University of Alberta

Behaviour of Reinforced Concrete Beams Strengthened in Shear with FRP Sheets

by

Christophe Deniaud ©

A thesis submitted to the Faculty of Graduate Studies and Research in partial fulfillment of the requirements for the degree of Doctor of Philosophy

in

Structural Engineering

Department of Civil and Environmental Engineering

Edmonton, Alberta

Fall 2000

National Library
of Canada

Acquisitions and
Bibliographic Services

395 Wellington Street
Ottawa ON K1A 0N4
Canada

Bibliothèque nationale
du Canada

Acquisitions et
services bibliographiques

395, rue Wellington
Ottawa ON K1A 0N4
Canada

Your file Votre référence

Our file Notre référence

The author has granted a non-exclusive licence allowing the National Library of Canada to reproduce, loan, distribute or sell copies of this thesis in microform, paper or electronic formats.

The author retains ownership of the copyright in this thesis. Neither the thesis nor substantial extracts from it may be printed or otherwise reproduced without the author's permission.

L'auteur a accordé une licence non exclusive permettant à la Bibliothèque nationale du Canada de reproduire, prêter, distribuer ou vendre des copies de cette thèse sous la forme de microfiche/film, de reproduction sur papier ou sur format électronique.

L'auteur conserve la propriété du droit d'auteur qui protège cette thèse. Ni la thèse ni des extraits substantiels de celle-ci ne doivent être imprimés ou autrement reproduits sans son autorisation.

0-612-59576-5

Canada

University of Alberta

Library Release Form

Name of Author: Christophe Deniaud

Title of Thesis: Behaviour of Reinforced Concrete Beams Strengthened in Shear with FRP Sheets

Degree: Doctor of Philosophy

Year this Degree granted: 2000

Permission is hereby granted to the University of Alberta Library to reproduce single copies of this thesis and to lend or sell such copies for private, scholarly or scientific research purposes only.

The author reserves all other publication and other rights in association with the copyright in the thesis, and except as herein provided, neither the thesis or any substantial portion thereof may be printed or otherwise reproduced in any form whatever without the author's prior written permission.

Christophe Deniaud

Christophe Deniaud
10741-University Avenue
Edmonton, Alberta
T6E 4P8

September 29, 2000

University of Alberta

Faculty of Graduate Studies and Research

The undersigned certify that they have read, and recommend to the Faculty of Graduate Studies and Research for acceptance, a thesis entitled Behaviour of Reinforced Concrete Beams Strengthened in Shear with FRP Sheets submitted by Christophe Deniaud in partial fulfillment of the requirements for the degree of Doctor of Philosophy in Structural Engineering.

J.J.R. Cheng, Supervisor

S. Alexander

S. Ariaratnam

A. Elwi

B. Jar

A. Nanni

September 21, 2000

ABSTRACT

The research work reported here investigates the behaviour of reinforced concrete beams strengthened in shear with Fibre Reinforced Polymer (FRP) sheets. A full-scale testing program was undertaken to expand the database on beams rehabilitated with FRP. This experimental data was used to develop a rational shear design method that includes and integrates all shear carrying components.

A series of four type G-girders removed from existing bridges were first strengthened with two types of FRP and two repair schemes. The shear capacity of the girders was increased significantly by the FRP sheets. However, due to the geometry of the girder and the loading set-up, the failure occurred in the end diaphragm of the hat-shaped beams. Three commonly used shear strength evaluation methods: a) Strut-and-Tie, b) Modified Compression Field Theory, and c) grid analysis were also investigated and the prediction results were compared to the experimental results. The shear capacity of each beam was accurately predicted but was limited to the ultimate shear load and to the elastic range of the load deflection curves.

The second part of the experimental study involved eight full-scale T-beams cast in laboratory conditions and extensively instrumented. Four parameters were studied: concrete strength, stirrup spacing, height of the beam web, and type of FRP. The contribution of the external FRP sheets was found dependant on the amount of internal reinforcement. The tri-axial glass fibre reinforcement exhibited a more ductile failure than the other beams reinforced by the other types of fibre.

The current shear design methods and the recently proposed models, which include the FRP contribution, were reviewed and were evaluated using the experimental data. From this analysis, new design equations based on the strip model and the shear friction approach were developed. The interaction of concrete, stirrups and FRP sheets is accounted for in these equations. The proposed design equations were validated with 35 available test results found in the literature and good predictions of the beam behaviour were observed.

A la mémoire de Marcelle et Louis

RÉSUMÉ

Le travail de recherche rapporté étudie le comportement des poutres en béton armé renforcées en cisaillement par des plaques en FRP (Polymères Renforcés de Fibres). Un program experimental grandeur nature a été entrepris pour augmenter la base de données de poutres réhabilitées avec des FRP. Ces nouvelles données experimentales ont été utilisées afin de de developper une methode rationnelle de design en cisaillement qui inclue and intègre tous les constituants supportant les forces de cisaillement.

Quatre poutres de Type G démantelées d'un pont ont été renforcées avec deux types de FRP et deux schémas de réparation. La capacité en cisaillement des poutres a été augmentée significativement par les laminés en FRP. Cependant, en raison de la géométrie des poutres et du montage du chargement, la rupture s'est produite dans le diaphragme d'extrémité des poutres en forme de U inversé. Trois méthodes d'évaluation du cisaillement généralement utilisées, à savoir les bielles et les tendons (Strut-and-Tie), la théorie modifiée du champ de compression (Modified Compression Field Theory) et l'analyse par grillage ont aussi été étudiées and comparées avec les resultats expérimentaux. La capacité en cisaillement de chaque poutre fut prédite avec précision mais fut aussi limitée à la charge de cisiallement ultime et à la partie élastique des courbes charge déflexion.

La seconde partie de l'étude experimentale comprenait huit poutres en T grandeur nature coulées au laboratoire et considérablement instrumentées. Quatre paramètres ont été étudiés: la résistance du béton, l'espacement des étriers, la hauteur de l'âme de la poutre et le type de FRP. Il a été observé que la contribution des plaques extérieures en FRP dépendaient de l'importance du renforcement interne. Le renforcement en fibre de verre tri-directionnel présente un mode de rupture plus ductile que les autres poutres renforcées par les autres types de fibres.

Les méthodes actuelles de design en cisaillement et les modèles incluant la contribution des FRP récemment proposés ont été revus et évalués avec ces données expérimentales. De cette analyse, de nouvelles équations basées sur l'approche du cisaillement par friction et de la méthode par bandes ont été développées. L'intéraction du béton, des étriers et des feuilles en FRP est incluse dans ces équations. Les équations proposées ont été validées

avec 35 résultats d'essais disponibles trouvés dans la litérature et de trés bonnes prédictions du comportement de ces poutres ont été observées.

RESUMEN

Este trabajo de investigación estudia el comportamiento de vigas de hormigón armado reforzadas a cortante con polímeros reforzados con fibras (FRP). El estudio incluye un extenso programa experimental de vigas de hormigón de tamaño real, encaminado a aumentar el número existente de ensayos en vigas rehabilitadas con FRP. Los resultados fueron utilizados para desarrollar un procedimiento racional de diseño que integre todos los componentes que participan en la transferencia de cortante en vigas de hormigón.

El programa experimental fué dividido en dos series. La primera incluye experimentos en cuatro vigas con sección transversal en forma de sombrero, comunmente denominadas del tipo G. Las vigas, obtenidas directamente de un puente de la vida real después de su desmantelamiento, fueron reforzadas con dos tipos de FRP, siguiendo dos esquemas diferentes de reparación. Los resultados demuestran que la capacidad a cortante de las vigas fué incrementada significativamente por el FRP. Sin embargo, debido a las propiedades geométricas de las vigas así como también a la manera como fueron cargadas, la falla tuvo lugar en los diafragmas extremos de las mismas. Cuatro métodos convencionales de diseño fueron utilizados para evaluar la capacidad a cortante de las vigas: a) el modelo de bielas de compresión y tensores (Strut and Tie), b) la teoría del campo de compresión modificada (Modified Compression Field Theory) , y c) un análisis de malla. La capacidad última a cortante de las vigas fué correctamente predicha por estos métodos, así como también su respuesta en el rango elástico.

La segunda serie comprende experimentos en ocho vigas T de hormigón armado fabricadas en el laboratorio. Las vigas fueron instrumentadas minuciosamente. Los ensayos se desarrollaron variando cuatro parámetros: la resistencia a la compresión del hormigón, el espaciamiento del refuerzo a cortante, la altura del alma de la viga y el tipo de hoja de FRP. Los resultados indican que la contribución de las hojas de FRP a la respuesta de las vigas depende de la cantidad de refuerzo interno existente. Las vigas con hojas de fibra de vidrio orientadas coplanarmente en tres dimensiones exhibieron una falla más dúctil que aquellas reforzadas con los otros tipos de FRP examinados. Con base en los resultados de esta segunda fase experimental, los actuales procedimientos de diseño para determinar la capacidad a cortante de vigas rehabilitadas con FRP fueron revisados, en particular aquellos que evalúan la llamada contribución del FRP. Como resultado, se propone un conjunto de ecuaciones de diseño basadas en el modelo de franjas y en el modelo de cortante por fricción. Las ecuaciones propuestas consideran el efecto interactivo existente entre el hormigón, el refuerzo interno a cortante y las hojas de FRP. Las ecuaciones propuestas fueron evaluadas y validadas con base en 35 resultados de laboratorio reportados previamente en la literatura.

ACKNOWLEDGEMENTS

This study was conducted with the financial assistance of the Natural Sciences and Engineering Research Council of Canada (NSERC) and the Canadian Network of Centres of Excellence on Intelligent Sensing for Innovative Structures (ISIS). The author also acknowledges supports, in the form of scholarships, provided by the University of Alberta, NSERC, and Vaughan Engineering.

The guidance and the supervision from Dr. Cheng throughout this project are greatly appreciated. I would also like to thank Dr. Neale of the Université de Sherbrooke in Québec for convincing me to undertake this endeavour. Equal thanks go to Dr. Labossière and Moni Rahhal for their encouragement to move West.

In France, I would like to thank my family for their constant support and encouragement despite the distance.

At the University of Alberta, the assistance of the technicians in the I.F. Morrison Structural laboratory, especially the resourceful Mr. Richard Helfrich, is acknowledged with thanks. Students Micheal Albert, Heng Aik Khoo, Scott Walbridge, Gaylene Kennedy, Patrick Del Col and Research Engineer Dr. Afhami were invaluable during the tests. The comments and suggestions of Dr. Alexander were very helpful in the development of the experimental part of this project. The photographs were all taken by Mr. Larry Burden.

Special thanks to my office colleagues Jeff DiBattista, Alfred Dorey and Marc Kuzik for all the constructive discussions and consultations regarding - or not - my thesis, and to Carlos Ospina and Georg Josi for sharing their passion of the world largest sport - soccer.

In industry, Mr. Dennis Sargent, Mr. Walter Tate and Mr. Ralston MacDonnell from Sargent and Vaughan Engineering shared kindly their practical bridge expertise and welcomed me in Victoria, B.C. The field application of some FRP repair techniques developed in this research was also made possible in Edmonton with the help of Mr. John Alexander from Stantec Consulting Group. The author also acknowledges the donation of the G-girders from Alberta Infrastructure and the FRP materials from Mitsubishi Canada Limited, Fyfe LLC Ltd, Owens Corning, and Sika Canada Inc.

Last, by not the least, I wish to extend a very special thank to Heather for her support and her editing skills.

TABLE OF CONTENTS

1 INTRODUCTION 1
- 1.1 Problem Statement 1
  - 1.1.1 Design Truck Loads 1
  - 1.1.2 Concrete Shear Strength 1
  - 1.1.3 Beam Shear Strengthening 2
- 1.2 Objectives and Scope 3
- 1.3 Thesis Format 4
- 1.4 Thesis Outline 4
- 1.5 References 6

2 SHEAR STRENGTHENING TECHNIQUES AND SHEAR EVALUATIONS OF REINFORCED CONCRETE BEAMS 7
- 2.1 Introduction 7
- 2.2 Shear Strengthening Methods for Reinforced Concrete Beams 8
  - 2.2.1 Traditional Techniques 8
  - 2.2.2 FRP Strengthening 9
    - *2.2.2.1 Laboratory Controlled Specimens* 9
    - *2.2.2.2 Rehabilitation of Existing Girders with FRP* 11
- 2.3 FRP Sheet Properties 12
  - 2.3.1 General Characteristics 12
  - 2.3.2 Bond Characteristics between Concrete and FRP 13
    - *2.3.2.1 General Behaviour* 13
    - *2.3.2.2 Interface Shear Strength Curves* 14
  - 2.3.3 Other Considerations 15
- 2.4 Shear Evaluation of Reinforced Concrete Members 16
  - 2.4.1 Current Shear Design Methods 16
    - *2.4.1.1 Truss Approach* 16
    - *2.4.1.2 Modified Compression Field Theory* 17
    - *2.4.1.3 Shear Friction* 18
  - 2.4.2 Shear Evaluation Models with FRP Strengthening 19
- 2.5 Conclusion 23
- 2.6 References 31

3 SHEAR REHABILITATION OF G-GIRDER BRIDGES IN ALBERTA USING FRP SHEETS 37
- 3.1 Introduction 37
- 3.2 Experimental Program 38
  - 3.2.1 Test Specimens 38
  - 3.2.2 Test Set-up and Instrumentation 39
- 3.3 Experimental Results 39
  - 3.3.1 Material Properties 39
  - 3.3.2 Girder Tests 40
- 3.4 Test Specimen Models 42

3.4.1 General Assumptions 43
3.4.2 Strut-and-Tie Model 43
3.4.3 Modified Compression Field Theory (MCFT) 44
3.4.4 Grid Analysis 45
3.5 Discussion 48
3.5.1 General 48
3.5.2 Comparison of the Models 49
3.6 Conclusion 50
3.7 References 64

4. REINFORCED CONCRETE T-BEAMS STRENGTHENED IN SHEAR WITH FRP SHEETS 65
4.1 Introduction 65
4.2 Experimental Program 67
4.2.1 Test Specimen 67
4.2.2 Test Set-up 68
4.2.3 Instrumentation 68
4.3 Experimental Results 69
4.4 Discussion 70
4.4.1 Initial Flexural Stiffness 70
4.4.2 Number of Stirrups 70
4.4.3 Strain Distribution Through the Depth 71
4.4.4 Beam and Arching Actions 71
4.4.5 Failure Modes 71
4.5 Mechanical Design Model 72
4.5.1 Strip Method 72
4.5.2 Shear Friction Method 75
4.5.3 Comments 76
4.6 Conclusion 76
4.7 References 87

5 SHEAR BEHAVIOUR OF RC T-BEAMS WITH EXTERNALLY BONDED FRP SHEETS 89
5.1 Introduction 89
5.2 Research Significance 90
5.3 Experimental Program 90
5.3.1 Test Specimens 90
5.3.2 Test Set-up 91
5.3.3 Instrumentation 92
5.4 Experimental Results 92
5.5 Discussion 94
5.5.1 Initial Flexural Stiffness 94
5.5.2 Number of Stirrups 94
5.5.3 Strain Distribution through the Depth 95

5.5.4 Beam and Arching Actions 95
5.5.5 FRP Strains 95
5.5.6 Failure Modes 96
5.5.6.1 General 96
5.5.6.2 Carbon Fibre Sheets 96
5.5.6.3 Glass Fibre Sheets 96
5.5.7 T6S2C90 Test 97
5.6 Mechanical Design Model 97
5.6.1 Strip Method 97
5.6.2 Shear Friction 98
5.6.3 Comments 99
5.7 Conclusion 100
5.8 References 112

6 REVIEW OF SHEAR DESIGN METHODS FOR RC BEAMS STRENGTHENED WITH FRP SHEETS 114
6.1 Introduction 114
6.2 Experimental Program 115
6.2.1 Test Specimens 115
6.2.2 Testing Results 116
6.3 Shear Evaluation Methods 117
6.3.1 Bond Models 118
6.3.2 CSA-S806 (2000) 120
6.3.3 Modified Compression Field Theory (MCFT) 120
6.3.4 Modified Shear Friction Method 121
6.3.5 Strut-and-Tie Model 122
6.4 Discussion 123
6.4.1 Comment on Each Model 123
6.4.2 Comparison of the Models 125
6.5 Conclusion 125
6.6 References 136

7 A SIMPLIFIED SHEAR DESIGN METHOD FOR CONCRETE BEAMS STRENGTHENED WITH FRP SHEETS 139
7.1 Introduction 139
7.2 Strip Method 140
7.2.1 General Description 140
7.2.2 Interface Shear Strength Curve 141
7.2.2.1 Interface Shear Strength Curve Development 141
7.2.2.2 Interface Shear Strength Curve Discussion 143
7.2.3 An Example of Using the Strip Method 144
7.2.3.1 Effect of the Concrete Crack Angle θ 144
7.2.3.2 Effect of the Number of Strips and the Strip Width 145
7.3 Parametric Study 145

7.3.1 Methodology 145
7.3.2 Development of the ε_{max} Equation 146
7.3.3 Development of the R_L Equation 147
7.4 Design Equation based on Shear Friction Method 148
7.4.1 Strength along the Weakest Plane through Stirrups 148
7.4.2 Continuous Equation 149
7.5 Validation of the Proposed Equations 150
7.5.1 Experimental Test Data 150
7.5.2 Discussion of the Design Equations 150
7.6 Illustration of the Proposed Equations 152
7.6.1 Design Example 152
7.6.2 Comparison Between the Discrete and Continuous Design Equations 153
7.7 Conclusion 154
7.8 References 165

8 SUMMARY, CONCLUSIONS AND RECOMMENDATIONS 169
8.1 Summary 169
8.2 Conclusions 170
8.3 Recommendations 172
8.4 References 173

Appendix A - Additional Type G-Girder Data 174
A.1 Photographs 174
A.2 Loaded Leg Shear Crack Patterns 188
A.3 Point Load Deflection Comparisons 196
A.4 Modified Compression Field Theory (MCFT) Detailed Procedure 200

Appendix B - Additional T400 Beam Data 202
B.1 Photographs 202
B.2 Schematic Shear Crack Patterns 210
B.3 Strain Distribution Through the Depth of the T-beam 219
B.4 Crack Pattern Prediction with a Linear FRP Strain Distribution 223

Appendix C - Additional T600 Beam Data 227
C.1 Photographs 227
C.2 Schematic Shear Crack Patterns 237
C.3 Beam and Arching Shear Actions 251
C.4 FRP Strain in the Principal Direction of the Fibres 254
C.5 Crack Pattern Prediction with a Uniform FRP Strain Distribution 257

Appendix D - Additional Shear Design Method Data 261
D.1 T400 Crack Pattern Prediction with a Uniform FRP Strain Distribution 261

D.2 Detailed Design Procedure Proposed by Malek and Saadatmanesh (1998) 264

Appendix E - Conference Papers 266
E.1 5th International Conference on Short and medium Span Bridges - July 13-16, 1998, Calgary, Alberta 266
E.2 27th Annual Conference of the Canadian Society for Civil Engineering - June 2-5, 1999, Regina, Saskatchewan (Paper #1) 278
E.3 27th Annual Conference of the Canadian Society for Civil Engineering - June 2-5, 1999, Regina, Saskatchewan (Paper #2) 288
E.4 3rd International Conference on Advance Composite Materials in Bridges and Structures - August 15-18, 2000, Ottawa, Ontario 298

LIST OF TABLES

Table **Page**

2.1 Mechanical Properties of Typical Materials (Kaw, 1997) 24

3.1 Test Matrix 52
3.2 Steel Coupon Tests 52
3.3 Fibre Reinforced Polymers Material Properties 52
3.4 Girder Test Results 53
3.5 Parameters Used for the Analysis of the Test Specimens 53
3.6 Material and Section Properties of the Girder Elements 54
3.7 Strength of the Girder Elements 55
3.8 Ultimate Point Load Predictions 55

4.1 Test Matrix of the T400 Series 78
4.2 Fibre Reinforced Plastics Material Properties 78
4.3 Maximum Loads and Loads Corresponding to the Change of Behaviour when Plane Section no Longer Remains Plane 78
4.4 Normalized Loads 79
4.5 Beam and Arching Shear Actions 79
4.6 Mechanical Model Results 79

5.1 Fibre Reinforced Polymer Material Properties 102
5.2 Test Matrix of the T600 Series 102
5.3 Maximum Loads and Loads Corresponding to the Change of Behaviour when Plane Section no Longer Remains Plane 102
5.4 Beam and Arching Shear Actions 103
5.5 Mechanical Model Results 103

6.1 Fibre Reinforced Polymer Material Properties 127
6.2 Test Matrix and Ultimate Loads 127
6.3 Chaallal *et al.* (1998) Model Predictions 128
6.4 Khalifa *et al.* (1998) Model Predictions 128
6.5 CSA-S806 (2000) Model Predictions 129
6.6 Malek and Saadatmanesh (1998) Model Predictions 129
6.7 Modified Shear Friction Model Predictions 130
6.8 Struts-and-Ties Model Predictions 130
6.9 Model comparison 131

7.1 Summary of the Strip Method Example with Nine Strips 155
7.2 Experimental Data on Shear Strengthening with FRP 156
7.3 Predicted Beam Strength using an Effective Concrete Area 157
7.4 Discrete Equation Results 158

LIST OF FIGURES

Figure **Page**

1.1 Number of ACI Shear Design Equation in ACI-318 over the Years (Collins *et al.*, 1999) 5

2.1 Internal and External Post-Tensioning (Emmons, 1993) 25
2.2 Beam and Slab Overlay (Emmons, 1993) 25
2.3 Bridge Girders in Alberta 26
2.4 Prestressed I-Shaped Beams with Bent-Legged Stirrups Tested in Manitoba (Hutchinson, 1999) 26
2.5 Typical Stress Strain Relationship for FRP 27
2.6 Potential Crack Paths (Karbhari, 1995) 27
2.7 Shear Stress Distribution Before and After Cracking (Brosens and Van Gemert, 1997) 28
2.8 Schematic Strain Distribution (Maeda *et al.*, 1997) 28
2.9 Tri-linear Bond Strength Curve (Alexander and Cheng, 1997) 29
2.10 FRP Strain Distribution across the Width at the Crack (Kamel *et al.*, 2000) 29
2.11 Various Anchoring Methods of FRP Sheets (Sato *et al.*, 1997) 30
2.12 FRP Sheet End Conditions 30

3.1 Typical Type G-Girder 56
3.2 Surface Preparation in the End Panel 57
3.3 Typical End Diaphragm Layout 57
3.4 Repair Schemes Used 58
3.5 Test Set-Up 59
3.6 Load vs. Point Load Deflection Curves for Specimens with Round End Diaphragm 59
3.7 Load vs. Point Load Deflection Curves for Specimens with Square End Diaphragm 60
3.8 Twisting of Carbon Fibres in Close Unloaded Corner (*Girder 4 West*) 60
3.9 Typical Shear Crack Patterns 61
3.10 Strut-and-Tie Scheme 61
3.11 Geometry for the Triangular Stress Block 62
3.12 Shear Friction Assumptions with FRP Sheets 62
3.13 Typical Point Load Deflection Comparisons (*Girder 3 West*) 63

4.1 T-beam Cross Section and Stirrup Layout with 200 mm Spacing 80
4.2 Isometric View of the Test Set-up 80
4.3 Strain Distribution Through the Depth of the T-beam from the Horizontal LVDT for T4S2 and T4S2G90 Specimens 81
4.4 Normalized Load Deflection Curves with no Stirrups 82

4.5 Normalized Load Deflection Curves with 400 mm Stirrup Spacing 82
4.6 Normalized Load Deflection Curves with 200 mm Stirrup Spacing 83
4.7 Normalized Load Deflection Curves with SEH51 Glass Fibres 83
4.8 Photo of the Crack Pattern for T4NS 84
4.9 Photo of the Crack Pattern for T4S2Tri 84
4.10 Vertical Equilibrium of one FRP Strip 85
4.11 Interface Shear Stress Curves 85
4.12 Crack Pattern Prediction for T4NS 86
4.13 Crack Pattern Prediction for T4S2Tri 86

5.1 T-beam Cross Section and Stirrup Layout with 200 mm Spacing 104
5.2 Isometric View of the Test Set-up 104
5.3 Horizontal LVDT Apparatus 105
5.4 Normalized Load Deflection Curves with 400 mm Stirrup Spacing 105
5.5 Normalized Load Deflection Curves with 200 mm Stirrup Spacing 106
5.6 Normalized Load Deflection Curves with Carbon Fibre Sheets 106
5.7 FRP Strain in the Vertical Direction with T6S4C90 at 501 kN 107
5.8 Beam and Arching Actions with 400 mm Stirrup Spacing 107
5.9 Photo of the Debonded Carbon Bands for T6S4-C90 108
5.10 Schematic FRP Debonding Growth 109
5.11 Photo of the Debonded Tri-Axial Glass Fibre Sheets 110
5.12 Stirrup Strains Comparison with 200 mmm Spacing 110
5.13 Interface Mean Shear Stress Curve 111
5.14 Effective Shear Friction Concrete Area 111

6.1 T-beam Geometry 132
6.2 FRP Designation 132
6.3 Effective Shear Friction Concrete Area 133
6.4 Strut-and-Tie Layouts for T600 Beams 133
6.5 Graphical Model Predictions 134
6.6 Graphical Modified Shear Friction Results (T6NSC45) 135

7.1 Dimensionless Bond Joint Capacity Plot 159
7.2 Dimensionless Interface Shear Strength Curves 159
7.3 FRP Strip Description used in the Example 160
7.4 Influence of the FRP Strip Width 161
7.5 FRP Sheet Anchorage and End Conditions 162
7.6 Inclined FRP Band Notation 162
7.7 Test Predictions using an Effective Concrete Area 163
7.8 Test Predictions using a Rectangular Concrete Section 163
7.9 Example Beam 164

A.1 Preparation and Mixing of the Epoxy 174
A.2 Epoxy Application on the Face of the Specimen 175

A.3 Soaking the Glass Fibres with Epoxy 176
A.4 GFRP Band Application inside the Leg of the Girder 177
A.5 GFRP Band Application in the Round End Diaphragm 178
A.6 Overall View of the Test Set-up 179
A.7 Close View of the Distributing Beam 179
A.8 Typical Round End Diaphragm Crack 180
A.9 Exposed Flexural Reinforcement Bars 181
A.10 Drilling of Concrete Cores 181
A.11 Underneath View of *Girder 1 East* at Ultimate 182
A.12 Underneath View of *Girder 2 West* at Ultimate 183
A.13 Underneath View of *Girder 3 West* at Ultimate 184
A.14 Underneath View of *Girder 4 East* at Ultimate 185
A.15 Underneath View of *Girder 4 West* at Ultimate 186
A.16 Concrete Cracks on the Exterior Face of the Loaded Leg without FRP Shear Strengthening (*Girder 1 East*) 187
A.17 Concrete Cracks on the Exterior Face of the Loaded Leg with FRP Shear Strengthening (*Girder 2 West*) 187
A.18 Cracking Growth of *Girder 1 East* 188
A.19 Cracking Growth of *Girder 1 West* 189
A.20 Cracking Growth of *Girder 2 East* 190
A.21 Cracking Growth of *Girder 2 West* 191
A.22 Cracking Growth of *Girder 3 East* 192
A.23 Cracking Growth of *Girder 3 West* 193
A.24 Cracking Growth of *Girder 4 East* 194
A.25 Cracking Growth of *Girder 4 West* 195
A.26 Point Load Deflection Comparisons (*Girder 1 East*) 196
A.27 Point Load Deflection Comparisons (*Girder 1 West*) 196
A.28 Point Load Deflection Comparisons (*Girder 2 East*) 197
A.29 Point Load Deflection Comparisons (*Girder 2 West*) 197
A.30 Point Load Deflection Comparisons (*Girder 3 East*) 198
A.31 Point Load Deflection Comparisons (*Girder 3 West*) 198
A.32 Point Load Deflection Comparisons (*Girder 4 East*) 199
A.33 Point Load Deflection Comparisons (*Girder 4 West*) 199

B.1 T4NS Specimen after Failure (Face A) 202
B.2 T4NS Specimen after Failure (Face B) 202
B.3 T4NSG90 Specimen after Failure (Face A) 203
B.4 T4NSG90 Specimen after Failure (Face B) 203
B.5 T4S4 Specimen after Failure (Face A) 204
B.6 T4S4 Specimen after Failure (Face B) 204
B.7 T4S4G90 Specimen after Failure (Face A) 205
B.8 T4S4G90 Specimen after Failure (Face B) 205
B.9 T4S2 Specimen after Failure (Face A) 206
B.10 T4S2 Specimen after Failure (Face B) 206

B.11 T4S2G90 Specimen after Failure (Face A) 207
B.12 T4S2G90 Specimen after Failure (Face B) 207
B.13 T4S2C45 Specimen after Failure (Face A) 208
B.14 T4S2C45 Specimen after Failure (Face B) 208
B.15 T4S2Tri Specimen after Failure (Face A) 209
B.16 T4S2Tri Specimen after Failure (Face B) 209
B.17 Cracking Growth of T4NS Specimen 210
B.18 Cracking of T4NSG90 Specimen at Ultimate 211
B.19 Cracking Growth of T4S4 Specimen 212
B.20 Cracking of T4S4G90 Specimen at Ultimate 213
B.21 Cracking Growth of T4S2 Specimen 214
B.22 Cracking Growth of T4S2G90 Specimen 216
B.23 Cracking Growth of T4S2C45 Specimen 217
B.24 Cracking Growth of T4S2Tri Specimen 218
B.25 Horizontal LVDT Data for T4NS and T4NSG90 Specimens 219
B.26 Horizontal LVDT Data for T4S4 and T4S4G90 Specimens 220
B.27 Horizontal LVDT Data for T4S2 and T4S2G90 Specimens 221
B.28 Horizontal LVDT Data for T4S2C45 and T4S2Tri Specimens 222
B.29 Crack Prediction for T4NS Specimen with a Linear FRP Strain Assumption 223
B.30 Crack Prediction for T4NSG90 Specimen with a Linear FRP Strain Assumption 223
B.31 Crack Prediction for T4S4 Specimen with a Linear FRP Strain Assumption 224
B.32 Crack Prediction for T4S4G90 Specimen with a Linear FRP Strain Assumption 224
B.33 Crack Prediction for T4S2 Specimen with a Linear FRP Strain Assumption 225
B.34 Crack Prediction for T4S2G90 Specimen with a Linear FRP Strain Assumption 225
B.35 Crack Prediction for T4S2C45 Specimen with a Linear FRP Strain Assumption 226
B.36 Crack Prediction for T4S2Tri Specimen with a Linear FRP Strain Assumption 226

C.1 Formworks and Bar Placement Prior to Casting the Concrete 227
C.2 Test Set-up 228
C.3 Horizontal LVDTs on the Side of the Beam 228
C.4 T6NS Specimen after Failure (Face A) 229
C.5 T6NS Specimen after Failure (Face B) 229
C.6 T6NSC45 Specimen after Failure (Face A) 230
C.7 T6NSC45 Specimen after Failure (Face B) 230
C.8 T6S4 Specimen after Failure (Face A) 231
C.9 T6S4 Specimen after Failure (Face B) 231

C.10 T6S4C90 Specimen after Failure (Face A) 232
C.11 T6S4C90 Specimen after Failure (Face B) 232
C.12 T6S4G90 Specimen after Failure (Face A) 233
C.13 T6S4G90 Specimen after Failure (Face B) 233
C.14 T6S4Tri Specimen after Failure (Face A) 234
C.15 T6S4Tri Specimen after Failure (Face B) 234
C.16 T6S2 Specimen after Failure (Face A) 235
C.17 T6S2 Specimen after Failure (Face B) 235
C.18 T6S2C90 Specimen after Failure (Face A) 236
C.19 T6S2C90 Specimen after Failure (Face B) 236
C.20 Cracking Growth of T6NS Specimen 237
C.21 Cracking Growth of T6NSC45 Specimen 238
C.22 Cracking Growth of T6S4 Specimen 240
C.23 Cracking Growth of T6S4C90 Specimen 241
C.24 Cracking Growth of T6S4G90 Specimen 243
C.25 Cracking Growth of T6S4Tri Specimen 245
C.26 Cracking Growth of T6S2 Specimen 247
C.27 Cracking Growth of T6S2C90 Specimen 249
C.28 Beam and Arching Actions for T6NS and T6NSC90 Specimens......... 251
C.29 Beam and Arching Actions for T6S4 and T6S4C90 Specimens......... 251
C.30 Beam and Arching Actions for T6S4 and T6S4G90 Specimens......... 252
C.31 Beam and Arching Actions for T6S4 and T6S4Tri Specimens........... 252
C.32 Beam and Arching Actions for T6S2 and T6S2C90 Specimens......... 253
C.33 FRP Strains for T6NSC45 Specimen at 400 kN 254
C.34 FRP Strains for T6S4C90 Specimen at 501 kN 254
C.35 FRP Strains for T6S4G90 Specimen at 464 kN 255
C.36 FRP Strains for T6S4Tri Specimen at 589 kN 255
C.37 FRP Strains for T6S2C90 Specimen at 585 kN 256
C.38 Crack Prediction for T6NS Specimen with a Uniform FRP Strain Assumption 257
C.39 Crack Prediction for T6NSC45 Specimen with a Uniform FRP Strain Assumption 257
C.40 Crack Prediction for T6S4 Specimen with a Uniform FRP Strain Assumption 258
C.41 Crack Prediction for T6S4C90 Specimen with a Uniform FRP Strain Assumption 258
C.42 Crack Prediction for T6S4G90 Specimen with a Uniform FRP Strain Assumption 259
C.43 Crack Prediction for T6S4Tri Specimen with a Uniform FRP Strain Assumption 259
C.44 Crack Prediction for T6S2 Specimen with a Uniform FRP Strain Assumption 260
C.45 Crack Prediction for T6S2C90 Specimen with a Uniform FRP Strain Assumption 260

D.1 Crack Prediction for T4NS Specimen with a Uniform FRP Strain Assumption 261
D.2 Crack Prediction for T4NSG90 Specimen with a Uniform FRP Strain Assumption 261
D.3 Crack Prediction for T4S4 Specimen with a Uniform FRP Strain Assumption 261
D.4 Crack Prediction for T4S4G90 Specimen with a Uniform FRP Strain Assumption 262
D.5 Crack Prediction for T4S2 Specimen with a Uniform FRP Strain Assumption 262
D.6 Crack Prediction for T4S2G90 Specimen with a Uniform FRP Strain Assumption 262
D.7 Crack Prediction for T4S2C45 Specimen with a Uniform FRP Strain Assumption 263
D.8 Crack Prediction for T4S2Tri Specimen with a Uniform FRP Strain Assumption 263

LIST OF ABBREVIATIONS AND SYMBOLS

Abbreviations

AASHTO	American Association of State Highway and Transportation Officials
ACI	American Concrete Institute
ASTM	American Society for Testing and Materials
CFRP	Carbon Fibre Reinforced Polymer
CSA	Canadian Standards Association
FRP	Fibre Reinforced Polymer
GPa	GigaPascal
kg	kilogram
kN	kiloNewton
LVDT	Linear Variable Differential Transducer
mm	millimetre
MCFT	Modified Compression Field Theory
MPa	MegaPascal
MTS	Material Testing System
$\mu\varepsilon$	microstrain (= 10^{-6} ε)

Arabic Symbols

a	Shear span
a_1, a_2, etc.	Regression coefficients
a_h	Anchor length underneath the flange
a_x	Interface length of the strip x
A_c	Effective concrete area
A_{cf}	Effective flange concrete area
A_{cv}	Area of the concrete section resisting shear transfer
A_{cw}	Web concrete area (= b_w h_w)
A_{FRP}	FRP sheet area

A_s	Longitudinal steel reinforcement area
A_v	Vertical steel area
A_{vf}	Area of shear friction reinforcement
b_f	Concrete flange width
b_{FRP}	Width of one FRP strip
b_{leg}	Width of one leg for a hat-shaped beam
b_w	Effective concrete web width
d	Effective beam depth (distance from extreme compression fibre to centroid of tension reinforcement)
d_{FRP}	FRP sheet height along the side of the beam web
d_s	Stirrup height
d_v	Distance between the resultant of the tensile and compressive forces due to flexure
E	Modulus of elasticity of steel
E_a	Elastic tensile modulus of the adhesive
E_c	Modulus of elasticity of concrete
E_{FRP}	Elastic tensile modulus of the FRP sheets in the principal direction of the fibres
f_1	Concrete principal tension stress
f_2	Concrete principal compression stress
f_{2max}	Limiting compressive stress in concrete strut
f_c'	Compressive strength of concrete
f_{cr}	Cracking strength of concrete
f_{FRP}	Effective FRP stress
f_t	Concrete tension stress
f_{tr}	Direct concrete tension strength
f_{ultFRP}	Ultimate strength of the FRP sheets in the principal direction of the fibers
f_v	Stress of the stirrups
f_{vy}	Yield strength of stirrups
f_y	Yield strength of longitudinal steel
F_{FRP}	Shear force carried by the FRP sheets

F_s	Shear force carried by the stirrups
F_u	Ultimate strength of longitudinal steel
G_c	Shear modulus of concrete
h	Beam height
h_f	Flange height
h_w	Web height (= $h - h_f$)
i	Integer
I_{cr}	Cracked moment of inertia
jd	Moment lever arm between the bottom and top chords
J	St. Venant torsion constant
k	Experimentally determined factor
k_a	Coefficient describing the anchorage conditions
k_e	Integer describing the number of debonding ends
k_1	Factor given in Equation (2.16b) or (6.9b)
k_f	Experimentally determined factor used for the flange
k_w	Experimentally determined factor used for the web
L	Available bond length
L_{eff}	Effective bond length
L_x	Available bond length of strip x
M	Moment occurring simultaneously with V
M_r	Resisting moment
$M^T{}_r$	Resisting moment with the triangular stress block
$M^R{}_r$	Resisting moment with the rectangular stress block
n	Number of effective strips
n	Number of spaces between stirrups
n_s	Total number of stirrups crossing the concrete shear plane
P	Ultimate load
P_{Joint}	Maximum load carried by the FRP bond joint
P_{Pred}	Predicted test load
P_{Test}	Experimental test load
P_y	Load level required to yield the vertical ties

R	Stress reduction factor
R_L	Remaining bonded width over the initial width ratio
s	Stirrup spacing
s_{FRP}	Spacing of FRP sheet bands
t	Thickness of the FRP sheets
t_a	Thickness of the adhesive
T	Tension force in the bottom chord
T_{cr}	Diaphragm cracking torque
T_{FRP}	Tension force in the FRP sheet between two consecutive stirrups
T_v	Tension force in the stirrups
V	Shear load
V_c	Shear load resistance attributed to the concrete
V_{exp}	Experimental shear load of the beam specimen
V_f	Factored shear load
V_{FRP}	Shear load resistance provided by the FRP sheets
V_i	Shear capacity given in Equation (2.29)
V_r	Total shear load resistance
V_s	Shear load resistance provided by the stirrups
$V_{(n,x)}$	Shear load computed at the strip x using a total of n strips
v	Concrete shear stress
v_c	Concrete shear strength
v_{FRP}	FRP shear stress
v_r	Shear friction resistance of the shear plane
v_s	Stirrup shear stress
w_{eff}	Effective FRP width given by Equation (2.22a) or (6.14a)
w_{FRP}	Width of one FRP sheet band
w_{Joint}	Width of the bonded FRP joint
w_x	Width of the FRP strip x
x	Strip number
y_x	Portion of the load carried by the strip x

Greek Symbols

α	Angle between the principal direction of the FRP sheets and the longitudinal axis of the beam
α_f	Angle between the principal direction of the FRP sheets and the shear plane
β	Concrete reduction factor
ΔN	Axial force due to the shear load
ε_1	Principal tensile strain in cracked concrete
ε_2	Principal compressive strain in cracked concrete
ε_{ave}	Effective average FRP strain over the remaining bonded length
ε_{cu}	Compressive uniaxial strain corresponding to f_c'
ε_{eff}	Effective FRP strain in the principal direction of the fibres
ε_{ext}	Extrapolated maximum FRP strain in the principal direction of the fibres at ultimate
ε_{FRP}	FRP strain in the principal direction of the fibres
ε_{long}	Longitudinal strain of flexural tension chord of the member
ε_{max}	Maximum FRP strain over the remaining bonded width
ε_t	Vertical strain
ε_{ultFRP}	Ultimate FRP strain
ε_x	Allowable FRP strain of a strip
ε_y	Yield strain of the steel stirrups
ϕ_c	Concrete resistance factor
ϕ_{FRP}	FRP resistance factor
ϕ_s	Steel resistance factor
γ_c	Density of concrete
ν_c	Concrete Poisson's ratio (= 0.2)
θ	Crack angle w.r.t. the longitudinal axis of the beam
θ_f	Crack angle w.r.t. the longitudinal axis of the beam in the flange
θ_w	Crack angle w.r.t. the longitudinal axis of the beam in the web

ρ_{FRP}	FRP reinforcement ratio
ρ_v	$= A_{vf}/A_{cv}$
ρ_w	Longitudinal reinforcement ratio
σ	Effective normal stress
σ_{FRP}	FRP stresses in the principal direction of the fibres
τ	Average concrete bond strength
τ_{eff}	Mean concrete bond strength over the effective bond length L_{eff}
τ_{ult}	Ultimate debonding shear stress
τ_x	Average bond strength associated with the strip x

1 INTRODUCTION

1.1 Problem Statement

Over 40% of the bridges in service today across North America were built 30 to 40 years ago. Most of these bridges are concrete bridges and most of them are now approaching their lifetime expectancy. Since the construction of these bridges, the design requirements have been reviewed and rewritten with the latest research developments. The shear design provisions have become more stringent as reported by COLLINS *et al.* (1996). As discussed, the ACI-318 shear design procedure required only four equations prior to 1963 whereas about 43 design equations were included in the 1995 ACI-318 code. Figure 1.1 illustrates the increase of the number of equations for shear design in ACI-318 Specifications. In addition, the allowable truck load weights for bridge design have also experienced significant increases. These two important elements of bridge design are described in more detail below.

1.1.1 Design Truck Loads

The bridges built in the early 50's and 60's in North America were designed using the AASHTO (1949) specifications. The design truck was the H20-S16 which corresponds to a total weight of 320.3 kN (36 t). The maximum wheel load was 71.2 kN. Today, bridges in Canada are designed with the CSA-S6 (1988) standard. The new current highway design truck in Canada is the CS-600 which indicates a total gross load of 600 kN. The maximum wheel load is now 90 kN which represents a 26.4% increase. However, some provinces use greater design truck loading which can lead to almost 45% increase (KORNELSEN and LOO, 1990). Same degrees of increase are also observed in the United States and elsewhere in the world.

1.1.2 Concrete Shear Strength

In 1973, following a series of research programs, a better understanding of the shear resistance of concrete members resulted in a complete review of the shear design provisions (ACI-ASCE COMMITTEE 426). Two major changes have been made: the concrete shear strength and the stirrup spacing requirements. For instance, using a typical concrete strength of 27.6 MPa (4000 psi) and a beam height of 400 mm, the AASHTO

(1949) and the CSA-S6 (1988) codes give different concrete shear strength evaluations and stirrup spacing requirements.

Concrete shear strength

[1.1]	$v_c = 0.03f'_c$	$v_c = 0.828$ MPa	AASHTO (1949)
[1.2]	$v_c = 0.19\sqrt{f'_c}$	$v_c = 0.998$ MPa	CSA-S6 (1988)

Stirrup spacing

[1.3a]	$s = \frac{1}{2}h$ when required to carry shear	$s = 203$ mm	
or			AASHTO (1949)
[1.3b]	$s = \frac{3}{4}h$ when not required	$s = 304$ mm	
[1.4]	$s = \frac{d}{2} \leq 600\,\text{mm}$	$s = 180$ mm	CSA-S6 (1988)

where h = height of the beam and d equals 0.9 h.

As shown, the concrete shear strength might be increased by 20.5%. But the spacing of the stirrups would need to be reduced from 304 mm to 180 mm, representing a 40.8% difference. Furthermore, in some cases the actual stirrup spacings did not meet the requirements of the 1949 standard at the time of construction by as much as 25% (ALEXANDER and CHENG, 1997).

CSA-S6 (1988) also stipulates that a minimum area of shear reinforcement must be provided where the design shear is greater than one half the shear resistance carried by the concrete alone. In other words, when the minimum stirrup requirements are not satisfied, the concrete shear strength should be reduced by half. In the above example, the concrete shear strength then becomes equal to 0.499 MPa which is then much smaller than 0.828 MPa.

1.1.3 Beam Shear Strengthening

The above evaluation shows that the bridge girder shear capacity may have decreased by as much as 40% while the applied loads increased by almost 45% during the past 40 years. These two effects, added to the natural aging of the bridges, have resulted in the shear deficiency of some of these bridges. Consequently, there is an urgent need to develop an efficient method of rehabilitation to address this structural deficiency.

The first option is to limit the traffic over the existing structures. This option, however, is not very practical since it requires redirection of the traffic. The second option is to replace the old one with a new bridge but this can be a very expensive remedy. The third option is to upgrade the existing structures to carry additional loads and normally is the most feasible solution.

The rehabilitation of structures is not new and various repair projects have been carried out in the world for many years. Steel has been the primary material used to strengthen deficient structural members. However, adding steel components to the structure increases the dead load, which may require additional substructure strengthening. Corrosion protection for the steel also needs to be considered. Fibre Reinforced Polymer (FRP) materials offer an attractive alternative for the strengthening of structures with their high strength to weight ratio, low weight to stiffness ratio, non-corrosiveness property, high fatigue strength and ease of application.

1.2 Objectives and Scope

The primary objective of this program is to evaluate the shear contribution of FRP sheets bonded externally on reinforced concrete beams. The potential of the FRP shear reinforcement was first investigated using existing bridge girders. Two types of FRP and two repair schemes were considered in these tests. Next, a series of laboratory controlled specimens were cast to investigate specifically the effects of the concrete strength, the stirrup spacing, the height of the beam web and the type of the FRP. The secondary objective is to evaluate the test results with various methods of analysis, such as the Strut-and-Tie model and the Modified Compression Field Theory (MCFT). The FRP design models available in the literature were also considered. Finally, with a better understanding of the behaviour of concrete beams strengthened in shear with FRP, the development of a more rigorous design model has been undertaken. In addition, this project provides a significant number of full-scale test results of concrete beams strengthened with FRP to the existing database.

1.3 Thesis Format

This thesis is prepared in accordance with the regulations for a Paper-Format Thesis as set out by the Faculty of Graduate Studies and Research at the University of Alberta (FGSR, 1999). Each chapter includes its own bibliography. Tables and figures are grouped at the end of each chapter before the bibliography. The nomenclature is consistent throughout the thesis and is listed in the prefatory pages. References to the chapters which have been submitted for publication take the form of "(DENIAUD and CHENG, 2000 [Chapter 4])", which refers to the paper by DENIAUD and CHENG that appears as Chapter 4 of this thesis.

Considerable information that was generated from this study is presented in Appendices. These appendices, except Appendix E, include typically photos, crack patterns, detail experimental data, details of calculation methods, and other essential information that are not provided in the main chapters. Appendix E presents a copy of the four conference papers that were presented during the course of this thesis.

1.4 Thesis Outline

This research studies the behaviour of the FRP sheets bonded externally to reinforced concrete beams. Chapter 2 reviews both the traditional and FRP shear strengthening techniques, as well as the principal FRP properties. The current shear design methods and the recently developed shear models, which include the FRP contribution, are also introduced. Chapter 3 focuses on the shear rehabilitation of four Type G-girders removed from existing bridges in Alberta. Chapters 4 and 5 present full-scale reinforced concrete beam tests having a height of 400 mm and 600 mm respectively. These beam specimens were cast and tested under fully-controlled laboratory conditions. Chapter 6 discusses the shear design models proposed in the literature to account for the FRP shear contribution. These model predictions are compared with the experimental data developed in this research study. Finally, Chapter 7 proposes a new shear design model which accounts for the interaction of the concrete, the stirrups, and the FRP components. This model is then validated with available experimental data reported in this study and other published sources. Finally, summary, conclusions, and recommendations for future study are presented in Chapter 8.

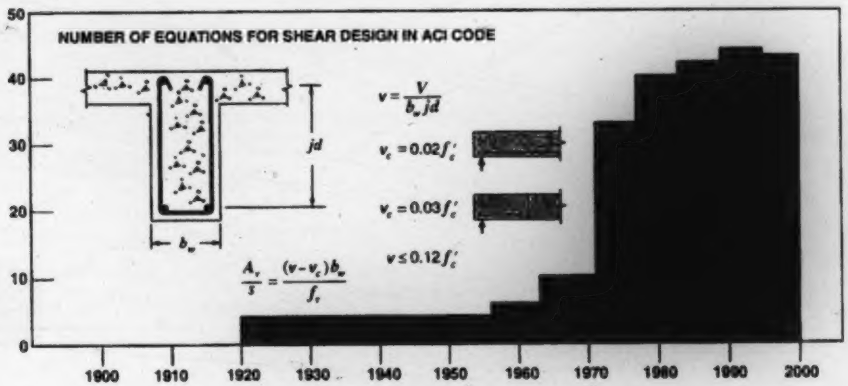

Figure 1.1 **Number of Shear Design Equations in ACI-318 over the Years (COLLINS *et al.*, 1996)**

1.5 References

AASHTO (1949). *Standard Specifications for Highway Bridges*, 5th edition, Washington, D.C.

ACI-318 (1995). *Building Code Requirements for Structural Concrete,* Detroit, MI.

ALEXANDER J. and CHENG J.J.R. (1997). *Shear Rehabilitation of G-Girder Bridges using CFRP Sheets*, Structural Engineering Report No 218, Department of Civil and Environmental Engineering, University of Alberta, Edmonton, AB, 181 p.

ASCE-ACI COMMITTEE 426 (1973). "The Shear Strength of Reinforced Concrete Members", *Journal of Structural Engineering*, ASCE, Vol. 99, No. ST6, June, pp. 1091-1187.

COLLINS M.P., MITCHELL D., ADEBAR P., and VECCHIO F.J. (1996) "A General Shear Design Method", *American Concrete Institute Structural Journal*, Vol. 93, No. 1, January-February, pp. 36-45.

CSA-S6 (1988). *Design of Highway Bridges*, Canadian Standards Association, Rexdale, ON.

FACULTY OF GRADUATE STUDIES AND RESEARCH (1999). *Thesis Handbook*, University of Alberta, Edmonton, AB, 17 p.

KORNELSEN R.W. and LOO T. (1990) *Bridge Rating – New Rating Truck Models*, Version 1.00, Alberta Transportation and Utilities, Edmonton, AB.

2 SHEAR STRENGTHENING TECHNIQUES AND SHEAR EVALUATIONS OF REINFORCED CONCRETE BEAMS

2.1 Introduction

The infrastructure deficits in North America and elsewhere in the world have reached an all time high because a large percentage of the inventory has reached its life expectancy. An estimated 40% of all bridges operating today have been found to be structurally deficient or obsolete and require repair, strengthening, upgrading or replacement (SEIBLE, 1996). These deficiencies are mainly due to environmental deterioration, insufficient detailing at the time of construction, inadequate maintenance and increased traffic load demands. Because of recent budget constraints and scarce funding, the owners of these structures, comprised mainly of government bodies, are interested in reliable, cost effective, rapid and sustainable alternative repair solutions.

Fibre Reinforced Polymers (FRPs) have been widely used in the aerospace and defence industries, but mainly due to economic reasons, applications in civil engineering sectors have been very limited. The high manufacturing costs of FRP and lack of experience of civil engineers in using these materials, compared to the cheaper and more well-established traditional construction materials, such as concrete and steel, made FRP a less common option. With the end of the Cold War, the excessive production of composite materials calls for alternative markets for the materials. Combined with the needs of rehabilitation market, researchers, infrastructure owners, and FRP sectors have started to explore the possibility of using FRP in construction applications, more specifically in the market of rehabilitation (HEAD, 1996). In the meantime, new FRP manufacturing techniques have helped reduce the production costs, making these high quality materials more competitive.

Over the last decade, a significant number of research projects and field applications have been carried out in the area of using FRP in civil engineering applications. NEALE (2000) surveyed the most recent progress in the use of FRP in structures and found that almost all aspects of structural members could and had been efficiently reinforced with these lightweight materials. FRP materials were mostly used with concrete structural elements to increase their flexural capacity (RITCHIE *et al.*, 1991; SAADATMANESH and EHSANI, 1991). FRP applications in masonry, wood or steel elements were also investigated (KUZIK *et al.*, 1999; ROWLANDS *et al.*, 1986; DOREY and CHENG, 1996; KENNEDY and CHENG, 1998).

Since this research focuses on the use of FRP in shear strengthening of reinforced concrete beams, only the area of shear strengthening of concrete beams will be considered in this chapter. The commonly used shear reinforcement techniques are briefly reviewed followed by the new FRP strengthening methods recently developed. The main characteristics of externally bonded FRP sheets are also presented. Finally, the shear evaluation methods currently available in design standards and other design models proposed by researchers to include the FRP sheet contribution are introduced.

2.2 Shear Strengthening Methods for Reinforced Concrete Beams

2.2.1 Traditional Techniques

Shear strengthening of concrete beams has traditionally been performed by adding steel elements to the deficient members. The most common traditional shear strengthening techniques were illustrated by EMMONS (1993) and will be reviewed briefly and discussed below. Further design details on bridge rehabilitation can be found elsewhere (XANTHAKOS, 1996).

Post-tensioning is a technique used to prestress reinforced concrete members. Either internally or externally placed post tensioning can be added to an existing beam web as shown in Figure 2.1. The main advantage of this technique is that it provides immediate active strengthening, which relieves the overstressed conditions of the beam web. However, the deck overlay needs to be removed and a large number of holes must be drilled through the member. The labour costs are very expensive and there is some inconvenience for the users since one part of the bridge would be closed at all times to facilitate the drilling process. The amount of steel weight added to a structure could also become a concern for some other bridge elements which, in turn, may also require strengthening.

Internal mild steel reinforcements can also be used as passive shear strengthening to increase the shear capacity of a member. Additional reinforcement dowels are placed perpendicular to the existing cracks. They are placed into drilled holes and then grouted into place with epoxy. This repair technique has the same problems associated with the post tensioning method. In addition, the passive reinforcements imply that the web can not be severely damaged since the new reinforcement will only be activated if additional loads are added to the member.

Another technique is to enlarge the cross section of the member to increase the area of load carrying concrete. An overlay can be cast either around the web or over the top slab as shown in Figure 2.2 or as a combination of the two. This technique effectively increases the stiffness and the flexural capacity of the member, but obviously involves the addition of considerable dead load. A consideration of the effects on the supporting structural elements, such as the piers or foundation piles, is also required. In some cases, this technique is therefore not possible due to the lack of capacity of the substructure components.

2.2.2 FRP Strengthening

2.2.2.1 Laboratory Controlled Specimens

In 1992, UJI reported eight RC specimens with and without internal shear reinforcement. The beams tested were 200 x 100 mm in cross section and 1300 mm long. Only carbon fibre sheets were used to strengthen the beams. The sheets were either wrapped around the beam or applied only on the sides with different amounts and directions of fibres. By applying the FRP, the shear capacity of the beams without stirrups was substantially increased. For the beam with stirrups, the shear force carried by the stirrups was reduced. The strain on FRP and stirrups were found different even at the same locations. Finally they observed that the tensile force of the FRP sheets was related to the debonded area and that the bond of the FRP to the concrete determined the shear capacity.

AL-SULAIMANI *et al.* (1994) built 16 beams deficient in shear and repaired them with FRP sheets. The specimens used were 150 x 150 mm in cross section and 1250 mm long. The reinforcement consisted of high-strength steel bars and stirrups spaced at 200 mm. The beams were designed to yield a flexural capacity 1.5 times higher than the shear capacity. The beams were loaded until the first visible cracks appear. Then, the beams were repaired using glass fibre sheets with three different repair schemes: strip, wing and jacket. The jacket gave the best improvement of the shear capacity, but flexural failure occurred in this case. Therefore, the full potential of this scheme could not be realized. The strips and wings yielded an increased shear capacity of 25% and 30%, respectively.

CHAJES *et al.* (1995) published results of 12 concrete T-beams externally bonded with FRP. They used three composite materials: Aramid, E-Glass and Graphite. No stirrups were provided in these beams. The beams were 1200 mm long and 190 mm deep with a flange of 140 mm wide. The shear failure occurs at the same location in the constant shear span for all the specimens. They found that the shear behaviour of the beam with FRP was similar to the flexural behaviour of a reinforced concrete before and after cracking. They concluded that full-scale tests should be conducted and more tests were required with varied internal shear reinforcement, different beam geometry, and variety of shear span to depth ratio in order to develop a more rigorous analytical model.

SATO *et al.* (1996) conducted six beam tests with carbon fibre sheet shear strengthening. The CFRP sheets were applied either to the sides of the beam or to both sides and the bottom of the beam. Only one of the test specimens had internal reinforcement. The beams had a rectangular cross section 200 mm wide and 300 mm deep. The repair scheme in a form of U-jacket was more effective than the FRP attached only to the sides. For the specimens without stirrups, the observed failure mode occurred by delamination of the FRP sheets along the shear crack.

In 1997, the Swiss Federal Institute of Technology tested seven rectangular beams reinforced in shear with FRP sheets (ADEY *et al.*). The beams were 200 x 400 mm in cross section, which represented the largest beams tested to date. The shear span was 750 mm. The performance of partially wrapped and fully wrapped specimens was investigated. The beams were only strengthened with carbon fibre sheets. This test series showed that the partially wrapped specimens resulted in much smaller increases in the load carrying capacity then observed for smaller specimens. The anchorage length of the FRP was also found to be a significant parameter affecting the beam strength. They then recommended focussing any future work on alternative methods for anchoring the FRP sheets.

Recently, TRIANTAFILLIOU (1998) increased the experimental database on shear strengthening of reinforced concrete beams using FRP. A series of eleven very shallow beams (70 mm wide by 110 mm deep) were cast and strengthened with various amount of fibres bonded only to the side of the specimens. Combined with all the test results available in the literature at that time, the effective FRP strain was found to be related to the axial rigidity of the FRP sheets bonded to the concrete. Further studies on full-scale test specimens were recommended to validate these observations and also to expand the experimental database.

2.2.2.2 Rehabilitation of Existing Girders with FRP

Concurrently, several researchers investigated the potential of FRP shear strengthening with existing bridge girders to solve specific deficiencies.

In 1994, DRIMOUSIS and CHENG presented results on type E-Girders strengthened by carbon fibre sheets. These tests were part of a research program in partnership with the Alberta Infrastructure at the University of Alberta. The purpose was to study the feasibility of using FRP in rehabilitation of concrete bridges. A typical cross section of a type E-girder is presented in Figure 2.3. The peculiarity of this girder type is that the stirrups alternate from leg to leg. This means that the maximum spacing is actually twice this distance if considering only one leg. All the tested girders failed in shear. Successful FRP repair schemes were found to strengthen this type of girders in shear capacity. The shear capacity was increased by an amount of 21% to 55% over the control beam with no reinforcement. However, it was pointed out that a more rigorous and controlled experimental program should be carried out.

Following this initial project, ALEXANDER and CHENG (1997) studied the reinforcement of type G-girders with FRP. Since the height of the G-girder is less than the type E-girder (see Figure 2.3), the first tests, conducted under concentric loading, did not fail in shear, but rather in bending. An eccentric loading system was then created to avoid premature bending failure. The failure by the combined shear and torsion occurred within the end diaphragm in all cases. Further investigations of the end panel strengthening for these girders were recommended.

FRP shear strengthening of prestressed girders were also investigated at the University of Manitoba (HUTCHINSON *et al.*, 1997). Four, ten meter long, I-shaped, precast, prestressed beams were fabricated using stirrups with a bent-legged shape identical to that used for the stirrups of existing bridge girders. This poor existing detail of the internal steel shear reinforcement in shown in Figure 2.4. Various repair scheme configurations, including vertical, horizontal and diagonal CFRP sheets, were investigated. Results showed that CFRP sheets were effective in reducing the tensile force in the stirrups under the same applied shear load. The application of both vertical and horizontal CFRP sheets improved the contribution of the sheets to the shear capacity of the beam. Diagonal CFRP sheets were also found more efficient than the horizontal and vertical CFRP combination.

2.3 FRP Sheet Properties

2.3.1 General Characteristics

FRP products consist of two or more separate materials that are glued together to form a single composite unit. The fibres provide the high strength and the stiffness of the FRP composites and the resin matrix provides the stress transfer among the fibres. Three types of fibres are commonly used for civil applications: glass, carbon and aramid. The fibres are embedded in a polymer matrix (i.e. epoxy) which binds the fibres together and protect them from breakage due to abrasion. The material properties of the fibres and the epoxy, as well as more commonly used FRPs, are shown in Table 2.1. The matrix has typically lower modulus of elasticity and greater rupture strain than the fibres (see Figure 2.5).
Randomly short directed fibres such as sprayed FRP (BANTHIA *et al.*, 1996) are also being used for the repair of existing structures. However, in most cases, continuous fibres, in one or more directions, are preferred for structural strengthening. The uniaxial FRP material is linear elastic up to rupture in the direction of the fibres, as shown in Figure 2.5. With unidirectional FRP sheets, the behaviour of the composite material in the direction perpendicular to the fibres depends on the matrix properties. Thus, the sheet is very weak in this direction. Woven FRP materials with cross-pattern fibre layout show enhanced lateral behaviour. Tri-axial laminates with fibre content equally oriented at 0, 60 and –60 degrees, are also an interesting category of laminates. This material displays in-plane stiffnesses that are independent of orientation and has been called quasi-isotropic because it displays isotropic properties within the plane of the laminates. It is often used when the loading directions are not well known in advance, since no particular direction, is favoured (SWANSON, 1997).
The FRP sheets can be tailored to a specific application and have a very light weight. The labour costs are then significantly reduced and negligible weight is added to the structure.

These advantageous capabilities helped promote the use of externally bonded FRP systems for the rehabilitation of existing structures over the last decade. Unfortunately, the relatively high cost of the FRP materials limited their application in civil engineering. However, due to the constant efforts of the FRP manufacturers over the last few years to reduce the production costs, FRP materials are now more affordable and more readily available.

The application of the FRP to a concrete structure is normally done using adhesives, such as epoxy. Thus, unless mechanical anchors are used, the efficiency of the FRP system relies essentially on FRP-to-concrete bond performance. The bond requirements for the FRP sheet anchorage are therefore very important to transfer shear loads.

2.3.2 Bond Characteristics between Concrete and FRP

2.3.2.1 General Behaviour

Over the last few years, the bond behaviour of FRP sheets glued to concrete has gained a lot of interest, since it is the key to a successful strengthening technique. KARBHARI (1995) identified five potential failure modes of the FRP sheet glued on concrete as shown in Figure 2.6. Although these potential crack paths were observed at the plate curtailment bonded underneath the beam, they may also describe the failure of FRP sheets bonded to the vertical side of the beam.

In 1997, BROSENS and VAN GEMERT studied the variation of the shear stress along the bond joint. Figure 2.7 shows the shear stress distribution on the concrete surface before and after cracking. They found that the tensile force from the FRP sheet was transferred into the concrete within an effective bond length. Therefore, when the bonded length exceeded the critical length, the fracture load of the joint remained constant. In other words, there is an effective bond length beyond which the load carried by the joint does not increase. Similar results were observed by other researchers but presented differently (CHAJES *et al.*, 1996; ALEXANDER and CHENG, 1997; MAEDA *et al.*, 1997; BIZINDAVYI and NEALE, 1999). In particular, MAEDA *et al.* presented a schematic strain distribution to describe the FRP strain profile of the bonded joint, as shown in Figure 2.8. They also observed a relationship between the effective bond length and the stiffness of the FRP sheet. The following equation was then proposed:

[2.1] $$L_{eff} = \exp[6.134 - 0.58\ln(t\,E_{FRP})]$$ (L_{eff} is in mm)

where t and E_{FRP} are the thickness and the elastic modulus of the bonded FRP sheet, respectively. In this equation, $t \cdot E_{FRP}$ has units of kN/mm and L_{eff} is given in mm.

2.3.2.2 Interface Shear Strength Curves

The average concrete bond strength τ is commonly used to characterize the FRP bond and is written as follows:

[2.2] $$\tau = \frac{P}{L\,w_{joint}}$$

where P is the ultimate load, L is the available length and w_{joint} the width of the joint. Since all the bond length provided is not being utilized, as mentioned earlier, the average bond strength will typically decrease as the available bond length increases (CHAJES *et al.*, 1996). Several researchers have, therefore, proposed interface shear curves to fully describe the FRP bonded joints.

ALEXANDER and CHENG (1997) proposed a tri-linear curve as shown in Figure 2.9. This relationship was developed from a few concrete block tests with 100 mm FRP joint width. This series of ancillary tests were performed to evaluate the shear strength of existing girders laterally strengthened with carbon fibre sheets. A few years later, BIZINDAVYI and NEALE (1999) published extensive bond test results with both glass and carbon sheets. They used a width of 25 mm for the bonded FRP sheets. They suggested an exponential formulation with different fitting coefficients for each type of FRP, as shown below.

[2.3a] $$\tau = 5.3662\exp(-0.0051\,L)$$ (Carbon fibres)

[2.3b] $$\tau = 8.6513\exp(-0.0090\,L)$$ (Glass fibres)

where L and τ are given in mm and MPa, respectively.

Recently, Kamel *et al.* (2000) observed that the width of the bonded FRP sheet significantly affected the average bond strength. Experimental results showed that as the FRP sheet width decreased, the mean average bond strength increased. This behaviour was partially attributed to the strain distribution across the sheet. With a narrow sheet, the strain distribution is roughly uniform, whereas with a wide sheet the edge FRP strain value can more than double the middle strain value, as shown in Figure 2.10. UEDA *et al.*

(1999) made similar observations, but explained this behaviour with the wider failure zone of the concrete surface than the FRP sheet. Further studies with finite element analysis are still required to simulate the strain distribution both across the width and along the length of the joint. The nonlinear behaviour caused by the cracking of the concrete should also be considered (MAEDA *et al.*, 1997).

2.3.3 Other Considerations

The anchoring capacity of FRP sheets can be significantly improved by mechanical anchors. SATO *et al.* (1997a) investigated several anchoring methods for carbon fibre sheets, as illustrated in Figure 2.11. The strengthening method with bolt and plate was found to be the most practical in actual repair since no simultaneous work was required above the beam slab. They also recommended using longer anchoring bolts which penetrate the whole width of the beam. SATO *et al.* (1997b) confirmed also that FRP sheets with mechanical anchorage were much more effective than strengthening without mechanical anchorage. They qualitatively demonstrated the shear strength improvement due to the mechanical anchors, but a quantitative assessment of the anchorage efficiency needed further study.

The durability of the materials used in rehabilitation is also a major factor of a successful repair technique. Since the use of FRP in civil engineering is fairly new, an appropriate assessment of the FRP material behaviour under environmental exposure must be considered. This document does not intend to provide a thorough review of all the durability aspects investigated in the past or in current research projects. The latest developments in FRP durability can be found in BENMOKRANE and RAHMAN (1998). However, some significant durability works related to external FRP strengthening are briefly reviewed.

Moisture, temperature, salt environments, freeze-thaw and wet-dry cycles have been examined with FRP flexural strengthening (KARBHARI and ENGINEER, 1996; BEAUDOIN *et al.*, 1998; RAÎCHE *et al.*, 1999; UOMOTO and NISHIMURA, 1999). The investigations related to moisture were found to be the most aggressive with respect to potential degradation of the composite - concrete interface when the solution was salty. The FRP sheets made of carbon fibres showed, in all cases, better durability than the other type of fibres. The beam tested by RAÎCHE *et al.* (1999) also had glass FRP sheets, in a form of

U-jacket, to anchor the FRP plate underneath the beams. The anchorage of the FRP plate was found to be the weakest element of the strengthening system, due to the bond degradation of the glass fibres under severe environmental exposures.

FERRIER *et al.* (1999) observed that the adhesive joint and the carbon FRP plates were strong enough for a fatigue loading of one million cycles.

Most of the durability tests on FRP reported in the literature were performed with flexural reinforcement. The effect of environmental exposure on external FRP shear strengthening requires further investigations.

2.4 Shear Evaluation of Reinforced Concrete Members

2.4.1 Current Shear Design Methods

2.4.1.1 Truss Approach

The shear strength of a beam element is traditionally evaluated using a simple truss analogy initially proposed 100 years ago by RITTER and later by MÖRSCH (ASCE-ACI COMMITTEE 445, 1998). This approach is still the basis of several current design codes (ACI-318, 1998; CSA-A23.3, 1994; CSA-S6, 1988). In this model, the truss consists of a top longitudinal concrete chord, a bottom longitudinal steel chord, vertical steel ties, and diagonal concrete struts inclined at 45°. This method also assumes that diagonally cracked concrete cannot resist tension. Therefore, no diagonal tension members perpendicular to the concrete struts are considered. The total shear resistance is then the sum of the concrete and shear reinforcement contributions as follows:

$$[2.4] \qquad V_r = V_c + V_s$$

The concrete contribution term is typically expressed as a function of the square root of the concrete compressive strength f_c' (CSA A23.3, 1994):

$$[2.5] \qquad V_c = 0.2\sqrt{f_c'}\,b_w d$$

where b_w and d are the width of the web and effective depth of the beam, respectively. Numerous restrictions are attached to the calculation of V_c and are included in this traditional method to account for parameters that affect the shear strength. These parameters include the amount and distribution of transverse and longitudinal reinforcements, prestressing, span to depth ratio, beam size, coexisting moments and axial forces.

For the usual case of transverse reinforcement oriented at 90° to the longitudinal reinforcement, the stirrup contribution is expressed as:

$$[2.6] \qquad V_s = \frac{A_v f_{vy} d}{s}$$

where A_v is the transverse steel area, f_{vy} is the yield strength of the stirrups and s is the spacing of the stirrups.

2.4.1.2 Modified Compression Field Theory

In 1973, ACI-ASCE COMMITTEE 426 published a state-of-the-art document on shear design for reinforced concrete members. The committee recommended further research to develop realistic shear design models. Along with extensive experimental research, COLLINS (1978) developed the Compression Field Theory (CFT) for shear. The angle of inclination θ of the diagonal compression strut was calculated in a rational manner but the tensile stresses in the concrete were still ignored.

A few years later, the Modified Compression Field Theory (MCFT) was proposed to account for the beneficial effects of small tensile stresses that still remain in diagonally cracked reinforced concrete members (VECCHIO and COLLINS, 1986). This variable angle truss method requires iterations to converge to the appropriate solution. Details of the solution technique can be found in COLLINS and MITCHELL (1987).

The MCFT is the basis for the general method in the current reinforced concrete design code CSA-A23.3 (1994). The equations of the MCFT were simplified for design purposes. Equation (2.5) was re-written as follows:

$$[2.7] \qquad V_c = \beta \sqrt{f'_c}\, b_w d_v$$

The β term is a factor which depends on the ability of the concrete to transmit tensile stresses. The amount of reinforcement and the levels of axial tension or compression, bending, and prestressing are the main parameters affecting its value. The d_v term is the effective shear depth of the beam defined differently from the effective depth of the beam.

With a variable angle θ, the steel shear reinforcement contribution is then given by:

[2.8] $$V_s = \frac{A_v f_{vy} d_v}{s} \cot\theta$$

The background of these design equation simplifications from the MCFT was recently published by RAHAL and COLLINS (1999).

2.4.1.3 Shear Friction

From Clause 11.1.3 in the CSA-A23.3 code (1994), the shear friction concept can be used for shear design when slippage may occur along an existing or potential-major crack. The shear stress resistance is then expressed with:

[2.9a] $$v_c = k\sqrt{\sigma f'_c} + \rho_v f_y \cos\alpha_f$$

with

[2.9b] $$\sigma = \rho_v f_y \sin\alpha_f$$

[2.9c] $$\rho_v = \frac{A_{vf}}{A_{cv}}$$

where k=0.6 for concrete placed monolithically, α_f is the angle between the shear friction reinforcement and the shear plane, f_y is the yield strength of the reinforcement crossing the shear plane, and A_{vf} and A_{cv} are the area of shear friction reinforcement and concrete section resisting shear transfer, respectively.

Recently, LOOV (1998) applied the shear friction concept to evaluate the shear strength of reinforced beams. Equation (2.9a) was re-written to evaluate the shear strength along a plane crossing *n* spaces and *n-1* stirrups:

[2.10] $$V_r = 0.25 k^2 f'_c b_w h \frac{d_s}{ns} + T_v(n-1)$$

where h and d_s are the beam and stirrup heights, respectively. The experimentally-determined factor k was studied by LOOV and PENG (1998) with concrete strengths ranging from 20 to 100 MPa. The following equation was proposed from a least squares analysis.

[2.11] $$k = 2.1(f'_c)^{-0.4}$$

T_v is the tension force in the stirrup and is expressed by:

[2.12] $$T_v = A_v f_{vy}$$

The governing shear strength is the lowest shear strength among all potential shear cracks along which slippage can occur. The discrete formulation presented in Equation (2.10) is therefore an upper bound solution. Assuming *n* to be continuous rather than discrete, LOOV (1998) derived the Equation (2.10) with respect to *n* to obtain the following continuous design equation, which was slightly conservative.

[2.13] $$V_r = k\sqrt{f_c^{'} b_w h T_v \frac{d_s}{s}} - T_v$$

The tension force T_v is then subtracted following the derivation. This subtraction means that no stirrups are crossing the most critical shear path until $n > 1$.

2.4.2 Shear Evaluation Models with FRP Strengthening

The use of FRP sheets for shear strengthening of reinforced concrete beams has received less attention than the flexural strengthening application. Consequently, the first shear evaluation models with specific application to FRP sheets were published only a few years ago. For consistency with the truss approach used in current codes, the FRP sheet contribution was added to the Equation (2.4) to give:

[2.14] $$V_r = V_c + V_s + V_{FRP}$$

CHAALLAL *et al.* (1998)

Based on the FRP sheet capability to stay bonded to the face of the web and assuming vertical strips, CHAALLAL *et al.* (1998) proposed the following expression for the contribution of the FRP sheets in form of U-jacket:

[2.15] $$V_{FRP} = \tau_{ult} b_{FRP} d_{FRP} \frac{d}{s_{FRP}}$$

with

[2.16a] $$\tau_{ult} = \frac{5.4}{1 + k_1 \tan 33^\circ}$$

[2.16b] $$k_1 = t_{FRP} \left(\frac{3 E_a}{E_{FRP} t^3 t_a} \right)^{0.25}$$

where b_{FRP} is the width, d_{FRP} is the effective height, s_{FRP} is the spacing and t is the thickness of one FRP strip, E_a is the modulus of elasticity and t_a is the thickness of the adhesive (i.e. the epoxy in this case). When the FRP sheets are glued only on the side of the web, τ_{ult} in Equation (2.16a) is reduced by half.

KHALIFA *et al.* (1998)

The same year, KHALIFA *et al.* (1998), identified two possible failure modes: FRP sheet rupture and delamination from the concrete surface. The FRP shear contribution with vertical FRP sheets on both sides of the web takes the form:

[2.17] $$V_{FRP} = 2 t b_{FRP} R f_{ultFRP} \frac{d_{FRP}}{s_{FRP}}$$

where f_{ultFRP} is the ultimate strength in the principal direction of the fibres and R is a reduction factor which describe each potential failure mode.

The design approach based on the fracture of the FRP was first investigated by TRIANTAFILLOU (1998). A relationship between the effective FRP strain and the axial rigidity of the fibres was determined as follows:

[2.18a] $$\varepsilon_{eff} = 0.0119 - 0.0205(\rho_{FRP} E_{FRP}) + 0.0104(\rho_{FRP} E_{FRP})^2 \quad \text{for } 0 < \rho_{FRP} E_{FRP} < 1\text{GPa.}$$

[2.18b] $$\varepsilon_{eff} = 0.00245 - 0.00065(\rho_{FRP} E_{FRP}) \quad \text{for } \rho_{FRP} E_{FRP} > 1\text{GPa.}$$

with

[2.19] $$\rho_{FRP} = \left(\frac{2t}{b_w}\right)\left(\frac{b_{FRP}}{s_{FRP}}\right)$$

KHALIFA *et al.* (1998) then improved the model with additional data and proposed a polynomial equation for the FRP sheet rupture as follows:

[2.20] $$R = 0.778 - 1.2188(\rho_{FRP} E_{FRP}) + 0.5622(\rho_{FRP} E_{FRP})^2$$

The design governed by the delamination of the FRP sheet bonded to the concrete surface was described with the following equation:

[2.21] $$R = \frac{0.0042 \left(f'_c\right)^{2/3} w_{eff}}{\left(E_{FRP}\, t\right)^{0.58} \varepsilon_{ultFRP}\, d_{FRP}}$$

with

[2.22a] $$w_{eff} = d_{FRP} - k_e L_{eff}$$

and

[2.22b] $$\varepsilon_{ultFRP} = \frac{f_{ultFRP}}{E_{FRP}}$$

where k_e is an integer describing the number of debonding ends as shown in Figure (2.12).

Finally, the upper limit of the reduction factor was taken as 0.5, based on the concrete integrity by limiting the shear crack width. The governing value of R is then taken as the lowest result among the above three limits.

MALEK and SAADATMANESH (1998)

Also in 1998, MALEK and SAADATMANESH used the MCFT to evaluate the shear capacity of a reinforced concrete member strengthened with FRP. Based on equilibrium of the section and following the procedures developed by COLLINS and MITCHELL (1987), the method proceeds by steps with several iterations. By doing so, this method considers a variable concrete crack angle, but assumes a prefect bond between the concrete and the FRP sheets. The principal steps of the method are reported below:

1. Assume the shear load, V, and the angle, θ.
2. Calculate the axial force ΔN developed in the longitudinal reinforcement.

[2.23] $$\Delta N = \frac{V}{\tan\theta}$$

3. Calculate the corresponding longitudinal axial strain, ε_{long}, neglecting the effect of the FRP sheets with respect to the longitudinal reinforcement.

[2.24] $$\varepsilon_{long} = \frac{\Delta N}{A_s E} \leq \frac{f_y}{E}$$

4. Compute the compressive stress in the concrete strut.

[2.25] $$f_2 = \frac{V}{b_w d_v \sin\theta\cos\theta}$$

5. Assume ε_1 and compute the maximum compressive stress f_{2max}.

[2.26] $$f_{2max} = \frac{f_c'}{0.8-0.34\dfrac{\varepsilon_1}{\varepsilon_{cu}}} \leq f_c'$$

6. Calculate the compression strain in the concrete strut.

[2.27] $$\varepsilon_2 = \varepsilon_{cu}\left(1-\sqrt{1-\frac{f_2}{f_{2max}}}\right)$$

where ε_{cu} is the compressive uniaxial strain corresponding to f_c'.

7. Knowing ε_{long} and ε_2, ε_l and ε_t are obtained using the transformation equations and Mohr's circle.

[2.28a] $$\varepsilon_l = \frac{\varepsilon_{long}\left(1+\tan^2\theta\right)-\varepsilon_2}{\tan^2\theta}$$

[2.28b] $$\varepsilon_t = \varepsilon_l\left(1+\tan^2\theta\right)+\varepsilon_{long}\tan^2\theta$$

8. The assumption on ε_l is then checked.
9. Once ε_l is verified, the total shear force resisted by the beam is then determined.

[2.29] $$V_i = F_{FRP} + F_s$$

with

[2.30a] $$F_s = E\varepsilon_t A_v \frac{d_v}{s\tan\theta} \leq f_{vy} A_v \frac{d_v}{s\tan\theta}$$

and

[2.30b] $$F_{FRP} = 2d_{FRP}\, t\left(\sigma_{12} + \frac{\sigma_{11}}{\tan\theta}\right)$$

where σ_{12} and σ_{11} are the shear and normal stresses of the FRP sheet along the crack in the direction 1 and 2. The laminate theory is used to transform the FRP sheet stiffness from the axis *long* and *t* to the axis 1 and 2.

Step 1 through 9 are repeated until the assumed shear load V and V_i converge for a given angle θ. The inclination angle θ corresponding to the maximum shear load is the governing angle.

The authors acknowledge that the contribution of the aggregate and the concrete in compression zone are not considered here. Therefore, once the governing angle θ is found, the concrete contribution V_c can be determined with the equation (2.7) and the appropriate value of β. The total shear capacity of the beam then becomes

[2.31] $$V_r = V_i + V_c$$

CSA-S806

The Canadian Standard Association (CSA-S806, 2000) is currently preparing a new design standard for the construction and rehabilitation of structures with FRP. The shear design section uses the truss model, with an assumed 45° concrete crack angle. The FRP shear contribution, with vertical sheets on both sides of the beam web, is simplified to

[2.32] $$V_{FRP} = \frac{2\,t\,b_{FRP}E_{FRP}\varepsilon_{eff}\,d_{FRP}}{s_{FRP}}$$

where the value of the effective FRP strain, ε_{eff}, is taken as 0.004 (or 4000$\mu\varepsilon$).

2.5 Conclusion

The latest advancements in reinforced concrete shear strengthening for existing structures were revisited. In this process, the current shear design codes and the FRP shear design models available in the literature were summarized. From this survey, the lack of test data on FRP shear strengthening with realistic beam depth specimens was continuously mentioned. Reliable experimental data on laboratory, using controlled, full-scale tests, are required to address this concern. A better understanding of the interaction between the concrete, the stirrups and the FRP sheets used in combination to carry shear loads in reinforced concrete beams is also needed. The results of this investigation will provide a rigorous database to evaluate the current design methods and the proposed FRP shear models. From this analysis, a simplified, but general FRP shear design formulation, including the effects of the FRP, will be developed and proposed.

Table 2.1 Mechanical Properties of Typical Materials (KAW, 1997)

Material	Density	Young's Modulus GPa	Ultimate Tensile Strength MPa
Graphite	1.8	230.0	2067
Aramid	1.4	124.0	1379
Glass	2.5	85.0	1550
Unidirectional graphite/epoxy	1.6	181.0	1500
Unidirectional glass/epoxy	1.8	38.6	1062
Cross-ply graphite/epoxy	1.6	96.0	373
Cross-ply glass/epoxy	1.8	23.6	88
Quasi-isotropic graphite/epoxy	1.6	69.6	276
Quasi-isotropic glass./epoxy	1.8	19.0	73
Steel	7.8	203.0	500
Aluminium	2.6	69.0	276
Epoxy	1.2	3.0	80

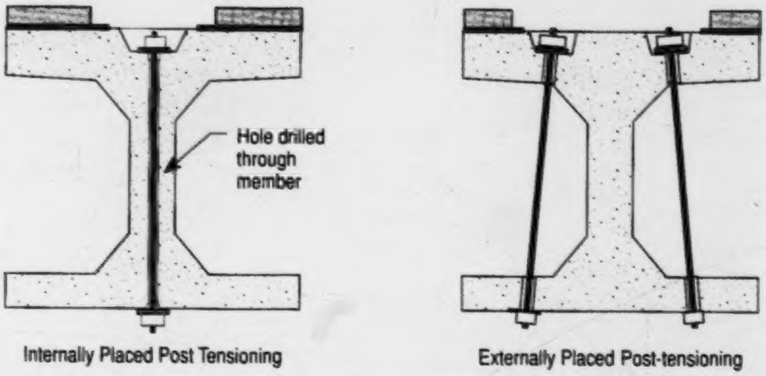
Hole drilled through member
Internally Placed Post Tensioning
Externally Placed Post-tensioning

Figure 2.1 Internal and External Post-Tensioning (Emmons, 1993)

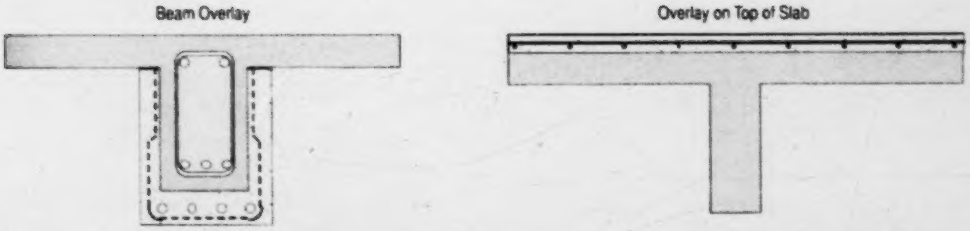
Beam Overlay
Overlay on Top of Slab

Figure 2.2 Beam and Slab Overlay (Emmons, 1993)

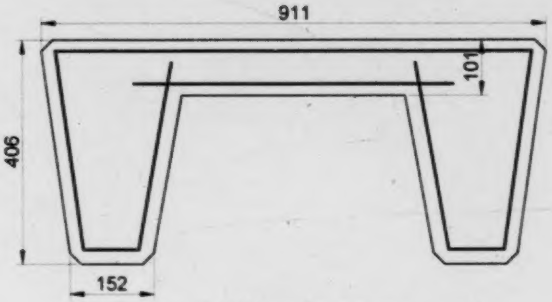
911
101
406
152

(a) Type G-girder

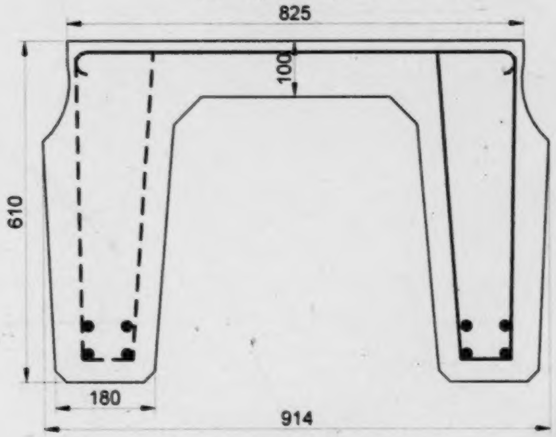
825
100
610
180
914

(b) Type E-girder

Figure 2.3 Bridge Girders in Alberta

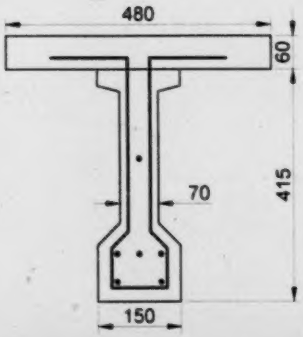
480
60
70
415
150

Figure 2.4 Prestressed I-Shaped Beams with Bent-Legged Stirrup Tested in Manitoba (HUTCHINSON, 1999)

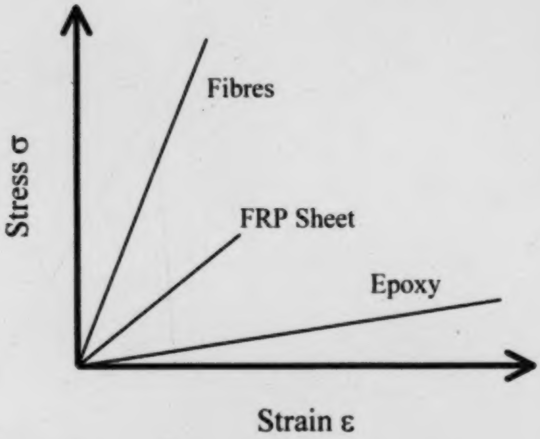

Figure 2.5 Typical Stress Strain Relationship for FRP

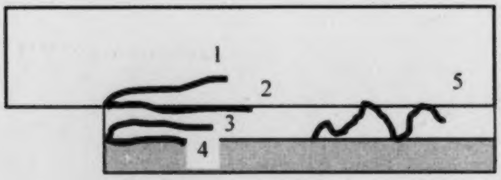

1: Peel failure into concrete
2: Interfacial failure between concrete and adhesive
3: Cohesive failure in the adhesive
4: Interfacial crack between the adhesive and the composite
5: Alternating crack path between the two interfaces

Figure 2.6 Potential Crack Paths (KARBHARI, 1995)

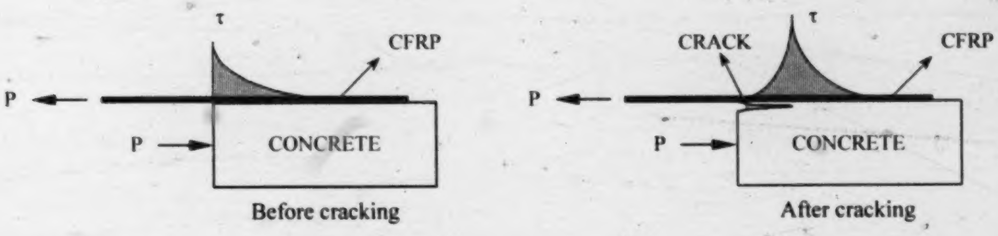
τ
CFRP
P
P
CONCRETE
Before cracking
CRACK
τ
CFRP
P
P
CONCRETE
After cracking

Figure 2.7 Shear Stress Distribution before and After Cracking (BROSENS and VAN GEMERT, 1997)

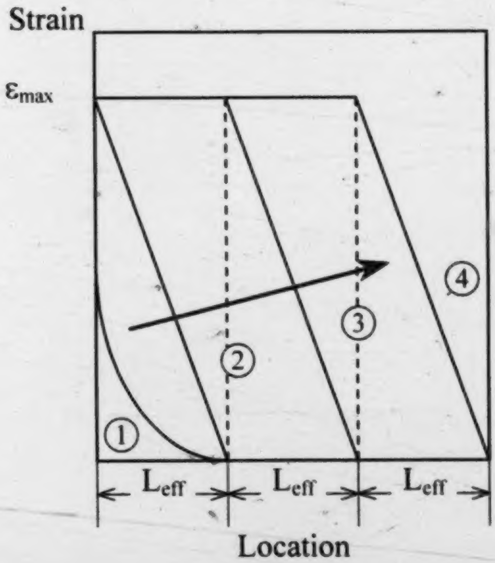
Strain
ε_{max}
①
②
③
④
L_{eff}
L_{eff}
L_{eff}
Location

Figure 2.8 Schematic Strain Distribution (MAEDA *et al.*, 1997)

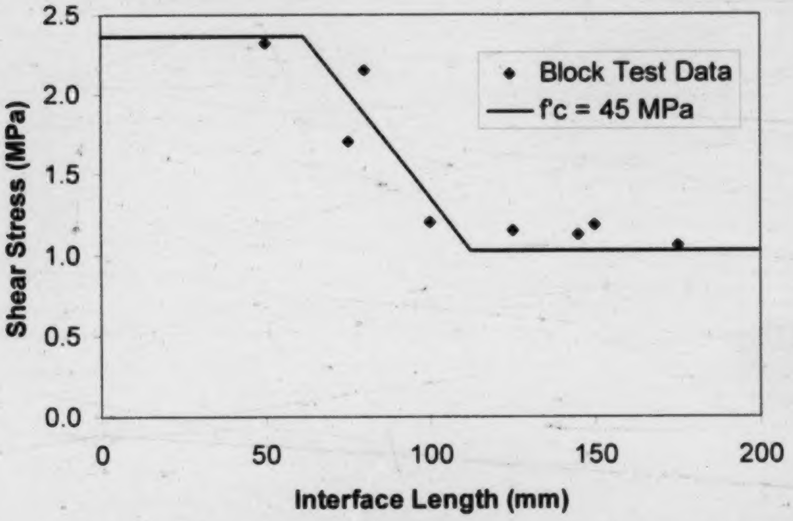

Figure 2.9 Tri-linear Bond Strength Curve (ALEXANDER and CHENG, 1997)

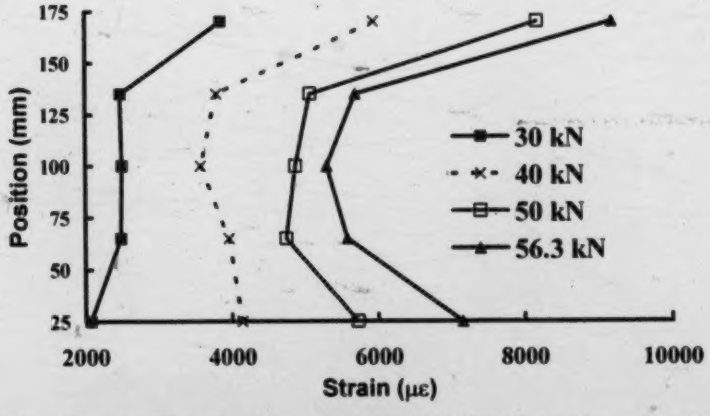

Figure 2.10 FRP Strain Distribution across the Width at the Crack (KAMEL *et al.*, 2000)

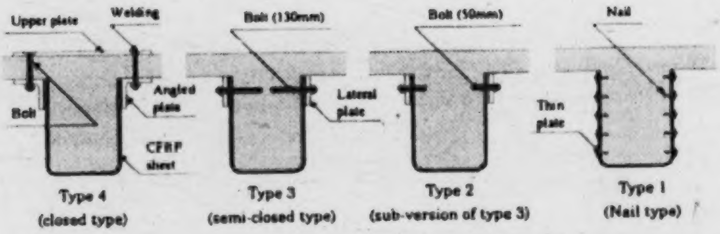
Upper plate
Welding
Angled plate
Bolt
CFRP sheet
Type 4
(closed type)
Bolt (130mm)
Lateral plate
Type 3
(semi-closed type)
Bolt (50mm)
Type 2
(sub-version of type 3)
Nail
Thin plate
Type 1
(Nail type)

Figure 2.11 Various Anchoring Methods of FRP Sheets (SATO *et al.*, 1997)

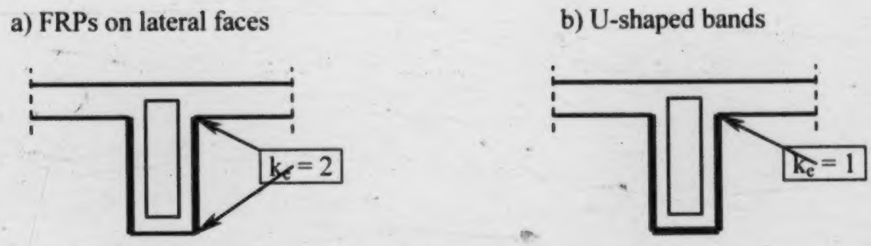
a) FRPs on lateral faces

b) U-shaped bands

Figure 2.12 FRP Sheet End Conditions

2.6 References

ACI-318 (1998). *Building Code Requirements for Structural Concrete*, American Concrete Institute, Detroit, MI, 369 p.

ADEY B., SAN-ROMÁN J. D. C., and BRÜHWILLER E. (1998). "Carbon Fibre Shear Strengthening of Rectangular Concrete Beams", *Final Report - 97.02*, École Polythechnique de Lausanne, Lausanne, Switzerland, 28 pp.

ALEXANDER, J., and CHENG, J.J.R. (1997). *Shear Rehabilitation of G-Girder Bridges using CFRP Sheets*, Structural Engineering Report No 218, Department of Civil and Environmental Engineering, University of Alberta, Edmonton, AB, 181 p.

AL-SULAIMANI G.J., ISTEM A., BASUNBUL A.S., BALUCH M.H., and GHALEB B.N. (1994). "Shear Repair for Reinforced Concrete by Fiberglass Plate Bonding", *American Concrete Institute Structural Journal*, Vol. 91, No. 3, July-August, pp. 458-464.

ASCE-ACI COMMITTEE 426 (1973). "The Shear Strength of Reinforced Concrete Members", *Journal of Structural Engineering*, ASCE, Vol. 99, No. ST6, June, pp. 1091-1187.

ASCE-ACI COMMITTEE 445 (1998). "Recent Approaches to Shear Design of Structural Concrete", *Journal of Structural Engineering*, ASCE, Vol. 124, No. 12, December, pp. 1375-1417.

BANTHIA N., YAN C., and NANDAKUMAR N. (1996). "Sprayed Fiber Reinforced Plastics (FRPs) for Repair of Concrete Structures", *Proceedings of Advanced Composite Materials in Bridges and Structures (ACMBS-2)*, CSCE, Montréal, Québec, pp. 537-545.

BENMOKRANE B. and RAHMAN H., Editors (1998). *Durability of Fibre Reinforced Polymer (FRP) Composites for Construction*, Department of Civil Engineering, Université de Sherbrooke, Sherbrooke, Qué.

BIZINDAVYI L., and NEALE K.W. (1999). "Transfer Lengths and Bond Strengths for Composites Bonded to Concrete", *Journal of Composites for Construction*, ASCE, Vol. 3, No. 4, November, pp. 153-160.

BEAUDOIN Y., LABOSSIÈRE P. and NEALE K.W. (1998). "Wet-Dry Action on the Bond between Composite materials and Reinforced Concrete Beams", *Proceedings of*

Durability of Fibre Reinforced Polymer Composites for Construction, Sherbrooke, Qué, pp. 537-546.

BROSENS K. and VAN DEMERT D. (1997). "Anchoring Stresses between Concrete and Carbon Fibre Reinforced Laminates", *Proceedings of the Non-Metallic (FRP) Reinforcement for Concrete Structures (3rd International Symposium)*, Sapporo, Japan, pp. 271-278.

CHAALLAL O., NOLLET M.-J., and PERRATON D. (1998). "Strengthening of Reinforced Concrete Beams with Externally Bonded Fiber-Reinforced-Plastic Plates: Design Guidelines for Shear and Flexure", *Canadian Journal of Civil Engineering*, Vol. 25, No. 4, August, pp. 692-704.

CHAJES M.J., JANUSZKA T.F., MERTZ D.R., THOMSON T.A., and FINCH W.W. (1995). "Shear Strengthening of Reinforced Concrete Beams using Externally Applied Composite Fabrics", *American Concrete Institute Structural Journal*, Vol. 92, No 3, May-June, pp. 295-303.

CHAJES M.J., FINCH W.W., JANUSZKA T.F., and THOMSON T.A. (1996). "Bond and Force Transfer of Composite Material Plates Bonded to Concrete", *American Concrete Institute Structural Journal*, Vol. 93, No. 2, March-April, pp. 208-217.

COLLINS M.P. (1978). "Toward a Rational Theory for RC Members in Shear", *Journal of Structural Engineering*, ASCE, Vol. 104, No. ST4, April, pp. 649-666.

COLLINS M.P., and MITCHELL D. (1987). *Prestressed Concrete Basics*, 1st Edition, Canadian Prestressed Concrete Institute, Ottawa, ON, 614 p.

CSA-A23.3 (1994). *Design of Concrete Structures*, Canadian Standard Association, Rexdale, ON.

CSA-S6 (1988). *Design of Highway Bridges*, Canadian Standard Association, Rexdale, ON.

CSA-S806 (2000). *Design and Construction of Building Components with Fiber Reinforced Polymers*, Draft, Canadian Standard Association, Rexdale, ON.

DOREY A. and CHENG J.J.R. (1996) *Glass Fiber Reinforced Glued Laminated Wood Beams*, Canadian Forest Service, Edmonton, AB, 88 p.

DRIMOUSSIS E.H. and CHENG J.J.R. (1994). *Shear Strengthening of Concrete Girders using Carbon Fiber Reinforced Plastic Sheets*, Structural Engineering Report No 205, University of Alberta, Edmonton, AB, 177 p.

EMMONS P. (1993). *Concrete Repair and Maintenance Illustrated*, R.S. Means Company, Kingston, MA, 295 p.

FERRIER E., NASSERI H. and HAMELIN P. (1999) "Fatigue Behavior of Composite Reinforcement for Concrete Structures", *Proceedings of Fiber Reinforced Polymer Reinforcement for Reinforced Concrete Structures (4th International Symposium)*, ACI-SP188, Baltimore, MD, pp. 535-545.

HEAD P.R. (1996) " Advanced Composites in Civil Engineering – A Critical Overview at this High Interest, Low Use Stage of Development", *Proceedings of Advanced Composite Materials in Bridges and Structures (ACMBS-2)*, CSCE, Montréal, Québec, pp. 3-16.

HUTCHINSON R., ABDELRAHMAN A., RIZKALLA S. and SMITH G. (1997). "Shear Strengthening using FRP Sheets for a Highway Bridge in Manitoba, Canada", *Proceedings of the Non-Metallic (FRP) Reinforcement for Concrete Structures (3rd International Symposium)*, Sapporo, Japan, pp. 531-538.

KAMEL A.S., ELWI A.E., and CHENG J.J.R. (2000). "Experimental Study on the Behavior of CFRP Sheets Bonded to Concrete", *Proceedings of the Advanced Composite Materials for Bridges and Structures (ACMBS-3)*, CSCE, Ottawa, ON, pp. 61-68.

KARBHARI V.M. (1995). "Characteristics of Adhesion between Composites and Concrete as Related to Infrastructure Rehabilitation", *Proceedings of the 27th International SAMPE Technical Conference*, SAMPE, Albuquerque, NM, pp. 1083-1094.

KARBHARI V.M. and ENGINEER M. (1996). "Effect of Environmental Exposure on the External Strengthening of Concrete with Composites – Short Term Bond Durability", *Journal of reinforced Plastics and Composites*, Vol. 15, December, pp. 1194-1216.

KAW A.K. (1997) *Mechanics of Composite Materials*, CRC Press, Boca Raton, FL, 329 p.

KENNEDY G.D. and CHENG J.J.R. (1998) *Repair of Cracked Steel Elements using Composite Fibre Patching*, Structural Engineering Report No 221, University of Alberta, Edmonton, AB, 173 p.

KHALIFA A., GOLD W.J., NANNI A., and AZIZ M.I. (1998). "Contribution of Externally Bonded FRP to Shear Capacity of RC Flexural Members", *Journal of Composites for Construction*, Vol. 2, No. 4, November, pp. 195-202.

KUZIK M., ELWI A.E.E. and CHENG J.J.R. (1999). *Cyclic Behaviour of Masonry Walls with FRP*, Structural Engineering Report No 228, University of Alberta, Edmonton, AB, 116 p.

LOOV R. (1998). "Review of A23.3-94 Simplified Method of Shear Design and Comparison with Results using Shear Friction", *Canadian Journal of Civil Engineering*, Vol. 25, No. 3, April, pp. 437-450.

LOOV R. and PENG L. (1998). "The Influence of Concrete Strength on Shear Friction Based Design of Reinforced Concrete Beams", *Proceedings of the International Conference on HPHSC*, Perth, Australia, pp. 505-519.

MAEDA T., ASANO Y., SATO Y., UEDA T., and KAKUTA Y. (1997). "A Study on Bond Mechanism of Carbon Fiber Sheet", *Proceedings of the Non-Metallic (FRP) Reinforcement for Concrete Structures (3rd International Symposium)*, Sapporo, Japan, pp. 279-286.

MALEK A.M., and SAADATMANESH H. (1998). "Analytical Study of Reinforced Concrete Beams Strengthened with Web-Bonded Fiber Reinforced Plastic Plates or Fabrics", *American Concrete Institute Structural Journal*, Vol. 95, No. 3, May-June, pp. 343-352.

NEALE, K. (2000). "FRPs for Structural Rehabilitation: A Survey of Recent Progress", Progress in Structural Engineering and Materials (in press).

RAHAL K.N. and COLLINS M.P. (1999) "Background to the General Method of Shear Design in the 1994 CSA-A23.3 Standard", *Canadian Journal of Civil Engineering*, Vol. 26, No. 6, December, pp. 827-839.

RAÎCHE A., BEAUDOIN Y. and LABOSSIÈRE P. (1999). "Durability of Composite Materials used as External Reinforcement for RC Beams", *Proceedings of the Annual Conference of the CSCE*, CSCE, Regina, pp. 155-164.

ROWLANDS R.E., VAN DEWEGHE R.P., LAUFENBERG T.L. and KRUEGER G.P. (1986) "Fiber Reinforced Wood Composites", *Wood and Fiber Science*, Vol. 18, No. 1, pp. 39-57.

RICHIE P.A., THOMAS D.A., LU L.-W., and CONNELLY G.M. (1991). "External Reinforcement of Concrete Beams using Fiber Reinforced Plastics", *American Concrete Institute Structural Journal*, Vol. 88, No. 4, July-August, pp. 490-500.

SAADATMANESH H. and EHSANI M.R. (1991). "RC beams Strengthend with GFRP Plates I: Experimental Study", *Journal of Structural Engineering*, ASCE, Vol. 117, No. 11, November, pp. 3417-3433.

SATO Y., UEDA T., KAKUTA Y., and TANAKA T. (1996). "Shear Reinforcing Effect of Carbon Fiber Sheet Attached to Side of Reinforced Concrete Beams", *Proceedings of Advanced Composite Materials in Bridges and Structures (ACMBS-3)*, CSCE, Montréal, Québec, pp. 621-628.

SATO Y., KATSUMATA H., and KOBATAKE Y. (1997a). "Shear Strengthening of Existing Reinforced Concrete Beams by CFRP Sheet", *Proceedings of the Non-Metallic (FRP) Reinforcement for Concrete Structures (3rd International Symposium)*, Sapporo, Japan, pp. 507-514.

SATO Y., UEDA T., KAKUTA Y., and ONO S. (1997b). "Ultimate Shear Capacity of Reinforced Concrete Beams with Carbon Fiber Sheet", *Proceedings of the Non-Metallic (FRP) Reinforcement for Concrete Structures (3rd International Symposium)*, Sapporo, Japan, pp. 499-506.

SEIBLE F. (1996) "Advanced Composite Materials for Bridges in the 21st Century", *Proceedings of Advanced Composite Materials in Bridges and Structures (ACMBS-2)*, CSCE, Montréal, Québec, pp. 17-30.

SWANSON S.R. (1997). *Introduction to Design and Analysis with Advanced Composite Materials*, Prentice Hall, Upper Saddle River, NJ, 249 p.

TRIANTAFILLOU T.C. (1998). "Shear Strengthening of Reinforced Concrete Beams using Epoxy-Bonded FRP Composites", *American Concrete Institute Structural Journal*, Vol. 95, No. 2, March-April, pp. 107-115.

UEDA T., SATO Y. and ASANO Y. (1999). "Experimental Study on Bond Strength of Continuous Carbon Fiber Sheet", *Proceedings of Fiber Reinforced Polymer*

Reinforcement for Reinforced Concrete Structures (4th International Symposium), ACI-SP188, Baltimore, MD, pp. 407-416.

UJI K. (1992). "Improving Shear Capacity of Existing Reinforced Concrete Members by Applying Carbon Fiber Sheets", *Transaction of the Japan Concrete Institute*, Vol. 14, pp. 254-266.

UOMOTA T. and NISHIMURA T. (1999). "Deterioration of Aramid, Glass, and Carbon Fibers Due to Alkali, Acid, and Water in Different Temperatures", *Proceedings of Fiber Reinforced Polymer Reinforcement for Reinforced Concrete Structures (4th International Symposium)*, ACI-SP188, Baltimore, MD, pp. 515-522.

VECCHIO F.J. and COLLINS M.P. (1986). "The Modified Compression Field Theory for Reinforced Concrete Elements Subjected to Shear", *American Concrete Institute Structural Journal*, Vol. 83, No. 2, March-April, pp. 219-231.

XANTHAKOS P. (1996). *Bridge Strengthening and Rehabilitation*, Prentice Hall, upper Saddle River, NJ, 966 p.

3 SHEAR REHABILITATION OF G-GIRDER BRIDGES IN ALBERTA USING FRP SHEETS[1]

3.1 Introduction

The Type G-girders shown in Figure 3.1 have been used extensively in Alberta for short span highway bridges constructed in the 1950's and 60's. Today, approximately 1500 of these bridges are still in service across the province. The bridges are typically simply supported with no shear keys between the girders. The G-girders were found to be deficient in shear based on current code requirements and evaluation specifications (CSA S6, 1988). This deficiency is due mainly to an increase in allowable truck loads over the last 40 years, as well as a better understanding of shear behaviour in reinforced concrete members since the early 1970's. Overall, the design shear requirement has increased by 40% and the applied loads have also increased by about 45% over the last 40 years. The combination of these two effects, plus the aging of the bridges, results in the shear deficiency problems for type G-girder bridges. Finding a reliable and economical technique to rehabilitate and strengthen these girders is a major concern for Alberta Infrastructure. A research program to assess these needs is carried out at the University of Alberta in collaboration with Alberta Infrastructure and ISIS Canada. A series of full-scale tests were conducted using G-girders removed from existing bridges.

A preliminary investigation of type G-girders conducted at the University of Alberta in 1997 (ALEXANDER and CHENG) indicated that type G-girders must be loaded eccentrically about the centroid of the cross section in order to fail the girders in a combination of shear and torsion. ALEXANDER and CHENG (1997) also showed that the end panel is the weakest part of the girder under eccentric loading. Special considerations are therefore required to reinforce not only the inner faces of the legs, but also the end diaphragm.

The objective of the current series of tests is to establish a comparison between the use of glass and carbon Fibre Reinforced Polymers (FRP) sheets with various sheet configurations, as a shear repair technique. The end diaphragm was also reinforced using composite sheets. A 9.5 mm thick steel plate was bonded along the bottom faces of the girders to avoid flexural failure.

---

[1] A version of this chapter has been accepted for publication in the October 2000 special issue of the *Canadian Journal of Civil Engineering*.

The following three commonly used shear strength evaluation methods were also investigated: a) the Strut-and-Tie model, b) the Modified Compression Field Theory (MCFT), and c) the grid analysis. The shear capacity predicted using these methods were compared to the experimental results.

3.2 Experimental Program

3.2.1 Test Specimens

A total of eight tests were conducted on four G-girders. Each end of the 6.1 m long girders was tested separately with a different shear strengthening detail, as shown in Table 3.1. Three of the four girders have round end diaphragms and one has square end panels, as shown in Figure 3.1.

Prior to application of the steel plates and composite sheets, the concrete surface of the specimens was prepared using a grinder to remove any bumps. The steel plates were sand blasted and then glued to the underside of each leg using *Sikadur 31 Hi Mod* epoxy provided by Sika Inc. In order to avoid sharp corners, putty was used to round the corners of the girders. Figure 3.2 shows a typical surface preparation of the end diaphragm. FRP sheets were then applied on the inner face of the girders. Additional photos of the specimen preparation can be found in Appendix A.1. One end of the sheet was extended underneath the flange and the other end extended on top of the steel plate or the end panel, as shown in Figure 3.3. At least 100 mm development length was provided for the FRP sheets.

The two types of uniaxial FRP sheets used were carbon fibre - *Replark Type 20* from Mitsubishi Canada Ltd. and glass fibre - SEH51 from Fyfe LLC Ltd. The two repair configurations used were 250 mm wide vertical sheets and 250 mm wide diagonal sheets at 45°. A 50 mm spacing between sheets was used in all the specimens. The round end panels were strengthened using 50 mm wide bands applied vertically while the square end panel (*G4 West*) was strengthened with horizontal carbon sheets. Table 3.1 provides a full description of the various specimen parameters. Both repair schemes are presented in Figure 3.4.

3.2.2 Test Set-up and Instrumentation

In order to provide an eccentric loading, a stiff steel beam was used to distribute the load from the MTS 6000 testing machine to the top of one leg of the girder, as shown in Figure 3.5. The load applied to the top of the girder was computed using four load cells located at each support or by subtracting the steel beam support reaction from the MTS 6000 load. The terminology used in the testing program, *Close*, *Far*, *Unloaded* and *Loaded*, is described in Figure 3.5.

The side of each leg of the girders was instrumented with several sets of Demec gauges while electrical strain gauges were applied on the steel plate. Eight cable displacement transducers were used to record vertical deflections along each leg and four Linear Variable Differential Transducers (LVDTs) were installed at two stirrup locations of interest. An additional LVDT was used to record the *Far Unloaded* support which was lifting up during each test.

After the first end of each girder was tested, the girder was repaired with external stirrups prior to testing the second end. The external stirrups consisted of two HSS steel tubes with tie rods on both ends.

3.3 Experimental Results

3.3.1 Material Properties

Coupon tests were carried out in accordance with ASTM Standard A-370 (1996) to determine the material properties of the steel components of each girder including the steel plate used as external reinforcement, the 28.6 mm diameter longitudinal reinforcing bars, and the 9.5 mm diameter stirrup bars. Table 3.2 gives the steel coupon test results.

For each type of FRP used, coupon specimens were made at the same time as the bands were being bonded to the girders. Material properties for the two composites are given in Table 3.3. It should be noted that premature failure was observed for the glass fibre coupons.

The concrete strength was determined from 100 mm diameter cores drilled from each girder, in accordance with the ASTM STANDARD C-42 (1994). Three cores were taken in each girder at three different locations. Core specimens were soaked for at least 48 hours prior to testing. Correction factors developed by BARTLETT and MACGREGOR (1994) were used to find the equivalent in situ strength presented in Table 3.4.

3.3.2 Girder Tests

The girder test results are summerized in Table 3.4. Figure 3.6 shows the Load vs. Deflection curves at the location of the point load for all tests with round end diaphragms, while the results of the two tests with square end diaphragms are presented in Figure 3.7.

General Behaviour

When the girders were eccentrically loaded over one leg, as described in Figure 3.5, about 70 to 75% of the total load was carried by the *Close Loaded* support reaction and 20 to 25% went to the *Far Loaded* support. The remainder of the load, no more than 7%, was carried by the *Close Unloaded* support. The *Far Unloaded* support was lifting up in all cases. From the observations, the load-sharing path was not significantly affected by the external steel plate or FRP strengthening. Furthermore, the loaded leg carried the majority of the shear load.

Failure Mode

The failure mode observed in all of the tests, except *Girder 2 East* and *Girder 3 West*, was shear cracks in the end diaphragm induced by the torsion applied in the end panel. Testing of *Girder 2 East* was terminated prematurely and Girder 3 West failed in shear in the *Loaded* leg with no crack in the end panel. The test results for *Girder 3 West* are the most promising for shear rehabilitation of this type of girder, as explained in the following sections. All of the test results showed that the FRP sheets helped to hold flexural reinforcement in place. This technique proved to be very efficient in avoiding premature failure due to steel plate debonding. No debonding of the steel plate was observed when composite materials were used.

End Panels Cracks - For the control test with the steel plate (*Girder 1 East*), the crack in the end panel was inclined at about 60 to 70 degrees from the soffit of the diaphragm. The 50 mm wide sheets applied vertically at the end panel prevented any horizontal cracks. The crack path in the diaphragm then became vertical because it was now the weakest orientation. This behaviour was clearly observed in *Girder 2 West*. *Girder 3 East* exhibited similar behaviour but the crack in the end panel was initiated by the peeling-off of an FRP band underneath the diaphragm.

For *Girder 3 West*, peeling did not occur since the woven glass fabric used had fibres at both 0° and 90°, with a ratio of 80 and 20%, respectively. This material was stronger perpendicular to the main fibre orientation when compared to the uniaxial carbon fibre. Although only 50 mm wide bands were used, horizontal tension could still be mobilized in this product and partially explains why the end panel did not fail in this case. Unfortunately, no strain in the horizontal direction was measured to confirm this hypothesis.

For the square end panel specimen, *Girder 4 West*, the carbon sheets were applied horizontally in the end panel. Therefore, the crack, which was running vertically along the *Close Unloaded* corner, was bridged by FRP. Although vertical cracks could still develop because of the sharp corner, the horizontal fibres were extremely effective. Twisting of the fibres can be seen in Figure 3.8. In this case, the horizontal sheets were long enough to provide sufficient anchorage and avoid peeling off.

Shear Span Cracks - Two major inclined cracks were typically observed in each shear span. The first one was initiated at the support location and the second one started to open up about 500 mm away from the support sloping toward the load point. These cracks were initially oriented at about 45 degrees. However, the ultimate crack orientation decreased to approximately 30 degrees.

The steel plate alone did not affect the inclination and initiation of the end panel cracks. However, the failure crack was closer to the beam without FRP, when compared to the failure crack of a girder strengthened by composites. For the later case, the failure crack was initiated at the leg-to-end panel joint, then widened and propagated toward the point load. The failure crack was therefore shifted away from the support face when the FRP was used, as shown in Figure 3.9 (see Appendix A.2 for the other girder shear crack patterns).

Maximum Load

The overall comparison of the total load applied on the girders is presented in Table 3.4. The results show that the external steel plate increases the capacity of the girder by 35%. This large increase is due to the significant stiffness the plate adds to the bottom of the legs. Deflection of the legs is reduced and the plate acts to hold the concrete in place, thereby allowing greater shear transfer to occur.

The effect of FRP, determined by superposition, was found to be equal to 5 and 12% for the vertical and inclined glass sheets, respectively. It should be noted that, although the total load for *Girder 2 East* increased by only 24%, the test was stopped prematurely. With the square end panel, and assuming the same percentage contribution from the external steel plate, the presence of carbon sheets increased the applied load by 17%. Although the difference in load increase between girders with inclined and vertical sheets is not large, the repair scheme using inclined sheets improved the performance, as shown in Figures 3.6 and 3.7. This phenomenon can be attributed to the absence of cracking in the gap between the sheets when the fibres are inclined and the presence of vertical cracks between vertical sheets observed during the test.

Strains in FRP and Steel Plates

Flexural capacity was not an issue when steel reinforcing plate was used since the steel plate did not yield in any of the tests. The strain values recorded in the FRP sheets for each test were relatively small compared to the maximum deformation that these materials can sustain. The maximum strain recorded was 0.18%, while the maximum elongation for FRP sheets typically exceeds 1%.

The measured strains for the inclined sheets were similar in magnitude in both legs. However, for the vertical sheets, the sheet on the loaded leg sustained twice the strains measured in the sheet on the unloaded leg. Therefore, it appears that the inclined repair scheme distributes the stress and strain more evenly to both legs. Torsion in the end panel is therefore reduced because the angle of rotation is reduced between the two legs.

3.4 Test Specimen Models

Three commonly used shear design methods: the Strut-and-Tie, MCFT, and grid analysis, were used to evaluate the shear capacity of the tested specimens. The development of the test specimen models using these three methods and the discussion of predicted behaviour and strength are summerized below, along with the test results.

3.4.1 General Assumptions

In all cases, the shear force was assumed to be carried by the loaded leg only, due to the combination of the applied bending and torsion forces as observed by the reactions in both *Unloaded* and *Loaded* legs. The bending moments were shared between the two legs. The bending contribution of the unloaded leg varied from test to test and decreased with the loading level. Therefore, the L/U (*Loaded/Unloaded*) ratio from the experimental results at ultimate was used and is reported in Table 3.5. No FRP strain measurements were recorded at the ultimate. Since FRP behaves linearly when stressed, a linear extrapolation was used from the last two Demec readings to evaluate the maximum FRP strains at the ultimate load, as listed in Table 3.5.

3.4.2 Strut-and-Tie Model

The loaded leg of the specimen was modeled as shown in Figure 3.10. Vertical ties were placed at the stirrup locations. A longitudinal bent bar was also introduced into the model. The 300 mm lever arm between the bottom tie and the top chord was used in all cases.

The effect of load sharing in flexure was accounted for by increasing the area of the bottom steel tie according to the L/U ratio given in Table 3.5. It was also assumed that the concrete stresses in any strut were not critical. The truss was loaded until the first tie reached its elastic limit based on the material properties of the steel. The yielded tie was then removed and a new strut-and-tie model was created. This process was repeated until the truss model collapsed due to yielding of all of the ties. The total applied load was the summation of all the load increments for each mechanism. The effect of the composite sheets was included by increasing the load level required to yield the vertical ties. The increased load level was determined as

$$P_y = A_v f_{vy} + \varepsilon_y E_{FRP} t s \qquad [3.1]$$

where A_v is the area, f_{vy} is the yield strength, s is the spacing, ε_y is the yield strain of the stirrups, and E_{FRP} is the elastic tensile modulus and t is the thickness of the sheets. The second term of the Equation (3.1) represents the FRP contribution to one stirrup tributary area and the FRP strain is limited to the yield of steel. Equation (3.1) is applied to the case when the fibres are parallel to the stirrups.

3.4.3 Modified Compression Field Theory (MCFT)

This variable angle truss method was developed by COLLINS and MITCHELL (1987) and is the basis of the general method described in CSA-A23.3 (1994). A computer program was created to include the contribution of the FRP sheets. The procedure requires iteration to converge to an appropriate solution. The solution technique is described briefly below. The detailed solution steps are presented in Appendix A.4. Detailed information on the method can be found in COLLINS and MITCHELL (1987).

The method starts with estimation of the inclination angle, θ, the stirrup stress, f_v, the FRP sheet stress, σ_{FRP}, and a chosen value for the principal tensile strain, ε_1. The shear load is then calculated including the contribution of the FRP sheets as

[3.2] $$V = v_s d_v b_w + v d_v b_w + v_{FRP} d_{FRP} b_w$$

where

[3.3a] $$v_s = \frac{A_v\ f_v}{b_w\ s\ \tan\theta}$$

[3.3b] $$v = \frac{f_1}{\tan\theta}$$

[3.3c] $$v_{FRP} = \frac{A_{FRP}\ \sigma_{FRP}}{b_w\ s_{FRP}}\left(\frac{\sin^2\alpha}{\tan\theta} + \sin\alpha\cos\alpha\right)$$

d_v and d_{FRP} are the effective shear depth and the height of the FRP sheets, respectively; b_w is the width of the web; A_{FRP} and s_{FRP} are the FRP sheet area and bands spacing, respectively; and α is the angle of the fibres with respect to the longitudinal axis of the section. Once the compression stress f_2 is found to be lesser than f_{2max}, the principal strain ε_2 is computed. The longitudinal strain ε_{long}, vertical strain ε_t and composite strain ε_{FRP} are found by strain transformation. The stirrup stress, f_v, and the FRP stress, σ_{FRP}, are determined from the calculated strains. Iteration continues until these stresses agree with the initial estimated values. Finally, a plane section analysis, with the strain at d set to ε_{long}, is performed to check the equilibrium of the axial load on the member.

This procedure is repeated for a specific moment by increasing ε_1 until the shear load drops, the fibres fail, or the concrete strut crushes. By repeating this procedure for different moments, the complete shear moment interaction diagram can be developed.

For this study, the maximum shear load was computed for the specified V/M ratio (which is a function of the L/U ratio) of each test (Table 3.5).

3.4.4 Grid Analysis

In this approach, the girder was modeled using beam elements. Two longitudinal beams spaced 660 mm apart represented the two legs, while two and seven transverse beams were used for the end panel and flange elements, respectively. The spacing between two consecutive transverse beams was 750 mm except for the first transverse element close to each end panel element where 660 mm spacing was used.

Material and Section Properties

The material properties of the girder were computed from the experimental data. The weight of the girder was obtained by summing the four reactions from the load cells in each support. The compression strength f'c from the concrete cores was used to estimate the modulus of elasticity (CSA-A23.3, 1994) from the equation

$$[3.4] \qquad E_c = \left(3000\sqrt{f'_c} + 6900\right)\left(\frac{\gamma_c}{2300}\right)^{1.5}$$

where γ_c is the density of the concrete. The shear modulus of the concrete was computed assuming an isotropic elastic material with Poisson's ratio, ν_c, equal to 0.2.

Section properties for each element were also determined. The moment of inertia of the leg elements was calculated using the transformed section method (CPCA, 1995) to account for cracking from service loads after 30 years of services.

The St. Venant torsional constant, J, was estimated using the membrane analogy by the finite differences method (ODEN and RIPPERGER, 1981). The cross section of the elements was discretized by a 2D mesh into a spreadsheet and several iterations were performed until convergence was reached for the points on the grid where the stress function was evaluated. Material and section properties are summarized in Table 3.6.

Cracking Torque of the Diaphragm

The cracking moment in the end panel was estimated from the stress function calculations. The shearing stresses were computed as well as the principal stresses at some discrete point of the grid. The maximum principal tensile stress was then compared to the direct cracking strength of the concrete, which was calculated based on COLLINS and MITCHELL (1987) as

[3.5] $$f_{cr} = 0.33\sqrt{f'_c}$$

The cracking torque in the end panel was then evaluated by linear interpolation.

From these calculations, the shear stress was found to be maximum along the inner face of the end diaphragm for the control specimens. When composite sheets were applied, the maximum shear stress shifted to the exterior face of the girder.

Flexural Strength of the Leg

The flexural strength of each individual leg was computed by a combination of two strength calculations. The first method assumed a triangular compression zone, as shown in Figure 3.11, to compute the flexural strength M^T_r. The second method used a rectangular compression block to obtain M^R_r. The former method accounts for an unsymmetric beam section (i.e. inverted L-shape when considering only half the hat-shaped G-girder) and the later describes symmetrical beam section behaviour.

The flexural strength M^R_r occurs at an L/U ratio (see Table 3.5) equal to 1.0, whereas the flexural strength M^T_r is assumed to occur when L/U reaches infinity. In order to obtain the flexural strength of the specimen, an exponential decay relationship between the flexural strength of the loaded leg and the L/U ratio was adopted. Based on this assumption, the flexural strength of each test was determined and is reported in Table 3.7.

Shear Strength of the Leg

The shear strength of the leg is the summation of the three contributing components, concrete, steel stirrups, and FRP sheets and can be expressed as

[3.6] $$V_r = V_c + V_s + V_{FRP}$$

Concrete Shear Strength V_c - The modified Zsutty's T-section formula, along with the concrete shear strength (1968), was used in calculating V_c:

[3.7] $$V_c = v_c\left(b_{leg}d + h_f^2\right)$$

where

[3.8] $$v_c = 2.137\left(f'_c\,\rho_w\,\frac{d}{a}\right)^{1/3}$$

b_{leg} is the web width of only one leg, h_f is the height of the flange, ρ_w is the longitudinal reinforcement ratio, and d and a are the effective depth and shear span, respectively.

Stirrups Shear Strength V_s – The stirrup contribution was computed by the simplified equation given in CSA-A23.3 (1994) Standard as

[3.9] $$V_s = \frac{A_v f_{vy} d}{s}$$

FRP Sheets Shear Strength V_{FRP} – The shear friction formulation in CSA-A23.3 (1994) is used here with some modifications for V_{FRP}. The adopted formulation takes the form

[3.10] $$V_{FRP} = (v_r - v_c) A_{cv} \sin\alpha_f$$

where

[3.11a] $$v_r = k\sqrt{\sigma f'_c} + \rho_v E_{FRP} \varepsilon_{ext} \cos\alpha_f$$

[3.11b] $$\sigma = \rho_v E_{FRP} \varepsilon_{ext} \sin\alpha_f$$

[3.11c] $$\rho_v = \frac{A_{vf}}{A_{cv}}$$

k = 0.6 for concrete placed monolithically

ε_{ext} is the maximum extrapolated strain (reported in Table 3.5) of the sheets, α_f is the angle between the shear friction reinforcement and the shear plane, and A_{vf} and A_{cv} are the area of shear friction reinforcement and concrete section resisting shear transfer, respectively. For consistency with the stirrup and concrete shear contributions previously defined, a shear plane of 45° was assumed. Since the FRP sheets were just glued to the inner face, only half of the concrete web was assumed to transfer shear stresses, as shown in Figure 3.12. These shear strength calculations are summerized in Table 3.7 for each test.

The elastic grid analysis was conducted using the commercial package SAP90. The boundary conditions of the grid model were such that the *Far Unloaded* support was able to lift up. The maximum load applied on the top of the girder was obtained when one of the elements reached its assumed capacity (see Table 3.7). Because the end diaphragm often failed first, a second elastic analysis was performed with the end diaphragm element removed. The maximum applied load was then given by the failure of one of the loaded leg elements.

3.5 Discussion

3.5.1 General

The ultimate load predictions from each method along with the test results are presented in Table 3.8. A comparison of the Load vs. Deflection curves for the three design methods investigated, along with the test results, is shown in Figure 3.13. Specimen *Girder 3 West* was selected as typical specimen. The Load vs. Deflection curves for all the specimens are presented in Appendix A.3. The ratio of *Loaded* over *Unloaded* leg deflection at the load point location was about 1.5 at the beginning, which is equivalent to 60% and 40% load sharing in bending for the Loaded and Unloaded leg, respectively. This value increased significantly at ultimate. This indicated that the girder no longer behaved linearly and as a whole inverted U section. Since this behaviour was difficult to assess fully with the methods presented, a more sophisticated analysis, such as the finite element method, could be performed.

The FRP stiffness per unit width (E_{FRP} times t) provided by the glass and carbon fibres are almost identical at 31.9 and 31.4 kN/mm, respectively. However, the fibres oriented at 45^o were found to perform better than the vertical sheets. In the former case, the concrete cracks were almost at right angle to the principal orientation of the fibres. The composite sheets were, therefore, very effective in controlling the crack widths. This effect is evident in the shear strengths of the girder elements in the grid method (see Table 3.7).

The strut-and-tie model is known to be a lower bound solution. The predicted results, as shown in Table 3.8, are conservative except for *Girder 2 East*, which was stopped prematurely.

The MCFT method considers only a rectangular concrete stress block when computing the bending moment for the T-beam section. This leads to an approximation of the capacity of the leg under an eccentric loading. The approximation can be improved, however, by using a triangular stress block as shown in Figure 3.11.

The grid analysis can accommodate various loading conditions or combinations. The initial stage of the load deflection curve can be predicted with reasonable accuracy, as shown in Figure 3.13. However, the flexural strength of the element needs to be evaluated with care since the load sharing between the two legs varies with the position of the applied load. Since this method is limited to elastic analysis, assessing the cracking moment in the end panel of the girder becomes difficult. *Girder 3 West*, for example, did not fail in the diaphragm, but the analysis predicts end panel cracking. The maximum predicted load is governed by flexural failure of the leg element rather than shear failure. However, if one ignores the cracking at the end diaphragm in the grid analysis, the predicted shear capacity of the leg element is at essentially the same load level as the previous prediction based on flexural failure.

The shear friction approach used to evaluate the contribution of the composite sheets gives simple but reasonable results. The Canadian standard CSA-A23.3 (1994), however, presents two methods that yield a range of shear strength. More research should be undertaken to refine or specify a preferred method between these two formulations when considering shear strengthening with composites.

3.5.2 Comparison of the Models

The predictions for each method are presented in Table 3.8. A ratio P_{Test} over P_{Pred} ranges from 1.11 to 1.69 (excluding *Girder 2 East* which was stopped prematurely) with a mean ratio of 1.33 and a coefficient of variation 11.0% for all of three methods. Because of the complex loading with combination of bending, shear, and torsion, it is unreasonable to expect better accuracy with the assumptions and simplifications necessary for the analysis. However, the three methods are consistent with each other and, in most cases, yield similar ultimate loads. Most of the predictions are conservative and, therefore, can be used for the design of strengthening elements.

A good correlation between the MCFT and the strut-and-tie model was found for almost all tests except *Girder 1 East*. In this test, the girder was strengthened only by a steel plate that gave a heavy longitudinal reinforcement. The stirrups spacing of 380 mm was too large to assume uniform concrete struts, as is required in the MCFT method (Collins and Mitchell, 1987).

A truss at 45° was assumed for the shear friction evaluation. A variable angle truss can also be used, as long as other strength evaluations are consistent. On the other hand, the MCFT can accommodate variable truss angle but requires computerized codes and software support.

Evaluating the material and cross sectional properties of the girder is a critical factor in order to achieve reliable predictions. However, it can be sometimes difficult to evaluate these properties in existing structures.

3.6 Conclusion

This series of tests investigated the benefit of using FRP sheets in the shear rehabilitation of type G-girders. A total of eight tests were performed on four type G-girders removed from existing bridges. Carbon and glass FRP sheets in two repair configurations were used in the rehabilitation. All of the girders were loaded eccentrically about the centroid of the cross section in order to fail the girders in combination of shear and torsion. Three commonly used shear strength evaluation methods, strut-and-tie model, MCFT, and grid analysis, were investigated.

The steel plate used to increase the flexural strength of the girders was found to provide significant increase in the shear capacity. The FRP sheets contributed to the increase of the total shear capacity of the girders by 5 to 17%. For the two repair schemes investigated, the inclined sheets were found to be more effective than the vertical sheets. The woven fabric glass materials performed better than the unidirectional carbon FRP sheets. The end panel was the weakest part of the girders under eccentric loading because it did not contain steel reinforcement. The vertical bands of FRP sheets applied in the inner face of the round end diaphragm were not effective, except for one case in which woven glass fibre was used. Better results were obtained when the horizontal sheets were used in the square end diaphragm. The FRP sheets did not fully develop their maximum capacity throughout the tests. Therefore, the maximum strength of the fibres was not a design criterion in this type of application.

The three shear evaluation methods presented in this study were consistent with each other. The test to predicted ratios based on these three methods ranged from 1.11 to 1.69 with a mean ratio of 1.33 and a coefficient of variation of 11.0%. The shear contribution of composite sheets at any angle can be accurately accounted for in the analysis. The strut-and-tie model and the MCFT are limited to the prediction of the ultimate shear capacity of the girders, while the grid analysis provides the complete load deflection curves with accuracy limited to the elastic range. Most of the predictions based on these three design methods are conservative and therefore can be used to design the shear rehabilitation of concrete girders using externally bonded FRP sheets.

Table 3.1 Test Matrix

Girder	Steel Plate	FRP Repair Scheme
G1 East	Yes	None
G1 West	No	None
G2 East	Yes	Vertical carbon
G2 West	Yes	Inclined carbon
G3 East	Yes	Vertical glass
G3 West	Yes	Inclined glass
G4 East*	No	None
G4 West*	Yes	Inclined carbon

* Square end diaphragm

Table 3.2 Steel Coupon Tests

	Bar Diameter mm	Yield Stress f_y MPa	Elastic Modulus E MPa	Ultimate Strength F_u MPa
Steel Plate		327	202000	502
Girder 2	28.6 (#9 Imp)	306	203000	494
	9.5 (#3 Imp)	311	186000	455
Girder 3	28.6 (#9 Imp)	263	191000	414
	9.5 (#3 Imp)	302	252000	423
Girder 4	28.6 (#9 Imp)	267	194000	448
	9.5 (#3 Imp)	336	203000	511

Table 3.3 Fibre Reinforced Polymers Material Properties

FRP Name	Type of fibres	Test source	Ultimate Strength MPa	Modulus of Elasticity MPa	Thickness mm
Replark Type 20	Carbon	Fibre strength*	3400	230000	0.11
		Coupon specimens	422	44800	0.70
SEH41	Glass	Fibre strength	-	-	-
		Coupon specimens	106**	17700	1.80

* Manufacture specified properties

** Premature failure

Table 3.4 Girder Test Results

Girder	*In Situ* f_c' MPa	Max. Load on girder kN	% Increase	Failure Mode
G1 East	45.9	382	35.5	Torsion in the end panel and plate debonding
G1 West	45.9	282	0.0	Torsion in end panel
G2 East	46.2	350	24.1	Shear in loaded leg
G2 West	46.2	412	46.1	Torsion in end panel/ partial concrete crushing
G3 East	42.8	394	39.4	Torsion in end panel
G3 West	42.8	415	47.2	Shear in loaded leg
G4 East*	32.5	259	0.0	Torsion in *Close Unloaded* corner
G4 West*	32.5	395	52.5	Torsion in *Close Unloaded* corner

*Square end diaphragm

Table 3.5 Parameters Used for the Analysis of the Test Specimens

Girder	L/U Ratio At Ultimate	ε_{ext} $\mu\varepsilon$	V/M Ratio m
G1W	1.62	-	1.147
G1E	3.95	-	0.889
G2E	2.11	1502	1.045
G2W	8.29	1783	0.795
G3E	4.07	2267	0.883
G3W	2.34	3907	1.012
G4E	3.99	-	0.887
G4W	4.50	1409	0.867

Table 3.6 Material and Section Properties of the Girder Elements

Girder	Density γ_c kg/m^3	E_c MPa	G_c MPa	Leg with two Ø 28.6 mm bars I_{cr} 10^6 mm^4	 J 10^6 mm^4	Leg with three Ø 28.6 mm bars I_{cr} 10^6 mm^4	 J 10^6 mm^4	Diaphragm J 10^6 mm^4
G1W	2084	25239	10516	932.2	137.9	1108.8	181.3	7742.1
G1E	2084	25239	10516	1663.8	231.6	1765.3	288.0	7742.1
G2	2111	25792	10747	1639.1	231.6	1740.4	288.0	7742.1
G3	1942	22109	9212	1820.6	231.6	1922.1	288.0	7742.1
G4E	2197	24002	10001	967.9	137.9	1148.8	181.3	1373.2
G4W	2197	24002	10001	1722.1	231.6	1823.8	288.0	1373.2

Table 3.7 Strength of the Girder Elements

	Diaphragm	Leg with two Ø 28.6 mm		Leg with three Ø 28.6 mm	
Girder	T_{cr} kN m	M_r kN m	V_r kN	M_r kN m	V_r kN
G1W	49.1	130.4	168.7	181.2	153.4
G1E	49.1	267.6	200.1	308.6	178.0
G2E	55.7	284.4	213.0	332.3	194.2
G2W	55.7	272.0	235.3	312.9	216.4
G3E	53.6	258.8	222.1	296.7	203.8
G3W	53.6	264.2	266.3	305.0	248.0
G4E	14.3	120.3	161.8	163.6	144.0
G4W	14.3	249.5	210.2	282.3	188.8

Table 3.8 Ultimate Point Load Predictions

	Test Results	Methods					
		Strut-and-tie		MCFT		Grid Analysis	
Girder	kN	kN	P_{Test}/P_{Pred}	kN	P_{Test}/P_{Pred}	kN	P_{Test}/P_{Pred}
G1W	281.9	230.2	1.225	210.6	1.339	195.9	1.439
G2E	351.0	409.5	0.857	393.3	0.892	281.1	1.248
G2W	412.6	313.4	1.316	320.1	1.289	310.5	1.329
G3E	393.0	319.1	1.232	330.4	1.190	293.1	1.341
G3W	414.8	364.6	1.138	373.8	1.110	340.6	1.218
G4E	259.0	172.6	1.501	171.1	1.514	179.5	1.443
G4W	395.7	315.7	1.254	313.7	1.261	277.4	1.427
G1E	383.1	331.7	1.155	226.3	1.693	264.1	1.451

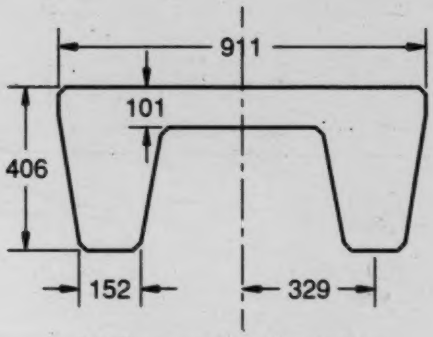
911
101
406
152
329

(a) Cross-section dimensions

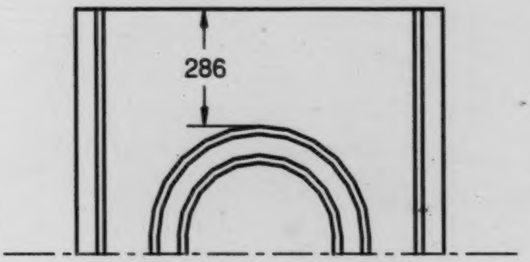

(b) Round diaphragm (plan view)

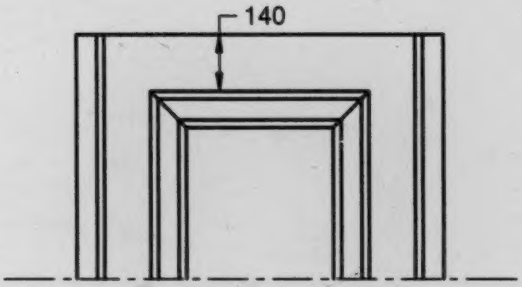

(c) Square diaphragm (plan view)

Figure 3.1 Typical Type G-Girder

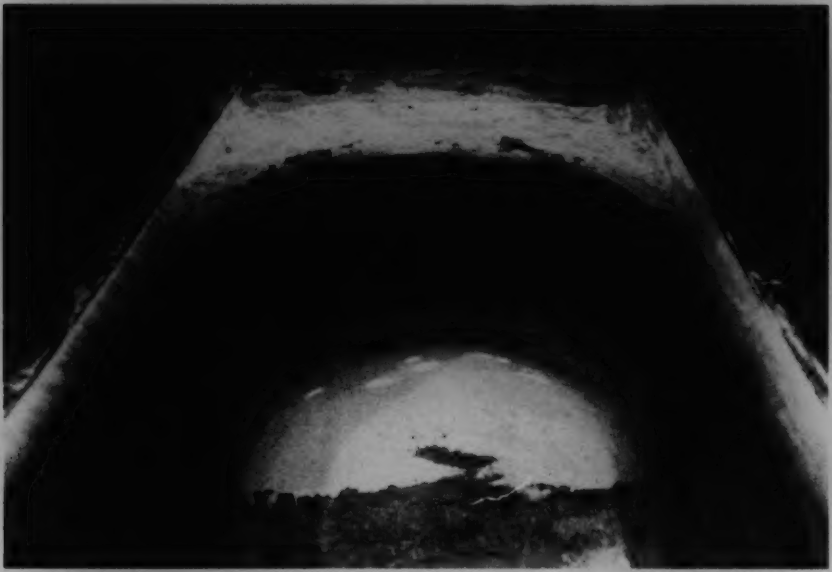

Figure 3.2 Surface Preparation in the End Panel

Figure 3.3 Typical End Diaphragm Layout

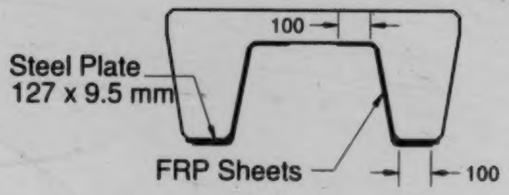
100
Steel Plate
127 x 9.5 mm
FRP Sheets
100

(a) Cross-section dimensions

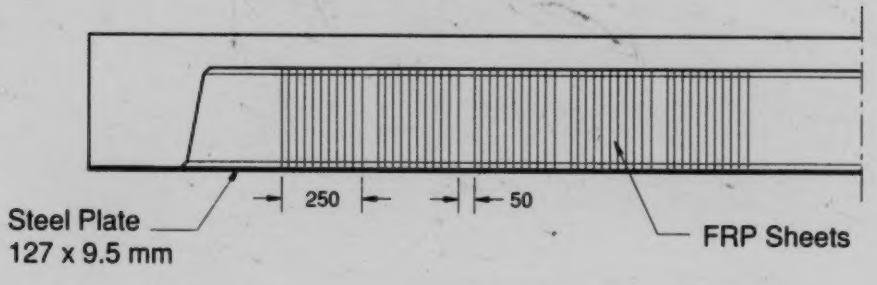
250
50
Steel Plate
127 x 9.5 mm
FRP Sheets

(b) Vertical sheets

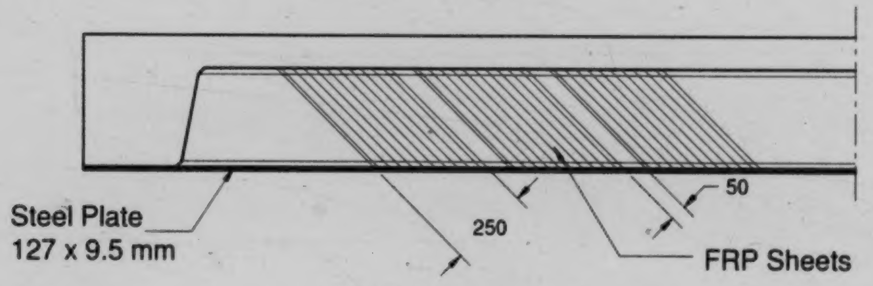
50
Steel Plate
127 x 9.5 mm
250
FRP Sheets

(c) Inclined sheets at 45°

Figure 3.4 Repair Schemes Used

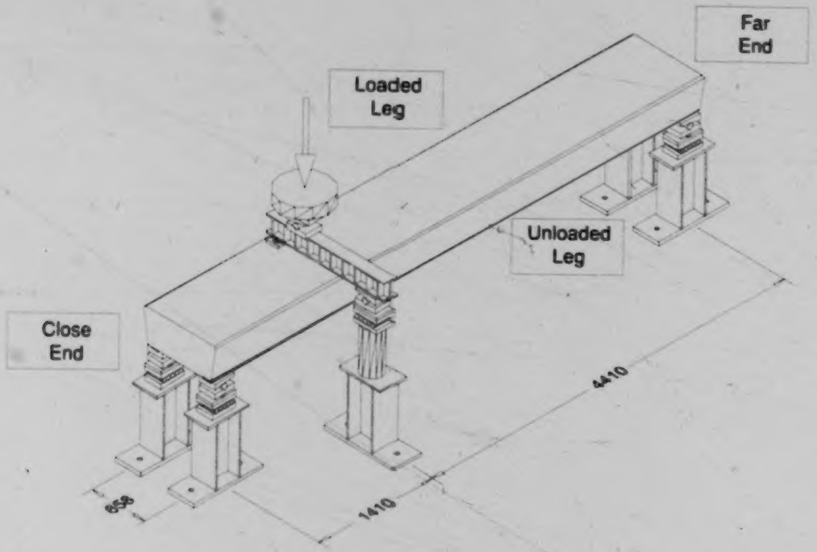
Far End
Loaded Leg
Unloaded Leg
Close End
4410
1410
858

Figure 3.5 Test Set-up

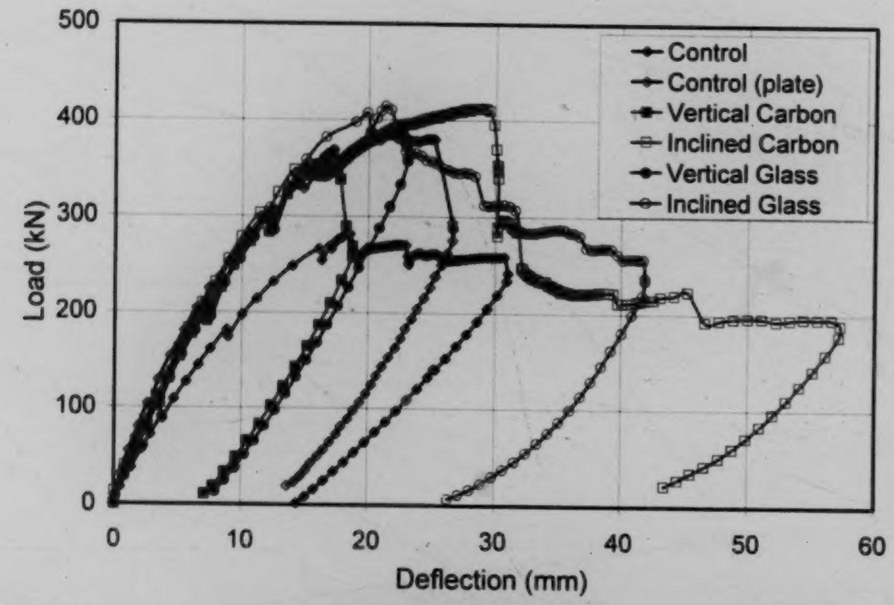

Figure 3.6 Load vs. Point Load Deflection Curves for Specimens with Round End Diaphragm

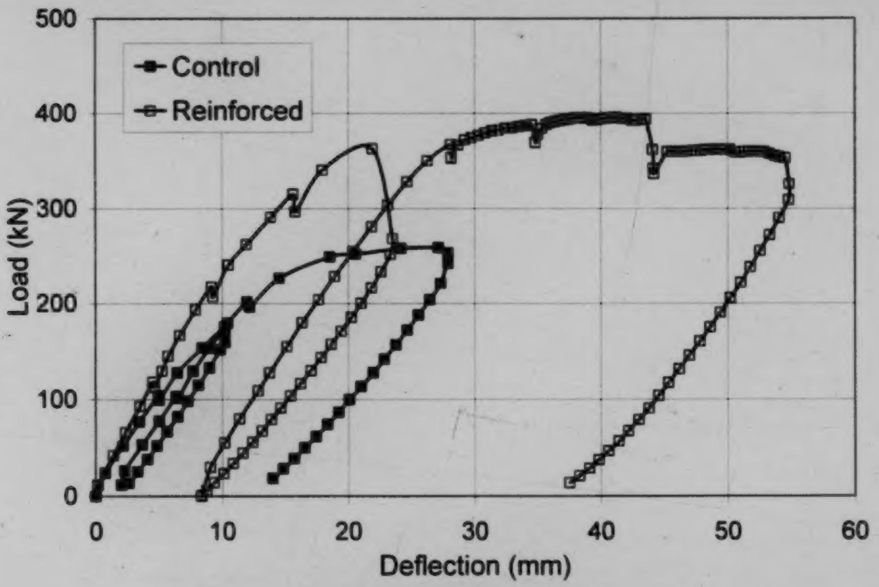

Figure 3.7 Load vs. Point Load Deflection Curves for Specimens with Square End Diaphragm

Figure 3.8 Twisting of Carbon Fibres in Close Unloaded Corner (*Girder 4 West*)

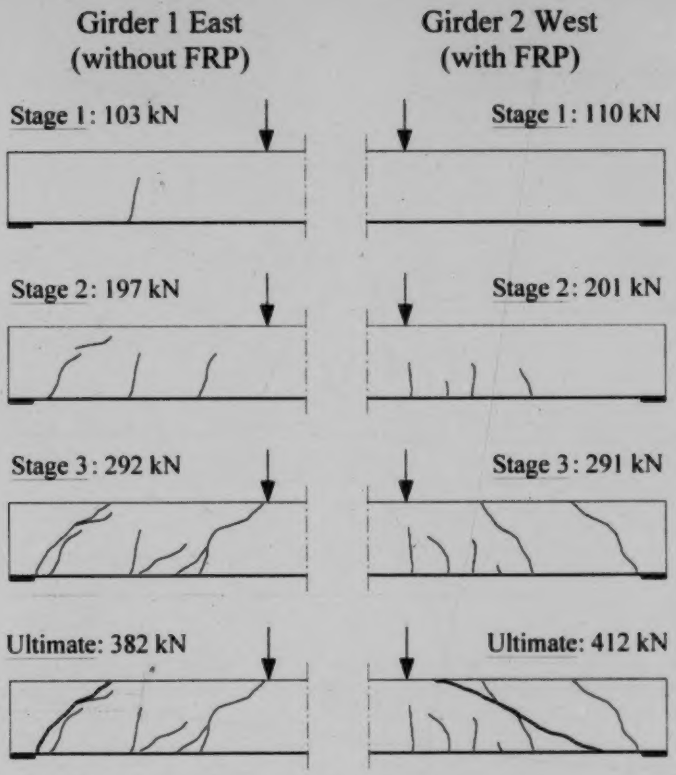
Girder 1 East
(without FRP)
Girder 2 West
(with FRP)
Stage 1: 103 kN
Stage 1: 110 kN
Stage 2: 197 kN
Stage 2: 201 kN
Stage 3: 292 kN
Stage 3: 291 kN
Ultimate: 382 kN
Ultimate: 412 kN

Figure 3.9 Typical Shear Crack Patterns

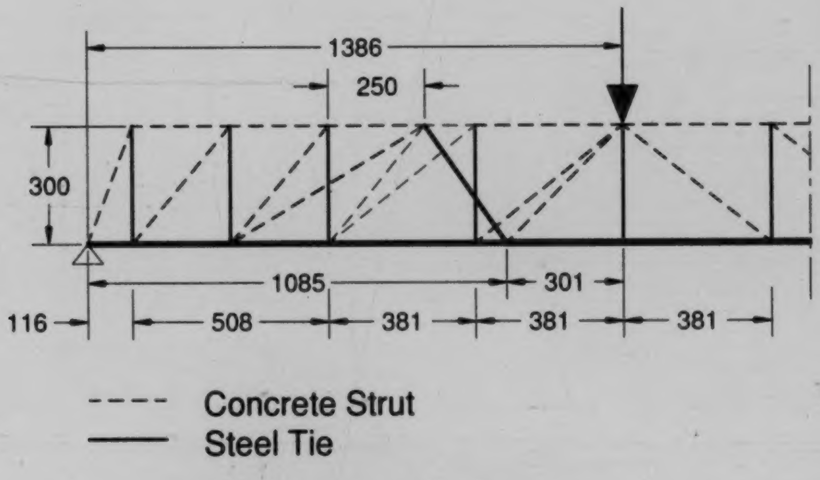
1386
250
300
1085
301
116
508
381
381
381
Concrete Strut
Steel Tie

Figure 3.10 Strut-and-Tie Scheme

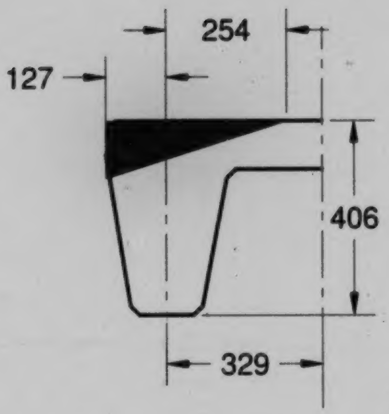
254
127
406
329

Figure 3.11 Geometry for the Triangular Stress Block

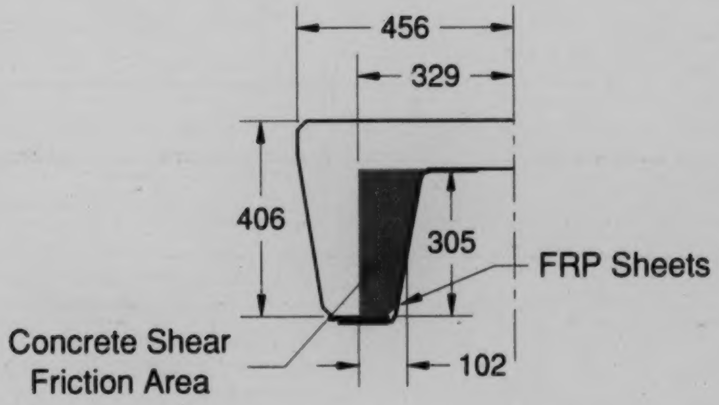
456
329
406
305
FRP Sheets
Concrete Shear
Friction Area
102

Figure 3.12 Shear Friction Assumptions with FRP Sheets

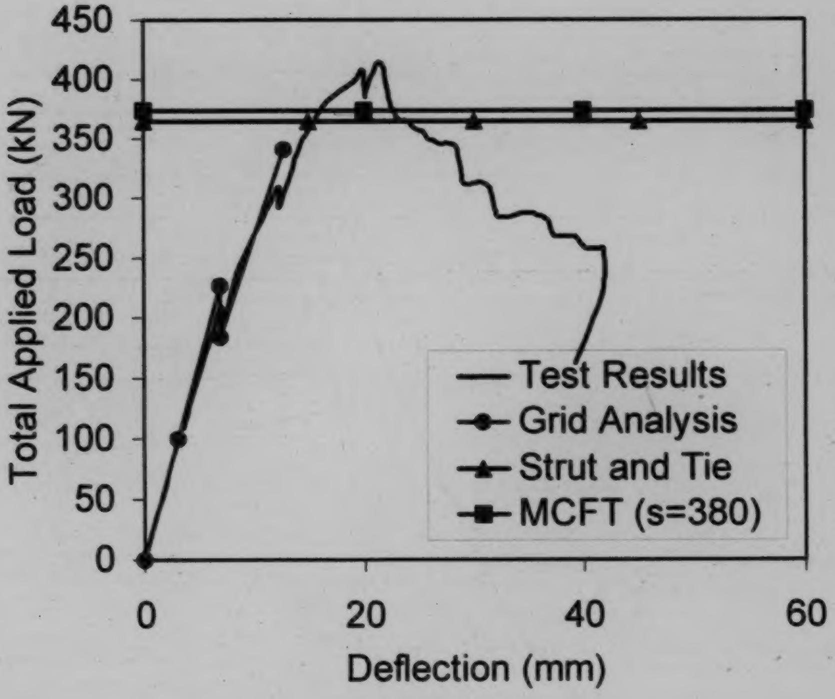

Figure 3.13 Typical Point Load Deflection Comparisons (*Girder 3 West*)

3.7 References

ALEXANDER J. and CHENG J.J.R. (1997). *Shear Rehabilitation of G-Girder Bridges using CFRP Sheets*, Structural Engineering Report No 218, Department of Civil and Environmental Engineering, University of Alberta, Edmonton, AB, 181 p.

ASTM A-370 (1996). *Standard Test Methods and Definitions for Mechanical Testing of Steel Products*, Annual Book of ASTM Standards, Philadelphia, PA.

ASTM C-42 (1994). *Standard Test Method for Obtaining and Testing Drilled Cores and Sawed Beams of Concrete*, Annual Book of ASTM Standards, Philadelphia, PA.

BARTLETT F.M. and MACGREGOR J.G. (1994). *Assessment of Concrete Strength in Existing Structures*, Structural Engineering Report No 198, Department of Civil and Environmental Engineering, University of Alberta, Edmonton, AB, 287 p.

COLLINS M.P. and MITCHELL D. (1987). *Prestressed Concrete Basics*, 1st Edition, Canadian Prestressed Concrete Institute, Ottawa, ON, 614 p.

CPCA (1995). *Concrete Design Handbook*, 2nd Edition, Canadian Portland Cement Association, Ottawa, ON.

CSA-A23.3 (1994). *Design of Concrete Structures*, Canadian Standards Association, Rexdale, ON.

CSA-S6 (1988). *Design of Highway Bridges*, Canadian Standards Association, Rexdale, ON.

ODEN J.T., and RIPPERGER E.A. (1981). *Mechanics of Elastic Structures*, 2nd Edition, MacGraw Hill, 460 p.

ZSUTTY T.C. (1968). “Beam Shear Strength Prediction by Analysis of Existing Data”, *American Concrete Institute Structural Journal*, Vol. 65, November, pp: 943-951.

4 REINFORCED CONCRETE T-BEAMS STRENGTHENED IN SHEAR WITH FRP SHEETS[1]

4.1 Introduction

During the post-World War II reconstruction, many concrete bridges were built both in North America and around the world. Since then, traffic volumes and allowable truck loads have steadily increased. As a result, most of the old bridges are now underdesigned according to current design codes, such as the American Association of State Highway and Transportation Officials Specification (AASHTO, 1994) and Canadian bridge design standard CSA-S6 (1988). At the same time, bridges are showing signs of aging, including corrosion of steel and spalling of concrete due to the use of de-icing salt.

Few design options are available to address these deficiencies. Limiting traffic loads over existing structures is not likely practical, as it requires the inconvenient redirection of the traffic. A second option, the construction of new bridges, is extremely expensive and can cause serious temporary traffic flow problems. The third option, in which structures are upgraded to carry additional loads, is the most feasible solution. The strengthening of existing structures has become a new engineering challenge and cost effective rehabilitation methods are in high demand.

The rehabilitation of infrastructures is not new, and various projects have been carried out around the world over the last two decades. Historically, steel has been the primary material used to strengthen concrete bridges and buildings. Bonded steel plates or stirrups have been applied externally to successfully repair concrete girders that are deficient in bending or in shear (SWAMY *et al.*, 1987; JONES *et al.*, 1988). However, steel used as a strengthening element adds additional dead load to the structure and normally requires corrosion protection.

Only a few years ago the construction market started to use Fibre Reinforced Polymers (FRP) for structural reinforcement, generally in combination with other construction materials, such as wood, steel, and concrete. The FRP's exhibit several main attractive properties such as low weight to strength ratios, non-corrosiveness, high fatigue strength and ease of application.

---

[1] A version of this chapter has been accepted August 7, 2000 for publication in the *ASCE Journal of Composites for Construction.*

The use of FRP sheets or plates bonded to concrete beams has been studied by several researchers (RITCHIE *et al.*, 1991). They have shown that bonded FRP plates are a feasible method of upgrading the flexural strength of reinforced concrete beams. AL-SULAIMANI *et al.* (1994) investigated the feasibility of using glass fibre sheets to repair shear deficient concrete beams. A series of small-scale concrete beam specimens deficient in shear were cast. The specimens were loaded until the first visible cracks appeared, then repaired with glass fibre sheets. But, even when the beams were designed to yield a flexural capacity of 1.5 times the shear capacity before repair, some beams still failed due to bending, and the full potential of the FRP shear strengthening could not be reached. Similar concrete beam specimens without stirrups were also tested by CHAJES *et al.* (1995), but they concluded that, both full-scale tests and more tests with internal shear reinforcement should be conducted.

The University of Alberta and the Alberta Transportation and Utilities (AT&U) have worked together to demonstrate the potential of FRP for bridge rehabilitation (Alexander and Cheng, 1996) in the field. Additionally, old concrete girders have been removed from existing bridges and were strengthened using carbon fibre reinforced plastic (CFRP) sheets, then tested in a laboratory setting (DRIMOUSSIS and CHENG, 1994; ALEXANDER and CHENG, 1997; DENIAUD and CHENG, 1998). Although the tests showed increased shear strength through the use of CFRP sheets, no information was obtained on the interaction between the internal stirrups and the CFRP sheets.

This project provides a series of laboratory controlled experiments using concrete beam specimens strengthened externally in shear with FRP sheets. The project objectives are to study the effects of the concrete strength, the stirrup spacing, the height of the beam web, and the type of FRP on the behaviour of the FRP-strengthened concrete beams. The experimental results of the first series of tests, using a beam height of 400 mm, are reported in this paper.

4.2 Experimental Program

4.2.1 Test Specimen

The specimen size was designed to provide a reasonably true behaviour of similar real life structural elements and to minimize the scale effect. A T-beam shape was selected to increase the flexural capacity relative to the shear resistance. In addition to the T shape, two high strength Dywidag bars with a 26 mm nominal diameter were used. The length of the beams was three meters long. Plain steel undeformed closed stirrups (6 mm diameter and 520 MPa yield strength) were used with three different spacings: 200 mm, 400 mm, and no stirrups. Figure 4.1 shows a typical cross section of a selected T-beam and the layout of the stirrups when 200 mm spacing was used. The beam was designed to provide a flexural capacity of between 2.0 and 3.5 times the shear capacity without FRP contribution. The specimens were cast with ready-mix concrete from a local supplier. Ancillary compressive concrete cylinder tests were performed throughout the test program and the concrete strength for each test was then evaluated with a best fit line by the least square method (see Table 4.1).

Three types of FRP were used to externally strengthen the web of the T-beams: a) uniaxial carbon fibre – *Replark Type 20* from Mitsubishi Canada Limited; b) uniaxial glass fibre – SEH51 from Fyfe LLC Limited; and c) triaxial [0°/60°/-60°] glass fibre – from Owens Corning. The glass fibres were applied at right angle to the longitudinal direction along the full length of the shear span. The carbon fibre sheets were placed at 45° angle to the longitudinal beam axis with a width of 50 mm and a gap of 50 mm perpendicular to the direction of the fibres. In all cases the fibres were extended underneath the flange to provide a minimum anchor length of 100 mm and wrapped under the web. The FRP sheets were bonded to the specimens prior to the test. At the same time the FRP sheets were glued on the test beams, coupon specimens were prepared in accordance with ASTM Standard D-3039M (1995). Table 4.2 summarizes the tested material properties of the FRP sheets.

This series tested four beams, but because both ends of each beam were tested separately, a total of eight tests were conducted. The test matrix for these four beams is presented in Table 4.1. The specimens were designated with a four character name: T4S*n* or T4NS, where T4 indicated a T-shape beam with 400 mm depth; S*n* was S2 or S4 indicating 200 mm or 400 mm stirrup spacing, respectively; and NS was for no internal stirrup. An additional designation was added to indicate the fibre type used (C45 – carbon fibre in 45°, G90 – glass fibre in 90°, and Tri – glass fibre in 0°/60°/-60°).

4.2.2 Test Set-up

The test set-up, shown in Figure 4.2, consisted of a four point loading system that created a region of constant moment at mid span. Because of the symmetric loading, the non-tested shear span of the beam was always strengthened using external stirrups in order to prevent premature failure. These stirrups consisted of two HSS steel tubes with tie rods on either end.

Two longitudinal Dywidag bars were extended 150 mm from the ends of the beams and anchored with a 50 mm thick steel plate. L-shaped steel angles were also used on each side of the web as a passive confinement for the anchor zone of the flexural reinforcement. These details (plate and angles), also shown in Figure 4.2, were included to prevent longitudinal de-bonding failure.

4.2.3 Instrumentation

Up to 20 electrical strain gauges were mounted on the FRP sheets on one side of the T-beam. These gauges were either vertically or horizontally orientated. The opposite side was instrumented with a number of sets of Demec gauges. A Demec gauge of 200 mm was used for most of the measurements. However, a Demec gauge of 50 mm was used to record vertical and 45° strains on the side of the web when glass fibre sheets and carbon fibre bands were glued, respectively.

Nine electrical strain gauges were mounted along the full length of each Dywidag bar. Both legs of each stirrup located in the shear span were also instrumented at mid height. These gauges were protected with waterproof coating and silicon prior to casting the concrete.

The flexural deflection was recorded using three cable transducers, one at each load point and one at mid span. A total of nine horizontal Linear Variable Differential Transformers (LVDTs), each with a gauge length of 400 mm, were also installed at two locations within the shear span (section #4 and section #6 in Figure 4.1, 470 mm and 870 mm from the support, respectively) and at mid span of the T-beam. They were used to measure the strain distribution through the depth of the beam. At each section, a steel apparatus was fixed on the side of the beam to hold three LVDTs located at the top and bottom of the flange and at the bottom of the web.

The total load applied by the MTS6000 testing machine on the top of the T-beam was recorded from a load cell and cross-checked against the two load cells provided at each support. The dead load of the specimen is not considered in the results presented here.

4.3 Experimental Results

The ultimate loads obtained from each test are summarized in Table 4.3. The strain distribution through the height of the beam was computed from the LVDT data using the least square method. Figure 4.3 shows the strain distributions through the depth of the beam at sections #4, #6, and mid-span for the specimen T4S2 and T4S2G90. The strain distributions for the remaining specimens are presented in Appendix B.3. The coefficient of variation (COV) of the compressive strain at the concrete extreme fibre was then calculated with the best fit line, first using all three LVDTs and then with only the first two. At the mid span the COV was never greater than 5%. This validates the assumption that the plane section remains plane. However, at sections #4 and #6 (470 mm and 870 mm from the support, respectively) this value increased drastically after certain loads, as shown in Figure 4.3, thus implying that the plane section no longer remains plane. The corresponding loads for each test when the plane section no longer remains plane at these two locations are also listed in Table 4.3.

For ease of comparison, the loads and deflections obtained from each test were normalized to the test results of the one with no FRP and no stirrups (T4NS). Figure 4.4 to Figure 4.6 show the normalized load vs. the normalized deflection curves for the three different stirrup arrangements. Figure 4.7 illustrates the increase of shear strength with the use of glass fibre and the decrease of stirrup spacing. Table 4.4 summarizes the normalized ultimate loads and the resultant net increase in shear strength over the respective control specimen.

The shear force V can be expressed by two components: arching action and beam action. At any location in a beam when a moment gradient $\frac{dM}{dx}$ is present, these two effects are combined to give the total shear resistance. For a cracked concrete member, these components can be written as follows:

$$[4.1] \qquad V = \frac{dM}{dx} \quad \text{and} \quad M = T \cdot jd$$

Where T and jd are the tensile force in the bottom chord and lever arm, respectively. Thus,

$$[4.2] \qquad V = T\frac{djd}{dx} + jd\frac{dT}{dx}$$

The first term of the above equation refers to the arching action while the second term describes the beam behaviour. These two effects can be evaluated between two known sections along the length of the beam, thus, Equation (4.2) can be re-written as:

$$[4.3] \qquad V = T\frac{\Delta jd}{\Delta x} + jd\frac{\Delta T}{\Delta x}$$

where Δ represents change between two sections.

Using the recorded strain gauge data in Dywidag bars at sections #4 and #6 and knowing the applied shear V, all terms of Equation (4.3) are known. Beam and arching actions were calculated between the sections #4 and #6 using Equation (4.3) and summarized in Table 4.5. Table 4.5 shows that shear force starts out being carried entirely by beam action, but ends with arching action as predominant. The load at which beam and arching actions share equally in carrying the applied shear is also given in the table.

4.4 Discussion

4.4.1 Initial Flexural Stiffness

As expected, the external and internal shear reinforcements did not increase the initial flexural stiffness of the beams. Figure 4.4 through Figure 4.7 show that the initial slope of the load – deflection curves is identical for all tests. Only the maximum load and the final deflection (ductility) were increased by the reinforcement.

4.4.2 Number of Stirrups

When the same type and amount of fibre (glass fibre SEH51) were used with various stirrup spacing, different levels of increase in the shear capacity were observed. With a 200 mm stirrup spacing (heavy internal shear reinforcement) a 21% net increase was recorded by using SEH51, while with no stirrups or with s = 400 mm, the glass fibre sheets provided approximately 40% increase in shear strength (see Table 4.4). These results indicate that the benefit from the use of FRP reinforcement was reduced when beams were heavily reinforced with internal shear stirrups.

4.4.3 Strain Distribution Through the Depth

Looking at the data recorded by the horizontal LVDTs (Figure 4.3), we can see that section #4, located at a distance of 470 mm from the support, did not behave as a plane section for most of the tests from the early stages of the loading. However, at section #6, 870 mm from the support, the external FRP reinforcement delayed the non-planar section behaviour (see also Appendix B.3). In all cases but one (test T4S2G90), the section strengthened with FRP did not remain plane when the maximum load level of the corresponding control test (T4S2, T4S4 and T4NS) with the same internal reinforcement was reached.

4.4.4 Beam and Arching Actions

As calculated using Equation (4.3) the shear components between sections #4 and #6 confirmed the results found with the LVDTs. At the beginning of the test, the shear is carried by beam action until the concrete cracks and the struts start to form (second column of Table 4.5). The equal share of the shear between beam action and arching action is reported in the third column of Table 4.5. The last column shows in percentage terms the remaining beam action that carries the shear. It should be noted that with no reinforcement in test T4NS, the load was transferred from the point load to the support only by the arching action. Therefore, 0% remaining beam action is shown in Table 4.5. No significant increase in percentage terms of the remaining beam action at the maximum load was observed for the beams with FRP. However, the arching action behaviour was delayed when FRP sheets were applied to the web of the specimens. An equal share between beam and arching actions occurred at a load level close to the loss of the plane section behaviour observed with the LVDTs (see Table 4.5).

4.4.5 Failure Modes

In general, for the tests with no FRP (control specimens), two major shear cracks were observed within the shear span, as shown in Figure 4.8. The ultimate load was reached when the concrete crack extended upward through the flange near the load point. The failure of both the uniaxial and tri-axial glass fibre reinforced specimens started the same web shear cracks as control specimens (see Appendix B.1). However, following the web shear crack formation, a vertical crack was formed on the top of the flange close to the support and propagated downward; the glass fibre was eventually tearing (unzipping) vertically, as shown in Figure 4.9. This effect can be explained by strain compatibility between the flange and the web. When the concrete strut formed in the web, it created a secondary effect in the top flange. At about 400 mm from the support, horizontal tensile strains were observed in the flange. Eventually, these strains reached the tensile strength of the concrete. A vertical crack therefore formed from the top of the flange and extended downward through the flange thickness until it reached the web and the FRP sheets and led to a vertical tearing (unzipping) of the fibres. This resulted a sudden drop of load with the uniaxial glass fibre as shown with the load-deflection curves in Figure 4.6. The horizontal strain gauges on the FRP sheets captured this behaviour where strains of up to 0.6% were observed at ultimate in the weak direction of the FRP sheets. The failure was progressive (see Figure 4.6) and the tearing (unzipping) of the fibre can be observed steadily throughout the test. The specimen reinforced by triaxial glass fibre (T4S2-Tri) was able to bridge this crack with the fibres inclined at ±60° that were crossing the vertical crack path. Therefore, the sudden tearing (unzipping) phenomenon observed in the uniaxial glass fibre reinforced specimens was effectively prevented. The unidirectional carbon bands at 45° were crossing the concrete cracks almost at right angles and were, therefore, very effective. However, with a gap of 50 mm these bands generated large shear stresses which were transferred from the surrounding concrete and thus the sheets peeled off suddenly from the face of the beam web after the bond strength of the fibre-concrete interface had been reached. This bond strength depends mainly on the anchorage at the end of the fibre.

4.5 Mechanical Design Model

4.5.1 Strip Method

The contribution of the FRP sheets was evaluated using the strip method, as developed by ALEXANDER and CHENG (1998). The model was developed from the observation that the fibre was first peeling off from the concrete surface at the top of the sheet where it has the smallest bond length above the shear crack on the beam web. The peeling area was graduately expanding from the initial debonding area under increasing applied load until the applied load exceeded the remaining bond strength between fibre and concrete. In the model, the FRP sheets are described by a series of strips crossing the concrete shear web crack. The load is distributed linearly between the strips from the bottom of the web to the flange (up to where the FRP sheets are glued) using the following equation:

$$[4.4] \qquad y_x = \frac{x}{\sum_{i=1}^{n} i}$$

where y_x is the portion of the load carried by the strip x, x is the strip number and n is the number of the strip which is still effective.

The maximum allowable strain (ε_x), which shall not exceed the ultimate tensile strain of the fibre (ε_{ultFRP}), for each strip is evaluated geometrically using the corresponding shear transfer length and taking into account the anchorage of the FRP sheets underneath the flange. From the vertical equilibrium of a unit FRP strip (shown in Figure 4.10), the force and moment equilibrium about the centroid of the fibre can be used to obtain:

$$[4.5] \qquad \varepsilon_x = \frac{0.5\, a_h\, f_t + a_x\, \tau_x}{t\, E_{FRP}} \quad \leq \quad \varepsilon_{ultFRP}$$

and

$$[4.6] \qquad f_t = \frac{6\tau_x\, a_x\, t}{a_h(2a_h - 3t)} \quad \leq \quad f_{tr}$$

a_h is the anchor length underneath the flange and a_x is the interface length of the strip x. τ_x is the average bond strength associated with the strip x. t and E_{FRP} are the thickness and the modulus of elasticity of the FRP sheets, respectively. Finally, f_{tr} is the concrete strength in direct tension and can be estimated by (Collins and Mitchell, 1987)

$$[4.7] \qquad f_{tr} = 0.33\sqrt{f'_c} \quad \text{in MPa}$$

Many researchers (Alexander and Cheng, 1997; Chajes *et al.*, 1996) have found that the average bond strength τ_x is a function of the bond length. The shear interface curve developed by Alexander and Cheng (1997) was used for this study. Because their concrete block bond tests were conducted using only a concrete strength of 45 MPa, some transformations must be performed for different concrete strengths. Most of the concrete strengths given in any design code indicate that the shear strength is proportional to the square root of f_c'. The experimental interface shear curve was therefore scaled accordingly, as shown in Figure 4.11, which uses an example concrete strength of 30 MPa.

For n number of strips used, the total shear load $V_{(n,x)}$ calculated from each individual strip x is given by

$$[4.8] \qquad V_{(n,x)} = \frac{w_x \, t \, E_{FRP} \, \varepsilon_x}{y_x} \sin\alpha$$

where w_x is the width of the FRP strip x and α is the angle between the fibre direction and the longitudinal axis of the beam. The governing shear is the minimum shear load computed with the above equation among the n strips that are still effective. Because the strip with the largest index carries the largest share of the load, it is likely to exceed its own maximum allowable strain. It will then either fail or debond and the load will be redistributed among the remaining strips. The number of effective strips decreases then to n-1. This process is continued until the governing shear load calculated with n-1 strips becomes lesser than the shear value computed in the previous step (i.e. with n strips). At this point the effective average FRP strain ε_{ave} over the remaining bonded width as well as the ratio R_L (remaining bonded over total widths), can easily be recorded.

The process described above can be repeated for a number of concrete crack angles. It can be shown that ε_{ave} and R_L do not vary with the concrete crack angle. However, the shear load increases when the angle θ becomes smaller because, of course, there are more fibre sheets bridging the concrete crack. To complete the evaluation of the load carried by the FRP sheets, we need to find the appropriate concrete shear crack angle θ. There are several shear design models, such as the modified compression field theory, available to determine the concrete shear crack angle. Since this paper is not intended to discuss the validity of using different shear design models in FRP strengthened beams, only the shear friction method is used and discussed in this paper. More details about the evaluation of various shear design models can be found in DENIAUD and CHENG (2000).

4.5.2 Shear Friction Method

Recently, LOOV (1998) reviewed the simplified method of shear design and compared it with results using the shear friction method, both methods are described in ACI-318 (1995) and Canadian Concrete Design Standard CSA-A23.3 (1994). He found that among all potential failure planes along which slippage can occur, the lowest shear strength is the governing shear strength. Using the shear friction method, the general equation of the shear strength of a beam having a cracking angle θ can be written as follows:

[4.9] $$V_r = 0.25 k^2 f_c' b_w h \tan\theta \quad + \quad T_v n_s$$

where k is an experimentally-determined factor, usually equals to 0.6 for design. b_w and h are the width of the effective web and the height of the beam, respectively. T_v is the tension force in the stirrups and n_s is the total number of stirrups, if any, crossing the concrete shear plane at angle θ.

Equation (4.9) is then modified twice. First, to include the contribution of the FRP sheets along with that of the stirrups, and, secondly, to account for the flange width as well as its corresponding k factor. Because cracked and uncracked concrete sections behave differently, the value of 0.6 for k is found to be unconservative for the former case, and conservative for the latter (LOOV, 1998). Therefore, k values of 0.7 and 0.5 were used for the flange (k_f) and the web (k_w), respectively:

[4.10] $$V_r = 0.25 f_c' \left(k_f^2 h_f b_f \tan\theta_f + k_w^2 h_w b_w \tan\theta_w \right) + T_v n_s + \frac{d_{FRP}\, t\, E_{FRP} \varepsilon_{ave}}{\tan\theta_w} R_L$$

where the subscripts f and w stand for *flange* and *web*, respectively. d_{FRP} is the height of the FRP sheets glued to the web of the beam (for this particular case in fact, $d_{FRP} = h_w$).

A computer program was written to perform the iterative procedure in evaluating the shear capacity of the beam with all potential concrete crack paths. Since the governing ε_{ave} and R_L are the same for all potential crack angles, the program first calculates the FRP components (ε_{ave} and R_L) with an assumed 45° crack. The program is then used to calculate Equation (4.10) with various combinations of θ_w and θ_f until the lowest shear load V_r is obtained. The results are presented in detail for all eight tests in Table 4.6.

4.5.3 Comments

The model described above gives a very good evaluation of the cracking pattern as well as the resisting shear force. The complete results are presented in Table 4.6. Figures 4.12 and 4.13 show the theoretical shear path and can be compared with the photos shown in Figures 4.8 and 4.9, respectively. The theoretical shear paths for all specimens are presented in Appendix B.4. The load predictions are conservative and the model also shows that FRP sheets are less effective at increasing the shear load when the beam is heavily reinforced with internal stirrups. The strip method can accommodate the FRP sheet shear contribution very well at any angle, but further studies are required to validate the assumptions made and in particular the linear load distribution among the strips. Finally, the mechanical model presented is based on a rational mechanism and does not require any experimental reading.

4.6 Conclusion

This series of tests investigated the behaviour of reinforced concrete beams with external FRP shear strengthening. Several conclusions can be drawn as follows:

1. The effectiveness of FRP strengthening to shear contribution is dependent on the amount of internal shear reinforcement. It appears that the composites are less effective when beams are heavily reinforced with internal shear reinforcement.
2. A plane section does not remain plane in the shear span after a certain load level is reached, but the external FRP sheets delay the loss of plane section behaviour.
3. The shear forces carried by arching action are also delayed when FRP is used. The remaining beam action at ultimate with significant shear reinforcement either by internal steel stirrups or external FRP sheets accounts for about 20% of the total shear force.
4. The failure mode of the beams reinforced by continuous uniaxial glass fibre was by vertical tearing (unzipping) of the fibres close to the support. The geometry of the T-beam is obviously a significant factor of such failure.
5. Tri-axial glass fibre reinforcement provided the beam with a more ductile failure than the ones strengthened by unidirectional glass fibres or unidirectional carbon fibres with a 50 mm gap.

6. The mechanical design model as presented calculates predicted values that are in excellent agreement with the experimental results. The behaviour of the FRP sheets can also be evaluated using a rational shear design model.

Table 4.1 Test Matrix of the T400 Series

Specimen	Concrete strength *MPa*	Stirrup Spacing *mm*	External FRP Reinforcement
T4S2	28.6	200	None
T4S2C45	29.4	200	Carbon sheets *Replark Type 20* at 45° (50 mm gap)
T4S4	29.9	400	None
T4S4G90	30.0	400	Glass fibres SEH51 at 90° (No gap)
T4NS	30.1	None	None
T4NSG90	30.2	None	Glass fibres SEH51 at 90° (No gap)
T4S2G90	30.3	200	Glass fibres SEH51 at 90° (No gap)
T4S2Tri	30.4	200	Tri-axial glass fibres (No gap)

Table 4.2 Fibre Reinforced Plastics Material Properties

FRP Name	Type of fibres	Test source	Ultimate Strength MPa	Modulus of Elasticity MPa	Thickness mm
Replark Type 20 (Mitsubishi)	Carbon	Fibre strength	3400	230000	0.11
		Coupon specimens	422	44800	0.70
Triaxial (Owens Corning)	Glass	Fibre strength	-	-	-
		Coupon specimens	124	8100	2.10
SEH51 (Fyfe LLC)	Glass	Fibre strength	-	-	-
		Coupon specimens	106*	17700	1.80

* Premature failure

Table 4.3 Maximum Loads and Loads Corresponding to the Change of Behaviour when Plane Section no Longer Remains Plane

Test	Maximum load *kN*	At Section #4 *kN*	At Section #6 *kN*
T4NS	230.8	34.6	155.4
T4NSG90	318.0	9.1	269.1
T4S4	313.9	0.0	140.6
T4S4G90	411.2	0.0	313.3
T4S2	402.5	83.2	232.1
T4S2C45	438.1	0.0	406.9
T4S2G90	451.2	0.0	361.8
T4S2Tri	485.3	59.4	415.6

Table 4.4 Normalized Loads

	Normalized Load			Stirrup contribution			FRP contribution		
	Stirrup Spacing (mm)			*Stirrup Spacing (mm)*			*Stirrup Spacing (mm)*		
FRP reinforcement	*None*	*400*	*200*	*None*	*400*	*200*	*None*	*400*	*200*
control	1.00	1.36	1.74	-	36.0%	74.4%	-	-	-
glass fibre SEH51	1.38	1.78	1.96	-	36.0%	74.4%	37.8%	42.2%	21.1%
carbon sheets at 45°	n.a.	n.a.	1.90	n.a.	n.a.	74.4%	n.a.	n.a.	15.4%
tri-axial glass	n.a.	n.a.	2.10	n.a.	n.a.	74.4%	n.a.	n.a.	35.9%

Table 4.5 Beam and Arching Shear Actions

Test	Beam action until *kN*	Equal share *kN*	Remaining beam action at P_{max} %
T4NS	83.0	136.8	0.0%
T4NSG90	214.0	276.0	12.2%
T4S4	65.5	162.2	16.1%
T4S4G90	85.7	313.3	19.6%
T4S2	62.8	162.8	24.8%
T4S2C45	59.8	303.1	20.3%
T4S2G90	111.5	313.2	21.8%
T4S2Tri	91.1	360.6	34.5%

Table 4.6 Mechanical Model Results

Test	θ_w *deg*	θ_f *deg*	ε_{ave} %	R_L	n_s	V_r *kN*	V_{exp}/V_r
T4NS	32.2	14.9	-	-	-	100.4	1.149
T4NSG90	38.0	13.2	0.157	0.796	-	129.2	1.231
T4S4	35.8	15.7	-	-	1	138.0	1.138
T4S4G90	40.3	14.1	0.156	0.800	1	163.8	1.255
T4S2	41.9	20.1	-	-	2	191.7	1.050
T4S2C45	42.7	19.8	0.142	0.868	2	205.5	1.066
T4S2G90	45.0	18.8	0.157	0.800	2	220.7	1.022
T4S2Tri	45.0	18.8	0.296	0.800	2	221.3	1.096

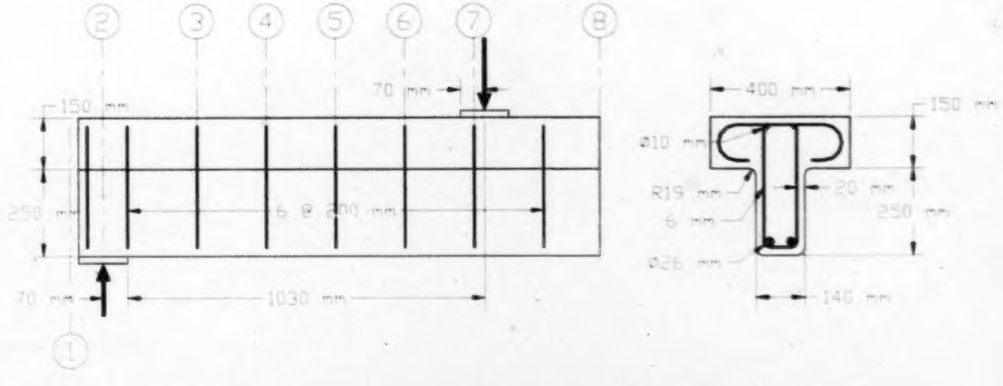
②
③
④
⑤
⑥
⑦
⑧
70 mm
150 mm
250 mm
6 @ 200 mm
70 mm
1030 mm
①
400 mm
150 mm
Ø10 mm
R19 mm
6 mm
20 mm
250 mm
Ø26 mm
140 mm

Figure 4.1 T-beam Cross Section and Stirrup Layout with 200 mm Spacing

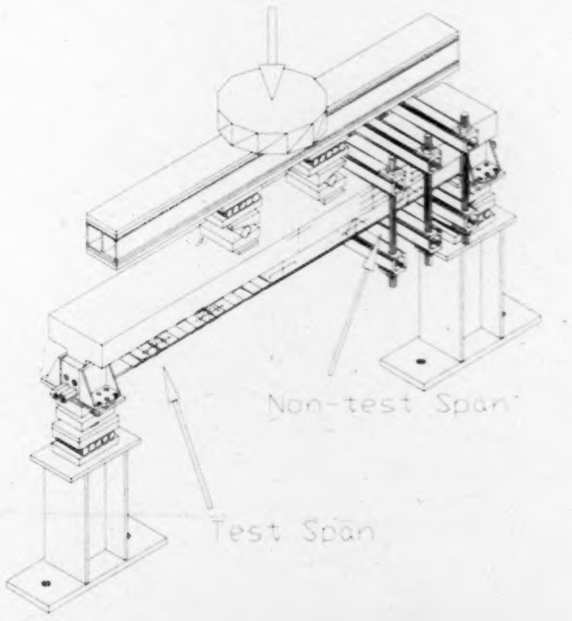
Non-test Span
Test Span

Figure 4.2 Isometric View of the Test Set-up

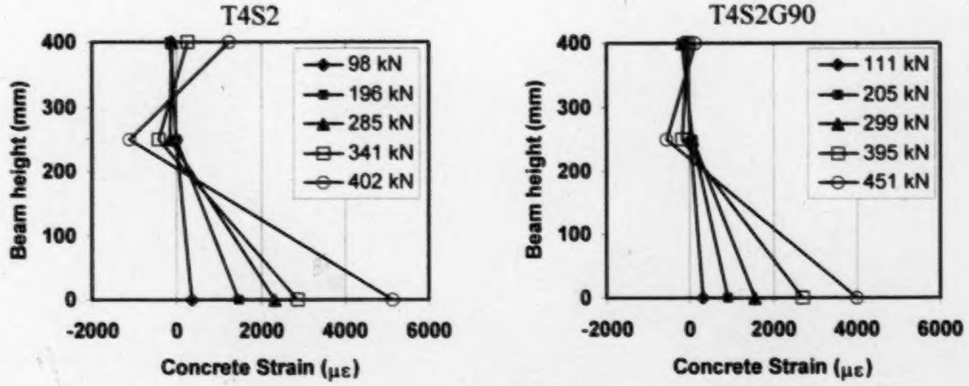

a) At section #4

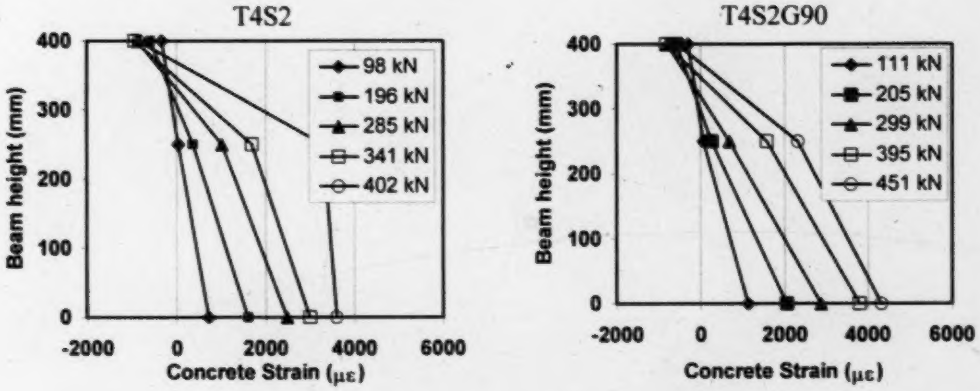

b) At Section #6

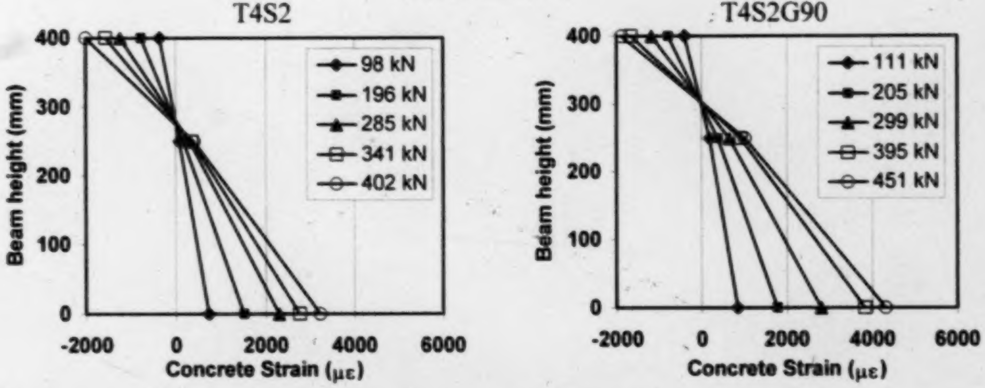

c) At section #8 (mid-span)

Figure 4.3 Strain Distribution Through the Depth of the T-beam from the Horizontal LVDT for T4S2 and T4S2G90 Specimens

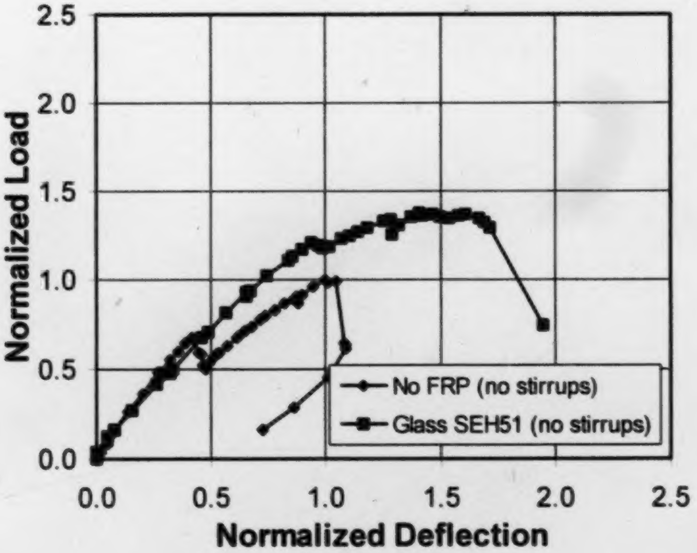

Figure 4.4 Normalized Load Deflection Curves with no Stirrups

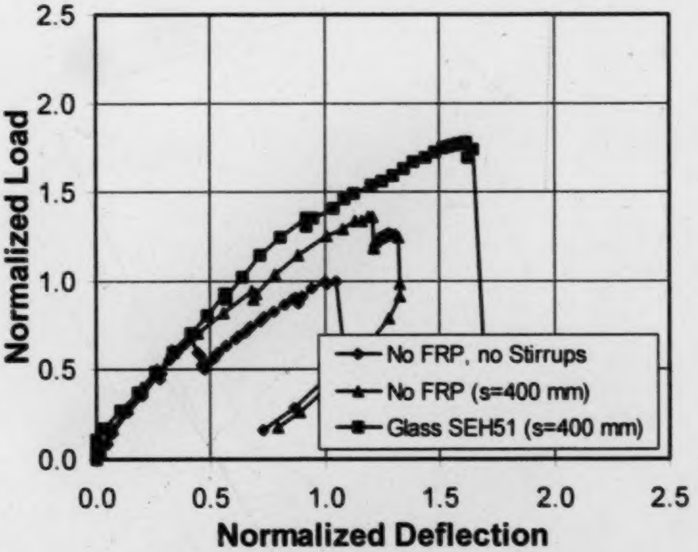

Figure 4.5 Normalized Load Deflection Curves with 400 mm Stirrup Spacing

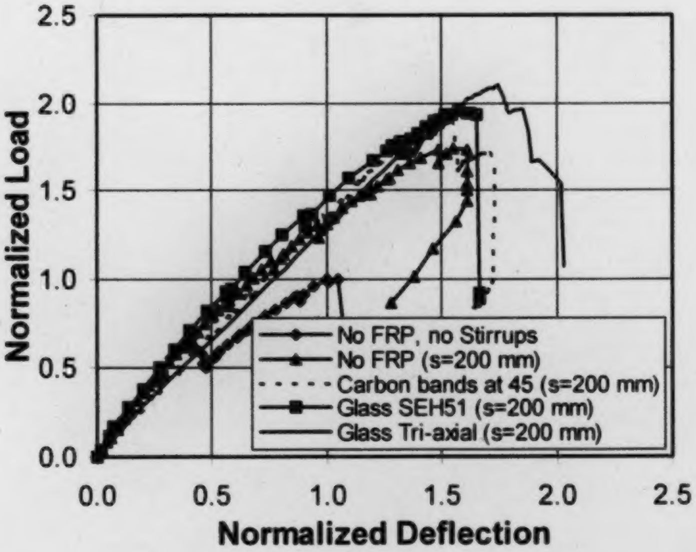

Figure 4.6 **Normalized Load Deflection Curves with 200 mm Stirrup Spacing**

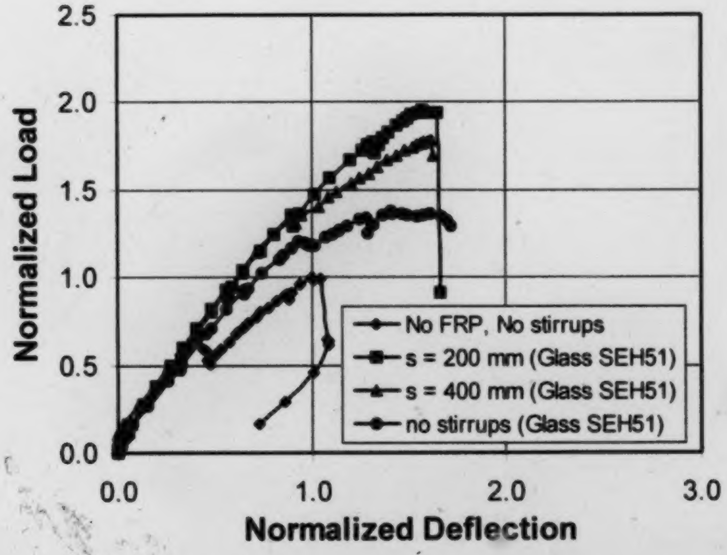

Figure 4.7 **Normalized Load Deflection Curves with SEH51 Glass Fibres**

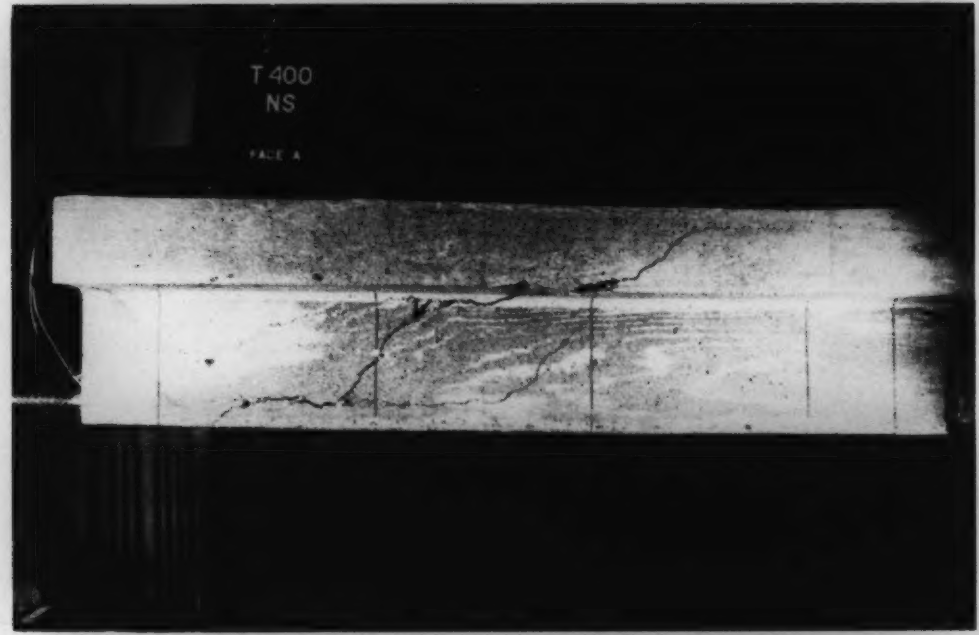
T 400
NS
FACE A

Figure 4.8 Photo of the Crack Pattern for T4NS

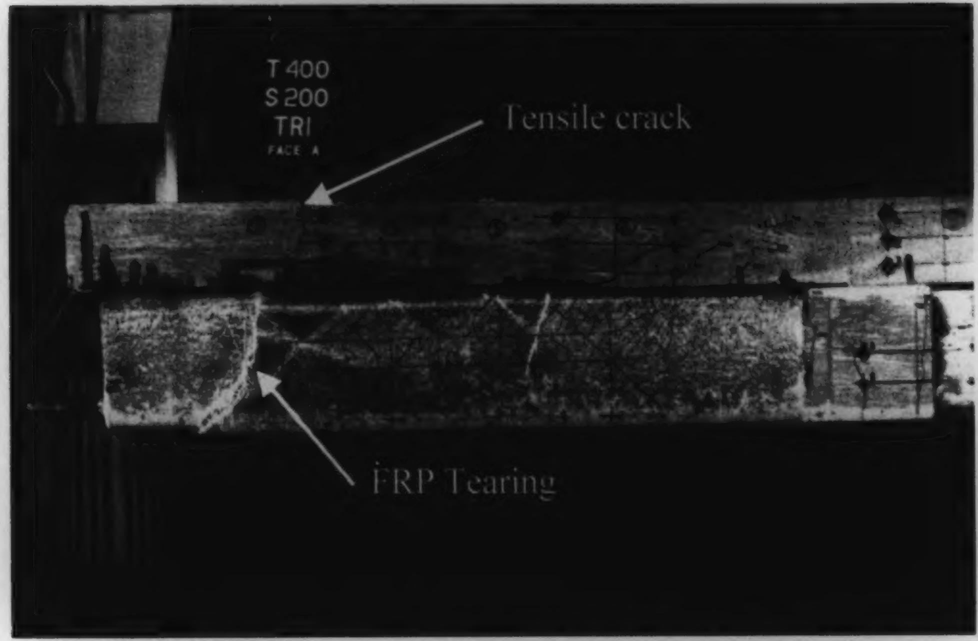
T 400
S 200
TRI
FACE A
Tensile crack
FRP Tearing

Figure 4.9 Photo of the Crack Pattern for T4S2Tri

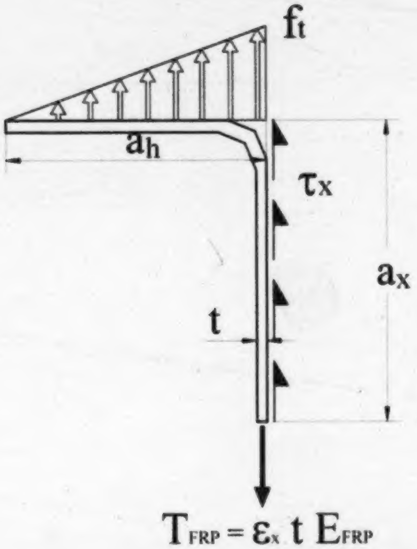

f_t
a_h
τ_x
a_x
t
$T_{FRP} = \varepsilon_x\ t\ E_{FRP}$

Figure 4.10 Vertical Equilibrium of one FRP Strip

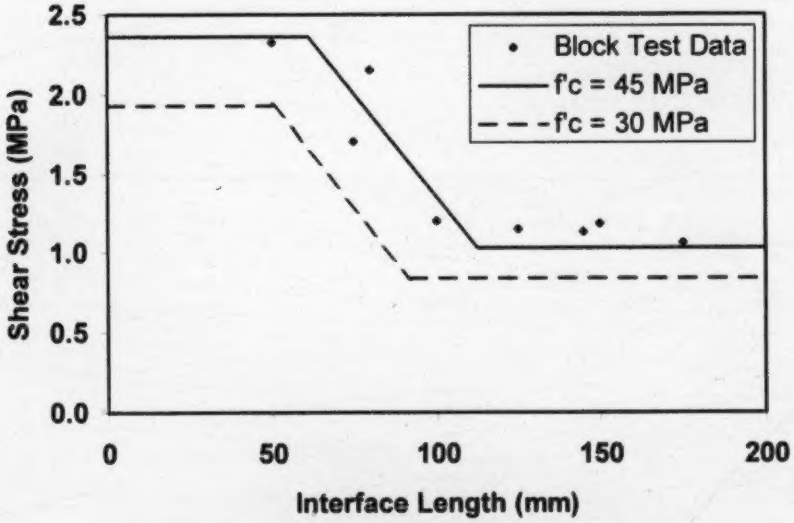

Figure 4.11 Interface Shear Stress Curves

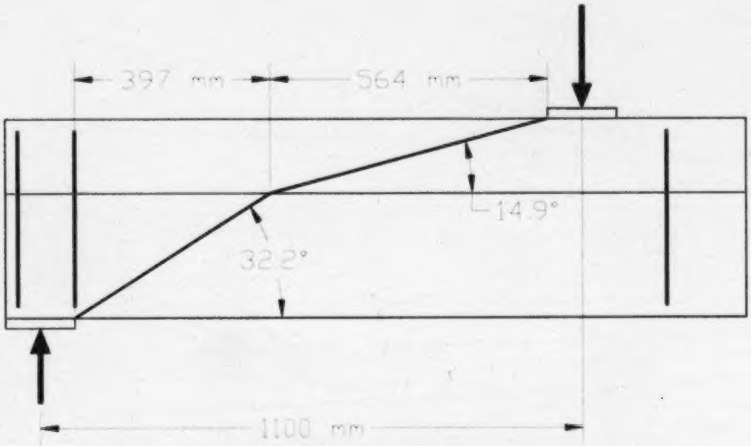
397 mm
564 mm
14.9°
32.2°
1100 mm

Figure 4.12 Crack Pattern Prediction for T4NS

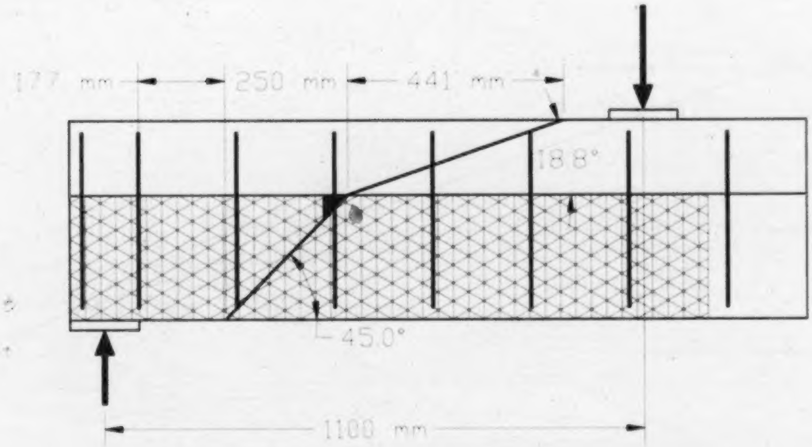
177 mm
250 mm
441 mm
18.8°
45.0°
1100 mm

Figure 4.13 Crack Pattern Prediction for T4S2Tri

4.7 References

AASHTO (1994). *Standard Specifications for Highway Bridges*, 14th edition, Washington, D.C.

ACI-318 (1995). *Building Code Requirements for Structural Concrete*, Detroit, MI.

ALEXANDER J. and CHENG J.J.R. (1998). "Shear Design Model of Concrete Girders Strengthened with Advanced Composite Materials." *Proceedings of Short and Medium Span Bridges (SMSB-5)*, CSCE, Calgary, Alberta.

ALEXANDER J. and CHENG J.J.R. (1997). *Shear Rehabilitation of G-Girder Bridges using CFRP Sheets*, Structural Engineering Report No 218, Department of Civil and Environmental Engineering, University of Alberta, Edmonton, AB, 181 p.

ALEXANDER J. and CHENG J.J.R. (1996). "Field Application and Studies of using CFRP Sheets to Strengthen Concrete Bridge Girders.", *Proceedings of Advanced Composite Materials in Bridges and Structures (ACMBS-2)*, CSCE, Montreal, Quebec, pp. 465-472.

ASTM D-3039M (1995). *Standard Test Methods for Tensile Properties of Polymer Matrix Composite Materials*, Annual Book of ASTM Standards, Philadelphia, Pa.

AL-SULAIMANI G.J., ISTEM A., BASUNBUL A.S., BALUCH M.H. and GHALEB B.N. (1994). "Shear Repair for Reinforced Concrete by Fiberglass Plate Bonding.", *American Concrete Institute Structural Journal*, Vol. 91, No. 3, july-August, pp. 458-464.

CHAJES M. J., FINCH W. W., JANUSZKA T. F., and THOMSON T. A. (1996). "Bond and Force Transfer of Composite Material Plates Bonded to Concrete", *American Concrete Institute Structural Journal*, Vol. 93, No.2, March-April, pp. 208-217.

CHAJES M.J., JANUSZKA T.F., MERTZ D.R., THOMSON T.A. and FINCH W.W. (1995). "Shear Strengthening of Reinforced Concrete Beams using Externally Applied Composite Fabrics", *American Concrete Institute Structural Journal*, Vol. 92, No. 3, May-June, pp. 295-303.

COLLINS M.P. and MITCHELL D. (1987). *Prestressed Concrete Basics;* 1st Edition, Canadian Prestressed Concrete Institute, Ottawa, ON, 614 p.

CSA-A23.3 (1994). *Design of Concrete Structures*, Canadian Standards Association, Rexdale, ON.

CSA-S6 (1988). *Design of Highway Bridges*, Canadian Standards Association, Rexdale, ON.

DENIAUD C. and CHENG J.J.R. (2000). "Evaluation of Shear Design Methods of reinforced Concrete Beams Strengthened with FRP Sheets." *Proceedings of Advanced Composite Materials in Bridges and Structures (ACMBS-3)*, CSCE, Ottawa, ON.

DENIAUD C. and CHENG J.J.R. (1998). "Shear Rehabilitation of Type G-girders using ACM: Experimental Study." *Proceedings of Short and Medium Span Bridges (SMSB-5)*, CSCE, Calgary, AB.

DRIMOUSSIS E.H. and CHENG J.J.R. (1994). *Shear Strengthening of Concrete Girders using Carbon Fiber Reinforced Plastic Sheets*, Structural Engineering Report No 205, Department of Civil Engineering, University of Alberta, Edmonton, AB, 177 p.

JONES R., SWAMY R.N. and CHARIF A. (1988). "Plate Separation and Anchorage of Reinforced Concrete Beams Strengthened by Epoxy-Bonded Steel Plates", *The Structural Engineer*, Vol. 66, pp. 85-94.

LOOV R. (1998). "Review of A23.3-94 Simplified Method of Shear Design and Comparison with Results using Shear Friction", *Canadian Journal of Civil Engineering*, CSCE, Vol. 25, pp. 437-450.

RITCHIE P.A., THOMAS D.A., LU L.W. and CONNELLY G.M. (1991). "External Reinforcement of Concrete Beams using Fiber Reinforced Plastics", *American Concrete Institute Structural Journal*, Vol. 88, No. 4, July-August, pp. 490-500.

SWAMY R.N., JONES R. and BLOXHAM J.W. (1987). "Structural Behaviour of Reinforced Concrete Beams Strengthened by Epoxy-Bonded Steel", *The Structural Engineer*, Vol. 65A, pp. 59-68.

5 SHEAR BEHAVIOUR OF RC T-BEAMS WITH EXTERNALLY BONDED FRP SHEETS[1]

5.1 Introduction

Many concrete bridges in use today were built in the 40s and 50s and have now exceeded their original design life. Meanwhile the code requirements and evaluation specifications have changed and improved over the years with a better understanding of the member behaviour. In particular, the shear requirements have become more stringent for concrete girders (ACI-318, 1995; AASHTO, 1994; CSA-S6, 1988; DRIMOUSSIS and CHENG, 1994). In addition, the allowable traffic loads have also increased over the last few decades. These combined factors lead to many existing bridges structurally deficient, especially in shear.

The rehabilitation or the strengthening of old concrete bridges becomes the new challenge for structural engineers today. In the last ten years, through intensive research and development, Fibre Reinforced Polymer (FRP) sheets have brought new and innovative solutions to this increasingly important market. The low strength to weight ratio, the non-corrodible and magnetically neutral behaviour, and the ease of construction make the FRP very attractive. Although the cost of the FRP products remains high, the reduced labour costs and minimal traffic disturances of an FRP rehabilitation solution make this repair technique competitive compared to more traditional rehabilitation methods.

Most of the past research has focused on the potential use of FRP for the flexural strengthening of concrete beams (SAADATMANESH and EHSANI, 1991; VARASTEHPOUR and HAMELIN, 1997; BUYUKOZTURK and HEARING, 1998). Very little research has been done in the area of using FRP in shear strengthening. Most of the research in shear strengthening has focused on promoting the use of FRP for specific application (DRIMOUSSIS and CHENG, 1994; ALEXANDER and CHENG, 1996; RIAD *et al.*, 1998). Relatively few experimental data in FRP shear strengthening is available for full-scale specimens (ADEY *et al.*, 1997; LAMOTHE *et al.*, 1998; DENIAUD and CHENG, 2000b [Chapter 4]).

---

[1] A version of this chapter has been accepted July 31, 2000 for publication in the *American Concrete Institute Structural Journal*.

This research project studies the interaction of the concrete, the steel stirrups, and the external FRP sheets in carrying shear loads using full-scale reinforced concrete T-beams. The first series of the test results using a beam height of 400 mm was presented in detail in a previous publication (DENIAUD and CHENG, 2000b [Chapter 4]). In this paper, the experimental results of the second series, using a beam height of 600 mm, are reported. The objective of the second series of tests is to further study the effects of different concrete strength and beam size on the shear behaviour of FRP strengthened beams.

5.2 Research significance

An experimental program was conducted using full-scale concrete T-beams strengthened externally using FRP sheets to study the interaction between FRP sheets and steel stirrups in carrying shear load. The test results show that FRP reinforcement significantly increases the maximum shear strengths over beams with no FRP. The magnitude of the increased shear capacity is dependent not only on the type of FRP, but also on the amount of internal shear reinforcement. This paper also presents a design model based on the failure mechanisms of the test specimens. Good agreement was obtained between test and predicted results using the proposed model.

5.3 Experimental Program

5.3.1 Test Specimens

The specimen size of 600 mm represents a typical full-scale beam used in bridges or buildings. The beam was designed to provide a flexural capacity much greater (between 2.0 and 3.5 times) than the shear capacity without FRP contribution. A T-beam shape was then selected and four high-strength Dywidag bars with a 26 mm nominal diameter were provided for the longitudinal reinforcement. The length of the beams was 3.7 m long. Plain, undeformed, steel-closed stirrups (6 mm diameter and 520 MPa yield strength) were used with three different spacings: 200 mm, 400 mm, and no stirrups. Figure 5.1 shows a typical cross section of the T-beams and the layout of the stirrups when 200 mm spacing was used. The specimens were cast with one batch of ready-mix concrete from a local supplier. Ancillary compressive concrete cylinder tests were performed throughout the test program and the average concrete strength was 44.1 MPa.

Three types of FRP were used to externally strengthen the web of the T-beams: a) uniaxial carbon fiber – *Replark Type 20* from Mitsubishi Canada Limited; b) uniaxial glass fibre – SEH51 from Fyfe LLC Limited; and c) triaxial [0°/60°/-60°] glass fibre – from Owens Corning. The glass fibres were applied at right angles along the full length of the shear span. The carbon fibre sheets were glued at 45^{o} or 90^{o} angles to the longitudinal beam axis with a width of 50 mm and a gap of 50 mm perpendicular to the direction of the fibres. In all cases, the fibres were extended underneath the flange to provide a minimum anchor length of 100 mm and wrapped under the web. All the FRP sheets were bonded to the specimens prior to the test. Coupon specimens were prepared in accordance with ASTM Standard D-3039M (1995) when the FRP sheets were glued to the test beams. Table 5.1 summarizes the material properties of the FRP sheets.

This test series tested four beams, but because both ends of each beam were tested separately, a total of eight tests were conducted. Table 5.2 presents the test matrix for these eight tests. A four character name designation was used: T6S*n* or T6NS, where T6 indicated a T-shape beam with 600 mm depth; S*n* was S2 or S4 indicating 200 mm or 400 mm stirrup spacing, respectively; and NS was for no internal stirrup. An additional designation was added to indicate the fibre type used: C45 – carbon fibre in 45°, G90 – glass fibre in 90°, and Tri – glass fibre in 0°/60°/-60°.

5.3.2 Test Set-up

The test set-up, shown in Figure 5.2, consisted of a four-point loading system that created a region of constant moment at mid span. In order to fail the beam in the tested shear span, external stirrups were provided to strengthen the non-tested span. These stirrups consisted of two HSS steel tubes with tie rods on either end.

Four longitudinal Dywidag bars were extended 150 mm from the ends of the beams and anchored with a 50 mm thick steel plate. L-shaped steel angles were also used on each side of the web as a passive confinement for the anchor zone of the flexural reinforcement. These details (plate and angles), shown in Figure 5.2, were included to prevent longitudinal de-bonding failure.

5.3.3 Instrumentation

Up to 20 electrical strain gauges were mounted on the FRP sheets on one side of the T-beam. These gauges were all vertically orientated, except when a set of three gauges was placed to form a strain rosette in order to determine the principal strains and directions. The opposite side of the T-beam was instrumented with a number of sets of Demec gauges, as shown in Figure 5.3. A Demec gauge of 200 mm was used for most of the measurements. However, a Demec gauge of 50 mm was used to record vertical or inclined at 45° strains on the side of the web when FRP sheets were glued.

Nine electrical strain gauges were mounted along the full length of each Dywidag bar. Both legs of each stirrup located in the shear span were also instrumented at mid height. These gauges were protected with waterproof coating and silicone prior to casting the concrete.

The flexural deflection was recorded at mid span with one cable transducer. A total of 12 horizontal Linear Variable Differential Transformers (LVDTs) were also installed at three locations (section #4, section #6, and section #8 in Figure 5.2) within the shear span (470 mm, 870 mm, and 1270 mm from the support, respectively) and at mid span of the T-beam. They were used to measure the strain distribution through the depth of the beam. At each section, a steel apparatus was fixed on the side of the beam to hold three LVDTs at various elevations (see Figure 5.3).

The two load cells provided at each support were used to record the total load applied on the top of the beam. The dead load of the specimen is not included in any of the results presented here.

5.4 Experimental Results

The total loads applied at ultimate on the top of the beam for each test are reported in Table 5.3. The strain distribution through the depth of the beam was recorded with the LVDT data using the least square method. The compression strain at the extreme fibre of the concrete was calculated with a best fit line, first using all three LVDTs and then with only the top two. The coefficient of variation (COV) could then be evaluated with these two values of the compression strain. At mid span the COV varied from 2% to 8% for all the tests. This validates the assumption that plane sections remain plane. However, at sections #4, #6, and #8 (470 mm, 870 mm, and 1270 mm from the support, respectively) the COV increases drastically, much greater than 8%, after certain loads, thus implying that the plane section does not remain plane in the shear span. Table 5.3 summarizes the corresponding loads for each test when the plane section no longer remains plane at these three locations.

For ease of comparison, the loads and deflections obtained from each test were normalized to the weakest beam test results with no stirrup and no FRP reinforcement (T6NS). Figures 4 and 5 show the normalized load vs. the normalized deflection for two different stirrup spacing arrangements. Figure 5.6 shows the effect of the stirrup spacing with the use of carbon fibre bands. The normalized ultimate loads and the resultant net increase in shear strength over the respective control specimen are summarized in Table 5.3.

The shear force V can be expressed by a combination of two components: arching action and beam action. At any location in a beam when a moment gradient $\frac{dM}{dx}$ is present, these two effects are combined to give the total shear resistance. For a cracked concrete member, these components can be written as follows:

[5.1] $$V = \frac{dM}{dx} \quad \text{and} \quad M = T \cdot jd$$

where T and jd are the tensile force in the bottom chord and lever arm, respectively. Thus,

[5.2] $$V = T\frac{djd}{dx} + jd\frac{dT}{dx}$$

The first term of the above equation refers to the arching action while the second term describes the beam behaviour. These two effects can be evaluated between two known sections along the length of the beam, thus Equation (5.2) can be re-written as:

[5.3] $$V = T\frac{\Delta jd}{\Delta x} + jd\frac{\Delta T}{\Delta x}$$

where Δ represents the change between two sections.

The recorded strain gauge data in Dywidag bars between sections #4 and #6, and #6 and #8, and the applied shear V, allow all terms in Equation (5.3) to be calculated. Beam and arching actions were calculated between sections #4 and #6, and #6 and #8, using

Equation (5.3). Table 5.4 summarizes the change of full beam action to partial arching action, the equal share between beam and arching actions, and the remaining beam action at the maximum load. It shows that shear force starts out being carried entirely by beam action, but ends with arching action as predominant. The load at which beam and arching actions share equally in carrying the applied shear is also given in the table.

Using the Demec and strain gauges on the FRP sheets, the strain distribution in the vertical direction along the shear span of the beam was drawn by interpolation from the known scattered gauge locations. Figure 5.7 shows a typical distribution with concrete cracks superimposed. Additional FRP strain distributions are presented in Appendix C.4.

5.5 Discussion

5.5.1 Initial Flexural Stiffness

Figure 5.4 to Figure 5.6 show that the initial slope of the curves remains identical for all the tests. Thus, the external and internal shear reinforcements did not increase the initial stiffness of the beams. However, the ultimate loads and the ductility of the beam were, of course, affected by the shear reinforcement provided.

5.5.2 Number of Stirrups

The increasing amount of internal reinforcement reduced the net increase of the FRP sheets with respect to the ultimate load. Take the carbon fibre sheet reinforcement for example: the CFRP sheets increased the shear carrying capacity by 94% for the specimen with no stirrup, but with s = 400 mm, the stirrups provided 70% increase and the CFRP sheets shear contribution was down to 78% for a total increase of the beam shear capacity of 148% (see Table 5.3). In previous tests (DENIAUD and CHENG, 2000a [Chapter 3]) the fibres oriented at 45° were found to be more effective than at 90°, but by only 7%. Thus, the change in the angle of the FRP bands orientation from 45° to 90° cannot solely explain the 17% drop in shear load carried by the carbon fibres. Furthermore, with s = 200 mm, the ultimate load of specimen T6S2C90 did not reach the maximum load of the corresponding control specimen (T6S2). This result seems, at first, a contradiction in engineering judgement, but this particular test is discussed in more detail below.

5.5.3 Strain Distribution through the Depth

For almost all the tests, the data recorded by the LVDTs (Table 5.4) shows that section #4, located at 470 mm from the support, did not behave as a plane section from the very beginning of each test. Section #6, 870 mm from the support, generally lost its plane section behaviour before section #8, 1270 mm from the support, except for T6S4C90 and T6S2. The external FRP reinforcement, however, delayed the non-plane section behaviour in all cases but one (T6S2C90).

5.5.4 Beam and Arching Actions

The FRP sheets delayed the formation of the concrete strut, as shown for most cases in Table 5.4. The contribution of the two shear action modes can be seen graphically by the normalized load and deflection curves, as shown in Figure 5.8 with typical examples using s = 400 mm and the tri-axial glass fibres (see also Appendix C.3 for additional curves). When FRP sheets were used, the shear load carried by beam action reached the ultimate load level of the corresponding control test. No noticeable differences between sections #4 and #6, and #6 and #8 were also observed in terms of the ratio of the beam and arching action; however, the delay in the strut formation was less pronounced with the FRP sheets when the stirrups were spaced at 200 mm.

5.5.5 FRP Strains

The FRP strain distribution in the vertical direction shown in Figure 5.7 gives valuable information on the behaviour of the FRP sheets. The measured maximum FRP strains at ultimate have reached values from 4000 to 6000 $\mu\varepsilon$. These strain levels were similar to those observed in the previous series (DENIAUD and CHENG, 2000b [Chapter 4]) and were well below the ultimate strain in tension that such FRP can sustain (see Table 5.1). Figure 5.7 shows that the fibres crossing a concrete crack experienced the same level of strain along the path of the crack. In other words, the load carried by the FRP sheet crossing the crack is uniformly distributed among those fibres. This observation differs from the linear strain distribution assumption made by others and by the authors in previously published work (ALEXANDER and CHENG, 1997; DENIAUD and CHENG, 2000b [Chapter 4]).

5.5.6 Failure Modes

5.5.6.1 General

All the tests failed in shear with the formation of a web shear concrete crack, which extended through the flange at ultimate. Photographs of all the failed specimens can be found in Appendix C.1. Two major concrete cracks appeared during the test, crossing at mid height of the sections #4 and #6, and at 470 and 870 mm, respectively. The critical shear crack path that led to failure was always the one close to the support. The angle of the principal strains, recorded with the Demec rosettes, got flatter at ultimate from 35° to 27° and 22° when the internal shear reinforcement decreased from s = 200 mm to s = 400 mm and no stirrups, respectively, for the three control tests. The flexural capacity of the beam was never reached as the measured Dywidag strains at mid span were always below the yield strain.

5.5.6.2 Carbon Fibre Sheets

The CFRP bands at 90° started to debond at section #5, located at 600 mm from the support, above a concrete crack that was crossing the fibres at about 60 to 75 mm below the flange. When further loads were added to the specimen, the band between sections #4 and #5 (500 mm from the support) peeled off. The shear load was then too high to be carried by the remaining strips. Thus, all the bands located between section #5 and the support peeled off in a very sudden manner above the concrete crack, as shown in Figure 5.9. The CFRP sheets at 45° also debonded all at once in a very sudden manner.

5.5.6.3 Glass Fibre Sheets

The GFRP sheets showed a debonded area surrounding the path of the crack. Once the debonded surface reached the flange, the debonding process accelerated along the corner of the web-flange toward the support. Eventually a large trapezoidal shape of debonded sheets formed close to the support. Figure 5.10 shows the typical debonded area growing process in the sheets as the load increased. Additional schematic debonding growths can be found in Appendix C.2.

Once a large area of GFRP sheets was debonded, the sheets behaved like a very thin shell. The compression concrete strut that formed ended up buckling the FRP sheets as shown in Figure 5.11 with the tri-axial glass fibres. Similar buckling was observed with the SEH51 glass fibres, but with a lower amplitude. Because the SEH51 product is not quasi-elastic, like the tria-axial fibres, it ended up tearing (unzipping) close to the support when vertical tensile strains started to appear at the top of the flange. This typical failure mode was also observed in smaller beams (DENIAUD and CHENG, 2000b [Chapter 4]).

5.5.7 T6S2C90 Test

This test was the most reinforced in shear, with a combination of internal stirrup at 200 mm and external CFRP bands. However, the maximum load for this test did not even reach the corresponding load of the control test with no CFRP. The load difference represented only 13% between these two tests. The variability of the experimental specimens can partly explain this behaviour. The T6S2C90 test failed suddenly when the CFRP bands debonded as described above. Inspection of the failed beam showed that the stirrups were cut at the shear crack locations. The recorded stirrup strains from both tests gave some clues to explain this unexpected premature failure. As shown in Figure 5.12, the stirrups of the T6S2C90 test barely reached their yield strain prior to failure of the CFRP bands. However, with the T6S2 test, four stirrups have clearly yielded well before the ultimate load was reached. The authors thus believe that at the time the CFRP failed, the energy released to the stirrups was so great that the beam slipped along the web shear crack and snapped the stirrups.

5.6 Mechanical Design Model

The evaluation of the shear capacity of the beams was performed using the combination of the strip method and the shear friction method described in a previous paper (DENIAUD and CHENG, 2000b [Chapter 4]). However, some modifications were added to this model based on the experimental observations from this test series as well as further improvements in the shear friction approach. These two methods are reviewed briefly and the modifications are presented below.

5.6.1 Strip Method

ALEXANDER and CHENG (1998) developed the strip method to evaluate the FRP sheet contribution. The FRP sheets crossing the concrete web crack are described as a series of strips. Each strip is evaluated individually to find its maximum allowable strain from the geometry of the FRP sheets. The geometry includes the bonded length of the strip above and below the crack as well as the anchorage of each end of the strip (rounded and bonded underneath the flange and wrapped at the bottom of the web in this case). Initially, this method assumed that the load was linearly distributed among the fibres; however, the experimental results presented in Figure 5.7 show a uniform strain distribution rather than a linear distribution. Thus, the uniform distribution was used to reflect the true behaviour of the fibres.

Figure 5.13 shows the interface mean shear stress curve developed from experimental concrete block tests (ALEXANDER and CHENG, 1997). This curve was used to evaluate the bond strength and the corresponding maximum allowable strain ε_x of each strip. From the uniform strain distribution assumption, the same strain level is applied to all the FRP strips crossing the concrete web shear crack. The maximum allowable strain ε_x of the strip close to the web-flange corner is very small due to the small bond length and will fail first, thus starting the sequential peeling off. The load is then redistributed to the remaining strip with a larger critical ε_x. Eventually, as the critical ε_x increases, the number of remaining strips decreases until the load carried by the remaining FRP strips reaches a maximum. At this point the maximum FRP strain ε_{max} as well as the ratio R_L (remaining bonded length over total length) are recorded.

5.6.2 Shear Friction

Recently, LOOV (1998) reviewed the simplified method of shear design and compared it with results using the shear friction method. Both methods are described in ACI-318 (1995) and Canadian Concrete Design Standard CSA-A23.3 (1994). He found that among all potential failure planes along which slippage can occur, the lowest shear strength is the governing shear strength. Using the shear friction method, the general equation of the shear strength of a beam having a cracking angle θ can be written as follows:

[5.4] $$V_r = 0.25 k^2 f_c' b_w h \tan\theta \quad + \quad T_v n_s$$

where k is an experimentally-determined factor; b_w and h are the width of the effective web and the height of the beam, respectively; T_v is the tension force in the stirrups and n_s is the total number of stirrups, if any, crossing the concrete shear failure plane at angle θ.

The experimentally-determined factor k is usually taken as 0.5 for normal concrete strength. However, Loov and Peng (1998) found that the value of k needed to be substantially reduced with higher concrete strengths based on the test results. From a least squares fit of given data with a concrete strength ranging from 20 to 100 MPa they proposed the following equation:

$$k = 2.1\left(f'_c\right)^{-0.4} \qquad [5.5]$$

Recently, Tozser and Loov (1999) observed that the concrete area $b_w h$ was too conservative for T-beams and I-beams. They suggested approximating the effective section of the flange that participates in the shear friction with a 45° angle as shown in Figure 5.14.

Equation (5.4) is then re-written to include the contribution of the FRP sheets and to account for the effective flange area. Thus, we obtain:

$$V_r = 0.25 k^2 f'_c \left(A_{cf} \tan\theta_f + A_{cw} \tan\theta_w\right) + T_v n_s + \frac{d_{FRP} t E_{FRP} \varepsilon_{max}}{\tan\theta_w} R_L \qquad [5.6]$$

A_{cf} is the effective concrete flange area and A_{cw} is the concrete web area, which is equal to the web height h_w times the web width b_w. The subscripts f and w stand for *flange* and *web*, respectively. d_{FRP} is the height of the FRP sheets glued to the web of the beam (for this particular case, $d_{FRP} = h_w$). t and E_{FRP} are the thickness and the modulus of elasticity of the FRP sheets, respectively.

The governing shear strength is the lowest shear strength given by Equation (5.6) among all the potential failure planes. A computer program was written to find the most critical shear path given the layout of the stirrups for each test and the shear span. The results are summarized in detail in Table 5.5.

5.6.3 Comments

The predicted shear capacities are in very good agreement with the test results. The V_{exp} over V_r ratios are close to one and the two unconservative predictions are within 10%. These two specimens failed by FRP buckling, but, unfortunately, the mechanical model used in its present form does not include this failure mode. The V_{exp}/V_r ratio for the test T6S2 presents the only high value, which also suggests an unusually strong specimen.

The FRP strains ε_{max} used in the mechanical model are similar to the observed values. The theoretical shear failure plane and, thus, the web and flange shear plane angles, are also in very good agreement with the experimental crack patterns. The uniform load distribution among the FRP strips seems adequate and gives reasonable results. Assuming a uniform strain distribution also makes the model easier to implement.

The total number of stirrups n_s crossing the concrete shear path reduces when the specimen is strengthened with FRP sheets. In other words, the FRP sheets change the critical shear path by increasing the web crack angle in the same manner as an increased amount of internal reinforcement does (see Table 5.5).

5.7 Conclusion

This series of tests investigated the behaviour of reinforced concrete T-beams with external FRP shear strengthening and with a beam height of 600 mm. Several conclusions can be drawn and are summarized below:

1. The contribution of the FRP sheets to the shear capacity of the beam is dependent on the amount of internal reinforcement. The FRP sheets are less effective when beams are heavily reinforced internally. The external FRP reinforcement can eventually reduce the shear capacity of the beam by changing the critical path that will lead to an even more sudden shear failure.
2. The FRP strains are uniformly distributed among the FRP strips crossing the concrete shear crack.
3. The failure mode of the beams strengthened with FRP is characterized by the debonding and the peeling of the sheets above the concrete shear crack. The debonded sheets then buckle like a thin shell when the sheets are continuously wrapped. The deep web height contributes largely to this behaviour.
4. The plane sections do not remain plane in the shear span after a certain load level is reached, but the external FRP sheets delay the loss of the plane section behaviour.
5. Arching action is delayed when FRP is used. Beam action can often represent over 40% of the ultimate load when FRP are used.
6. The mechanical design model based on combination of the strip method and the shear friction approach calculates predicted values that are in very good agreement with the

experimental results. The behaviour of the beams strengthened by FRP sheets can be evaluated and described by using the proposed design model.

Table 5.1 Fibre Reinforced Polymer Material Properties

FRP Name	Type of Fibres	Test source	Ultimate Strength *MPa*	Modulus of Elasticity *MPa*	Thickness *mm*
Replark Type 20	Carbon	Fibre strength	3400	230000	0.11
(Mitsubishi)		Coupon specimens	422	44800	0.70
Triaxial	Glass	Fibre strength	-	-	-
(Owens Corning)		Coupon specimens	124	8100	2.10
SEH51	Glass	Fibre strength	-	-	-
(Fyfe LLC)		Coupon specimens	106*	17700	1.80

* Premature failure

Table 5.2 Test Matrix of the T600 Series

Specimen	Stirrup Spacing *mm*	External FRP Reinforcement
T6NS	None	None
T6NSC45	None	Carbon sheets *Replark Type 20* at 45° (50 mm wide, 50 mm gap)
T6S4	400	None
T6S4C90	400	Carbon sheets *Replark Type 20* at 90° (50 mm wide, 50 mm gap)
T6S4G90	400	Glass fibres SEH51 at 90° (No gap)
T6S4Tri	400	Tri-axial glass fibres (No gap)
T6S2	200	None
T6S2Tri	200	Carbon sheets *Replark Type 20* at 90° (50 mm wide, 50 mm gap)

Table 5.3 Maximum Loads and Loads Corresponding to the Change of Behaviour when Plane Section no Longer Remains Plane

Test	Maximum Load *kN*	Normalized Load	At Section #4 *kN*	At Section #6 *kN*	At Section #8 *kN*
T6NS	220.2	1.00	0.0	204.7	213.7
T6NSC45	427.2	1.94	0.0	378.6	427.2
T6S4	375.1	1.70	154.5	288.8	343.8
T6S4C90	545.6	2.48	0.0	500.7	461.8
T6S4G90	594.9	2.70	0.0	404.5	518.4
T6S4Tri	633.4	2.88	0.0	462.9	608.5
T6S2	713.7	3.24	0.0	389.0	235.7
T6S2C90	619.6	2.81	n.a.	363.5	n.a.

Table 5.4 Beam and Arching Shear Actions

	Between sections #4 and #6			Between sections #6 and #8		
Test	Beam action until *kN*	Equal share *kN*	Remaining beam action at P_{max}	Beam action until *kN*	Equal share *kN*	Remaining beam action at P_{max}
T6NS	92.6	96.8	34.4%	50.9	70.0	20.7%
T6NSC45	136.0	157.4	38.8%	171.6	187.7	39.4%
T6S4	72.4	150.3	26.8%	45.5	132.0	43.1%
T6S4C90	56.0	-	52.5%	142.3	204.0	36.8%
T6S4G90	122.7	235.1	21.1%	111.7	201.4	7.8%
T6S4Tri	106.9	298.9	31.5%	158.3	291.0	20.4%
T6S2	106.1	121.6	25.0%	92.8	166.7	8.3%
T6S2C90	72.5	299.3	46.3%	127.3	330.1	44.8%

Table 5.5 Mechanical Model Results

Test	θ_w *deg*	θ_f *deg*	ε_{max} %	R_L	n_s	V_r *kN*	V_{exp}/V_r
T6NS	25.2	18.2	-	-	-	103.2	1.067
T6NSC45	27.1	15.7	0.471	0.891	-	148.1	1.443
T6S4	28.4	19.1	-	-	2	173.7	1.079
T6S4C90	31.4	15.3	0.469	0.851	1	223.0	1.224
T6S4G90	45.4	18.5	0.468	0.851	1	326.0	0.912
T6S4Tri	45.4	18.5	0.536	0.851	1	326.4	0.970
T6S2	31.8	22.2	-	-	4	250.4	1.425
T6S2C90	39.3	24.5	0.469	0.851	3	289.8	1.069

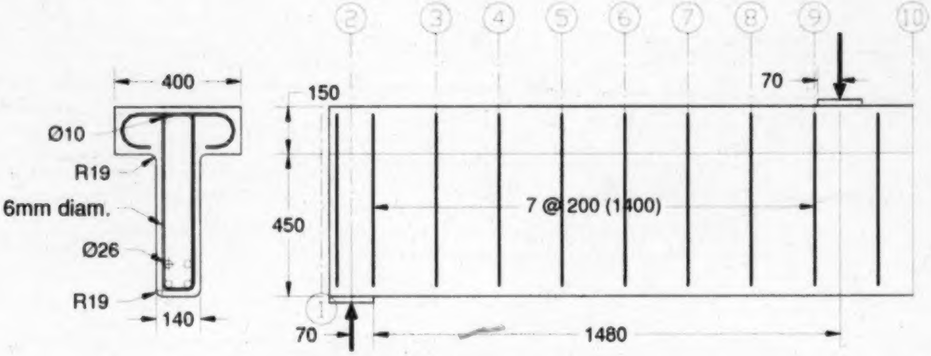
②
③
④
⑤
⑥
⑦
⑧
⑨
⑩
400
Ø10
R19
6mm diam.
Ø26
R19
140
150
70
450
7 @ 200 (1400)
①
70
1480

Figure 5.1 T-beam Cross Section and Stirrup Layout with 200 mm Spacing

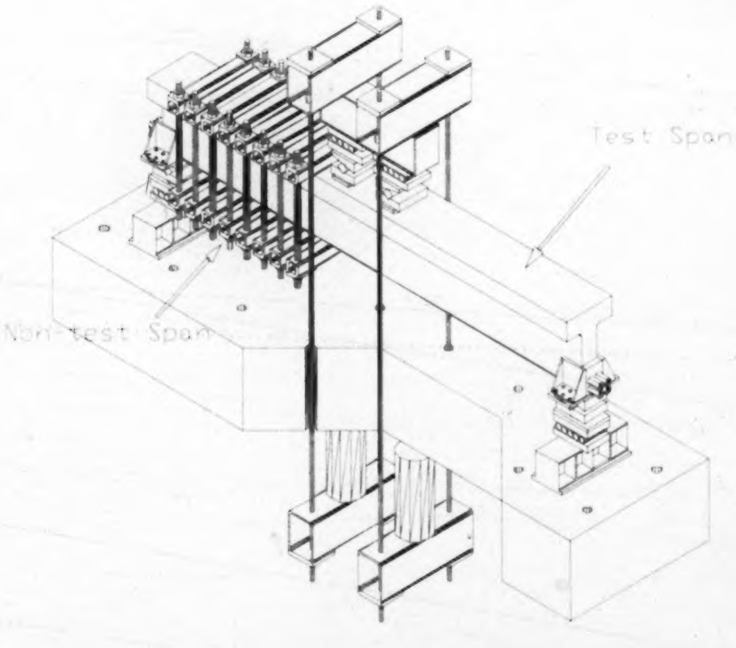
Test Span
Non-test Span

Figure 5.2 Isometric View of the Test Set-up

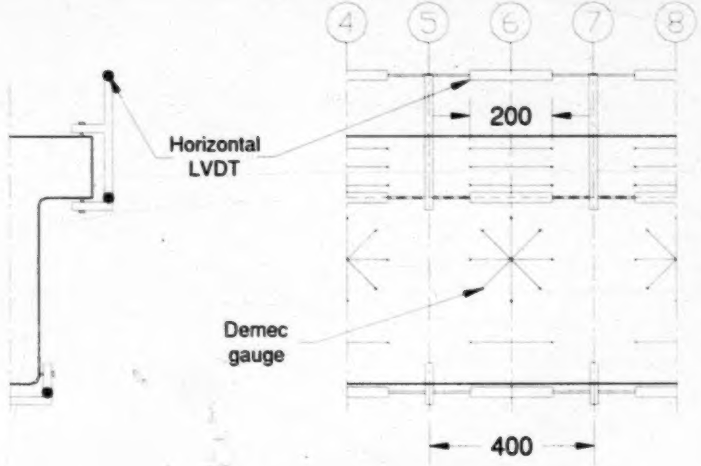
4
5
6
7
8
200
Horizontal LVDT
Demec gauge
400

Figure 5.3 Horizontal LVDT Apparatus

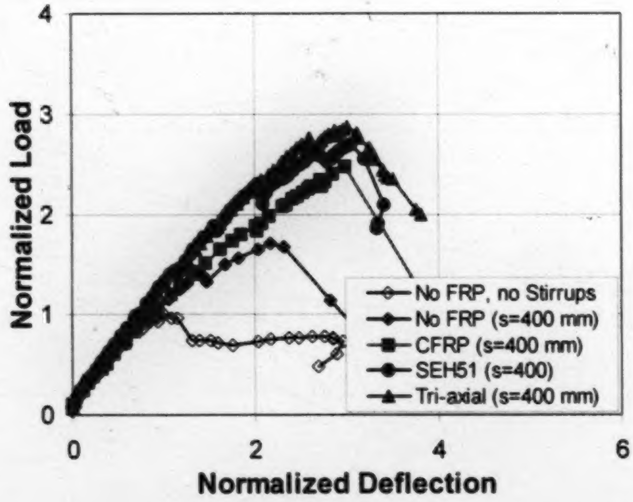

Figure 5.4 Normalized Load Deflection Curves with 400 mm Stirrup Spacing

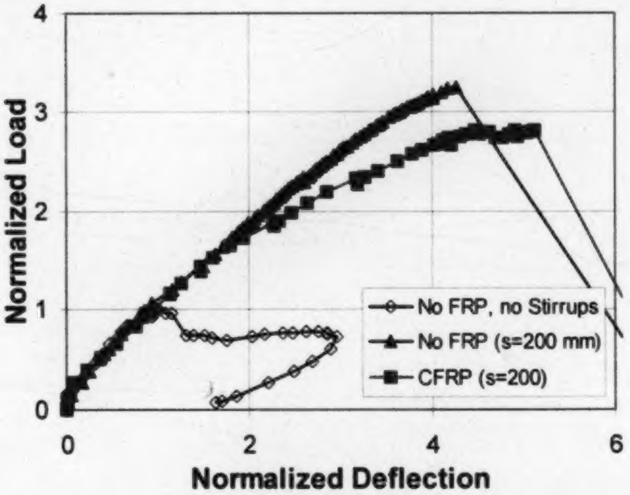

Figure 5.5 Normalized Load Deflection Curves with 200 mm Stirrup Spacing

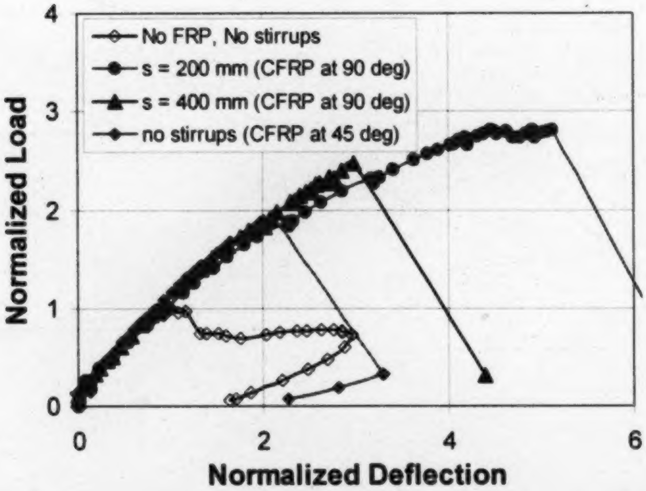

Figure 5.6 Normalized Load Deflection Curves with Carbon Fibre Sheets

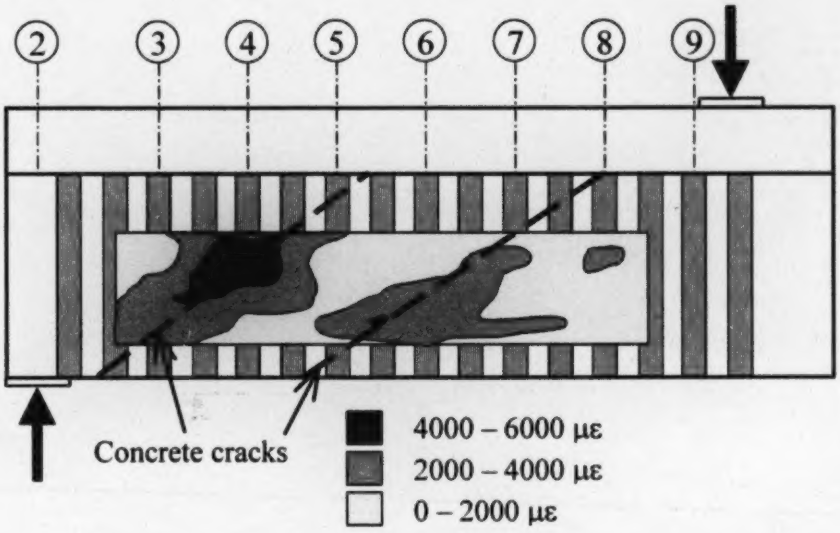
②
③
④
⑤
⑥
⑦
⑧
⑨
Concrete cracks
4000 – 6000 με
2000 – 4000 με
0 – 2000 με

Figure 5.7 FRP Strain in the Vertical Direction with T6S4C90 at 501 kN

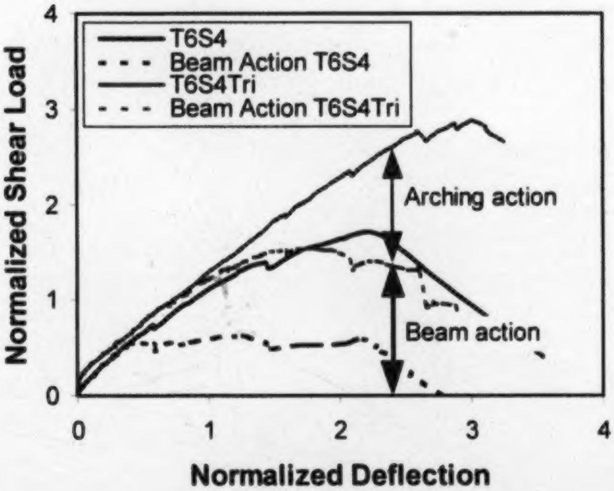

Figure 5.8 Beam and Arching Shear Actions with 400 mm Stirrup Spacing

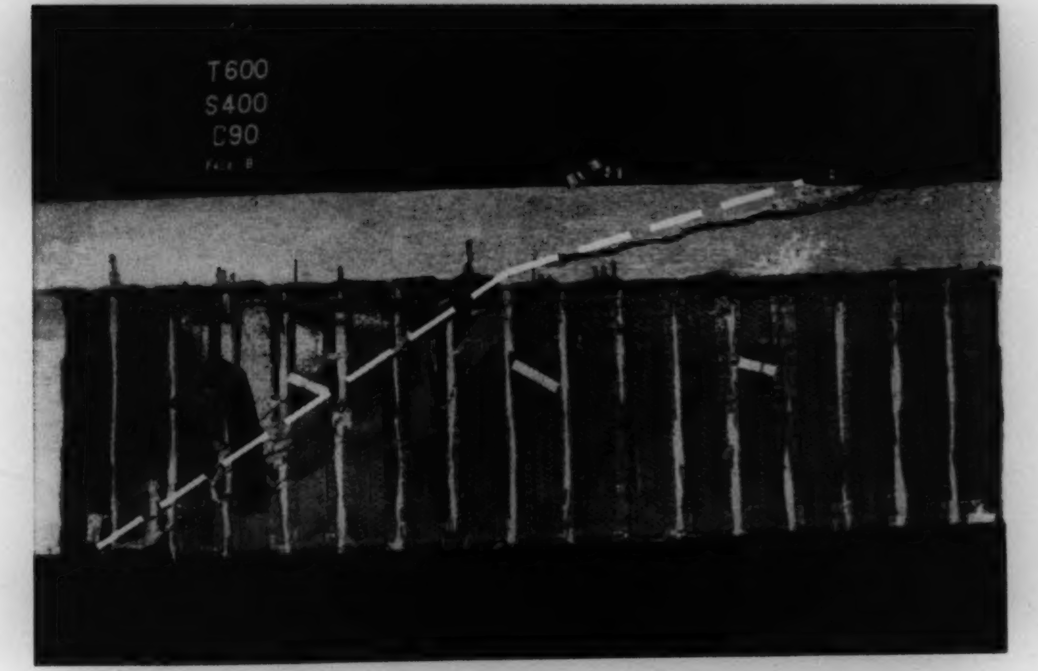
T600
S400
C90
Face B

Figure 5.9 Photo of the Debonded Carbon Bands for T6S4C90

At 506 kN

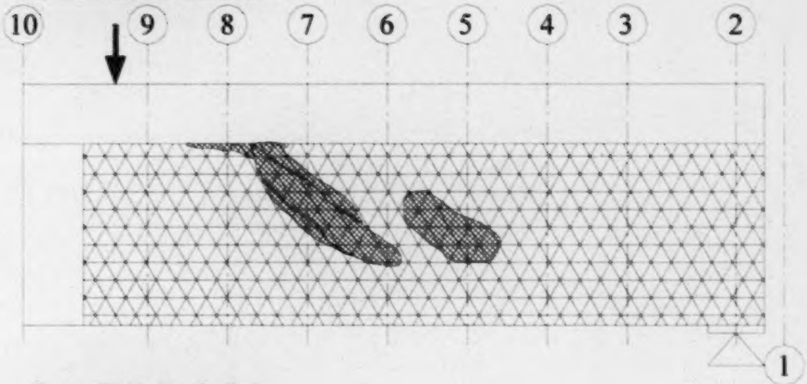
10
9
8
7
6
5
4
3
2
1

At 589 kN

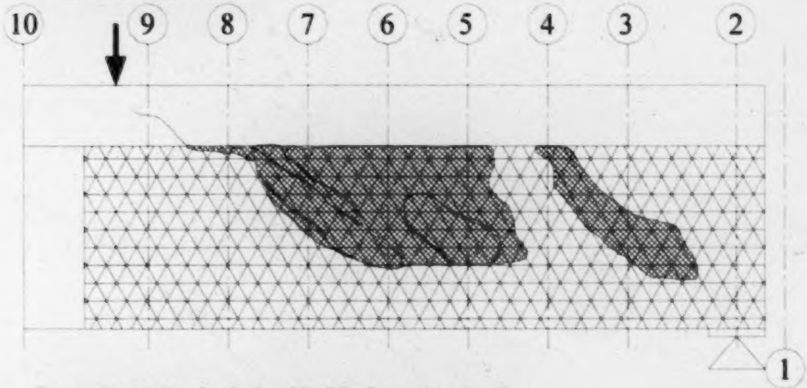
10
9
8
7
6
5
4
3
2
1

At 633 kN (Ultimate)

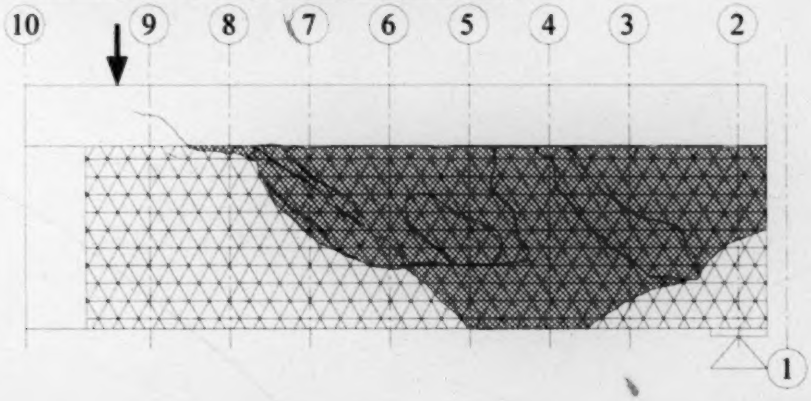
10
9
8
7
6
5
4
3
2
1

Figure 5.10 Schematic FRP Debonding Growth

Figure 5.11 Photo of the Debonded Tri-Axial Glass Fibre Sheets

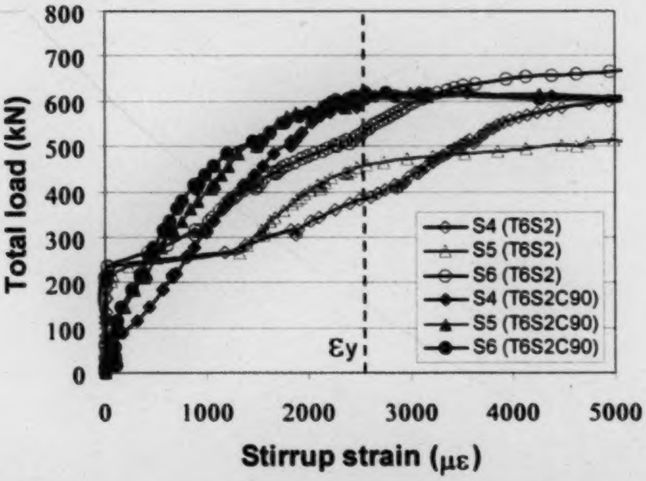

Figure 5.12 Stirrup Strains Comparison with 200 mm Spacing

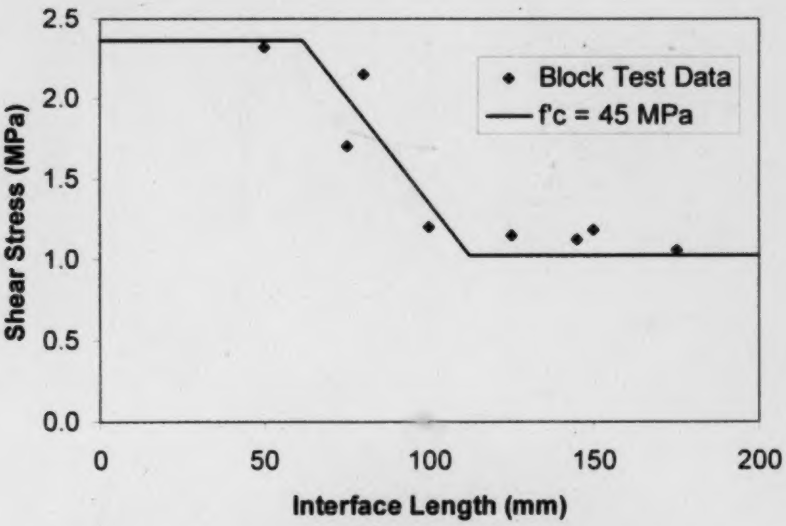

Figure 5.13 Interface Mean Shear Stress Curve

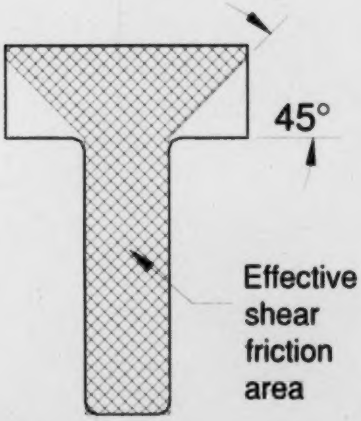
45°
Effective
shear
friction
area

Figure 5.14 Effective Shear Friction Concrete Area

5.8 References

AASHTO (1994). *Standard Specifications for Highway Bridges*, 14th edition, American Association of State Highway and Transportation Officials, Washington, DC.

ACI-318 (1995). *Building Code Requirements for Reinforced Concrete*, American Concrete Institute, Farmington Hills, MI.

ADEY B., SAN-ROMÁN J. d. C., and BRÜHWILLER E. (1998). *Carbon Fibre Shear Strengthening of Rectangular Concrete Beams*, Final Report - 97.02, École Polythechnique de Lausanne, Lausanne, Switzerland, 28 p.

ALEXANDER J. and CHENG J.J.R (1998). "Shear Design Model of Concrete Girders Strengthened with Advanced Composite Materials", *Proceeding of Short and Medium Span Bridges (SMBS-5)*, CSCE, Calgary, AB.

ALEXANDER J. and CHENG J.J.R. (1997). *Shear Rehabilitation of G-Girder Bridges using CFRP Sheets*, Structural Engineering Report No 218, Department of Civil and Environmental Engineering, University of Alberta, Edmonton, AB, 181 p.

ALEXANDER J. and CHENG J.J.R. (1996). "Field Application and Studies of using CFRP Sheets to Strengthen Concrete Bridge Girders", *Proceedings of Advanced Composite Materials in Bridges and Structures (ACMBS-2)*, CSCE, Montreal, PQ, pp. 465-472.

ASTM D-3039M (1995). "Standard Test Methods for Tensile Properties of Polymer Matrix Composite Materials", Annual Book of ASTM Standards, Philadelphia, PA, pp. 98-144.

BUYUKOZTURK O. and HEARING B. (1998). "Failure Behavior of Precracked Concrete Beams Retrofitted with FRP", *Journal of Composites for Construction*, ASCE, Vol. 2, No. 3, August, pp 138-144.

CSA-S6 (1988). *Design of Highway Bridges*, Canadian Standard Association, Rexdale, ON.

CSA-A23.3 (1994). *Design of Concrete Structures*, Canadian Standard Association, Rexdale, ON.

DENIAUD C. and CHENG J.J.R. (2000a). "Shear Rehabilitation of G-Girders Bridges in Alberta using FRP Sheets", Accepted for publication in *Canadian Journal of Civil Engineering* (in press) [Chapter 3].

DENIAUD C. and CHENG J.J.R. (2000b). "Reinforced Concrete T-beams Strengthened in Shear with FRP Sheets", Accepted for publication in *Journal of Composites for Construction* [Chapter 4].

DRIMOUSSIS E.H. and CHENG J.J.R. (1994). *Shear Strengthening of Concrete Girders using Carbon Fiber Reinforced Plastic Sheets*, Structural Engineering Report No 205, Department of Civil and Environmental Engineering, University of Alberta, Edmonton, AB, 177 p.

LAMOTHE P., LABOSSIÈRE P. and NEALE K. W. (1998). "Post-Strengthening of Reinforced Concrete T-Beams with Composite Materials", *Proceedings of the Annual Conference of the CSCE*, CSCE, Halifax, NS, pp 623-631.

LOOV R. (1998). "Review of A23.3-94 Simplified Method of Shear Design and Comparison with Results using Shear Friction", *Canadian Journal of Civil Engineering*, CSCE, Ottawa, ON, Vol. 25, No. 3, April, pp. 437-450.

LOOV R. and PENG L. (1998). "The Influence of Concrete Strength on Shear Friction based Design of Reinforced Concrete Beams", *Proceedings of the International Conference on HPHSC*, Perth, Australia, pp. 505-519.

RIAD A., SAYED-AHMED E.Y., TADROS G., LOOV R., and SHRIVE N.G. (1998). "Design Recommendations for HC-Type Bridge Girders Retrofitted with CFRP-Strips", *Proceedings of Short and Medium Span Bridges (SMBS-5)*, CSCE, Calgary, AB.

SAADATMANESH H. and EHSANI M. R. (1991). "RC Beams Strengthened with GFRP Plate I: Experimental Study", *Journal of Structural Engineering*, ASCE, Vol. 117, No. 11, November, pp. 3417-3433.

TOZSER O. and LOOV. R. (1999). "Shear Design of Prestressed Beams using Shear Friction", *Proceedings of the Annual Conference of the CSCE*, CSCE, Regina, SK, pp. 195-204.

VARASTEHPOUR H. and HAMELIN P. (1997). "Strengthening of Concrete Beams using Fiber-Reinforced Plastics"; *Materials and Structures*, RILEM, Cachan, France, V. 30, No. 197, April, pp. 160-166.

6 REVIEW OF SHEAR DESIGN METHODS FOR RC BEAMS STRENGTHENED WITH FRP SHEETS[1]

6.1 Introduction

The rehabilitation of concrete structures using Fibre Reinforced Polymer (FRP) materials has become a growing area in the construction industry over the last few years. Many research projects in Canada and elsewhere in the world were carried out to promote this efficient repair technique to extend the service life of existing concrete structures (NEALE, 2000). The low strength to weight ratio, the non-corrosive and magnetically neutral properties, and the ease of construction make the FRP very attractive. Most of the research and development in this area was focused on the flexural reinforcement (SAADATMANESH and EHSANI, 1991; VARASTEHPOUR and HAMELIN, 1997; BUYUKOZTURK and HEARING, 1998). As a result, the flexural design methods are well developed and accepted in design offices. In opposition, few researchers have proposed design methods to evaluate the shear capacity of beams strengthened in shear by FRP.

Reinforced concrete beams strengthened in shear using externally bonded FRP sheets were investigated successfully with laboratory controlled specimens (AL-SULAMANI *et al.*, 1994; CHAJES *et al.* 1995; HUTCHINSON, 1999). Girders removed from existing bridges were also strengthened in shear with FRP and tested in laboratory (DRIMOUSSIS and CHENG, 1994; ALEXANDER and CHENG, 1997; DENIAUD and CHENG, 2000a [Chapter 3]). The Strut-and-Tie model, the Modified Compression Field Theory (MCFT) and the shear friction method (CSA-A23.3, 1994) were used to evaluate the test results and were found to yield reasonable and conservative predictions (DENIAUD AND CHENG, 2000a [Chapter 3]). These three methods are commonly used in design offices and were slightly modified to account for the contribution from the FRP sheets.

In 1998, several researchers developed design equations and analytical models to evaluate specifically the FRP contribution to the shear strength of reinforced concrete beams (TRIANTAFILLOU; MALEK and SAADATMANESH; KHALIFA *et al.*; CHAALLAL *et al.*).

---

[1] A version of this chapter has been accepted September 20, 2000 for publication in the *Canadian Journal of Civil Engineering*.

These approaches were found successfully in predicting the beam shear strength. However, the experimental specimens considered were small in scale with the depth less than 300 mm. COLLINS and MITCHELL (1980), and MACGREGOR (1997) mentioned that the size of the beam is one of the important factors affecting the shear strength of reinforced concrete beams. Conceptually, beams strengthened in shear with FRP sheets should also be affected by scale-effect. Furthermore, some of the specimens considered have FRP sheets fully wrapped around the beams. In most of practical cases, the accessibility of the beams during rehabilitation is often limited. Normally only the bottom and the sides of the beams can be strengthened. CHAJES *et al.* (1995) concluded that full-scale specimens should be studied and more tests were required with different amounts of internal reinforcement, different geometry, and various shear span to depth ratio. DENIAUD and CHENG (2000b [Chapter 4], 2000c [Chapter 5]) have also shown that the amount of internal reinforcement can affect the net shear contribution from the FRP sheets.

This paper aims to review and discuss six recently published FRP shear design models. Experimental test results from a series of full-scale reinforced concrete beam specimens with various stirrup spacing and external FRP shear reinforcement (DENIAUD and CHENG, 2000b [Chapter 4]; 2000c [Chapter 5]) are used in this study to compare the predicted loads from each model investigated.

6.2 Experimental Program

A brief description of the test specimens is presented below as well as a summary of the testing results. The testing program details have been published elsewhere and will not be discussed here (DENIAUD and CHENG, 2000b [Chapter 4]; 2000c [Chapter 5]).

6.2.1 Test Specimens

A total of eight T-beams were cast in the program. Two web heights of 250 and 450 mm were used (four T-beams of each height). The beams had a length of 3 m and 3.7 m, respectively. All the beams have flange of 400 mm wide and 150 mm thick and web of 140 mm thick, as shown in Figure 6.1. The specimens were subjected to four point loading. The shear spans were 1100 and 1550 mm for the short and long beams, respectively.

Each end of the specimens was tested separately while the other end was strengthened using external stirrups made of 19 mm diameter steel rods. The flexural reinforcement was provided by two and four Dywidag bars for the 3 m and the 3.7 m beams, respectively, both with a nominal diameter of 26 mm and a yield strength of 950 MPa. The design provided a flexural capacity between 2.0 and 3.5 times the shear capacity without FRP contribution. The beams were cast with ready-mix concrete from a local supplier. The concrete strength was 29 and 44 MPa for the short and the long beams, respectively. The Dywidag bars were anchored at the end of the beam by using a 50 mm thick steel plate to avoid longitudinal de-bonding shear failure. Closed stirrups of plain undeformed steel (6 mm diameter, 550 MPa yield strength) were used with three spacings: 200 mm, 400 mm, and no stirrups.

Three types of FRP were used to strengthen externally the web of the T-beams: a) uniaxial glass fibre - SEH51 from Fyfe LLC; b) triaxial [0/60/-60] glass fibre – from Owens Corning; and c) uniaxial carbon fibre – *Replark Type 20* from Mitsubishi. The glass fibres were applied at right angles along the full length of the shear span. The carbon fibre sheets were placed either inclinedly at 45^{0} or at right angles, both cases with a width of 50 mm carbon sheets and a gap of 50 mm perpendicular to the direction of the fibres. Tension coupon specimens were prepared in accordance with ASTM Standard D-3039M (1995) when the FRP sheets were glued on the test beams. Table 6.1 summarizes the material properties of the FRP sheets used.

The test matrix with the total load applied to each specimen at ultimate are presented in Table 6.2. A four character name designation was used: T4 or T6 indicated a T-shape beam with 400 or 600 mm depth; S*n* was S2 or S4 indicating 200 mm or 400 mm stirrup spacing, respectively; and NS was for no internal stirrup. An additional designation was added to indicate the fibre type used (C45 – carbon fibre in 45°, G90 – glass fibre in 90°, and Tri – glass fibre in 0°/60°/-60°).

6.2.2 Testing Results

The contribution of the FRP strengthening to the shear capacity of the beam was dependent on the amount of internal reinforcement. The FRP sheets were less effective when beams were heavily reinforced with internal shear reinforcement. The external FRP reinforcement could eventually reduced the shear capacity of the beam by changing the critical path that led to an even more sudden shear failure (DENIAUD and CHENG, 2000c [Chapter 5]). The FRP strains were found to be uniformly distributed among the FRP strips crossing the concrete shear crack.

The failure mode of the beams strengthened with FRP was significantly affected by the web height of the T-beam as well as the layout and the type of the FRP sheets. With the 400 mm beam height, two major shear cracks formed within the shear span and extended upward toward the load point. Following the web shear cracks, vertical crack formed on the top of the flange closed to the support and propagated downward. Eventually, the FRP sheet was tearing (unzipping) vertically when this vertical crack reached the web. This effect can be explained by strain compatibility between the flange and the web due to the shallow geometry of the beam with a very wide top flange. The failure mode of the 600 mm beams was mostly affected by the layout of the FRP. The CFRP bands with a 50 mm gap peeled off above the concrete shear crack. The GFRP sheets fully wrapped without any gap showed a debonded area surrounding the path of the concrete shear crack. Once a large area of GFRP sheets was debonded, the sheets behaved like a thin shell. The compression concrete strut ended up buckling the FRP sheets.

6.3 Shear Evaluation Methods

Most of the current concrete design codes (CSA A23.3, 1994; ACI–318, 1998) in North America evaluate individually the shear contribution of each material used in the structural member. The general formulation of the shear capacity of any reinforced concrete beam including the FRP strengthening can be written as follows:

[6.1] $$V_r = V_c + V_s + V_{FRP}$$

where the subscripts c, s and FRP stand for concrete, steel and FRP sheets, respectively.

The shear contribution of the concrete can be expressed with:

[6.2] $$V_c = \beta \sqrt{f'_c}\, \frac{b_w\, d_v}{\tan\theta}$$

where β is a reduction factor accounting for cracked concrete, $f_c^{'}$ is the compressive concrete strength; b_w and d_v are the effective web width and the stirrup height, respectively; and θ_c is the angle of the concrete crack to the longitudinal axis of the beam. The transverse steel reinforcement V_s is commonly written as:

$$[6.3] \qquad V_s = A_v f_{vy} \frac{d_v}{s \tan\theta}$$

where A_v and f_{vy} are the cross-sectional area of two legs of stirrups and the yield strength of the steel stirrups, respectively; and s is the spacing of stirrups.

Similarly, the FRP shear contribution with α the angle of the principal direction of the fibres to the longitudinal axis of the beam, as shown in Figure 6.2, is defined by:

$$[6.4] \qquad V_{FRP} = A_{FRP} f_{FRP} \frac{d_{FRP} \sin\alpha}{s_{FRP} \tan\theta}(\sin\alpha + \cos\alpha \tan\theta)$$

with $A_{FRP} = 2\ b_{FRP}\ t$; b_{FRP} and t are the width and the thickness of one FRP strip, respectively. From the Figure 6.2, s_{FRP} and d_{FRP} are the spacing and the effective height of the FRP strips, respectively. f_{FRP} is the effective FRP stress in the principal direction of the fibres. The effective FRP stress, f_{FRP}, is probably the most difficult and sensitive parameter to evaluate. Many researchers have published different expressions for f_{FRP} that are summarized below using the same notations.

6.3.1 Bond Models

In these bond models, the angle θ is assumed equal to 45° and β in Equation (6.2) is taken as 0.2 for sections having either: at least the minimum amount of transverse reinforcement or an effective depth not exceeding 300 mm. For all the other cases, β in Equation (6.2) is computed as follows:

$$[6.5] \qquad \beta = \frac{260}{1000 + d} \geq 0.10 \quad (\text{d in mm})$$

The Equations (6.3) and (6.4) are also simplified to:

$$[6.6] \qquad V_s = A_v f_{vy} \frac{d_v}{s}$$

$$[6.7] \qquad V_{FRP} = A_{FRP} f_{FRP} \frac{d_{FRP}}{s_{FRP}}\left((\sin\alpha)^2 + \cos\alpha \sin\alpha\right)$$

CHAALLAL et al. (1998)

In their formulation, the effective FRP stress f_{FRP} is determined based on the FRP sheets capability to stay bonded to the web surface:

[6.8]
$$f_{FRP} = \tau_{ult} \frac{b_{FRP}\, d}{A_{FRP}} \leq f_{ultFRP}$$

for FRP sheets in a form of U-jacket,

[6.9a]
$$\tau_{ult} = \frac{5.4}{1 + k_1 \tan 33^{o}}$$

[6.9b]
$$k_1 = t_{FRP} \left(\frac{3\, E_a}{E_{FRP}\, t^3\, t_a} \right)^{0.25}$$

where d is the distance from the extreme compression fibre to the centroid of the tension steel reinforcement; f_{ultFRP} and E_{FRP} are the ultimate strength and the modulus of elasticity in the principal direction of the fibres, respectively; E_a and t_a are the modulus of elasticity and the thickness of the adhesive (i.e. the epoxy in this case), respectively.

KHALIFA *et al.* (1998)

KHALIFA *et al.* expressed the effective FRP stress as a fraction of the ultimate FRP strength with the use of a reduction factor R. Thus, f_{FRP} is written as:

[6.10]
$$f_{FRP} = R\, f_{ultFRP}$$

They provided three requirements for the value of the reduction factor R:

The effective FRP strain governs the first limit state. In a previous work, TRIANTAFILLOU (1998) presented a relationship between the axial rigidity of the FRP and the effective FRP strain. KHALIFA *et al* (1998) then made a minor modification to the model to include more test results. The limit on the FRP sheet rupture takes the form of a polynomial equation as follows:

[6.11]
$$R = 0.778 - 1.2188 (\rho_{FRP} E_{FRP}) + 0.5622 (\rho_{FRP} E_{FRP})$$

with

[6.12]
$$\rho_{FRP} = \left(\frac{2\, t}{b_w} \right) \left(\frac{b_{FRP}}{s_{FRP}} \right)$$

The second limit comes from the bond mechanism of the FRP sheet glued to the concrete surface with the following equation:

[6.13] $$R = \frac{0.0042\left(f_c^{'}\right)^{2/3} w_{eff}}{\left(E_{FRP}\,t\right)^{0.58} \varepsilon_{ultFRP}\, d_{FRP}}$$

with

[6.14a] $$w_{eff} = d_{FRP} - e^{(6.134 - 0.58\ln(t\,E_{FRP}))}$$

[6.14b] $$\varepsilon_{ultFRP} = \frac{f_{ultFRP}}{E_{FRP}}$$

The last limit ensures the shear integrity of the concrete. By experience and common practice, the upper limit of the reduction factor is taken as 0.5. The governing value of R is then the lowest result among the three limits.

6.3.2 CSA-S806 (2000)

The Canadian Standard Association is currently preparing a new design standard for the construction of building with FRP. The shear design criteria uses the simplified approach of the CSA – A23.3 (1994) with θ equals 45^o and β=0.2 in Equation (6.2). The effective FRP stress, f_{FRP}, is simply given by:

[6.15] $$f_{FRP} = E_{FRP}\,\varepsilon_{eff}$$

where the effective FRP strain ε_{eff} is equal to 0.004 (or 4000 $\mu\varepsilon$).

6.3.3 Modified Compression Field Theory (MCFT)

In 1998, MALEK and SAADATMANESH have worked out the section equilibrium of the forces acting along a concrete crack inclined at an angle θ. The method follows the iteration procedures similar to the MCFT developed by COLLINS and MITCHELL (1989). This method considers a variable concrete crack angle and assumes a prefect bond between the concrete and the FRP sheets. The laminate theory is used to transform the FRP sheet stiffness from the local axis of the FRP to the principal axes along the concrete crack angle θ. The inclination angle θ corresponding to the maximum shear load is the governing angle. The authors acknowledge that the contribution of the aggregate and the concrete in compression zone are not considered in the derivation. Therefore, once the governing angle θ is found, the concrete contribution V_c, which can be calculated using Equation (6.2) and the appropriate value of β, is added to the shear capacity of the beam (see Appendix D.2 for the detailed procedure).

6.3.4 Modified Shear Friction Method

The shear friction method was first presented by LOOV (1998) to review the simplified method of shear design in the Canadian concrete design standard CSA-A23.3 (1994). Using the shear friction approach, the shear contribution of the concrete is expressed as follows:

[6.16] $$V_c = 0.25 k^2 f_c' b_w h \tan\theta$$

where k is an experimentally determined factor and h is the height of the beam. The factor k was studied by LOOV and PENG (1998) for a concrete strength ranging from 20 to 100 MPa. The following equation was proposed from a least squares fit:

[6.17] $$k = 2.1 \left(f_c'\right)^{-0.4}$$

Recently, TOZSER and LOOV (1999) observed the concrete area $b_w h$ was too conservative for T-beams and I-beams. They suggested approximating the effective section of the flange that participates in the shear friction with a 45° angle as shown in Figure 6.3. Equation (6.16) is then modified as follows:

[6.18] $$V_c = 0.25 k^2 f_c' \left(A_{cf} \tan\theta_f + A_{cw} \tan\theta_w\right)$$

A_{cf} is the effective flange concrete area and A_{cw} is the web concrete area which is equal to the web height h_w times the web width b_w. The subscripts f and w stand for *flange* and *web*, respectively.

The shear contribution of the stirrups is expressed by:

[6.19] $$V_s = A_v f_{vy} n_s$$

where n_s is the total number of stirrups, if any, crossing the concrete shear plane at angle θ.

The main advantage of the shear friction approach is that the strain compatibility is not required. The shear strength calculations are therefore easier to perform without any iteration. In a previous work, DENIAUD and CHENG (2000c [Chapter 5]) extended the shear friction method to include the effect of the FRP sheets. The effective FRP stress in Equation (6.4) is expressed by the equation:

[6.20] $$f_{FRP} = E_{FRP}\, \varepsilon_{max}\, R_L$$

where ε_{max} and R_L are evaluated with the strip model proposed by ALEXANDER and CHENG (1997) and summarized below.

The FRP sheets crossing the concrete web crack are described as a series of strips. Each strip is evaluated individually to find its maximum allowable strain ε_x from the geometry of the FRP sheets. The geometry includes the bonded length of the strip above and below the concrete crack as well as the anchorage detail at each end of the strip. The load is assumed linearly distributed among the fibres (DENIAUD and CHENG, 2000c [Chapter 5]). With the FRP sheets in a form of U-jacket, the maximum allowable strain ε_x of the strip close to the web-flange corner is very small (due to the available bond length) and will fail first. The load is then redistributed to the remaining strips with a larger critical strain ε_x. Eventually, as the critical ε_x increases, the number of remaining strip decreases until the load carried by the remaining FRP strips reaches the maximum. At this point the maximum FRP strain ε_{max} as well as the ratio R_L (remaining bonded width over total width crossing the concrete web crack) are recorded.

Finally, the general modified shear friction equation is the addition of Equations (6.18), (6.19), and (6.4) with f_{FRP} obtained from the Equation (6.20). The lowest shear strength among all potential failure planes is the governing shear strength. Given the layout of the stirrups for each test and the shear span, the most critical shear path can be found. A simple computer program was written to scan all potential concrete shear paths to find the lowest shear capacity of the beam. The predicted shear crack path for the T400 and T600 beams can be found in Appendices C.5 and D.1, respectively.

6.3.5 Strut-and-Tie Model

Strut-and-tie model uses a truss to describe the shear span of a concrete beam. The bottom and vertical steel reinforcements represent the tension ties. The concrete is shown as an inclined compressive strut between the vertical stirrups. For a beam without stirrups, AL-NAHLAWI and WIGHT (1992) have successfully proposed a truss model with tension concrete ties. Their approach was thus used with the beam specimens having no internal reinforcement.

The layout of the trusses is presented in Figure 6.4 for the T600 beams. The concrete compressive struts were assumed adequate and were not checked. The predicted failure load was obtained when the vertical steel reinforcement yielded or when the tension concrete ties exceeded the cracking strength of the concrete. The effect of the composite sheets was integrated in the method by increasing the load level required to yield the vertical ties and to crack the concrete tension ties.

6.4 Discussion

The above methods were used to predict the 16 experimental test results. The experimental shear strength to predicted shear strength ratios, V_{exp}/V_r, were computed to evaluate each model efficiency and for comparison between the models. Figure 6.5 shows graphically the model results.

6.4.1 Comment on Each Model

CHAALAL *et al.* (1998)

Table 6.3 presents the principal components of the method as well as the ratio V_{exp}/V_r. With this model the FRP stresses were limited by the ultimate strength of the sheets for all the tests (4th column in Table 6.3). In other words, the beam web wrapped by the FRP was tall enough that the bond shear stresses at the end of the sheets did not govern the failure. This model thus assumed that the full strength of the sheets could be mobilized to enhance the shear capacity of the beam. This is contrary to the actual behavior that was governed by FEP debonding. Fortunately, the assumed 45° concrete crack angle limited the overall shear capacity of the FRP U-jacket. All the specimens strengthened with the glass fibre sheet SEH51 were largely over-estimated. Furthermore, allowing the full strength of the FRP sheets implies also that the ultimate FRP strain could be reached. In most cases, the ultimate FRP strain as high as 1% would have a significant impact on the concrete integrity.

KHALIFA *et al.* (1998)

The major components and the predicted shear capacities of this model are summarized in Table 6.4. In this model, three possible failure modes are identified. The T400 beams strengthen with the glass fibre SEH51 are found to be governed by the bond limit. But for all the other cases, in particular when the beam height increases to 600 mm, the FRP sheet rupture becomes the governing failure mode. As shown in Table 6.4, the governing stress reduction factor for the FRP material is roughly equal to 0.33. Combined with the assumed 45° concrete crack angle, the predicted values were found conservative even if predicted failure modes were incorrect.

CSA-S806 (2000)

Table 6.5 presents the FRP shear contribution using Equation (6.15) as well as the predicted beam capacity and V_{exp}/V_r ratio. The simple limitation of the FRP strain to 4000 $\mu\varepsilon$ gives conservative results. This method is very efficient and can then be used for a preliminary design. However, the mode of failure of the FRP cannot be determined by the method.

Malek and Saadatmanesh (1998)

The principal components of this model are summarized in Table 6.6. This model uses the compatibility of the stirrups and FRP strains without crushing the concrete strut. The vertical shear components are then evaluated consistently with each other. The model tends to overestimate the FRP shear contribution when fewer steel stirrups are present. In fact, the method converges to a smaller concrete crack angle, which leads directly to a substantial increase of the fully wrapped FRP sheets. This method does not provide any insight for the FRP failure mode.

Modified Shear Friction Method

Table 6.7 summarizes the principal components of the modified shear friction method. The model can predict with a very good accuracy the critical crack path as shown in Figure 6.6. The shear contribution of the FRP sheets and the number of stirrups crossing the concrete crack are also accurately evaluated. As mentioned in a previous work (DENIAUD and CHENG, 2000c [Chapter 5]) the model does not address at this point the buckling failure of the wrapped FRP sheets. Two test results (T6S4-G90 and T6S4-Tri) are thus overestimated by this model. But the predicted capacity remains within 10% difference from the test results. Since this approach is an upper bound solution, care should be taken in the evaluation of all potential concrete crack paths. This includes checking any potential cracks between two FRP bands when the gap is wide enough to allow cracking to develop between two consecutive FRP bands.

Strut-and-Tie Model

The predicted shear load V_r and the ratio V_{exp}/V_r are presented in Table 6.8. The Strut-and-tie model is a lower bound solution. Therefore, conservative values were expected and indeed this approach underestimated the capacity of all the specimens. The FRP shear contribution is also limited in this method by the yield strain of the stirrup or the tensile strength of the concrete. The full tensile potential of the FRP sheets is thus significantly reduced.

6.4.2 Comparison of the Models

For ease of comparison, the mean, the standard deviation and the coefficient of variation were computed with the 16 V_{exp}/V_r ratios found for each model. Table 6.9 summarizes these calculations. From the table, the modified shear friction method seems to yield the most accurate and reliable predictions with a mean value of 1.233 and a coefficient of variation of 16.7%. The method also provides accurate estimate of the concrete crack angles and the description of failure modes. The models proposed by CSA-S806 (2000) and KHALIFA *et al.* (1998) follow quite closely with a mean value of roughly 1.5 and a coefficient of variation of about 20%. However, the CSA-S806 equation is simple and easy to use but is lacking in providing the sense of the FRP failure modes. The other three models presented in this study have very scattered results with a coefficient of variation over 30% (see also Figure 6.5).

Only three methods (including modified shear friction method) address the FRP modes of failure. Unfortunately, models presented by CHAALLAL *et al.* (1998) and KHALIFA *et al.* (1998) miss the debonding of the FRP sheets when the beam height gets taller. They also assume a conservative concrete crack angle of 45°, which is not representative of the experimental results when the beams are internally reinforced with stirrups.

Three approaches give conservative results for all the 16 tests used in this study: CSA-S806 (2000), KHALIFA *et al.* (1998) and Strut-and-Tie Model. The modified shear friction method is also conservative except for the two specimens that failed by FRP buckling. But none of the methods investigated here has addressed this mode of failure.

6.5 Conclusion

Several FRP shear design models proposed recently in the literature were reviewed and compared with 16 full-scale reinforced concrete T-beam tests. All the test specimens were failed in shear. Except the modified shear friction method, all the design models yield very conservative and scattered predictions with a test to predicted coefficient of variation exceeding 20%. The modified shear friction method seems very promising in evaluating the shear contribution of the FRP sheets. The method provides the most reliable and consistent predictions among the models investigated with a mean test to predicted ratio of 1.233 and a coefficient of variation of 16.7%. The method also provides the accurate estimate of concrete crack angles and the description of failure modes.

The test results show that the size of the beam affects significantly the FRP shear behavior of the specimens. More tests are needed to substantiate the size effect. This factor must be accounted for in any shear evaluation method. The buckling of the FRP sheet needs to be addressed as a potential failure mode in the design. None of the presented shear models includes this failure mode.

Table 6.1 Fibre Reinforced Polymer Material Properties

FRP Name	Type of fibres	Test source	Ultimate Strength *MPa*	Modulus of Elasticity *MPa*	Thickness *mm*
Replark Type 20	Carbon	Fibre strength	3400	230000	0.11
(Mitsubishi)		Coupon specimens	422	44800	0.70
Triaxial*	Glass	Fibre strength	-	-	-
(Owens Corning)		Coupon specimens	124	8100	2.10
SEH51	Glass	Fibre strength	-	-	-
(Fyfe LLC)		Coupon specimens	250**	17700	1.80

* In 0° fibre direction.

** Assumed with roughly ε_{ultFRP}=1.5%.

Table 6.2 Test Matrix and Ultimate Loads

Specimen	Stirrup Spacing *mm*	External FRP Reinforcement	Ultimate load *kN*
T4NS	None	None	230.8
T4NSG90	None	Glass fibres SEH51 at 90° (No gap)	318.0
T4S4	400	None	313.9
T4S4G90	400	Glass fibres SEH51 at 90° (No gap)	411.2
T4S2	200	None	402.5
T4S2C45	200	Carbon sheets *Replark Type 20* at 45° (50 mm wide, 50 mm gap)	438.1
T4S2G90	200	Glass fibres SEH51 at 90° (No gap)	451.2
T4S2Tri	200	Tri-axial glass fibres (No gap)	485.3
T6NS	None	None	220.2
T6NSC45	None	Carbon sheets *Replark Type 20* at 45° (50 mm wide, 50 mm gap)	427.2
T6S4	400	None	375.0
T6S4C90	400	Carbon sheets *Replark Type 20* at 90° (50 mm wide, 50 mm gap)	545.6
T6S4G90	400	Glass fibres SEH51 at 90° (No gap)	594.9
T6S4Tri	400	Tri-axial glass fibres (No gap)	633.4
T6S2	200	None	713.7
T6S2Tri	200	Carbon sheets *Replark Type 20* at 90° (50 mm wide, 50 mm gap)	619.6

Table 6.3 CHAALLAL *et al.* (1998) Model Predictions

Specimen	k_1	τ_{ult} *MPa*	f_{FRP} *MPa*	V_{FRP} *kN*	V_r *kN*	V_{exp}/V_r
T4NS	-	-	-	-	52.3	2.208
T4NSG90	0.978	3.302	250.0	162.5	214.7	0.741
T4S4	-	-	-	-	81.2	1.934
T4S4G90	0.978	3.302	250.0	162.5	243.6	0.844
T4S2	-	-	-	-	107.6	1.870
T4S2C45	0.602	3.882	425.0	45.8	153.4	1.428
T4S2G90	0.978	3.302	250.0	162.5	270.1	0.835
T4S2Tri	1.092	3.159	127.4	96.6	204.2	1.188
T6NS	-	-	-	-	83.7	1.315
T6NSC45	0.602	3.882	425.0	67.3	151.0	1.414
T6S4	-	-	-	-	137.4	1.365
T6S4C90	0.602	3.882	425.0	78.8	216.2	1.262
T6S4G90	0.978	3.302	250.0	238.5	375.9	0.791
T6S4Tri	1.092	3.159	127.4	141.8	279.2	1.134
T6S2	-	-	-	-	176.2	2.025
T6S2C90	0.602	3.882	425.0	78.8	255.0	1.215

Table 6.4 KHALIFA *et al.* (1998) Model Predictions

Specimen	R_{bond}	R_{stress}	V_{FRP} *kN*	V_r *kN*	V_{exp}/V_r
T4NS	-	-	-	52.3	2.208
T4NSG90	0.286	0.340	64.2	116.5	1.365
T4S4	-	-	-	81.2	1.934
T4S4G90	0.286	0.340	64.2	145.4	1.414
T4S2	-	-	-	107.6	1.870
T4S2C45	0.428	0.345	25.6	133.3	1.644
T4S2G90	0.286	0.340	64.2	171.9	1.313
T4S2Tri	0.442	0.381	51.0	158.6	1.530
T6NS	-	-	-	83.7	1.315
T6NSC45	0.645	0.345	46.2	129.9	1.644
T6S4	-	-	-	137.4	1.365
T6S4C90	0.645	0.345	46.2	183.5	1.486
T6S4G90	0.430	0.340	137.6	275.0	1.082
T6S4Tri	0.675	0.381	91.8	229.2	1.382
T6S2	-	-	-	176.2	2.025
T6S2C90	0.645	0.345	46.2	222.4	1.393

Table 6.5 CSA-S806 (2000) Model Predictions

Specimen	V_{FRP} *kN*	V_r *kN*	V_{exp}/V_r
T4NS	-	54.7	2.109
T4NSG90	63.7	118.4	1.343
T4S4	-	81.2	1.934
T4S4G90	63.7	144.9	1.419
T4S2	-	107.6	1.870
T4S2C45	31.4	139.0	1.576
T4S2G90	63.7	171.3	1.317
T4S2Tri	55.8	163.4	1.485
T6NS	-	98.5	1.117
T6NSC45	56.4	155.0	1.378
T6S4	-	137.4	1.365
T6S4C90	56.4	193.8	1.407
T6S4G90	114.7	252.1	1.180
T6S4Tri	100.5	237.9	1.331
T6S2	-	176.2	2.025
T6S2C90	56.4	232.7	1.332

Table 6.6 MALEK and SAADATMANESH (1998) Model Predictions

Specimen	θ *deg*	V_c *kN*	V_s *kN*	V_{FRP} *kN*	V_r *kN*	V_{exp}/V_r
T4NS	34.0	40.4	-	-	40.4	2.859
T4NSG90	28.0	20.5	-	181.3	201.8	0.788
T4S4	21.1	30.0	67.1	-	97.1	1.616
T4S4G90	27.3	22.4	50.3	69.4	142.1	1.447
T4S2	25.9	23.6	106.8	-	130.4	1.544
T4S2C45	28.1	21.4	97.1	30.5	148.9	1.471
T4S2G90	30.2	21.1	89.1	60.0	170.2	1.325
T4S2Tri	30.8	20.8	87.1	68.2	176.0	1.378
T6NS	37.0	48.8	-	-	48.8	2.256
T6NSC45	22.3	49.4	-	265.1	314.5	0.679
T6S4	19.1	66.0	117.3	-	183.3	1.023
T6S4C90	22.7	58.6	96.9	77.9	233.3	1.169
T6S4G90	27.9	41.6	76.7	339.7	458.0	0.649
T6S4Tri	28.5	40.2	74.7	355.3	470.1	0.674
T6S2	18.2	54.5	170.2	-	224.8	1.588
T6S2C90	25.9	56.5	167.3	65.6	289.4	1.071

Table 6.7 Modified Shear Friction Model Predictions

Specimen	θ_w *deg*	θ_f *deg*	ε_{max} *%*	R_L	n_s	V_r *kN*	V_{exp}/V_r
T4NS	25.8	18.7	-	-	0	68.3	1.691
T4NSG90	38.5	13.1	0.316	0.792	0	132.2	1.203
T4S4	29.2	19.8	-	-	1	105.3	1.490
T4S4G90	39.5	14.3	0.314	0.792	1	163.7	1.256
T4S2	34.7	25.0	-	-	2	154.7	1.301
T4S2C45	35.6	24.2	0.311	0.848	2	167.3	1.310
T4S2G90	42.1	20.0	0.317	0.792	2	205.4	1.098
T4S2Tri	42.1	20.0	0.364	0.792	2	205.6	1.180
T6NS	25.2	18.2	-	-	0	103.0	1.069
T6NSC45	27.1	15.7	0.471	0.891	0	148.0	1.443
T6S4	28.4	19.1	-	-	2	173.8	1.079
T6S4C90	31.4	15.3	0.469	0.851	2	222.9	1.224
T6S4G90	45.4	18.5	0.468	0.851	1	326.0	0.912
T6S4Tri	45.4	18.5	0.536	0.851	1	326.4	0.970
T6S2	31.8	22.2	-	-	4	250.4	1.425
T6S2C90	39.3	24.5	0.469	0.851	3	289.7	1.069

Table 6.8 Struts-and-Ties Model Predictions

Specimen	V_r *kN*	V_{exp}/V_r
T4NS	36.4	3.172
T4NSG90	42.9	3.707
T4S4	65.7	2.389
T4S4G90	120.9	1.701
T4S2	95.0	2.118
T4S2C45	133.9	1.636
T4S2G90	150.2	1.502
T4S2Tri	157.2	1.544
T6NS	70.6	1.560
T6NSC45	125.4	1.703
T6S4	99.9	1.877
T6S4C90	137.6	1.983
T6S4G90	159.4	1.866
T6S4Tri	175.1	1.809
T6S2	129.2	2.762
T6S2C90	166.9	1.857

Table 6.9 Model Comparison

Model Name	Average	Sdt dev.	c.o.v. %
CHAALLAL *et al.* (1998)	1.348	0.456	33.8
KHALIFA *et al.* (1998)	1.561	0.305	19.6
CSA-S806	1.512	0.304	20.1
MALEK and SAADATMANESH (1998)	1.346	0.590	43.8
Modified Shear Friction	1.233	0.206	16.7
Struts-and-Ties	2.074	0.632	30.5

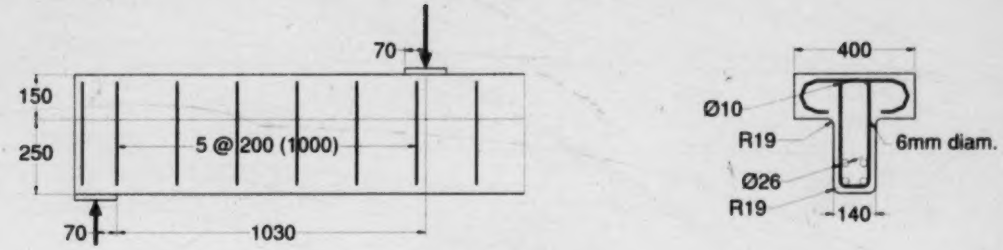
70
150
250
5 @ 200 (1000)
70
1030
400
Ø10
R19
6mm diam.
Ø26
R19
140

(a) T400 beams

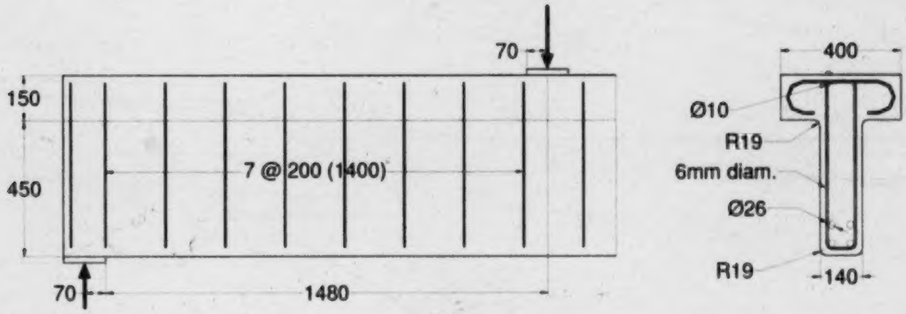
70
150
450
7 @ 200 (1400)
70
1480
400
Ø10
R19
6mm diam.
Ø26
R19
140

(b) T600 beams

Figure 6.1 T-beam Geometry

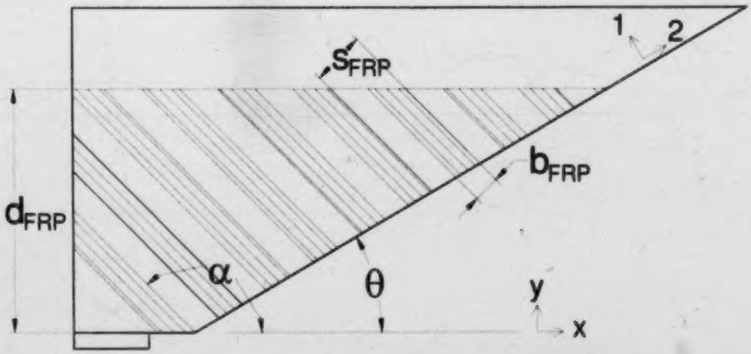
1
2
s_{FRP}
b_{FRP}
d_{FRP}
α
θ
y
x

Figure 6.2 FRP Designation

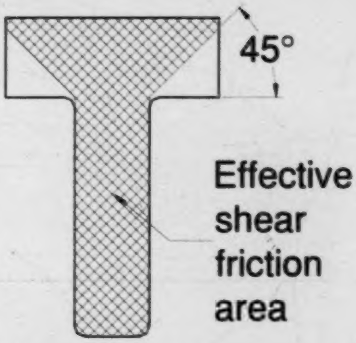
45°
Effective shear friction area

Figure 6.3 Effective Shear Friction Concrete Area

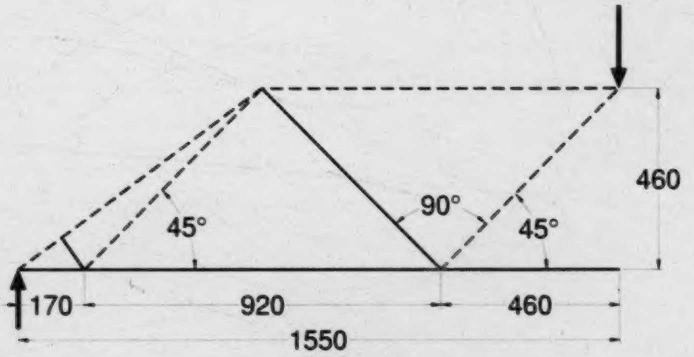
460
90°
45°
45°
170
920
460
1550

(a) With stirrups

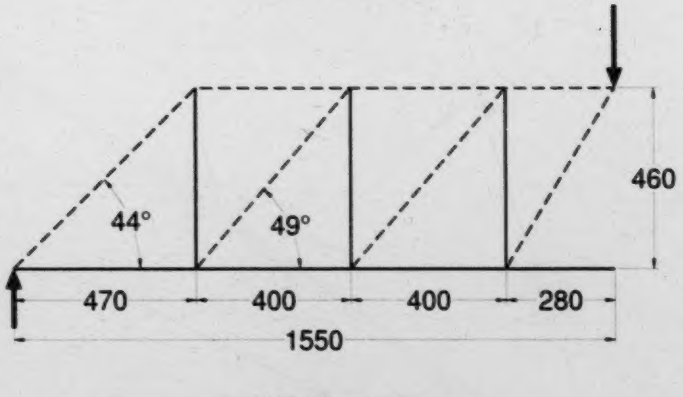
460
44°
49°
470
400
400
280
1550

(b) Without stirrups

Figure 6.4 Strut-and-Tie Layouts for T600 beams

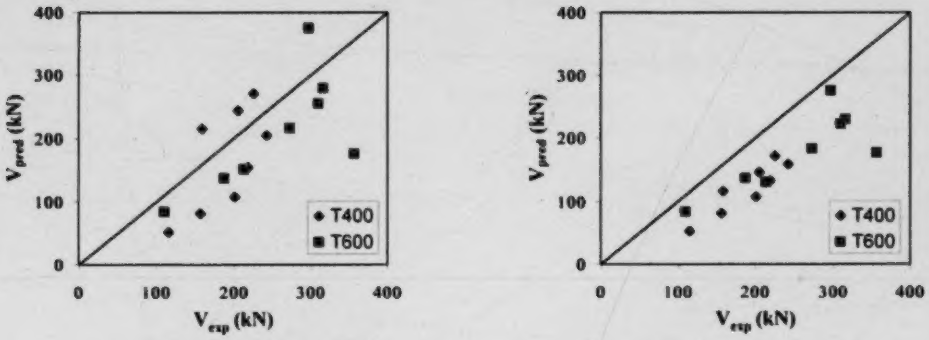

(a) CHAALLAL *et al.* (1998)

(b) KHALIFA *et al.* (1998)

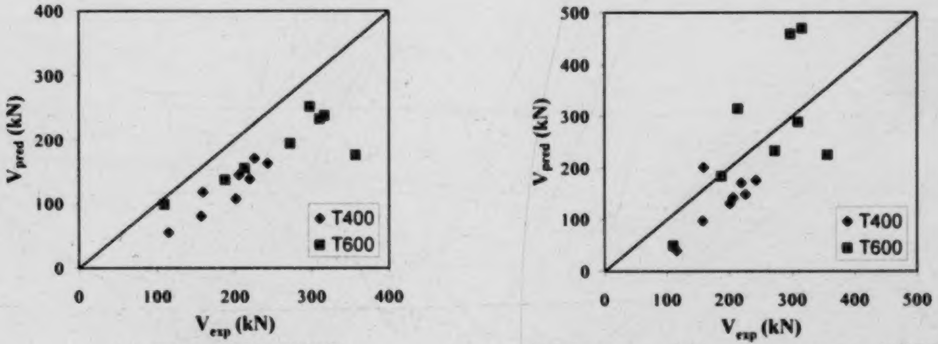

(c) CSA-S806 (2000)

(d) MALEK and SAADATMANESH (1998)

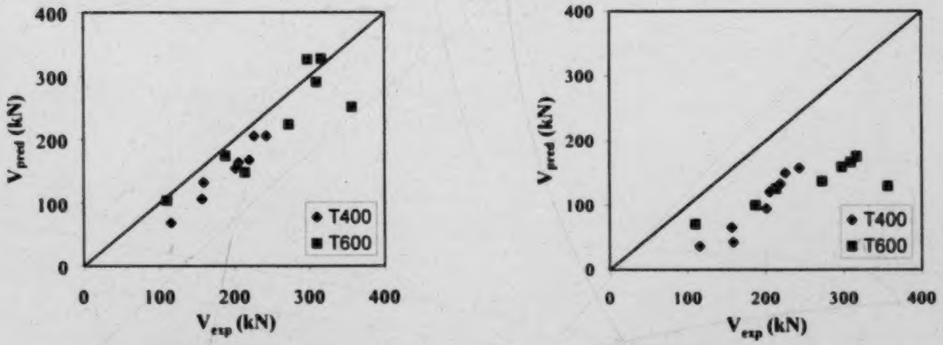

(e) Modified Shear Friction

(f) Strut-and-Tie

Figure 6.5 Graphical Model Predictions

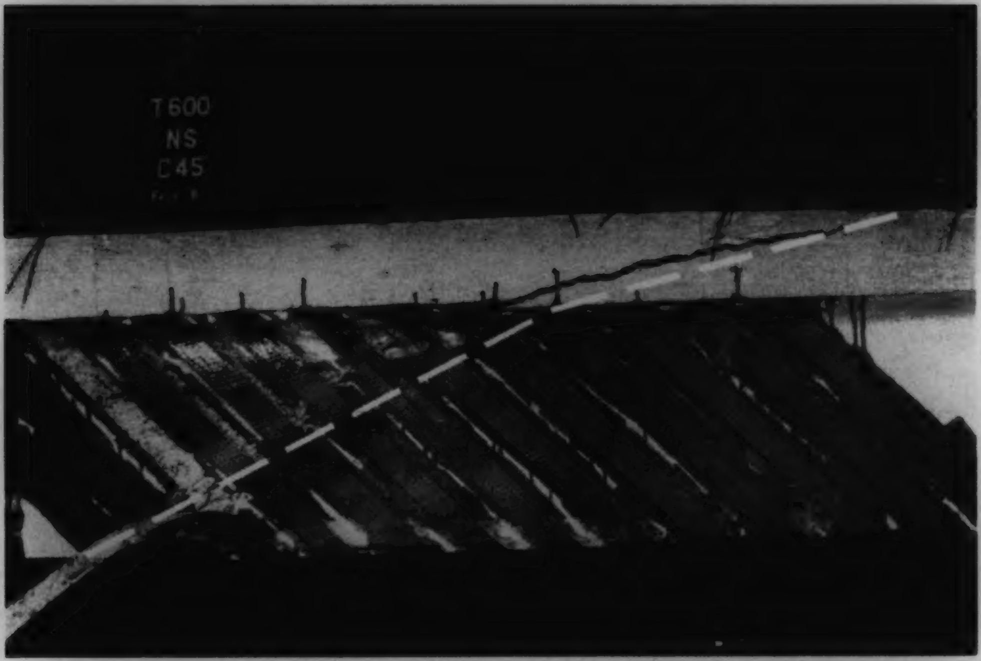

Figure 6.6 Graphical Modified Shear Friction Results (T6NSC45)

6.6 References

ACI-318 (1998). *Building Code Requirements for Structural Concrete*, American Concrete Institute, Detroit, MI, 369 p.

ALEXANDER J. and CHENG J.J.R. (1997). *Shear Rehabilitation of G-Girder Bridges using CFRP Sheets*, Structural Engineering Report No 218, Department of Civil and Environmental Engineering, University of Alberta, Edmonton, AB, 181 p.

AL-NAHLAWI K.A., and WIGHT J.K. (1992). "Beam Analysis using Concrete Tensile Strength in Truss Models", *American Concrete Institute Structural Journal*, Vol. 89, No. 3, May-June, pp. 284-289.

AL-SULAIMANI G.J., ISTEM A., BASUNBUL A.S., BALUCH M.H., and GHALEB B.N. (1994). "Shear Repair for Reinforced Concrete by Fiberglass Plate Bonding", *American Concrete Institute Structural Journal*, Vol. 91, No. 3, July-August, pp. 458-464.

ASTM. D-3039M (1995). "Standard Test Methods for Tensile Properties of Polymer Matrix Composite Materials", *Annual Book of ASTM Standards*, Philadelphia, PA, pp. 98-144.

CHAALLAL O., NOLLET M.-J., and PERRATON D. (1998). "Strengthening of Reinforced Concrete Beams with Externally Bonded Fiber-Reinforced-Plastic Plates: Design Guidelines for Shear and Flexure", *Canadian Journal of Civil Engineering*, Vol. 25, No. 4, August, pp. 692-704.

CHAJES M.J., JANUSZKA T.F., MERTZ D.R., THOMSON T.A., and FINCH W.W. (1995). "Shear Strengthening of Reinforced Concrete Beams using Externally Applied Composite Fabrics", *American Concrete Institute Structural Journal*, Vol. 92, No. 3, May-June, pp. 295-303.

COLLINS M.P., and MITCHELL D. (1987). *Prestressed Concrete Basics*, 1st Edition, Canadian Prestressed Concrete Institute, Ottawa, ON, 614 p.

COLLINS M.P., and MITCHELL D. (1980). "Shear and Torsion Design of Prestressed and Non-Prestressed Concrete Beams", *Prestressed Concrete Institute Journal*, Vol. 5, pp. 1-70.

CSA-A23.3. (1994). *Design of Concrete Structures*, Canadian Standard Association, Rexdale, ON.

CSA-S806 (2000). *Design and Construction of Building Components with Fiber Reinforced Polymers*, Draft, Canadian Standard Association, Rexdale, ON.

DENIAUD C., and CHENG J.J.R., (2000a). "Shear Rehabilitation of Type G-girders in Alberta using FRP Sheets", *Canadian Journal of Civil Engineering*, (in press) [Chapter 3].

DENIAUD C., and CHENG J.J.R., (2000b). "Reinforced Concrete T-beams Strengthened in Shear with FRP Sheets", Accepted for publication in ASCE *Journal of Composites for Construction*, [Chapter 4].

DENIAUD C., and CHENG J.J.R., (2000c). "Shear Behavior of RC T-beams with Externally Bonded FRP Sheets", Accepted for publication in the *American Concrete Institute Structural Journal* [Chapter 5].

DRIMOUSSIS E.H., and CHENG J.J.R. (1994). *Shear Strengthening of Concrete Girders using Carbon Fiber Reinforced Plastic Sheets*, Structural Engineering Report No 205, Department of Civil Engineering, University of Alberta, Edmonton, AB, 177 p.

HUTCHISON, R. (1999). *The Use of Externally Bonded CFRP Sheets for Shear Strengthening of I-Shaped Prestressed Concrete Bridge Girders*, Ph.D. Thesis, University of Manitoba, Winnipeg, MA, 270 p.

KHALIFA A., GOLD W.J., NANNI A., and AZIZ M.I. (1998). "Contribution of Externally Bonded FRP to Shear Capacity of RC Flexural Members", *Journal of Composites for Construction*, Vol. 2, No. 4, November, pp. 195-202.

LOOV R. (1998). "Review of A23.3-94 Simplified Method of Shear Design and Comparison with Results using Shear Friction", *Canadian Journal of Civil Engineering*, Vol. 25, No. 3, April, pp. 437-450.

LOOV R., and PENG L. Z(1998). "The Influence of Concrete Strength on Shear Friction based Design of Reinforced Concrete Beams", *Proceedings of the International Conference on HPHSC*, August, Perth, Australia pp. 505-519.

MALEK A.M., and SAADATMANESH H. (1998). "Analytical Study of Reinforced Concrete Beams Strengthened with Web-Bonded Fiber Reinforced Plastic Plates or Fabrics", *American Concrete Institute Structural Journal*, Vol. 95, No. 3, May-June, pp. 343-352.

MACGREGOR J.G. (1997). *Reinforced Concrete – Mechanics and Design*, 3rd edition, Prentice Hall, Upper Saddle River, NJ, 939 p.

NEALE K. (2000). "FRPs for Structural Rehabilitation: A Survey of Recent Progress", *Progress in Structural Engineering and Materials* (in press).

TOZSER O. and LOOV. R. (1999). "Shear Design of Prestressed beams using Shear Friction", *Proceedings of the Annual Conference of the CSCE*, CSCE, Regina, SK, pp. 195-204.

TRIANTAFILLOU T.C. (1998). "Shear Strengthening of Reinforced Concrete Beams using Epoxy-Bonded FRP Composites", *American Concrete Institute Structural Journal*, Vol. 95, No. 2, March-April, pp. 107-115.

7 A SIMPLIFIED SHEAR DESIGN METHOD FOR CONCRETE BEAMS STRENGTHENED WITH FRP SHEETS[1]

7.1 Introduction

The use of Fibre Reinforced Polymers (FRP) for the rehabilitation of existing concrete structures has grown very rapidly over the last few years (NEALE, 2000). Researches (DRIMOUSSIS and CHENG, 1994) have shown that FRP can be used very efficiently in strengthening the concrete beams weak in shear. Unfortunately, the current concrete design standards (ACI-318, 1995; CSA-A23.3, 1994) do not include any provisions for the shear strengthening of structural members with FRP materials. This lack of design standards led to the formation of partnerships between the research community and industry to investigate and to promote the use of FRP in shear rehabilitation of existing structures (DRIMOUSSIS and CHENG, 1994; ALEXANDER and CHENG, 1997; HUTCHINSON *et al.*, 1997). From these projects, design procedures were often proposed, but were generally limited to each specific project.

Several researchers have recently published design equations and analytical models to specifically evaluate FRP shear strengthening of reinforced concrete beams. Most of theses methods assumed a 45° concrete crack angle (TRIANTAFILLOU, 1998; KHALIFA *et al.*, 1998), which is consistent with the assumption of the shear design provisions in the current codes (ACI-318, 1995; CSA-A23.3, 1994). This simplified truss model is known to be conservative (COLLINS and MITCHELL, 1987), but a variable concrete crack angle will give a more realistic prediction of the behaviour and strength of beams failing in shear (MACGREGOR, 1997). MALEK and SAADATMANESH (1998) successfully extended the Modified Compression Field Theory (MCFT) proposed by Collins and Mitchell (1987) to include the contribution of the FRP sheets with variable concrete crack angles. However, the MCFT involves iterative process to calculate the shear strength of a beam element that may not be feasible in design offices when minimal design time is often required. Recently, RAHAL (2000) proposed a simplification of the equations used in the MCFT method to eliminate the iterative procedures and found comparable accuracy.

---

[1] A version of this chapter is in preparation for publication in the *ASCE Structural Journal*

Further research is still required to extend this simplified model to FRP shear strengthening.

DENIAUD and CHENG (2000c [Chapter 6]) revisited the different shear evaluation models specifically developed for FRP shear strengthening. They showed that the strip model, combined with the shear friction approach, was the most reliable and consistent model. The strip model is based on the bond mechanism observed from the tests. The shear friction approach assumes a formation of a concrete web shear crack along which slippage occurs, whereas the MCFT assumes a uniform concrete strut along the shear span with no discontinuity. Since the FRP sheets bonded to the beam sides are only activated after a concrete web crack has formed, the shear friction model is, therefore, better suited to describe this behaviour.

However, the strip and shear friction models require finding all potential shear crack paths to yield the lowest shear capacity. To find this lower bound solution by iteration was then the drawback of this otherwise viable design method.

A new simplified shear design method, which is based on the strip model (ALEXANDER and CHENG, 1997; DENIAUD and CHENG, 2000b [Chapter 5]) and the shear friction approach (LOOV, 1998), is developed here for the shear evaluation of reinforced concrete beams strengthened externally in shear with FRP sheets. The method, eliminating the need of iteration, is covered in this paper in detail, and the method is also validated with experimental data available in the literature.

7.2 Strip Method

7.2.1 General Description

The shear contribution of FRP sheets using the strip method was first developed by ALEXANDER and CHENG (1997). In their model, the FRP sheets crossing the concrete web crack are described as a series of strips. Each strip is evaluated individually to find its maximum allowable strain from the geometry of the FRP sheets. The geometry includes the bonded length of the strip above and below the crack, as well as the anchorage at each end of the strip. A free body diagram of a unit FRP strip can be used to work out the force and moment equilibrium (DENIAUD and CHENG, 2000a [Chapter 4]). In the original model proposed by ALEXANDER and CHENG (1997), the load was assumed to be linearly distributed between the strips from the bottom of the web to the flange. However, further experimental results showed a uniform strain distribution rather than linear distribution among the fibres crossing the concrete web crack (DENIAUD and CHENG, 2000b [Chapter 5]). Thus, the uniform distribution will be used here to reflect the experimentally observed behaviour of the fibres.

The interface mean shear stress curve is used to evaluate the bond strength and the corresponding maximum allowable strain, ε_x, of each strip. From the uniform strain distribution assumption, the same strain level is applied to all the FRP strips crossing the concrete web shear crack. The ε_x of the strip closest to the web-flange corner is very small due to its small bond length. As a result, it will then fail first, thereby, starting a sequential peeling off. The load in this peeled strip is then redistributed to the remaining strips. Eventually, as the strain ε_x increases, the number of remaining strips decreases until the load carried by the remaining FRP strips reaches a maximum. At this point the maximum FRP strain ε_{max}, as well as the ratio R_L (remaining bonded over total length), are recorded.

To complete the model, an interface mean shear stress curve is needed and is presented in the following section.

7.2.2 Interface Shear Strength Curve

7.2.2.1 *Interface Shear Strength Curve Development*

The interface shear strength curve used initially by ALEXANDER and CHENG (1997) in the strip model was developed with the results of a few concrete block tests. Recently, many other researchers have also published concrete and FRP bond test results using various test set-ups (CHAJES *et al.*, 1996; MAEDA *et al.*, 1997; Brosens and Van Gemert, 1999; BIZINDAVYI and NEALE, 1999; KAMEL *et al.*, 2000). The existence of an ultimate load beyond which no further increase of the load carried by the FRP-concrete bond joint occurs was commonly observed. A corresponding minimum transfer or effective bond length corresponding to the load could also be found. MAEDA *et al.* (1997) found that the effective bond length is a function of the FRP stiffness per unit length, $t \cdot E_{FRP}$, and proposed the equation

[7.1] $$L_{eff} = \exp[6.134 - 0.58 \ln(t\,E_{FRP})]$$

where $t \cdot E_{FRP}$ is in GPa·mm and L_{eff} is in mm.

Figure 7.1 presents the experimental data from various researchers using dimensionless axes P/P_{Joint} vs. L/L_{eff}. A curve is proposed to fit these data and is also included in the figure. The proposed relationship uses a quadratic curve up to L equal to L_{eff}, followed by a constant joint load when P reaches P_{Joint}, as shown in Equation (7.2).

[7.2a] $$\frac{P}{P_{Joint}} = -\left(\frac{L}{L_{eff}}\right)^2 + 2\frac{L}{L_{eff}} \qquad \text{when } L < L_{eff}$$

[7.2b] $$\frac{P}{P_{Joint}} = 1 \qquad \text{when } L \geq L_{eff}$$

The quadratic equation was selected to create a continuous curve and a smooth transition when L/L_{eff} equals one. The maximum load P_{Joint} carried by the joint can be expressed by

[7.3] $$P_{Joint} = \tau_{eff}\, L_{eff}\, w_{Joint}$$

where τ_{eff} is the mean concrete bond strength over the effective bond length L_{eff}, and w_{Joint} is the width of the FRP joint. Similarly, the load P carried by any joint length L can be written as

[7.4] $$P = \tau\, L\, w_{Joint}$$

where τ is the average concrete bond strength over the joint length L. Substituting Equations (7.3) and (7.4) into Equation (7.2) it can be show that

[7.5a] $$\frac{\tau}{\tau_{eff}} = \left(2 - \frac{L}{L_{eff}}\right) \qquad \text{when } L < L_{eff}$$

[7.5b] $$\frac{\tau}{\tau_{eff}} = \frac{L_{eff}}{L} \qquad \text{when } L \geq L_{eff}$$

Let $\tau_{eff} = \beta\sqrt{f_c'}$, Equations (7.5a) and (7.5b) can be rewritten as

[7.6a] $$\frac{\tau}{\sqrt{f_c'}} = \left(2 - \frac{L}{L_{eff}}\right)\beta \qquad \text{when } L < L_{eff}$$

[7.6b] $$\frac{\tau}{\sqrt{f_c'}} = \frac{L_{eff}}{L}\beta \qquad \text{when } L \geq L_{eff}$$

where β is a factor accounting for the concrete bond shear resistance evaluated at $L/L_{eff} = 1$. With a best fit regression and using the data from the University of Alberta

(ALEXANDER and CHENG, 1997; KAMEL *et al.*, 2000), β was found to be equal to 0.23. The coefficient of multiple determination R^2 for this regression was 0.87.

The proposed interface shear strength curve is plotted in Figure 7.2, as well as the test data from the literature. Shear strength curves proposed by other researchers (ALEXANDER and CHENG, 1997; BIZINDAVYI and NEALE, 1999) are also included.

7.2.2.2 Interface Shear Strength Curve Discussion

The bond strength curves proposed in the literature well described the data from which they were defined. However, large discrepancy and scattering between these curves are shown in Figure 7.2.

In the figure, it clearly indicates that the width of the FRP sheets bonded to the concrete block has a significant effect. In fact, as the width of the FRP sheets becomes smaller, the bond strength increases. The difference in strength between the 25 mm and 100 mm FRP widths has a factor of two to three times. The strain distribution along the width of the FRP sheets can provide a rational explanation for such behaviour. KAMEL *et al.* (2000) observed that the strain values at the edge are much higher than at the centre of the sheet. They also found that the difference was increasing as the ultimate load was reached. Using narrow FRP sheets bonded to the concrete, the strain distribution along the width is likely to be fairly uniform. Since high strain concentrations exist at the edge of wide FRP sheets, the maximum load per unit width of the joint can then be significantly reduced.

Therefore, for conservative reason, the bond strength data from the University of Alberta (ALEXANDER and CHENG, 1997; KAMEL *et al.*, 2000), were used for the proposed interface bond strength curve (Equation (7.6) with β = 0.23), as shown in Figure 7.2. The proposed β value (= 0.23) is very similar to the coefficient commonly used in the concrete design codes (ACI-318, 1995; CSA-A23.3, 1994) where the concrete shear strength v_c is express as

$$[7.7] \qquad v_c = 0.2\sqrt{f_c'}$$

Further investigations should be conducted to evaluate specifically the effect of the FRP width bonded to the concrete. Such studies are however beyond the scope of this research.

7.2.3 An Example of Using the Strip Method

A beam strengthened externally by FRP sheets, as shown in Figure 7.3, is used to illustrate the typical procedures of strip method. Assume that the FRP sheets have a height of 450 mm with $t \cdot E_{FRP}$ = 35.85 kN/mm and ε_{ultFRP} = 2.0%. These values were taken from the available manufactures' data of glass fibre product *Tyfo SEH51* (FYFE CO. LLC, 1999). From Equation (7.1), L_{eff} equals 57.9 mm. The sheets are bonded to the side of the concrete beam without any gap at 90° from the longitudinal axis of the beam. The top end of the sheet is free whereas the bottom end of the sheet is wrapped underneath the web. The concrete strength of the beam is 45 MPa.

Assume that the concrete crack has a 45° angle and the width of the strip is 50 mm (see Figure 7.3). The average bond length, L_x, of each individual strip above the crack is then easily computed from the given geometry. Using Equation (7.6), the mean bond strength τ_x of each strip can be evaluated. For this particular example, the maximum allowable strain ε_x is then given by

$$[7.8] \qquad \varepsilon_x = \frac{\tau_x L_x}{t E_{FRP}} \leq \varepsilon_{ultFRP}$$

Strip #9 has the lowest allowable strain (= 0.00132) due to its shortest bond length and will fail first. The shear load carried by all the FRP strips just prior to failure of the strip #9 is

$$V_{FRP} = 0.00132 \cdot (9) \cdot (50) \cdot (35.85) = 21.31 \text{ kN}$$

These calculations are summarized in Table 7.1. The load is then redistributed among the remaining strips. This process is continued until the maximum shear load carried by the FRP sheet reaches a value of 27.95 kN, as shown in Table 7.1. The maximum FRP strain ε_{max} is then found to be 0.195% and the ratio R_L equal to 0.889.

The effects of the crack angle θ, the number of strips and the strip widths are investigated below to study the sensitivity of the strip method.

7.2.3.1 Effect of the Concrete Crack Angle θ

The above example was computed with a 45° concrete crack angle. Consider a new crack angle of 26.6° (2 to 1 slope) and assume the same number of nine strips. The width of each individual strip becomes 100 mm. However, the bond length and, therefore, the bond strength of each individual strip remains the same. Thus, the maximum allowable strain, ε_x, is unchanged. Since the FRP sheet crossing the concrete crack is twice as wide, the load carried by the FRP sheet will double. However, the peak FRP load will occur at the same step once the strip #9 has failed.

The maximum FRP strain ε_{max} and the ratio R_L are thus independent of the concrete crack angle θ. However, the load carried by the FRP sheet is, of course, a function of the number of FRP strips crossing the crack.

7.2.3.2 *Effect of the Number of Strips and the Strip Width*

The number of strips and the strip width are obviously related to each other for any given overall width. Consider the data given in the above example with an increasing number of strips and, consequently, a decreasing strip width. A computer program was written to calculate the FRP components ε_{max} and R_L. The strip number was increased from 1 to 450 at which time the width of each individual strip was 1 mm. Figure 7.4 shows the variation of ε_{max} and R_L with respect to the strip width.

From these results, it can be seen that the number of strips does not affect the maximum FRP strain value, given in percent up to three decimal digits. Graphically, these very slight changes are barely noticed (Figure 7.4a).

A strip width of 450 mm in this example means that only one strip is considered. The sequential failure mechanism described by the strip method can obviously not be applied. Figure 7.4b shows that the bonded to total length ratio R_L converges when the FRP strips become smaller than 50 mm wide. In other words, any reasonable strip width, that has dimensional and physical meaning, can be selected to obtain an accurate result.

7.3 Parametric Study

7.3.1 Methodology

A computer program was written to generate data for use in the strip method. For this study, five variables were identified: the concrete strength f'_c, the height and the stiffness per unit width of the FRP sheets (d_{FRP} and $t \cdot E_{FRP}$, respectively), the angle of the principal direction of the fibre, and the anchorage of the FRP sheets. The concrete strength varied from 20 to 50 MPa in increments of 10 MPa. The height of the FRP ranged from 250 to

1250 mm in increments of 200 mm. The stiffness per unit width of the FRP sheets started at 5 kN/mm and was increased in steps of 5 kN/mm up to 50 kN/mm. Four principal direction angle of the fibre were used: 30°, 60°, 75°, and 90°. Finally, the FRP sheets were assumed to be either bonded only to the side of the web, wrapped underneath the web, or/and were extended underneath the flange with a 100 mm anchor length. A slight modification of the program was included to account for the end of the FRP sheets bonded underneath the flange. The anchorage detail of the FRP sheet was made using a free body diagram and is fully describe elsewhere (DENIAUD and CHENG, 2000a [Chapter 4]). The ultimate FRP strain, ε_{ultFRP}, was not used as a limiting factor when the data were generated, but this constraint is discussed later.

This set of parameters was selected to cover the practical ranges and conditions for the use of FRP in rehabilitation projects for most applications. The maximum FRP strain and the remaining bonded to total lengths were then calculated for each combination of the parameter investigated. The commercially available statistical software package SigmaPlot 5.0 (SPSS, 1999) was used to perform the non-linear regression. The coefficient of multiple determination (R^2) was also used to measure the predictive ability of a proposed regression equation (DEVORE, 1991).

7.3.2 Development of the ε_{max} Equation

The value of the maximum FRP strain was first determined using only the data generated with the FRP sheets bonded to the side of the beam or wrapped underneath the web. After several trials, the following equation was found to give the greatest value of R^2:

$$[7.9] \qquad \varepsilon_{max} = a_1 (f_c')^{a_2} (d_{FRP})^{a_3} (t\,E_{FRP})^{a_4} (\sin\alpha)^{a_5} (k_a)^{a_6} \qquad \text{(in percent)}$$

with the optimal regression coefficients of the non-linear analysis given below:

$a_1 = 3.03318$ $a_3 = 0.160524$ $a_5 = -0.09557$

$a_2 = 0.51503$ $a_4 = -1.53175$ $a_6 = -0.111054$

where f_c', d_{FRP} and $t{\cdot}E_{FRP}$ are in MPa, mm and kN/mm, respectively. k_a describes the anchorage end conditions, as shown in Figure 7.5. For this equation, R^2 was found equal to 0.99331, which means that 99.3% of the predicted data describes the response perfectly.

The values of the regression coefficients were further studied and were rounded to provide a more compact equation without losing significantly the predictive ability of the equation. The compact equation takes the form

$$[7.10] \qquad \varepsilon_{max} = \frac{3\sqrt{f'_c}\, d_{FRP}^{\ 0.16}}{\left(t\, E_{FRP}\right)^{0.67}\left(k_a \sin\alpha\right)^{0.1}} \qquad \text{(in percent)} \quad (R^2 = 0.99296)$$

From this analysis, ε_{max} was found to be primarily a function of the concrete strength, the FRP stiffness and, to a lesser degree, the FRP sheet height. The anchorage conditions and the orientation of the fibre showed comparatively less effect.

Equation (7.10) was then used to calibrate the anchorage factor k_a when the FRP sheets were extended underneath the beam flange. The optimal value of k_a was then found equal to 0.79 with $R^2 = 0.99421$. The detail of this anchorage is also shown in Figure 7.5. With this method, the effectiveness of any anchor system can be demonstrated and an appropriate value for the anchorage factor k_a can be easily found for each anchor system. If the anchorage provided is such that no bond failure can occur (fully wrapping for instance), $k_a = 0$ shall be used and ε_{max} from Equation (7.10) then reaches infinity. In other words, the maximum FRP strain is not governed by the bond failure mechanism.

As mentioned earlier, ε_{FRPult} was not used as variable in the generated data. Therefore, in order to complete the formulation following the above discussion, the designer should also check that the value of ε_{max} given in Equation (7.10) is less than or equal to ε_{FRPult}.

7.3.3 Development of the R_L Equation

Similarly, the generated data were visually screened and, after several trials, the following form of the R_L equation was found with the greatest R^2 value.

$$[7.11] \qquad R_L = 1 - a_1 \exp\left[-\left(\frac{d_{FRP}}{k_e\, L_{eff} \sin\alpha}\right)^{a_2}\right]$$

where k_e is an integer describing the number of debonding ends, as shown in Figure 7.5. The optimal coefficients a_1 and a_2 of the non-linear regression analysis were found equal to 1.196 and 0.4008, respectively ($R^2 = 0.99365$). The equation coefficients were again rounded to give the more simplified equation

[7.12] $$R_L = 1 - 1.2\exp\left[-\left(\frac{d_{FRP}}{k_e\, L_{eff}\, \sin\alpha}\right)^{0.4}\right]$$ ($R^2 = 0.99356$)

This equation is in dimensionless form and the concrete strength is not an influencing parameter. The effective length L_{eff}, which is dependent on the stiffness of the FRP sheet ($t \cdot E_{FRP}$), and the depth and its orientation angle of FRP are found to be the most significant variables influencing the remaining bonded area ratio.

7.4 Design Equation based on Shear Friction Method

7.4.1 Strength along the Weakest Plane through Stirrups

In 1998, LOOV reviewed the CSA-A23.3 (1994) simplified method of shear design using the shear friction approach. The shear strength along a plane crossing *n* spaces and intersecting *n-1* stirrups can be written as

[7.13] $$V_r = 0.25 k^2 f_c' b_w h \frac{d_s}{ns} + T_v(n-1)$$

where the experimentally determined factor k is given by (LOOV and PENG, 1998):

[7.14] $$k = 2.1\left(f_c'\right)^{-0.4}$$

and b_w is the width of the web and h is the height of the beam; d_s is the height of the stirrups and s is the stirrup spacing. T_v is the tension force in a stirrup and can be expressed as:

[7.15] $$T_v = A_v f_{vy}$$

A_v and f_{vy} are the area and the yield strength of the stirrups, respectively.

The effect of the FRP sheets bonded to the side of the beam web can be added and Equation (7.13) is then re-written as

[7.16] $$V_r = 0.25 k^2 f_c' b_w h \frac{d_s}{ns} + T_v(n-1) + nT_{FRP}$$

with

[7.17] $$T_{FRP} = \frac{s}{d_s} d_{FRP}\, t\, E_{FRP}\, \varepsilon_{max}\, R_L$$

In the above equation, T_{FRP} represents the contribution of the FRP sheets applied without any gap between two stirrups. All the terms of the Equation (7.17) are defined in the previous sections.

For design purposes, it is conservative to ignore the contribution of the concrete flange for T-beams and I-beams. However, Tozser and Loov (1999) suggested approximating the effective concrete section of the flange that participates in the shear friction with a 45° angle. Deniaud and Cheng (2000b [Chapter 5]) have also used the effective concrete section in the analysis of their test results with good success.

For members with inclined FRP sheets and with an FRP width band of w_{FRP}, as shown in Figure 7.6, the T_{FRP} contribution of the FRP sheets becomes

$$[7.18] \qquad T_{FRP} = d_{FRP}\, t\, E_{FRP}\, \varepsilon_{max}\, R_L \left(\frac{w_{FRP}}{s_{FRP}}\right)^2 \left(\frac{s}{d_s}\sin\alpha + \cos\alpha\right)\sin\alpha$$

Finally, the governing shear strength of the beam is given by the lowest shear strength among all potential failure planes, calculated with Equation (7.16). With the formulation presented in Equation (7.18) the gap between the FRP bands is assumed very small. This assumption implies that the governing shear strength of the beam does not bypass the FRP bands. Similar to steel shear reinforcement, Khalifa *et al.* (1998) suggested limiting the spacing of the FRP bands to

$$[7.19] \qquad s_{FRP} \;\le\; w_{FRP} + \frac{d}{4}$$

The other way to check whether the FRP bands are wide enough to allow the formation of a diagonal crack without intercepting a band is to actually calculate the shear strength of this failure mode. The following equation should then be checked.

$$[7.20] \qquad V_r \;\le\; 0.25k^2 f'_c\, b_w\, h \frac{d_{FRP}}{s_{FRP} - w_{FRP}} \;+\; T_v n_s$$

where n_s is the number of stirrups crossing the clear distance between two consecutive FRP bands, if any.

7.4.2 Continuous Equation

Equation (7.16) was developed in a discrete format. Therefore, all the potential shear planes must be evaluated to find the weakest shear strength of the beam. In some cases, several repetitive computations are needed. Although a computer program can be written to find the critical shear path given the layout of the stirrups and the shear span, it is desirable to have a continuous design equation to avoid the need of iteration. If we assume *n* to be continuous rather than discrete, Equation (7.16) can be differentiated with respect to *n* and set equal to zero.

$$[7.21] \qquad \frac{\partial V_r}{\partial n} = -0.25k^2 f_c' A_c \frac{d_s}{n^2 s} + T_v + T_{FRP} = 0$$

The number of spaces corresponding to the weakest shear plane is then given as

$$[7.22] \qquad n = 0.5k\sqrt{\left(\frac{f_c' A_c}{T_v + T_{FRP}}\right)\left(\frac{d_s}{s}\right)}$$

By inserting *n* from Equation (7.22) into (7.21), the continuous shear friction design equation can be derived:

$$[7.23] \qquad V_r = k\sqrt{f_c' A_c \left(T_v + T_{FRP}\right)\frac{d_s}{s}} - T_v$$

It should be noted that the negative sign is not a typographical error but follows the derivation. It simply means that no stirrups are crossing until n > 1.

7.5 Validation of the Proposed Equations

7.5.1 Experimental Test Data

The available test data were used to validate the proposed design method. The data include both small-scale specimens (SATO *et al.*, 1996; UJI, 1992; AL-SULAIMANI et al., 1994; CHAJES *et al.*, 1995; TRIANTAFILLOU, 1998) and full-scale specimens (DRIMOUSSIS and CHENG, 1994; ADEY *et al.*, 1997; DENIAUD and CHENG, 2000a [Chapter 4] and 2000b [Chapter 5]). The beam specimens fully wrapped by FRP sheets reported by TRIANTAFILLOU (1998) were not considered here. In rehabilitation projects, it is often not practical to fully wrap the beams due to limited access. Table 7.2 describes the available experimental data. In total, 35 test specimens strengthened with FRP sheets were considered.

7.5.2 Discussion of the Design Equations

Equation (7.23) was used to predict the available experimental test results. The corresponding values, using an effective concrete area, used in the equation are listed in

Table 7.3. For comparison purposes, both the rectangular beam cross section and the effective concrete area were investigated and the results are shown in Figures 7.7 and 7.8, respectively. As expected, the predictions using a rectangular cross section for the T-beams (both Drimoussis and Cheng's and Deniaud and Cheng's data in the figures) are found more conservative than the predicted values using effective concrete area, as recommended by TOZSER and LOOV (1999).

As mentioned earlier, the proposed method does not include, in this present form, the effect of the FRP width when bands are used. Therefore, some results were found very conservative as noted in the Figure 7.7.

CHAJES *et al.* (1995) reported that the fabric did not debond prior to failure in any of their tests. Just prior to failure of the concrete, the FRP strain measurement also indicated that the fabrics had not reached their full tensile capacity. This premature FRP sheet failure may explain the non-conservative predictions. With all but one of their tests, the maximum FRP strain calculated with Equation (7.10), as shown in Table 7.3, was limited by the ultimate strain of the FRP (see Table 7.2). It is therefore possible that the use of ultimate FRP strains for the beam strength predictions were not appropriate. Further investigations are required to study this particular failure mode.

The experimental results reported by DRIMOUSSIS and CHENG (1994) are slightly over-estimated, as shown in Figures 7.7 and 7.8. The legs of the type E-girder were tapered and only the average width of the girder legs was reported in Table 7.2. These bridge girders were also designed with a large shear key slot on both side of the flange. With less concrete area in the flange, the capacity of the beam is then decreased. This reduction in concrete area was not taken into account in Equation (7.22).

The conservative predictions with the test specimens presented by UJI (1992) cannot be rationally explained by the author. Possible explanations, such as the scale effect or the variability of the experimental test (including the concrete cylinder tests), can only be suggested.

7.6 Illustration of the Proposed Equations

7.6.1 Design Example

The design example (Example 4.4) used in the CPCA Design Handbook (1995) is used here to illustrate the design procedures using the proposed method. Figure 7.9 shows the beam dimensions, support conditions and other details including the stirrups spacing. The beam has a simple span of 11 m, a cantilever span of 3.5 m, and is loaded uniformly. Assume that the beam needs to carry a 30% more live load. The factored uniform design load then becomes

$$w_f = 1.25w_D + 1.5w_L = 1.25 \times 30 + 1.5 \times (\mathit{1.3}) \times 35 = 106 \text{ kN/m}$$

The shear at the support toward the interior span is found to be 642 kN. Given that d_v = 844 mm at the negative moment location, f_c' = 25 MPa (normal concrete), f_y = 400 MPa, ϕ_c = 0.60, ϕ_s = 0.85 and A_v = 200 mm^2. The critical section for shear is located at a distance d_v from the face of the support and is calculated as

$$V_f = 642 - 106\text{x}(0.15+0.844) = 536.6 \text{ kN}$$

The first step in the design is to calculate k using the Equation (7.14):

$$k = 2.1(25)^{-0.4} = 0.580$$

From Equation (7.15):

$$T_v = 200\text{x}400\text{x}10^{-3} = 80 \text{ kN}$$

Re-arranging Equation (7.23) to solve for T_{FRP}, including the concrete, steel and FRP resistance factors ϕ_c, ϕ_s and ϕ_{FRP}, respectively, we have

$$[7.24] \qquad \phi_{FRP}\,T_{FRP} \geq \left(\frac{V_f + \phi_s T_v}{k}\right)^2 \frac{s}{d_s \phi_c f_c' A_c} - \phi_s T_v$$

$$\phi_{FRP}\,T_{FRP} \geq \left(\frac{536.6 + 0.85 \times 80}{0.580}\right)^2 \frac{400}{910(0.6 \times 25)(1000 \times 450)10^{-3}} - 0.85 \times 80 = 2.76\,\text{kN}$$

Assume that the manufactured glass fibres *Tyfo SEH51* (Fyfe Co. LLC, 1999) were selected for the shear reinforcement of the beam and have the same material properties of the FRP previously given in section 7.2.3. Also assume that a resistance factor ϕ_{FRP} of 0.50 is used as suggested for the glass FRPs (ISIS, 2000), Equation (7.1) gives:

$$L_{eff} = \exp\left(6.134 - 0.58\ln(35.85)\right) = 57.9\,\text{mm}$$

Now, assume that the FRP sheets are to be bonded to the side and on both faces of the beam with the principal fibres oriented at 90° from the longitudinal axis of the beam. Thus, $k_a = 2.0$, $k_e = 2$ and $\alpha = 90^{\circ}$. Consider also that only the first 2/3 of the beam height were accessible which gives $d_{FRP} = 666$ mm. From Equation (7.10)

$$\varepsilon_{max} = \frac{3\sqrt{25} \times 666^{0.16}}{35.85^{1.5} \times (2 \times \sin 90^{\circ})^{0.1}} = 0.185\ \% \quad \leq \quad 2\%$$

From Equation (7.12)

$$R_L = 1 - 1.2\exp\left(-\left(\frac{666}{2 \times 57.9 \times \sin 90^{\circ}}\right)^{0.4}\right) = 0.840$$

Next, assume that 40 mm clear cover top and bottom to the No. 10 stirrups was required, thus $d_s = 910$ mm. Finally, Equation (7.18) can be re-arranged and solved for the ratio w_{FRP} over s_{FRP} as

$$[7.25] \qquad \frac{w_{FRP}}{s_{FRP}} \geq \sqrt{\frac{T_{FRP}}{\phi_{FRP}\, d_{FRP}\, tE_{FRP}\, \varepsilon_{max}\, R_L} \frac{d_s}{s}}$$

$$\frac{w_{FRP}}{s_{FRP}} \geq \sqrt{\frac{2.76}{0.5 \times 666 \times 35.85 \times 0.185/100 \times 0.840} \times \frac{910}{400}} = 0.582$$

If we assume that $w_{FRP} = 200$ mm, then we find $s_{FRP} < 344$ mm. Use 100 mm gap. The maximum spacing of the FRP bands is also found to be adequate with Equation (7.19). Given d=937.5 mm,

$$s_{FRP} \leq 200 + \frac{937.5}{4} = 434\,\text{mm}$$

Equation (7.20) can also be used to check the adequacy of the spacing s_{FRP}.

7.6.2 Comparison between the Discrete and Continuous Design Equations

In the above example, the factored shear resistance provided can be found using Equations (7.18) and (7.23), which give $T_{FRP} = 7.25$ kN and $V_r = 539.7$ kN.

As mentioned earlier, the discrete formulation more accurately represents the critical shear path. Several calculations were performed using Equation (7.16) and an increasing number of spacings, *n*, to scan the potential crack paths and find the weakest shear strength. The resistance factors were added in Equation (7.16) to give comparable values with the above example. Table 7.5 summarizes the results. The weakest shear plane was found when three stirrups (four spaces) are crossing the shear plane. In this case, the beam shear strength is 541 kN, which is slightly higher than the prediction by the continuous equation.

In fact conservative results will always be obtained with the continuous equation. Both equations lead to the same shear strength only when the number of spaces given by Equation (7.22) yields an integer number.

7.7 Conclusion

A simple design formulation for the evaluation of reinforced concrete beam strengthened in shear with FRP sheets was presented. The proposed equations are based on the strip model and the shear friction approach. From this study, the following conclusions can be drawn:

1. The proposed design formulation can conservatively predict the experimental test results. The steps in calculating the strength of the beam are simple and easy to use without any iteration.
2. A parametric study was carried out to investigate the FRP sheet shear contribution with well-defined variables within their useful range of application. The maximum bond strain and the remaining bond area at the time of FRP debonding failure were presented using two simple equations from the regression analyses.
3. The strip method used to evaluate the FRP contribution can also be adapted for other FRP sheet anchorage configurations. The description of the anchor should, however, be evaluated with care.
4. The interface bond strength curve requires further study. In particular, further investigations are required to fully assess the width effect of the FPR bands when the FRP sheets are not continuously bonded to the concrete beam along the shear span.
5. Despite the simplicity of the method, the proposed method well describes the interaction between the concrete, the stirrups and the FRP sheets. Since the concrete crack angle is no longer limited to 45°, the variable angles therefore enhances the accuracy of the model predictions.

Table 7.1 Summary of the Strip Method Example with Nine Strips

Strip # i	Bond Length L_x mm	Bond Strength τ_x MPa	Maximum Allowable Strain ε_x %	FRP Shear Load V_{FRP} kN
1	425	0.164	0.195	3.49
2	375	0.186	0.195	6.99
3	325	0.215	0.195	10.48
4	275	0.254	0.195	13.98
5	225	0.311	0.195	17.47
6	175	0.399	0.195	20.96
7	125	0.559	0.195	24.46
8	75	0.932	0.195	27.95
9	25	1.894	0.132	21.31

Table 7.2 Experimental Data on Shear Strengthening with FRP

Specimen*	h mm	b_w mm	f_c' MPa	$t \cdot E_{FRP}$ kN/mm	ε_{FRPult} %	d_{FRP} mm	s mm	d_s mm	α deg	V_{exp} kN
Dr(2NE)	610	206	28.0	24.0	1.67	430	860	543	90	198.0
Dr(2SW)	610	206	28.0	24.0	1.67	485	705	543	90	229.0
Dr(3NE)	610	206	28.0	24.0	1.67	510	660	543	90	235.0
Dr(3SW)	610	206	28.0	24.0	1.67	445	625	543	90	146.5
D(T4NSG90)	400	140	30.2	31.9	1.41	250	1100	400	90	159.0
D(T4S4G90)	400	140	30.0	31.9	1.41	250	400	354	90	205.6
D(T4S2G90)	400	140	30.3	31.9	1.41	250	200	354	90	225.6
D(T4S2C45)	400	140	29.4	31.4	0.95	250	200	354	45	219.1
D(T4S2Tri)	400	140	30.4	20.3	1.29	250	200	354	90	242.7
D(T6NSC45)	600	140	44.1	31.4	0.95	450	1550	600	45	213.6
D(T6S4C90)	600	140	44.1	31.4	0.95	450	400	554	90	272.8
D(T6S4G90)	600	140	44.1	31.9	1.41	450	400	554	90	297.5
D(T6S4Tri)	600	140	44.1	20.3	1.29	450	400	554	90	316.7
D(T6S2C90)	600	140	44.1	31.4	0.95	450	200	554	90	309.8
A(B2)	400	200	46.4	29.9	1.52	267	750	400	45	210.7
A(B5)	400	200	46.4	29.9	1.52	267	150	334	45	271.7
S(S2)	300	200	45.2	25.5	1.51	300	700	300	90	160.5
S(S3)	300	200	41.3	25.5	1.51	300	700	300	90	202.1
S(S4)	300	200	37.5	25.5	1.51	300	700	300	90	156.3
S(S5)	300	200	39.7	25.5	1.51	300	700	300	90	198.2
U(5)	200	100	24.1	22.4	1.15	200	425	200	90	89.3
U(6)	200	100	26.9	22.4	1.15	200	425	200	56	113.8
U(7)	200	100	26.9	44.7	1.15	200	425	200	90	89.3
C(A)	191	64	46.9	11.5	2.03	127	406	191	90	34.4
C(E)	191	64	45.1	6.5	1.20	127	406	191	90	35.4
C(G)	191	64	45.5	12.3	0.89	127	406	191	90	36.0
C(G45)	191	64	44.5	12.3	0.89	127	406	191	45	42.4
A-S(SO)	150	150	37.7	46.7	1.29	150	200	94	90	41.5
A-S(WO)	150	150	37.7	46.7	1.29	120	200	94	90	42.0
T(S1-90)	110	70	30.0	36.2	1.40	110	320	110	90	20.6
T(S1-45)	110	70	30.0	36.2	1.40	110	320	110	45	22.3
T(S2-90)	110	70	30.0	36.2	1.40	110	320	110	90	22.6
T(S2-45)	110	70	30.0	36.2	1.40	110	320	110	45	23.7
T(S3-90)	110	70	30.0	36.2	1.40	110	320	110	90	20.1
T(S3-45)	110	70	30.0	36.2	1.40	110	320	110	45	20.4

* Dr=Drimoussis and Cheng (1994); D=Deniaud and Cheng (2000a and 2000b) [Chapter 4 and 5]; A=Adey *et al.* (1997); S=Sato *et al.* (1996); U=Uji (1992); C=Chajes *et al.* (1995);A-S=Al-Sulaimani *et al.* (1994); T=Triantafilliou (1998)

Table 7.3 Predicted Beam Strength using an Effective Concrete Area

Specimen	A_c (eff. area) mm^2	k_a	k_e	L_{eff} mm	T_v kN	ε_{max} %	R_L	V_r kN
Dr(2NE)	135660	2.00	2	73.1	56.3	0.34	0.743	210.4
Dr(2SW)	135660	2.00	2	73.1	56.3	0.34	0.762	236.1
Dr(3NE)	135660	0.79	1	73.1	56.3	0.38	0.864	260.2
Dr(3SW)	70490	0.79	1	73.1	56.3	0.37	0.845	158.6
D(T4NSG90)	78100	0.79	1	62.0	none	0.23	0.791	139.6
D(T4S4G90)	78100	0.79	1	62.0	29.3	0.23	0.791	163.1
D(T4S2G90)	78100	0.79	1	62.0	29.3	0.23	0.791	205.0
D(T4S2C45)	78100	0.79	1	62.5	29.3	0.23	0.838	176.8
D(T4S2Tri)	78100	0.79	1	80.5	29.3	0.45	0.751	213.0
D(T6NSC45)	106100	0.79	1	62.5	none	0.32	0.904	133.1
D(T6S4C90)	106100	0.79	1	62.5	29.3	0.31	0.867	214.4
D(T6S4G90)	106100	0.79	1	62.0	29.3	0.30	0.868	310.4
D(T6S4Tri)	106100	0.79	1	80.5	29.3	0.59	0.836	332.5
D(T6S2C90)	106100	0.79	1	62.5	29.3	0.31	0.867	286.8
A(B2)	80000	2.00	2	64.3	none	0.30	0.742	151.5
A(B5)	80000	2.00	2	64.3	24.5	0.30	0.742	265.8
S(S2)	60000	2.00	2	70.4	none	0.36	0.690	83.2
S(S3)	60000	1.00	1	70.4	none	0.37	0.799	86.2
S(S4)	60000	2.00	2	70.4	none	0.33	0.690	138.2
S(S5)	60000	1.00	1	70.4	none	0.37	0.799	157.1
U(5)	20000	2.00	2	76.1	none	0.30	0.607	52.4
U(6)	20000	2.00	2	76.1	none	0.33	0.639	53.7
U(7)	20000	2.00	2	50.9	none	0.11	0.676	48.3
C(A)	15000	1.00	1	112.0	none	1.15	0.581	52.7
C(E)	15000	1.00	1	155.4	none	2.62	0.523	38.4
C(G)	15000	1.00	1	107.9	none	1.03	0.587	47.9
C(G45)	15000	1.00	1	107.9	none	1.05	0.648	43.0
A-S(SO)	22500	2.00	2	49.7	25.4	0.12	0.631	27.5
A-S(WO)	22500	2.00	2	49.7	25.4	0.17	0.592	38.0
T(S1-90)	7700	2.00	2	57.5	none	0.15	0.551	10.5
T(S1-45)	7700	2.00	2	57.5	none	0.16	0.612	9.4
T(S2-90)	7700	2.00	2	57.5	none	0.15	0.551	14.0
T(S2-45)	7700	2.00	2	57.5	none	0.16	0.612	12.3
T(S3-90)	7700	2.00	2	57.5	none	0.15	0.551	21.0
T(S3-45)	7700	2.00	2	57.5	none	0.16	0.612	18.4

Table 7.4 Discrete Equation Results

spaces n	V_r kN
1	1293
2	720
3	577
4	541
5	548

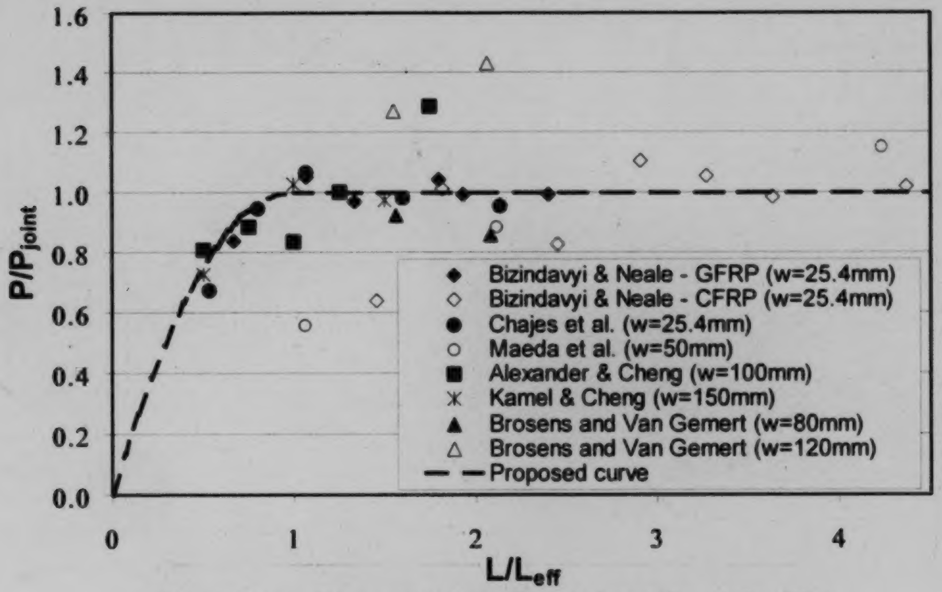

Figure 7.1 Dimensionless Bond Joint Capacity Plot

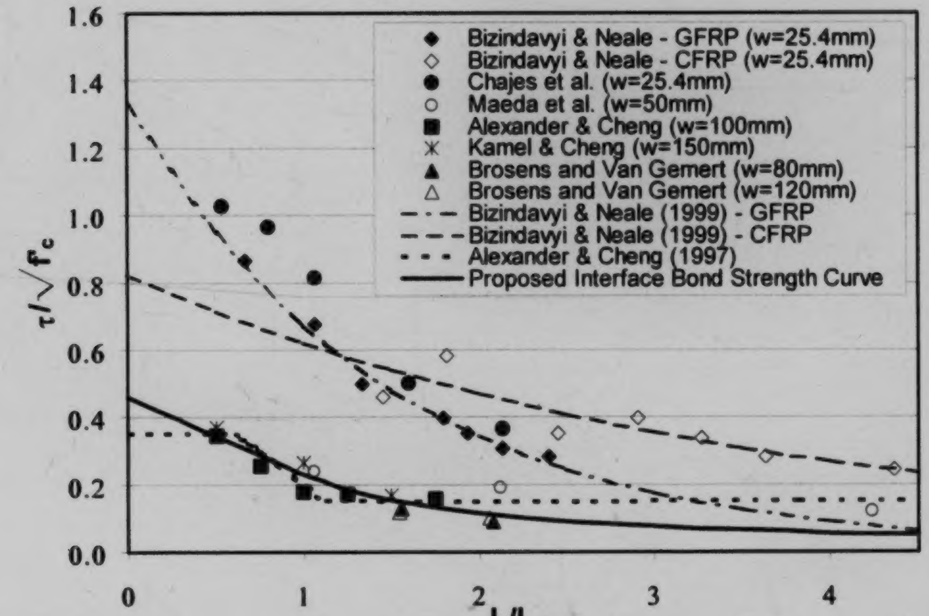

Figure 7.2 Dimensionless Interface Shear Strength Curves

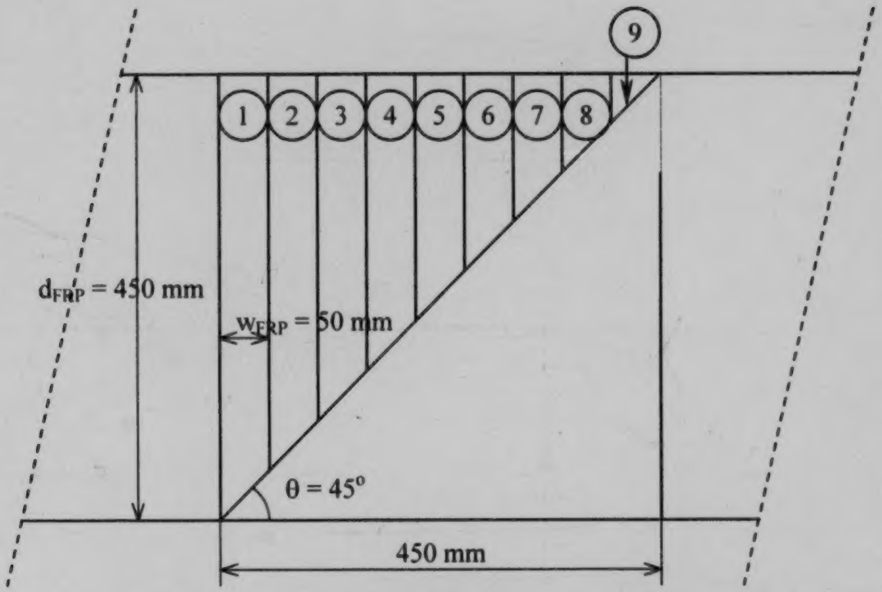
9
1
2
3
4
5
6
7
8
d_{FRP} = 450 mm
w_{FRP} = 50 mm
θ = 45°
450 mm

Figure 7.3 FRP Strip Description used in the Example

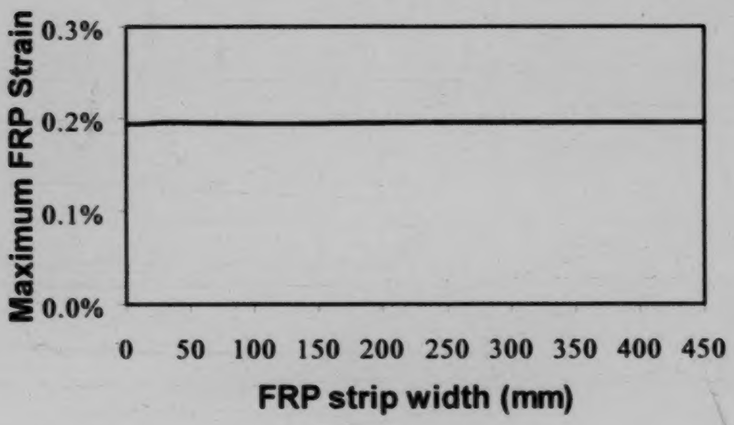

a) ε_{max} variation

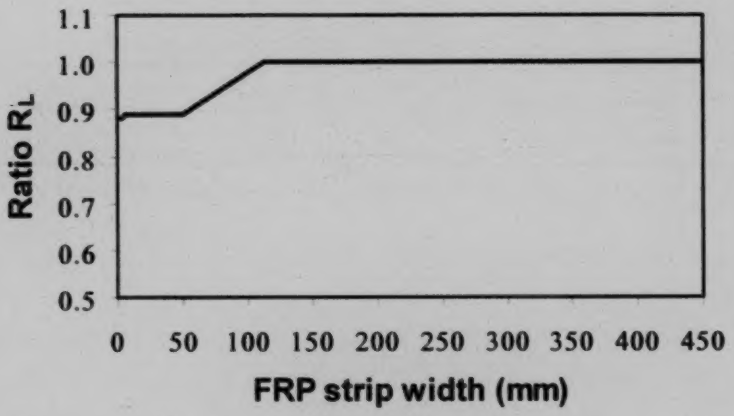

b) R_L variation

Figure 7.4 Influence of the FRP Strip Width

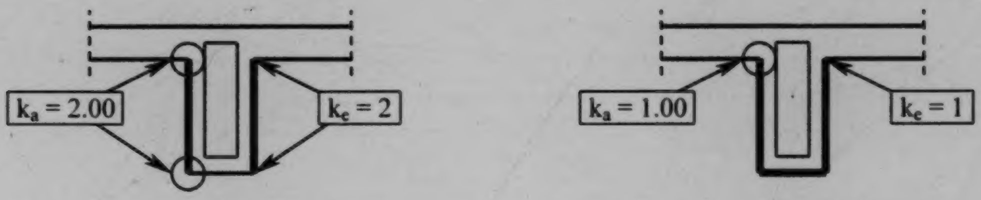
$k_a = 2.00$
$k_e = 2$
$k_a = 1.00$
$k_e = 1$

a) FRPs on lateral faces

b) U-shaped bands

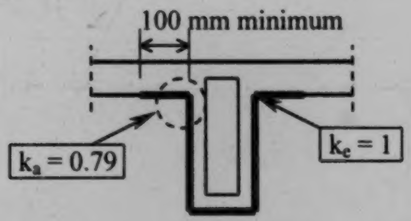
100 mm minimum
$k_a = 0.79$
$k_e = 1$

c) U-shaped bands extended underneath the flange

Figure 7.5 FRP Sheet Anchorage and End Conditions

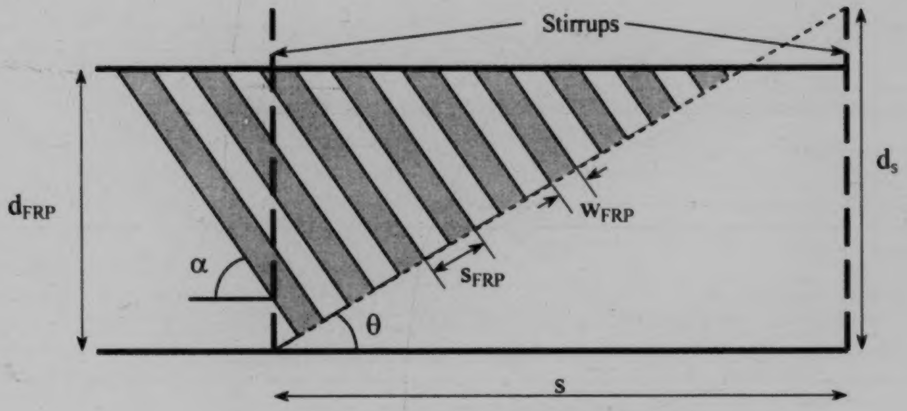
Stirrups
d_{FRP}
d_s
w_{FRP}
s_{FRP}
α
θ
s

Figure 7.6 Inclined FRP Band Notation

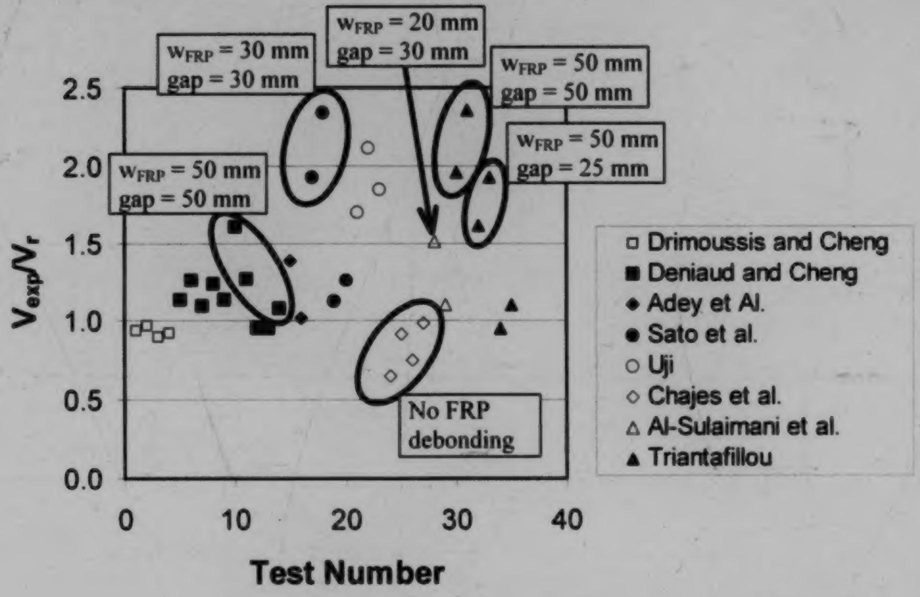

Figure 7.7 Test Predictions Using an Effective Concrete Area

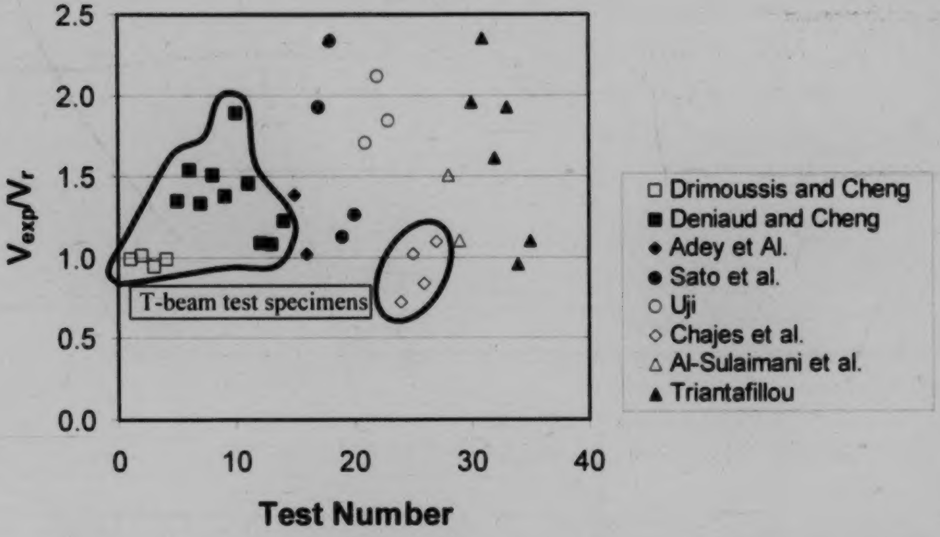

Figure 7.8 Test Predictions Using a Rectangular Concrete Section

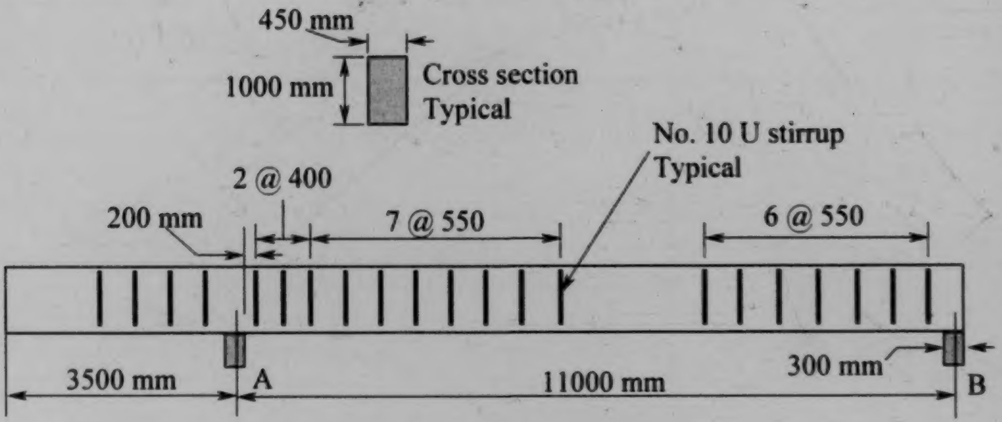
450 mm
1000 mm
Cross section
Typical
No. 10 U stirrup
Typical
2 @ 400
200 mm
7 @ 550
6 @ 550
3500 mm
A
11000 mm
300 mm
B

Figure 7.9 Example Beam

7.8 References

ACI-318 (1995). *Building Code Requirements for Reinforced Concrete*, American Concrete Institute, Farmington Hills, MI.

ADEY B., SAN-ROMÁN J. d. C., and BRÜHWILLER E. (1998). "Carbon Fibre Shear Strengthening of Rectangular Concrete Beams", *Final Report - 97.02*, École Polythechnique de Lausanne, Lausanne, Switzerland, 28 pp.

ALEXANDER, J., and CHENG, J.J.R. (1997). *Shear Rehabilitation of G-Girder Bridges using CFRP Sheets*, Structural Engineering Report No 218, Department of Civil and Environmental Engineering, University of Alberta, Edmonton, AB, 181 p.

AL-SULAIMANI G.J., ISTEM A., BASUNBUL A.S., BALUCH M.H., and GHALEB B.N. (1994). "Shear Repair for Reinforced Concrete by Fiberglass Plate Bonding", *American Concrete Institute Structural Journal*, Vol. 91, No. 3, July-August, pp. 458-464.

BIZINDAVYI L., and NEALE K.W. (1999). "Transfer Lengths and Bond Strengths for Composites Bonded to Concrete", *Journal of Composites for Construction*, ASCE, Vol. 3, No. 4, November, pp. 153-160.

BROSENS K. and VAN GEMERT D. (1999). "Anchorage Design for Externally Bonded Carbon Fiber reinforced Polymer Lamintes", *Proceedings of the Fiber Reinforced Polymer Reinforcement for Reinforced Concrete Structures (4th International Symposium)*, ACI SP-188, Baltimore, MD, pp. 635-645.

CHAJES M.J., FINCH W.W., JANUSZKA T.F., and THOMSON T.A. (1996). "Bond and Force Transfer of Composite Material Plates Bonded to Concrete", *American Concrete Institute Structural Journal*, Vol. 93, No. 2, March-April, pp. 208-217.

CHAJES M.J., JANUSZKA T.F., MERTZ D.R., THOMSON T.A., and FINCH W.W. (1995). "Shear Strengthening of Reinforced Concrete Beams using Externally Applied Composite Fabrics", *American Concrete Institute Structural Journal*, Vol. 92, No 3, May-June, pp. 295-303.

COLLINS M.P., and MITCHELL D. (1987). *Prestressed Concrete Basics*, 1st Edition, Canadian Prestressed Concrete Institute, Ottawa, ON, 614 p.

CPCA (1995). *Concrete Design Handbook*, 2nd Edition, Canadian Portland Cement Association, Ottawa, ON.

CSA-A23.3 (1994). *Design of Concrete Structures*, Canadian Standard Association, Rexdale, ON.

DENIAUD C. and CHENG J.J.R. (2000a). "Reinforced Concrete T-beams Strengthened in Shear with FRP Sheets", Accepted for publication in ASCE *Journal of Composite for Construction* [Chapter 4].

DENIAUD C. and CHENG J.J.R. (2000b)."Shear Behavior of RC T-beams with Externally Bonded FRP Sheets", Accepted for publication in *ACI Structural Journal* [Chapter 5].

DENIAUD C. and CHENG J.J.R. (2000c). "Review of Shear Design Methods for RC Beams Strengthend with FRP Sheets", Accepted for publication in *Canadian Journal of Civil Engineering* [Chapter 6].

DEVORE J.L. (1991). Probability and Statistics for Engineering and the Sciences, 3rd Edition, Brooks/Cole Publishing Company, Pacific Grove, California.

DRIMOUSSIS E.H. and CHENG J.J.R. (1994). *Shear Strengthening of Concrete Girders using Carbon Fiber Reinforced Plastic Sheets*, Structural Engineering Report No 205, University of Alberta, Edmonton, AB, 177 p.

FYFE CO. LLC (1999). "Tyfo Systems for Beams and Slabs", The Fibrwrap® Company, San Diego, USA.

KAMEL A.S., ELWI A.E., and CHENG J.J.R. (2000). "Experimental Study on the Behavior of CFRP Sheets Bonded to Concrete", *Proceedings of the Advanced Composite Materials for Bridges and Structures (ACMBS-3)*, CSCE, Ottawa, ON, (accepted).

KHALIFA A., GOLD W.J., NANNI A., and AZIZ M.I. (1998). "Contribution of Externally Bonded FRP to Shear Capacity of RC Flexural Members", *Journal of Composites for Construction*, American Society of Civil Engineering, Vol. 2, No. 4, November, pp. 195-202.

HUTCHINSON R., ABDELRAHMAN A., RIZKALLA S. and SMITH G. (1997). "Shear Strengthening using FRP Sheets for a Highway Bridge in Manitoba, Canada", *Proceedings of the Non-Metallic (FRP) Reinforcement for Concrete Structures (3rd International Symposium)*, Sapporo, Japan, pp. 531-538.

ISIS (2000). *Strengthening Reinforced Concrete Structures with Externally-Bonded Fibre Reinforced Polymers*, Design Manual-M05 (Draft), Intelligent Sensing for Innovative Structures, Winnipeg, Manitoba.

LOOV R. (1998). "Review of A23.3-94 Simplified Method of Shear Design and Comparison with Results using Shear Friction", *Canadian Journal of Civil Engineering*, Vol. 25, No. 3, April, pp. 437-450.

LOOV R. and PENG L. (1998). "The Influence of Concrete Strength on Shear Friction based Design of Reinforced Concrete Beams", *Proceedings of the International Conference on HPHSC*, Perth, Australia, pp. 505-519.

MAEDA T., ASANO Y., SATO Y., UEDA T., and KAKUTA Y. (1997). "A Study on Bond Mechanism of Carbon Fiber Sheet", *Proceedings of the Non-Metallic (FRP) Reinforcement for Concrete Structures (3rd International Symposium)*, Sapporo, Japan, pp. 279-286.

MALEK A.M., and SAADATMANESH H. (1998). "Analytical Study of Reinforced Concrete Beams Strengthened with Web-Bonded Fiber Reinforced Plastic Plates or Fabrics", *American Concrete Institute Structural Journal*, Vol. 95, No. 3, May-June, pp. 343-352.

MACGREGOR J.G. (1997). *Reinforced Concrete – Mechanics and Design*, 3rd edition, Prentice Hall, Upper Saddle River, NJ, 939 p.

NEALE, K. (2000). "FRPs for Structural Rehabilitation: A Survey of Recent Progress", Progress in Structural Engineering and Materials (in press).

RAHAL K.N. (2000). "Shear Strength of reinforced Concrete: Part II-Beams Subjected to Shear, Bending Moment, and Axial Load", *American Concrete Institute Structural Journal*, ACI, Vol. 97, No. 2, March-April, pp. 219-224.

SATO Y., UEDA T., KAKUTA Y., and TANAKA T. (1996). "Shear Reinforcing Effect of Carbon Fiber Sheet Attached to Side of Reinforced Concrete Beams", *Proceedings of Advanced Composite Materials in Bridges and Structures (ACMBS-2)*, CSCE, Montréal, Québec, pp. 621-628.

SPSS, Inc (1999). *SigmatPlot 5.0* (computer software), SPSS Inc, Chicago, Illinois.

TRIANTAFILLOU T.C. (1998). "Shear Strengthening of Reinforced Concrete Beams using Epoxy-Bonded FRP Composites", *American Concrete Institute Structural Journal*, Vol. 95, No. 2, March-April, pp. 107-115.

TOZSER O. and LOOV. R. (1999). "Shear Design of Prestressed beams using Shear Friction", *Proceedings of the Annual Conference of the CSCE*, CSCE, Regina, pp. 195-204.

UJI K. (1992). "Improving Shear Capacity of Existing reinforced Concrete members by Applying carbon Fiber Sheets", *Transaction of the Japan Concrete Institute*, Vol. 14, pp. 254-266.

8 SUMMARY, CONCLUSIONS, AND RECOMMENDATIONS

8.1 Summary

The primary objective of this research was to expand the database for reinforced concrete beams strengthened in shear with FRP sheets, using full-scale specimens. As reported in the literature by several researchers (Al-SULAIMANI *et al.*, 1994; CHAJES *et al.*, 1995), the beam specimens repaired with FRP sheets and tested to failure were very shallow with few or no stirrups. The shear capacity evaluation of beams strengthened with FRP was also limited to basic design methods. The FRP contribution was simply derived from the steel stirrup formulation with minor modifications to account for the properties of the FRP. The intent throughout this study has been to find, or develop, a rational design method that includes and integrates all shear carrying components.

Four type G-girders removed from existing bridges were first tested in the I.F. Morrison Structural Testing Laboratory at the University of Alberta. The type G-girders have been found deficient in shear and torsion when loaded eccentrically about the centroid of the cross section (ALEXANDER and CHENG, 1997). Glass and carbon fibre materials were used with various sheet configurations as a shear repair technique to enhance the load capacity of the girders. Three commonly used shear strength evaluation methods: a) Strut-and-Tie, b) Modified Compression Field Theory, and c) grid analysis were investigated and the results compared to the experimental data. The shear capacity of each beam was accurately predicted, but was limited to the ultimate shear load and to the elastic range of the load deflection curves.

In the second part of the experimental program, eight full-scale T-beams were cast in laboratory conditions and were extensively instrumented. Both ends of each beam were tested separately to provide a total of 16 test results. The objective was to study the effects of the concrete strength, the stirrups spacing, the height of the beam web and the type of FRP on the behaviour of the FRP-strengthened concrete beams. This experimental work provided data to enhance basic understanding of the interaction between concrete, internal stirrups and FRP sheets in carrying shear load.

The current shear design methods, as well as the recently proposed models which include the FRP contribution, were then reviewed. The experimental T-beam data was used to compare the predicted loads from each model investigated. From this analysis, design equations, which account for the interaction of the concrete, the steel stirrups and the FRP sheets, were developed. The method adopted the strip model for the FRP and the shear friction approach for the shear capacity of the strengthened beam. The proposed equations were validated with the available data found in the literature and very good predictions of the beam behaviour were observed.

8.2 Conclusions

The G-girder tests revealed that the shear capacity could be increased effectively using FRP sheets. The inclined sheets were found to be more efficient than the vertical sheets and the woven glass fabric performed better than the unidirectional carbon/glass sheets. However, the end panel of the girder remained the weakest part under eccentric loading.

The T-beam testing program provided a significant database on full-scale reinforced concrete beam specimens strengthened in shear with FRP that has not been investigated or reported in the literature. The experimental findings are reported below:

1. The effectiveness of FRP strengthening to the shear contribution is dependent on the amount of internal reinforcement. The FRP sheets are less effective when beams are heavily reinforced with internal reinforcement. Eventually, the external FRP reinforcement can reduce the shear capacity of the beam by changing the critical path that will lead to an even more sudden shear failure.
2. The FRP strains are uniformly distributed among the FRP strips crossing the concrete shear crack.
3. The height and the geometry of the beam affect the failure mode of the FRP sheets. With a 400 mm high specimen, the continuous glass fibres failed by vertical tearing (unzipping) of the fibres close to the support. With a 600 mm high T-beam, the FRP sheets debonded and peeled above the concrete shear crack. The debonded sheets then buckled like a thin shell when the sheets were longitudinally wrapped without any gap.
4. Tri-axial glass fibre reinforcement provides the beam with a more ductile failure than the ones strengthened by unidirectional glass fibres or unidirectional carbon fibres with a 50 mm gap.

5. Plane sections do not remain plane in the shear span after a certain load level is reached, but the external FRP sheets delay the loss of the plane section behaviour.
6. The shear forces carried by arching action are delayed when FRP is used. The beam action can often represent between 20% to 40% of the ultimate load when FRP are used.

Several FRP shear design models recently proposed in the literature were reviewed and compared with the experimental data collected during this investigation. From this analysis, the mechanical design model based on combination of the strip model (ALEXANDER and CHENG, 1997) and the shear friction approach (LOOV, 1998) provided the most reliable and consistent predictions. This modified shear friction method predicted also accurate estimate of concrete crack angles and an accurate description of the failure modes. Data were generated by the strip method with well-defined variables within their useful range of application. A regression analysis reduced this data to the following two simple equations for the maximum FRP strain ε_{max} and the remaining bonded to total lengths ratio R_L

[8.1] $$\varepsilon_{max} = \frac{3\sqrt{f_c'}\, d_{FRP}^{\;0.16}}{(t\,E_{FRP})^{3/2}(k_a \sin\alpha)^{1/10}} \qquad \text{(in percent)}$$

[8.2] $$R_L = 1 - 1.2\exp\left[-\left(\frac{d_{FRP}}{k_e\, L_{eff} \sin\alpha}\right)^{0.4}\right]$$

where f_c' is the concrete strength, d_{FRP} is the height, t is the thickness, E_{FRP} is the elastic modulus, and α is the principal fibre direction of the FRP sheets. f_c', d_{FRP} and $t \cdot E_{FRP}$ have units of MPa, mm and kN/mm, respectively. k_e and k_a are two parameters describing the anchorage conditions. The effective bond length L_{eff} is given by

[8.3] $$L_{eff} = \exp[6.134 - 0.58\ln(t\,E_{FRP})] \qquad (L_{eff} \text{ is in mm})$$

Finally, a simple shear design formulation based on the modified shear friction approach was derived as

[8.4] $$V_r = k\sqrt{f_c' A_c (T_v + T_{FRP})\frac{d_s}{s}} - T_v$$

with

[8.5a] $$k = 2.1\left(f_c'\right)^{-0.4}$$

[8.5b] $$T_v = A_v\, f_{vy}$$

[8.5c] $$T_{FRP} = d_{FRP}\, t\, E_{FRP}\, \varepsilon_{max}\, R_L \left(\frac{w_{FRP}}{s_{FRP}}\right)^2 \left(\frac{s}{d_s}\sin\alpha + \cos\alpha\right)\sin\alpha$$

where A_c is the effective concrete area, d_s and s are the length and the spacing of the stirrups, A_v and f_{vy} are the cross-sectional area and the yield strength of the stirrups, and w_{FRP} and s_{FRP} are the width and the spacing of the FRP bands. The Equation (8.4) is easy to use and has the advantage of taking into account not only the contribution of the concrete, the stirrups and the FRP sheets but also the interaction of all these shear resisting components. It was also determined that the concrete crack angle is no longer limited to 45°. Variable angles can indeed be used, thereby enhancing the accuracy of the model predictions. Equation (8.4) is therefore a significant improvement compared to the current design equations found in the literature.

8.3 Recommendations

To refine the design approach developed and presented in this research, further studies should be undertaken. Because the FRP sheets are externally bonded to the concrete surface, a better understanding of the bond characteristics of the FRP and concrete interface is required. In particular, the effect of the FRP fibre direction and the principal loads should be investigated. Many researchers have published bond test results with unidirectional fibres. The bond properties of other types of FRP material such as the Tri-axial and the woven fabrics, should also be rigorously evaluated. Further investigations are also required to fully assess the width effect of the FRP bands when the FRP sheets are not continuously bonded to the concrete beam along the shear span.

Because access to deficient concrete beams is often limited in shear rehabilitation projects, usually the FRP sheets are only partially wrapped on the member. A good anchorage on both ends of the FRP sheets is recommended and many anchorage systems for the FRP sheets have been proposed in the literature. Often, the performance of each anchor is only qualitatively defined and should be rationally evaluated. The strip method has the potential to describe any FRP sheet anchorage configuration using a free body diagram.

The shear friction approach was used to determine the concrete shear crack angle in this study for the simplicity of the method. The Modified Compression Field Theory (MCFT) is also available to determine the shear crack angle. A validation of the equations used in the MCFT to predict the behaviour of reinforced concrete beams strengthened in shear with FRP should be undertaken.

This research was limited to reinforced concrete members but the proposed shear design equations should also be able to extend to prestressed concrete beams. Further study in the applicability of the proposed method to prestressed concrete members should be conducted.

Finally, the long-term performance and the durability of the FRP shear strengthening techniques should be studied. The FRP behaviour for shear strengthening in fatigue and under cyclic loading has not yet been assessed and should be investigated.

8.4 References

ALEXANDER, J., and CHENG, J.J.R. (1997). *Shear Rehabilitation of G-Girder Bridges using CFRP Sheets*, Structural Engineering Report No 218, Department of Civil and Environmental Engineering, University of Alberta, Edmonton, AB, 181 p.

AL-SULAIMANI G.J., ISTEM A., BASUNBUL A.S., BALUCH M.H., and GHALEB B.N. (1994). "Shear Repair for Reinforced Concrete by Fiberglass Plate Bonding", *American Concrete Institute Structural Journal*, Vol. 91, No. 3, July-August, pp. 458-464.

CHAJES M.J., JANUSZKA T.F., MERTZ D.R., THOMSON T.A., and FINCH W.W. (1995). "Shear Strengthening of Reinforced Concrete Beams using Externally Applied Composite Fabrics", *American Concrete Institute Structural Journal*, Vol. 92, No 3, May-June, pp. 295-303.

LOOV R. (1998). "Review of A23.3-94 Simplified Method of Shear Design and Comparison with Results using Shear Friction", *Canadian Journal of Civil Engineering*, Vol. 25, No. 3, April, pp. 437-450.

APPENDIX A ADDITIONAL TYPE G-GIRDER DATA

A.1 Photographs

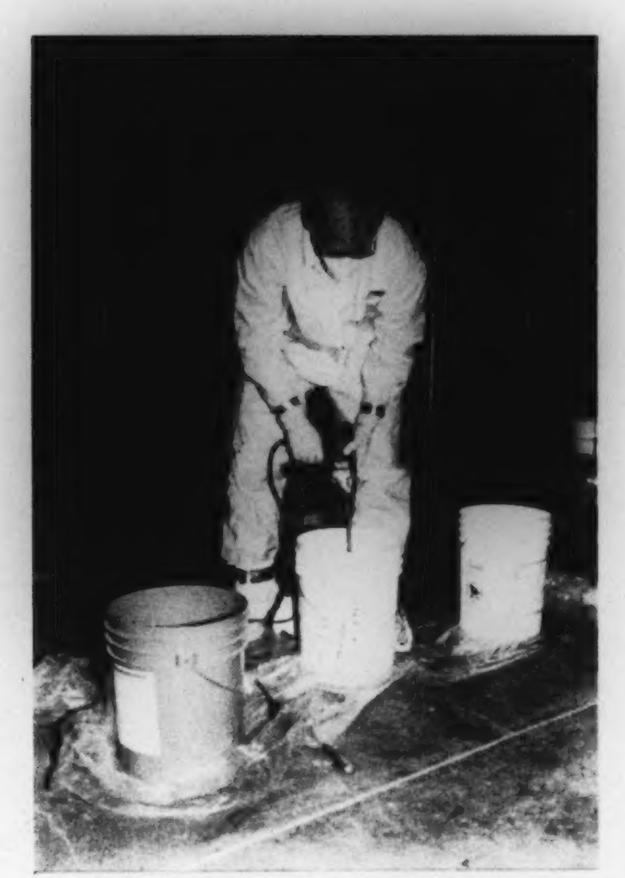

Figure A.1 Preparation and Mixing of the Epoxy

Figure A.2 Epoxy Application on the Face of the Specimen

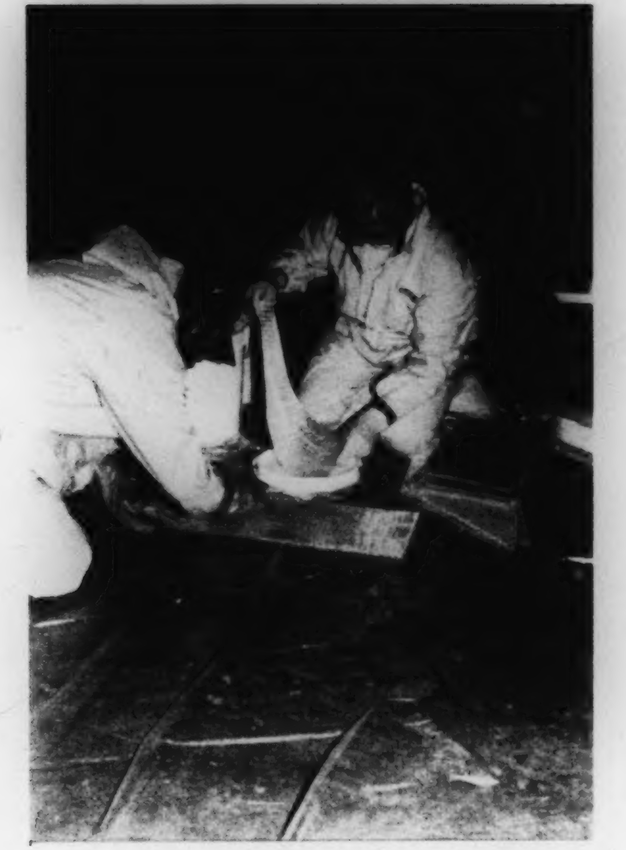

Figure A.3 Soaking the Glass Fibres with Epoxy

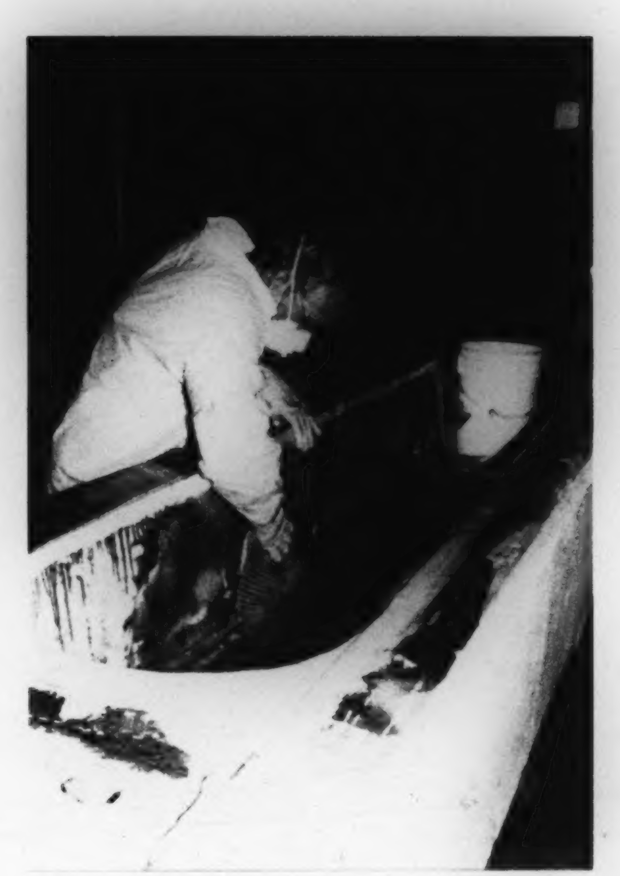

Figure A.4 GFRP Band Application Inside the Leg of the Girder

Figure A.5 GFRP Band Application in the Round End Diaphragm

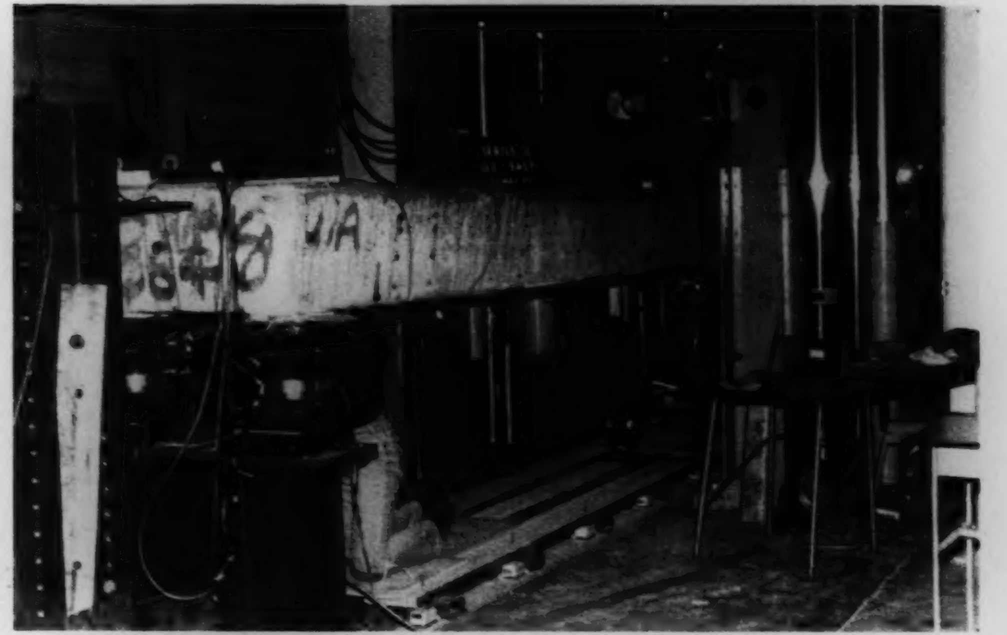
Figure A.6 Overall View of the Test Set-up

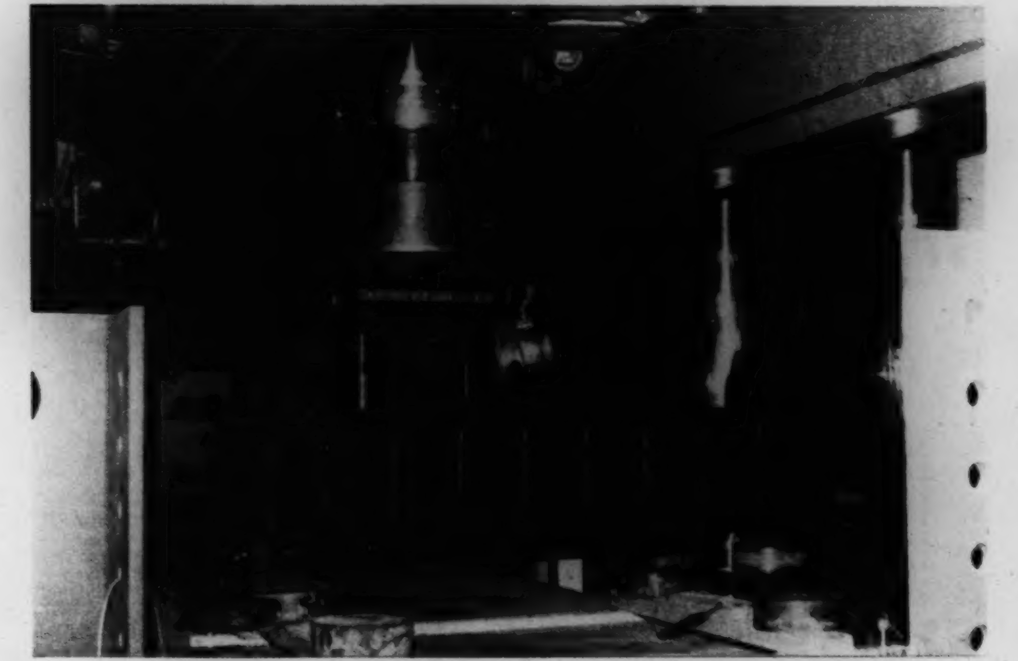
Figure A.7 Close View of the Distributing Beam

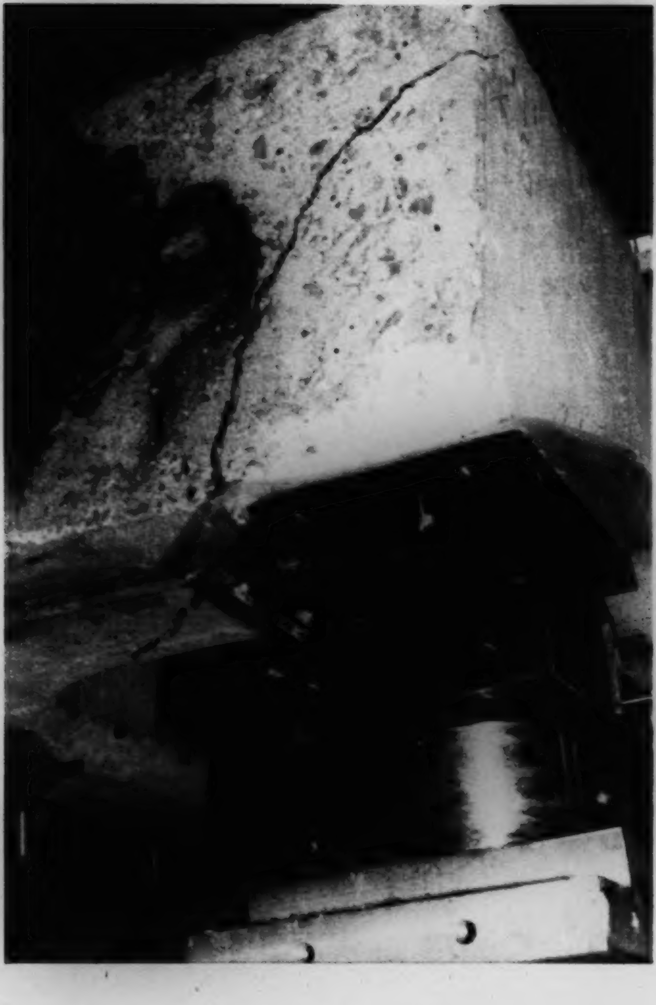

Figure A.8 Typical Round End Diaphragm Crack

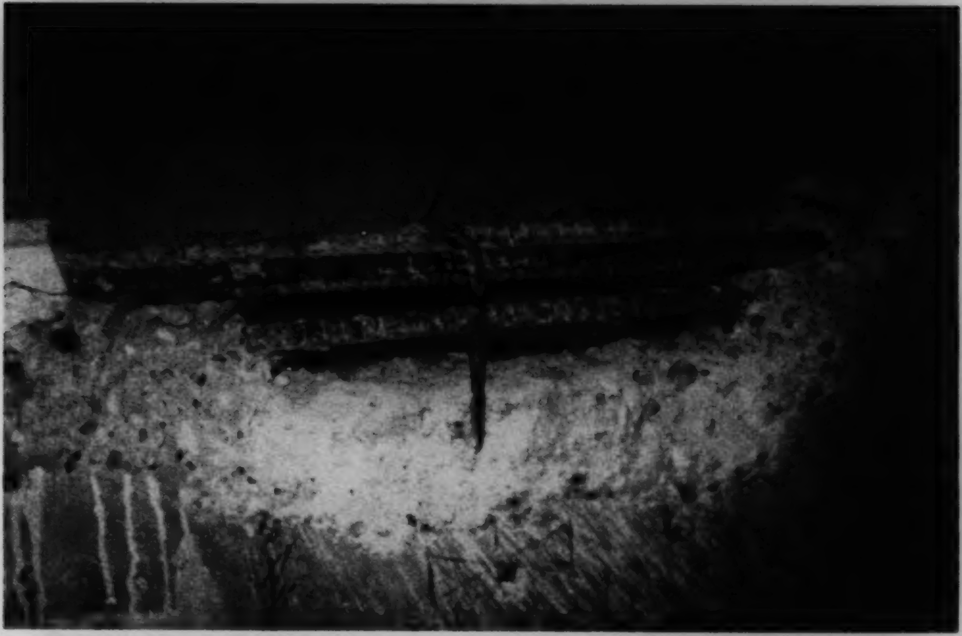

Figure A.9 Exposed Flexural Reinforcement Bars

Figure A.10 Drilling of Concrete Cores

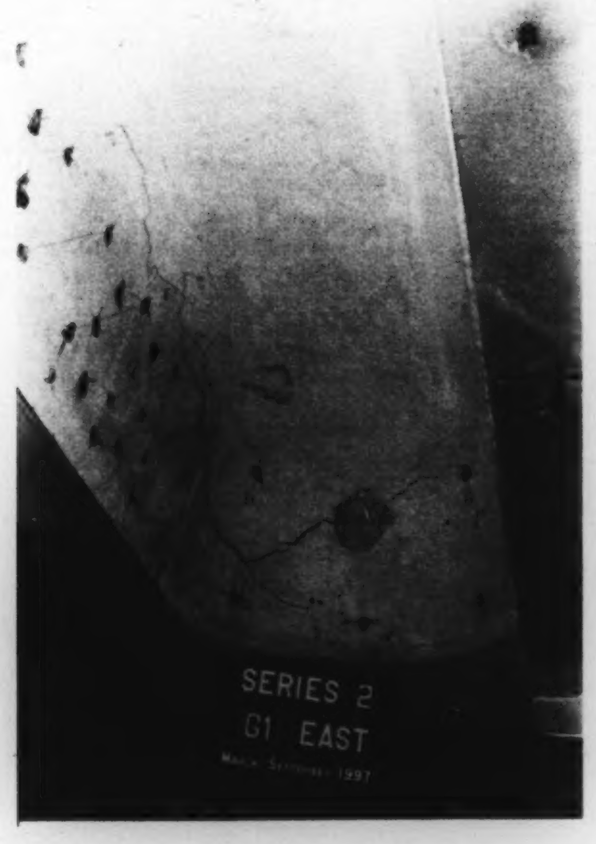
SERIES 2
G1 EAST

Figure A.11 Underneath View of *Girder 1 East* at Ultimate

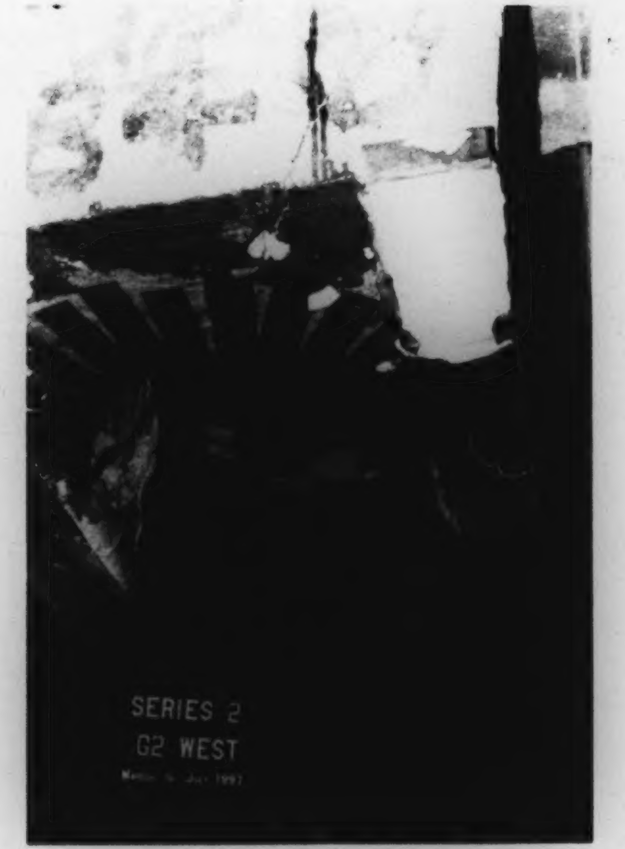
SERIES 2
G2 WEST

Figure A.12 Underneath View of *Girder 2 West* at Ultimate

SERIES 2
G3 WEST
MARCH 18 JULY 1997

Figure A.13 Underneath View of *Girder 3 West* at Ultimate

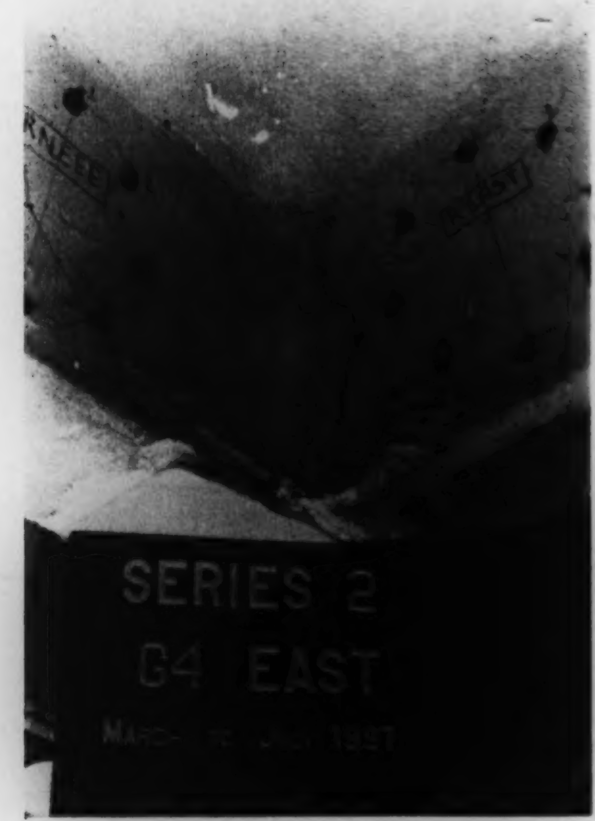
KNEE
SERIES 2
G4 EAST

Figure A.14 Underneath View of *Girder 4 East* at Ultimate

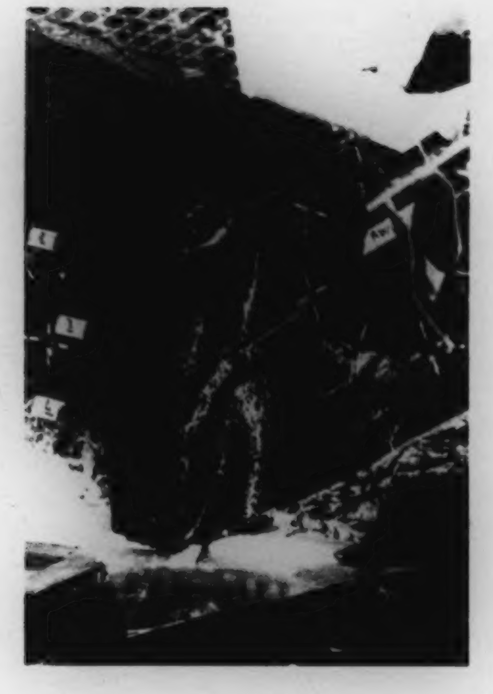

Figure A.15 Underneath View of *Girder 4 West* at Ultimate

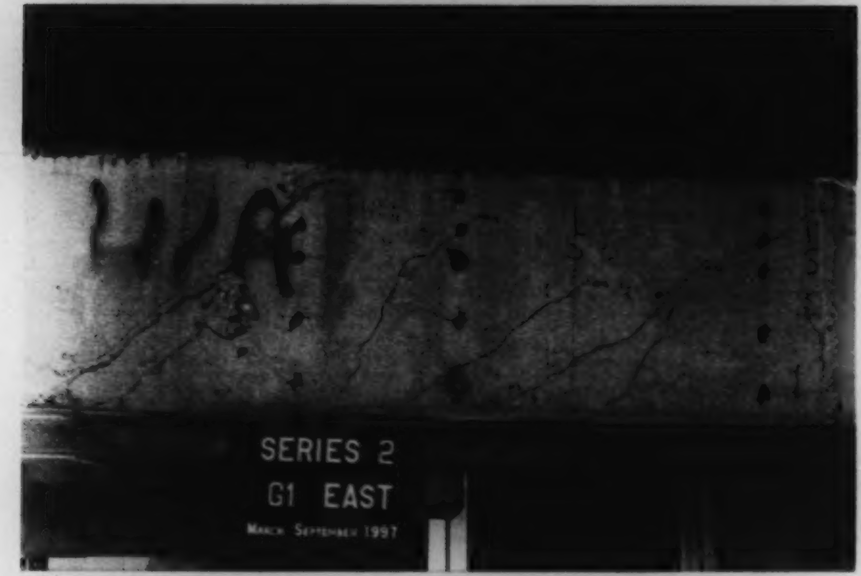
SERIES 2
G1 EAST
MARCH SEPTEMBER 1997

Figure A.16 Concrete Cracks on the Exterior Face of the Loaded Leg without FRP Shear Strengthening (*Girder 1 East*)

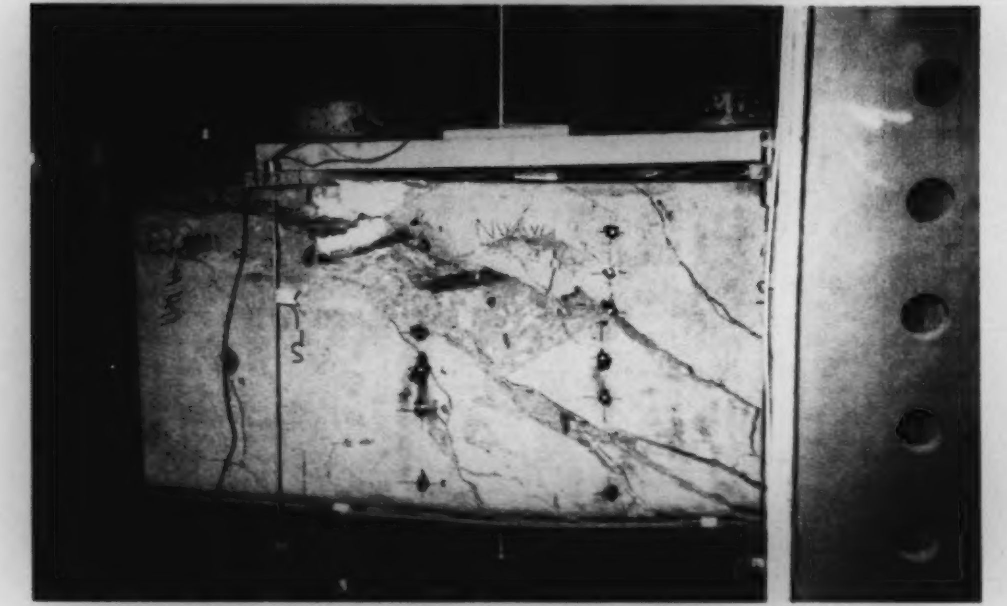

Figure A.17 Concrete Cracks on the Exterior Face of the Loaded Leg with FRP Shear Strengthening (*Girder 2 West*)

A.2 Loaded Leg Shear Crack Patterns

a) At 103 kN

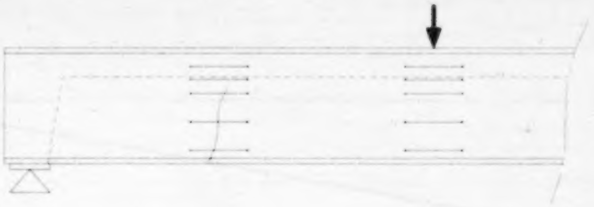

b) At 198 kN

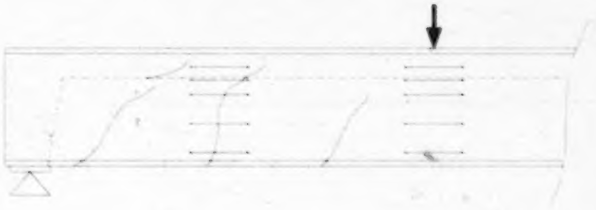

c) At 292 kN

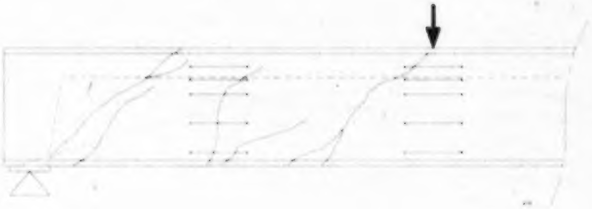

d) At 383 kN (Ultimate)

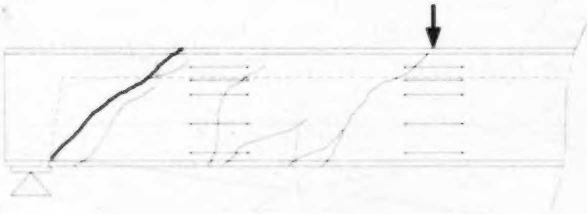

Figure A.18 Cracking Growth of *Girder 1 East*

a) At 176 kN

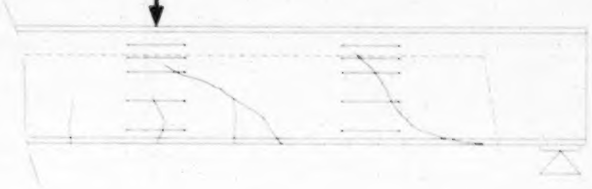

b) At 255 kN

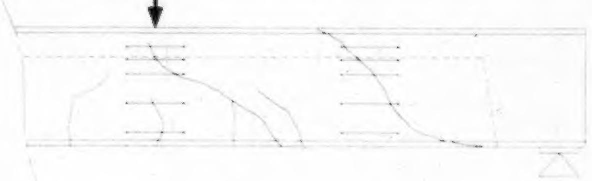

c) At 276 kN (Ultimate)

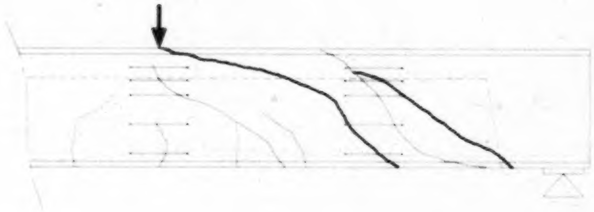

Figure A.19 Cracking Growth of *Girder 1 West*

a) At 98 kN

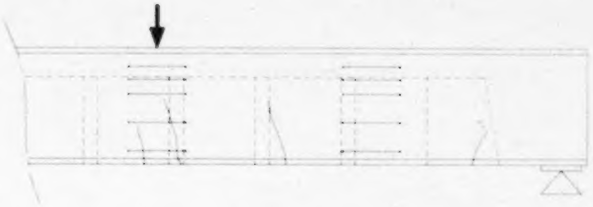

b) At 183 kN

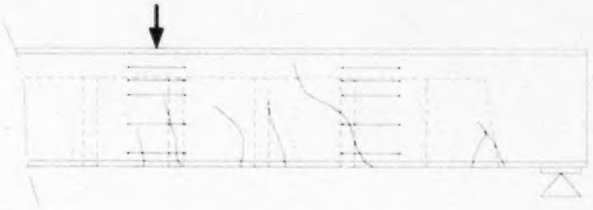

c)At 272 kN

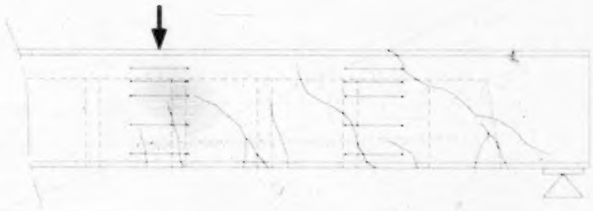

d) At 340 kN (Ultimate)

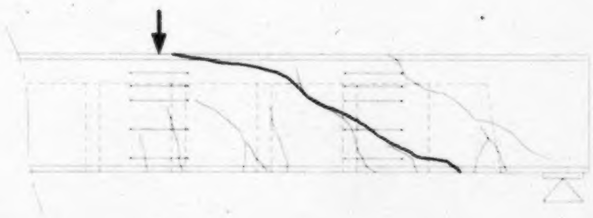

Figure A.20 Cracking Growth of *Girder 2 East*

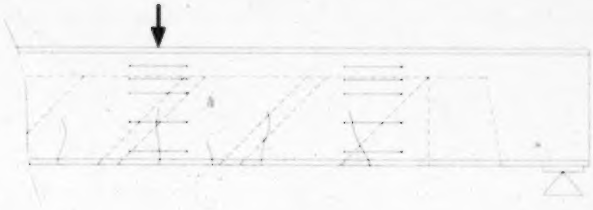

a) At 202 kN

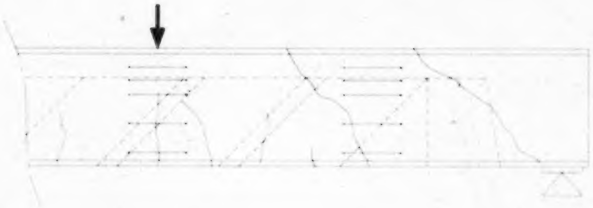

b) At 295 kN

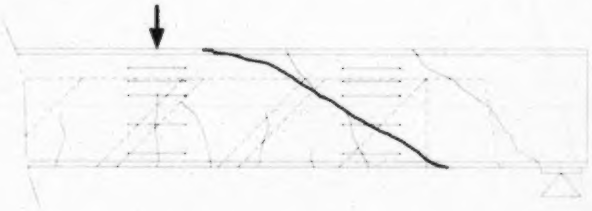

c) At 406 kN (Ultimate)

Figure A.21 Cracking Growth of *Girder 2 West*

a) At 103 kN

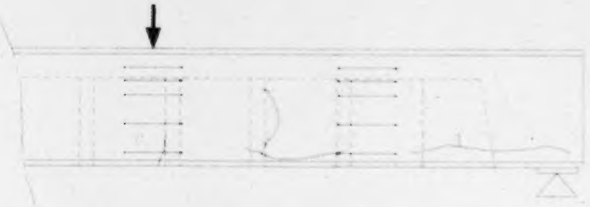

b) At 194 kN

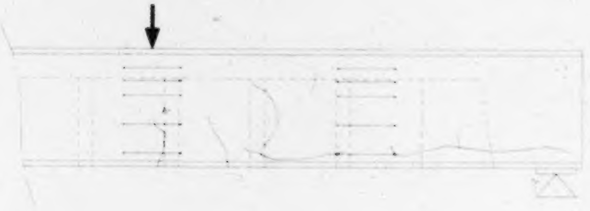

c)At 281 kN

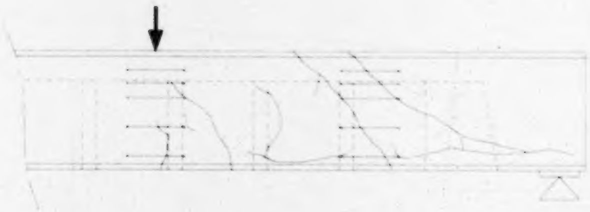

d) At 394 kN (Ultimate)

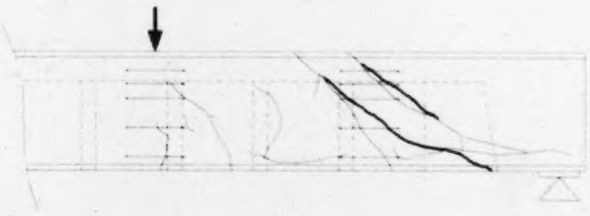

Figure A.22 Cracking Growth of *Girder 3 East*

a) At 108 kN

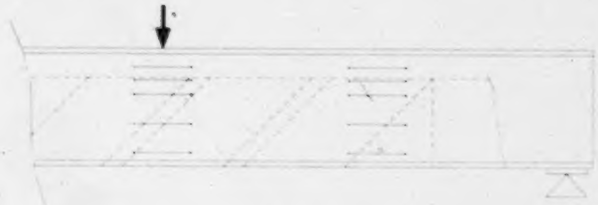

b) At 194 kN

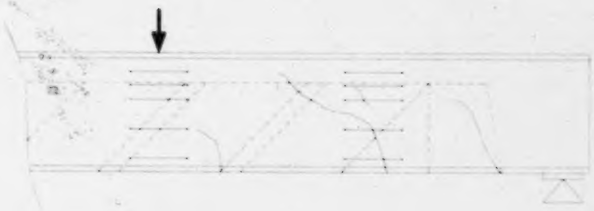

c)At 290 kN

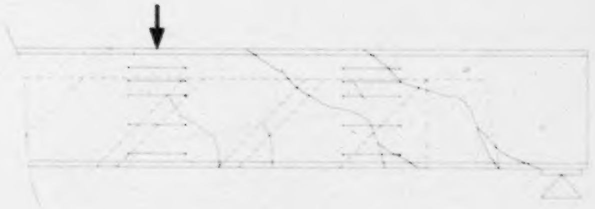

d) At 414 kN (Ultimate)

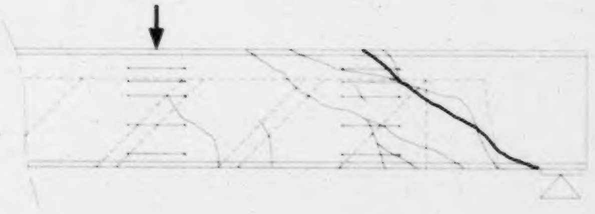

Figure A.23 Cracking Growth of *Girder 3 West*

a) At 99 kN

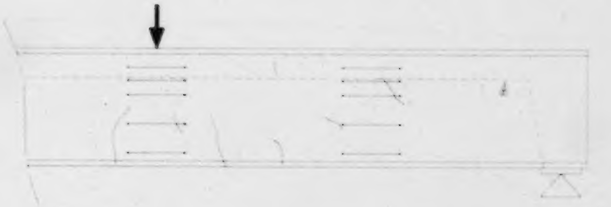

b) At 196 kN

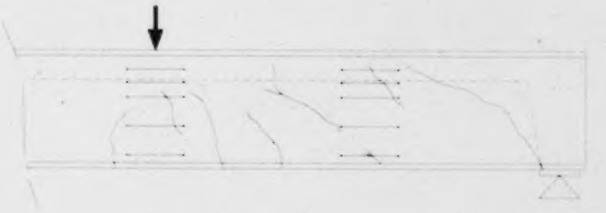

c) At 259 kN (Ultimate)

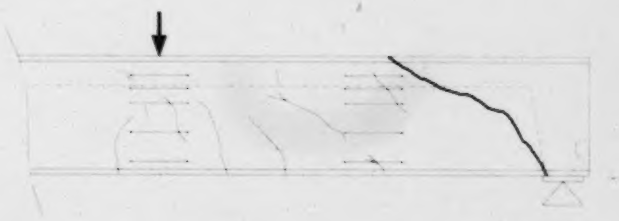

Figure A.24 Cracking Growth of *Girder 4 East*

a) At 103 kN

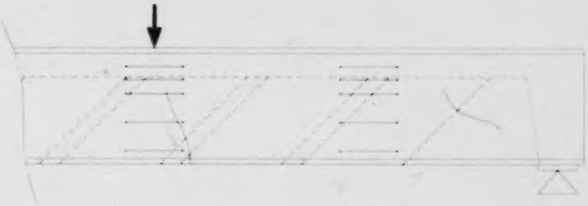

b) At 198 kN

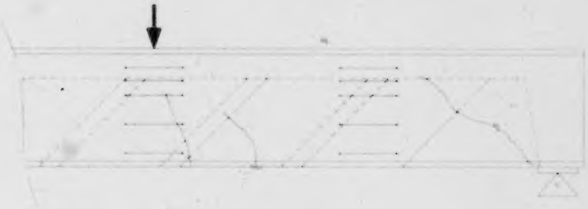

c)At 292 kN

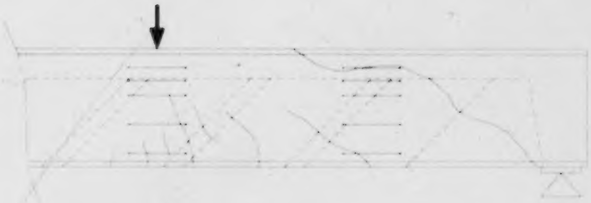

d) At 383 kN (Ultimate)

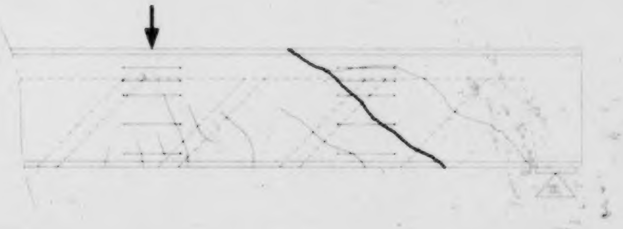

Figure A.25 Cracking Growth of *Girder 4 West*

A.3 Point Load Deflection Comparisons

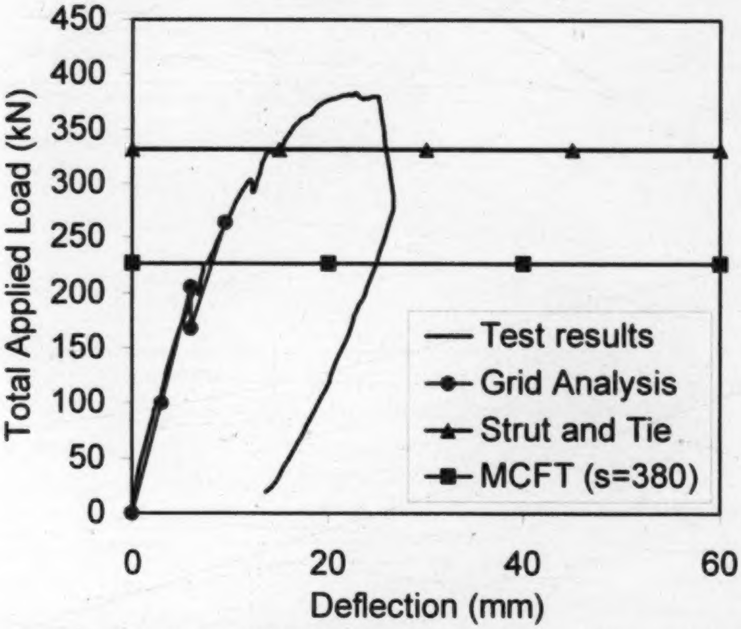

Figure A.26 Point Load Deflection Comparisons (*Girder 1 East*)

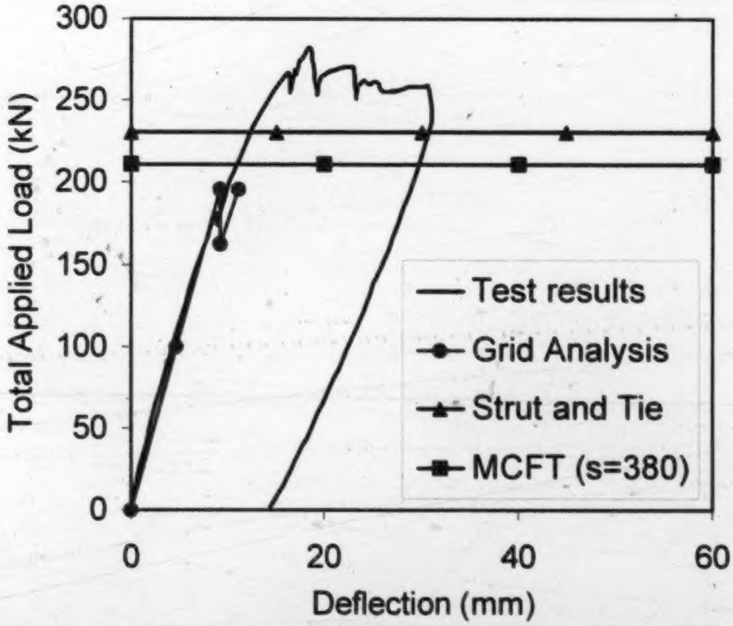

Figure A.27 Point Load Deflection Comparisons (*Girder 1 West*)

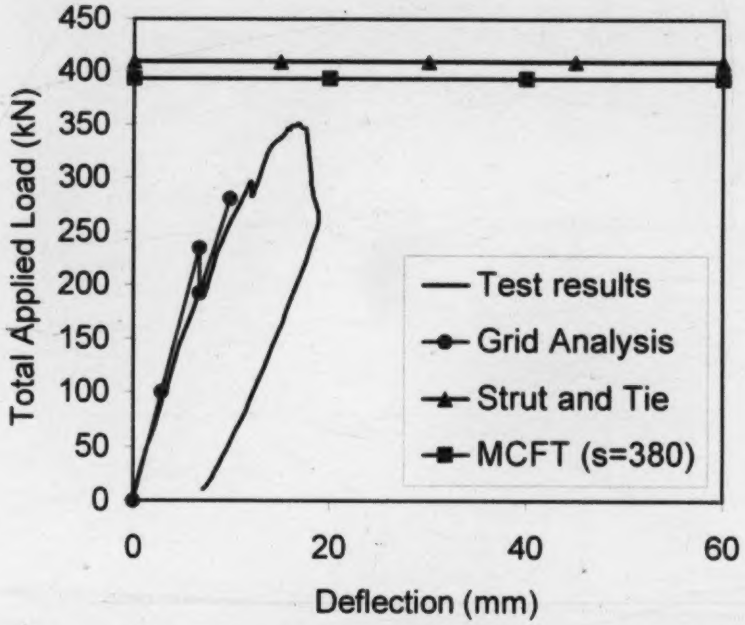

Figure A.28 Point Load Deflection Comparisons (*Girder 2 East*)

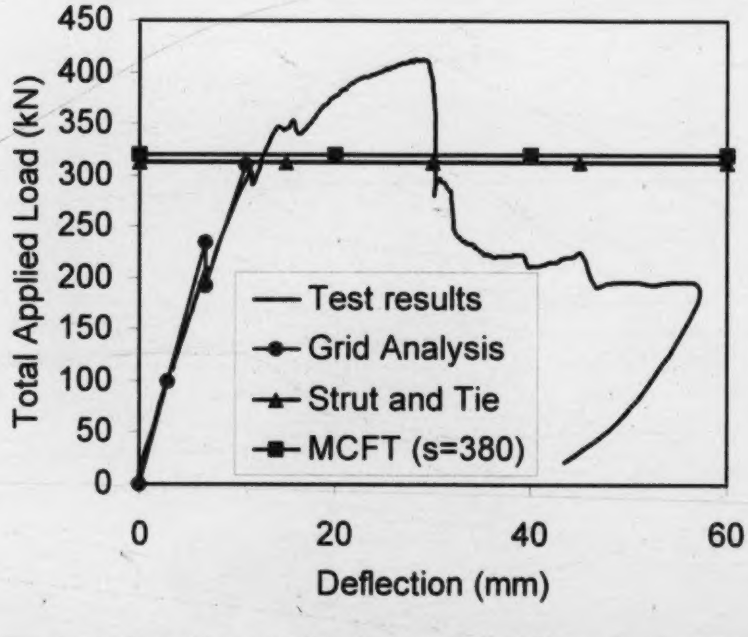

Figure A.29 Point Load Deflection Comparisons (*Girder 2 West*)

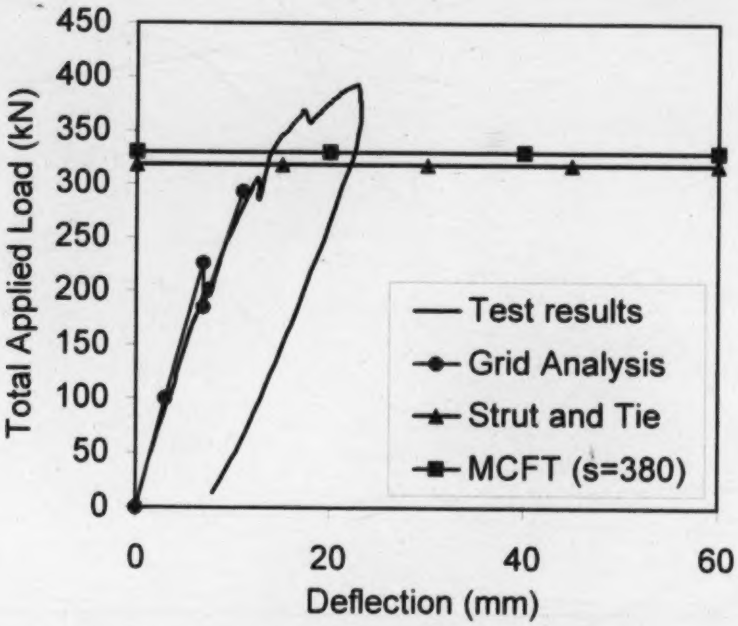

Figure A.30 Point Load Deflection Comparisons (*Girder 3 East*)

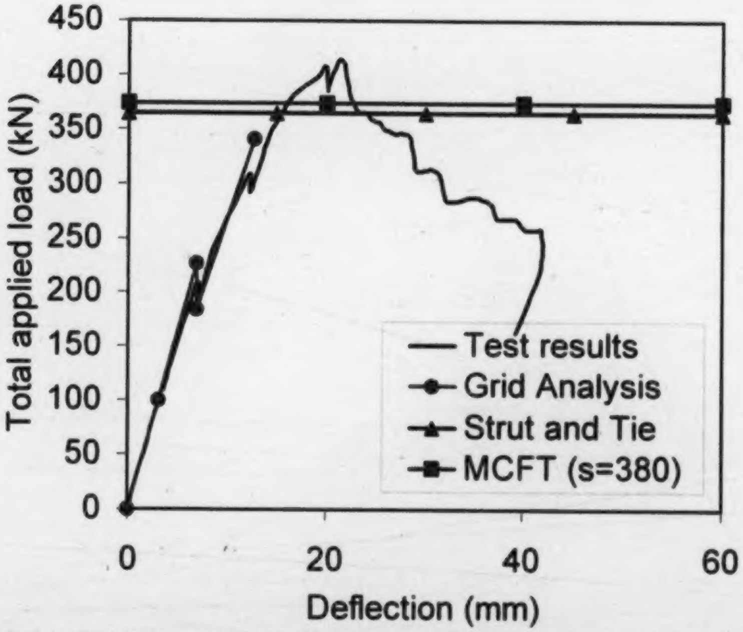

Figure A.31 Point Load Deflection Comparisons (*Girder 3 West*)

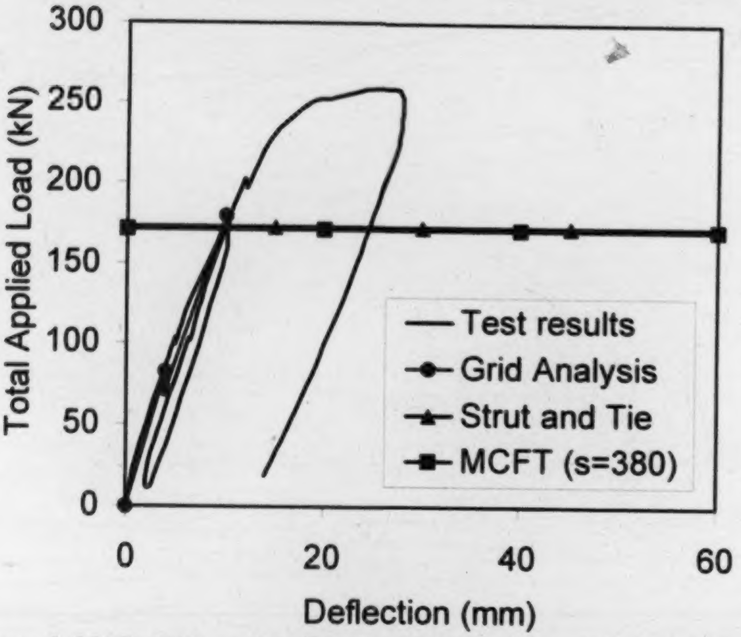

Figure A.32 Point Load Deflection Comparisons (*Girder 4 East*)

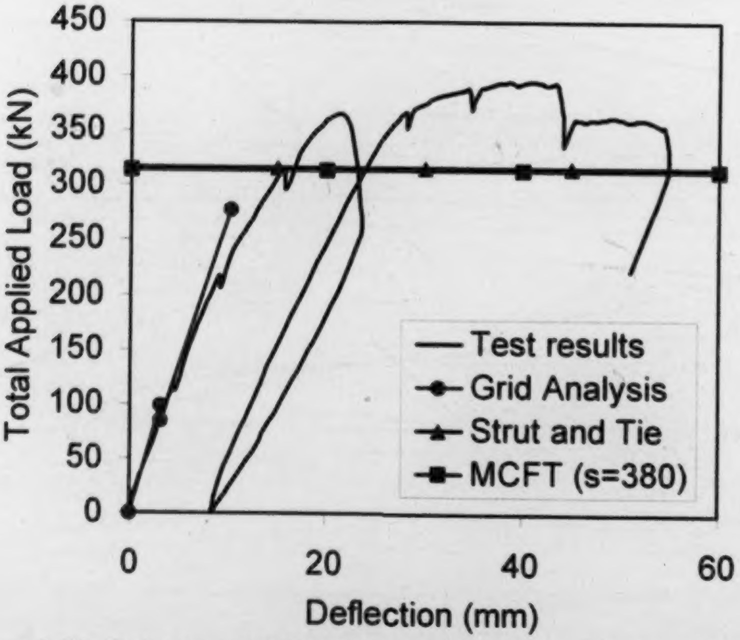

Figure A.33 Point Load Deflection Comparisons (*Girder 4 West*)

A.4 Modified Compression Field Theory (MCFT) Detailed Procedure

This method was developed by COLLINS and MITCHELL (1987). It is the basis of the general method used in CSA-A23.3 (1994) with a variable angle truss model. A computerized program was created to include the contribution of the FRP sheets. The procedure requires iterations to converge to the appropriate solution. The solution technique is described briefly below but complementary information of the method can be found in COLLINS and MITCHELL (1987).

Step 1: Choose a value of the principal tensile strain ε_1 at which to perform the calculation.

Step 2: Estimate the inclination θ.

Step 3: Estimate the stresses in the stirrups f_v and in the composite sheets σ_{FRP}.

Step 4: Calculate the diagonal tensile stress f_1.

Step 5: Calculate the shear load with

[A.1a] $$v_s = \frac{A_{sv}\ f_v}{b_w\ s\ \tan\theta}$$

[A.1b] $$v = \frac{f_1}{\tan\theta}$$

[A.1c] $$v_{FRP} = \frac{A_{FRP}\ \sigma_{FRP}}{b_w\ s_{FRP}}\left(\frac{\sin^2\alpha}{\tan\theta} + \sin\alpha\cos\alpha\right)$$

and

[A.1d] $$V = v_s d_v b_w + v d_v b_w + v_{FRP} d_{FRP} b_w$$

where α is the angle of the fibres with respect to the longitudinal axis of the section.

Step 6: Calculate the diagonal compression stress f_2

Step 7: Calculate the maximum allowable compression stress f_{2max}

Step 8: Check that $f_{2max}<f_2$. If not, solution is not possible. Return to step 2 and choose larger θ or return to step 1 and choose smaller ε_1.

Step 9: Calculate principal compressive strain ε_2.

Step 10: Calculate longitudinal strain ε_x, vertical strain ε_t and composite strain ε_{FRP}.

Step 11: Calculate f_v and σ_{FRP} from previous strains.

Step 12: Check estimates of f_v and σ_{FRP} . If necessary, revise estimates and return to step 3.

Step 13: Calculate the axial load on the member with

[A.2a] $$N_s = -\frac{v_s}{\tan\theta} b_w d_v$$

[A.2b] $$N_c = \left(\frac{-v}{\tan\theta} + f_1 \right) b_w d_v$$

[A.2c] $$N_{FRP} = \frac{-v_{FRP}}{\tan\theta} b_w d_v + \frac{A_{FRP}\sigma_{FRP} d_{FRP} \cos\theta}{s_{FRP}} \left(\frac{\sin\alpha}{\tan\theta} + \cos\alpha \right)$$

and

[A.2d] $$N_v = N_s + N_c + N_{FRP}$$

Step 14: Using a plane section analysis with the strain at d set to ε_x, find the strain distribution which corresponds to the desired moment and then determine the corresponding axial load N_p.

Step 15: Check if N_p-N_v equals zero. If it does not, make a new estimate of θ and return to step 2.

This procedure is repeated for a specific moment by increasing ε_1 until the shear load drops, or the fibres fail, or the concrete strut crushes. By repeating this procedure for various moments, the complete shear moment interaction diagram can be found.

APPENDIX B ADDITIONAL T400 BEAM DATA

B.1 Photographs

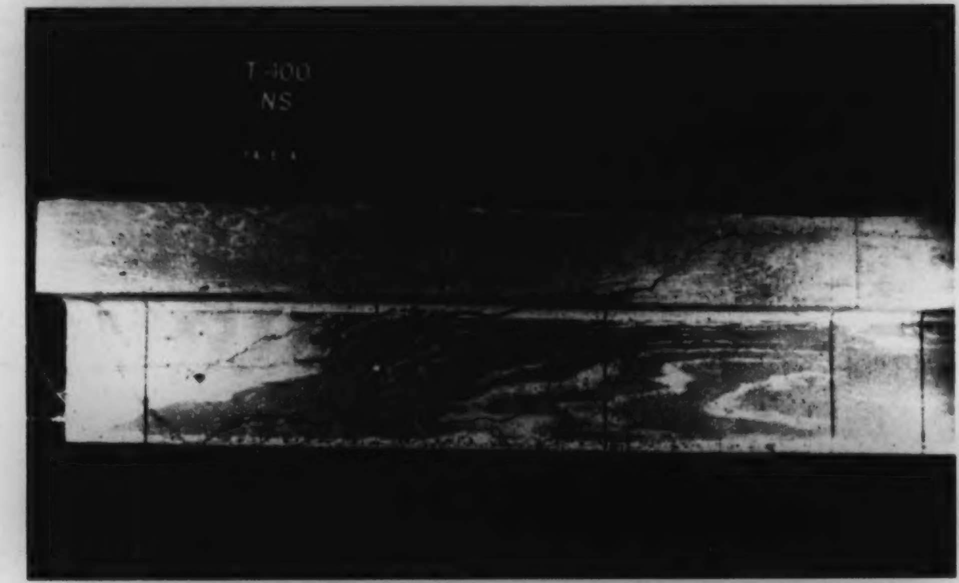
T 400
NS
FACE A

Figure B.1 T4NS Specimen after Failure (Face A)

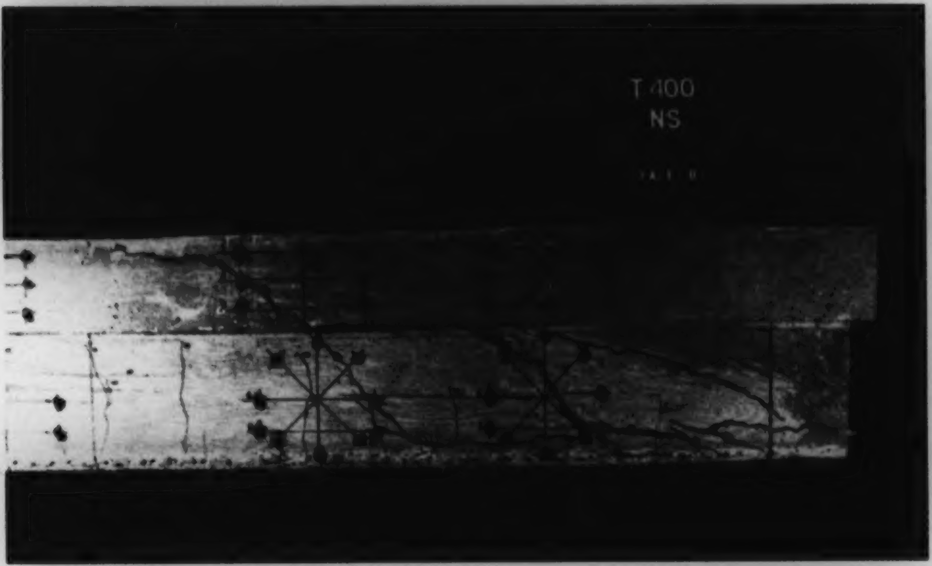
T 400
NS
FACE B

Figure B.2 T4NS Specimen after Failure (Face B)

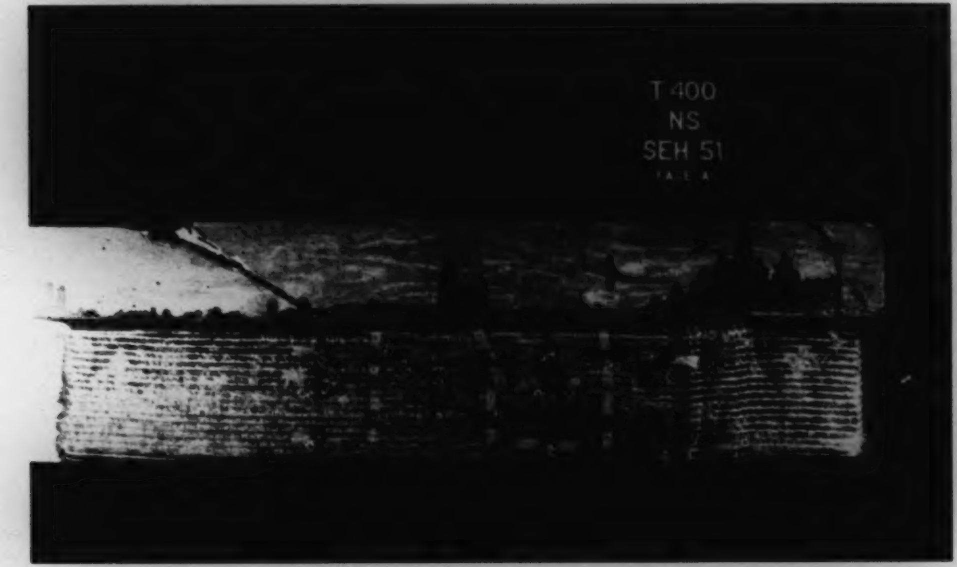
T 400
NS
SEH 51
FACE A

Figure B.3 T4NSG90 Specimen after Failure (Face A)

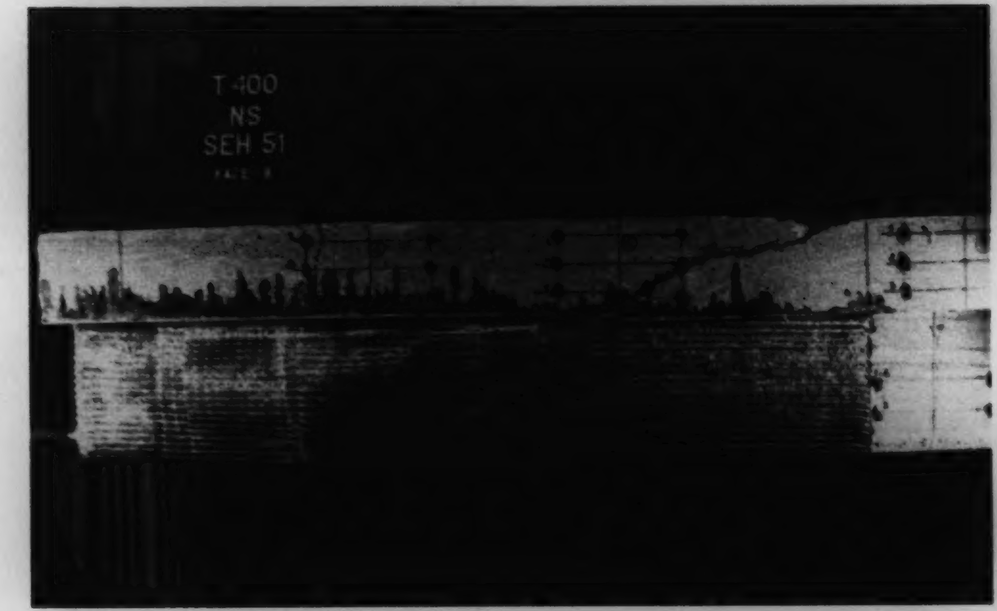
T 400
NS
SEH 51
FACE B

Figure B.4 T4NSG90 Specimen after Failure (Face B)

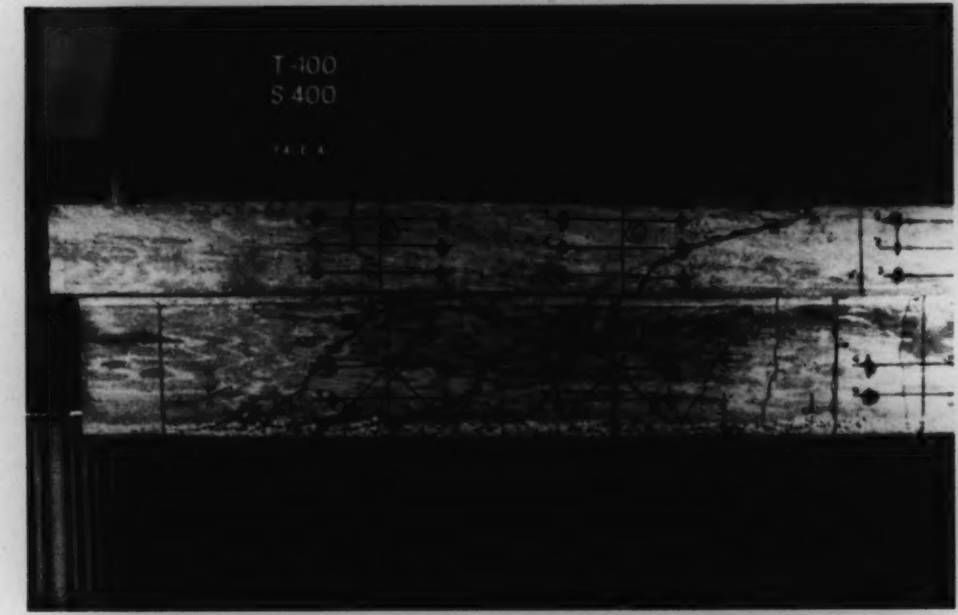
T 400
S 400
FACE A

Figure B.5 T4S4 Specimen after Failure (Face A)

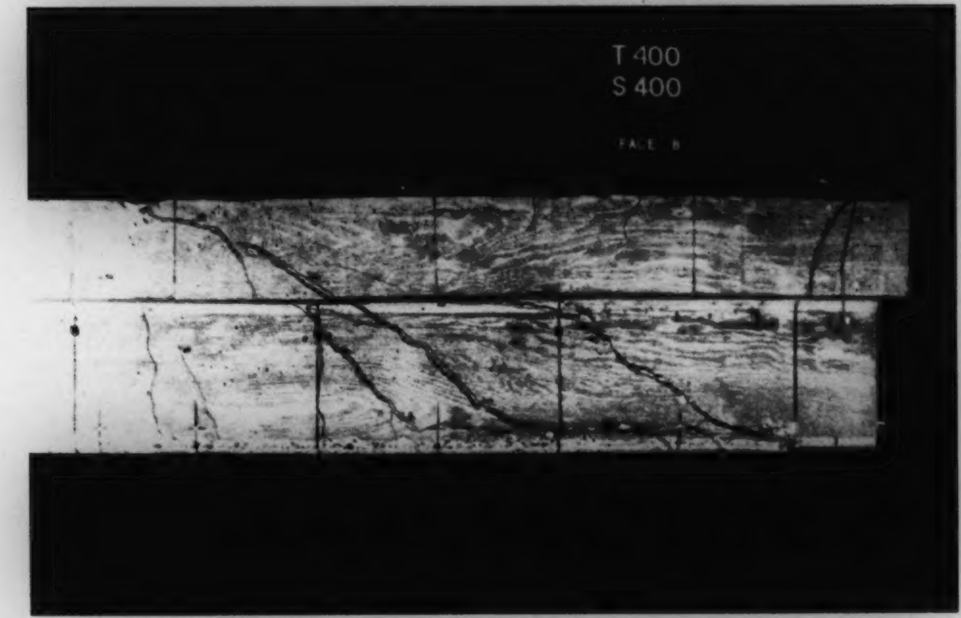
T 400
S 400
FACE B

Figure B.6 T4S4 Specimen after Failure (Face B)

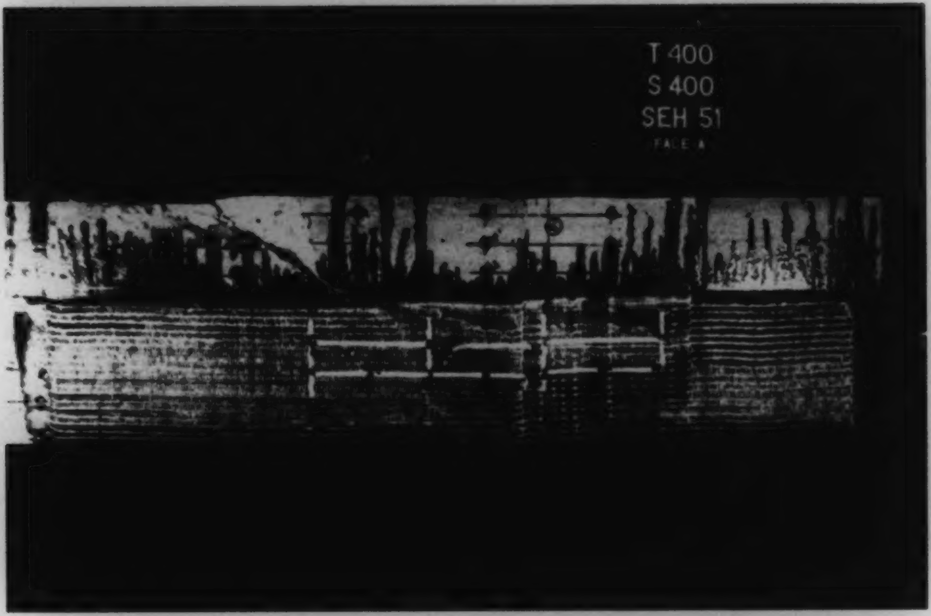
T 400
S 400
SEH 51
FACE A

Figure B.7 T4S4G90 Specimen after Failure (Face A)

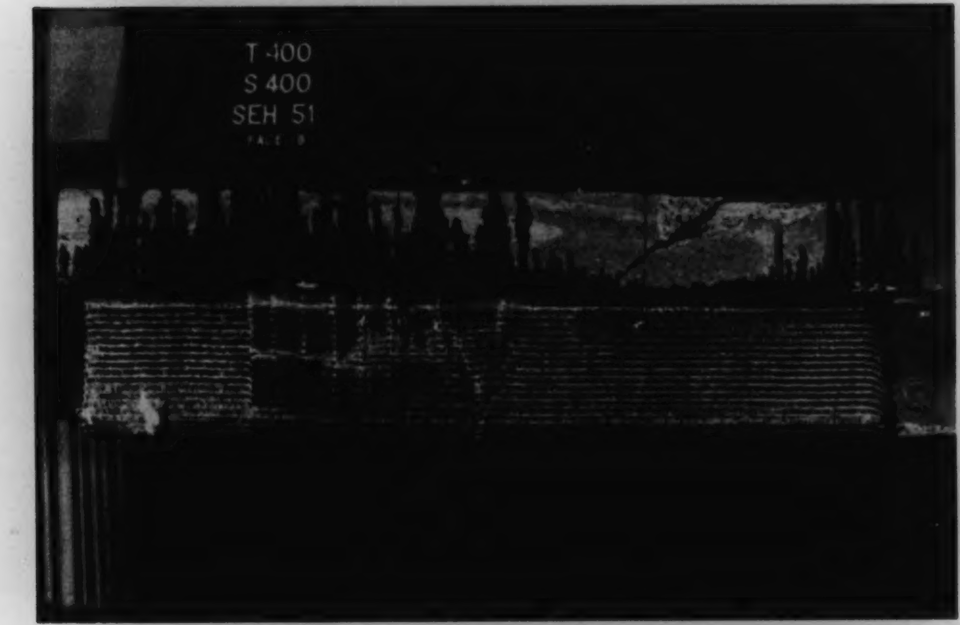
T 400
S 400
SEH 51
FACE B

Figure B.8 T4S4G90 Specimen after Failure (Face B)

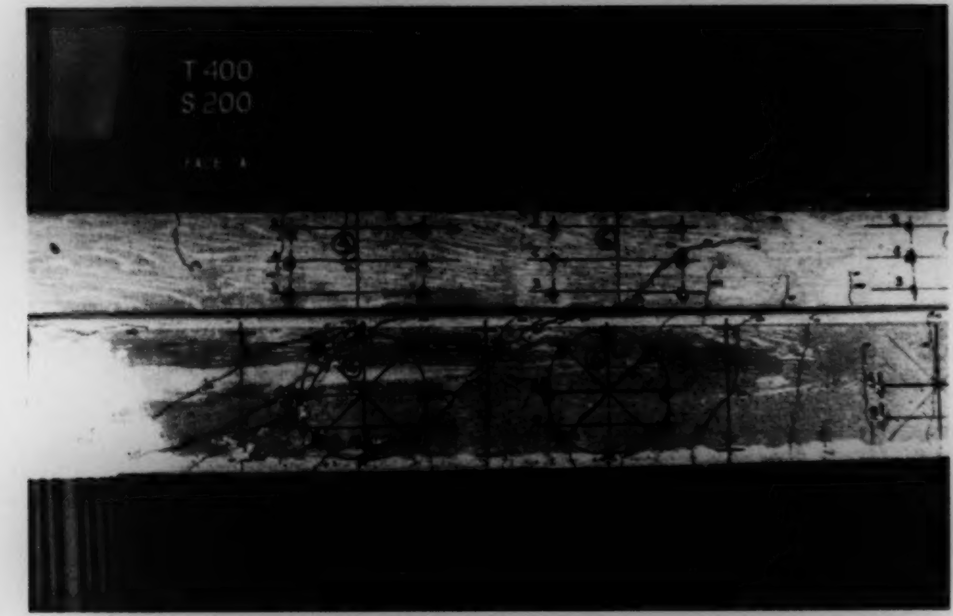

Figure B.9 T4S2 Specimen after Failure (Face A)

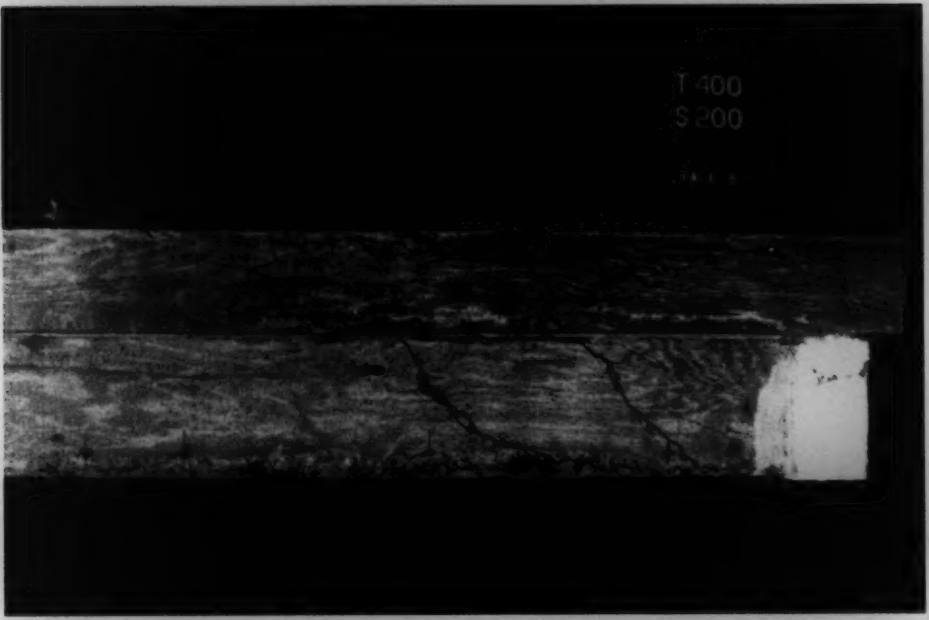

Figure B.10 T4S2 Specimen after Failure (Face B)

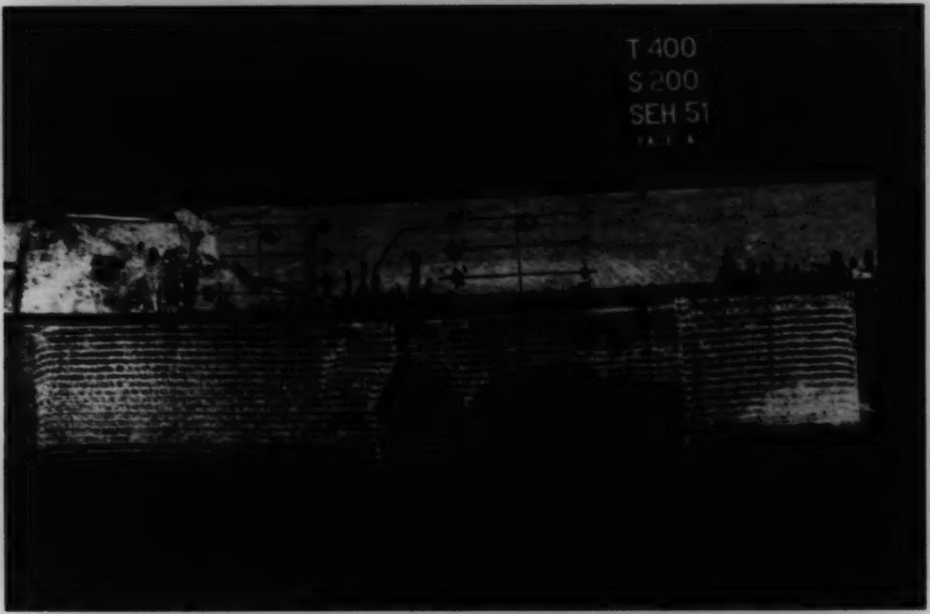
T 400
S 200
SEH 51
FACE A

Figure B.11 T4S2G90 Specimen after Failure (Face A)

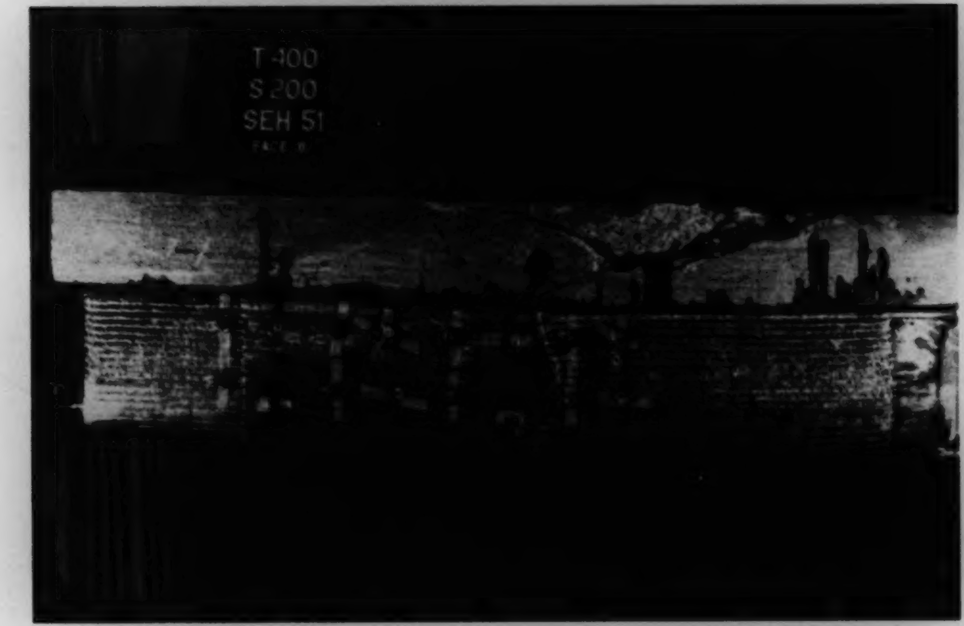
T 400
S 200
SEH 51
FACE B

Figure B.12 T4S2G90 Specimen after Failure (Face B)

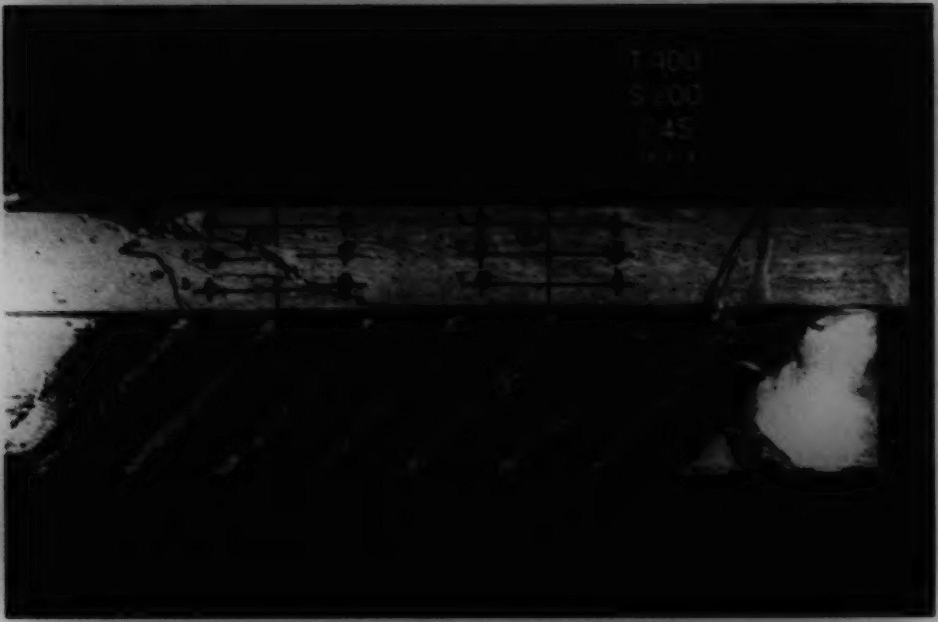

Figure B.13 T4S2C45 Specimen after Failure (Face A)

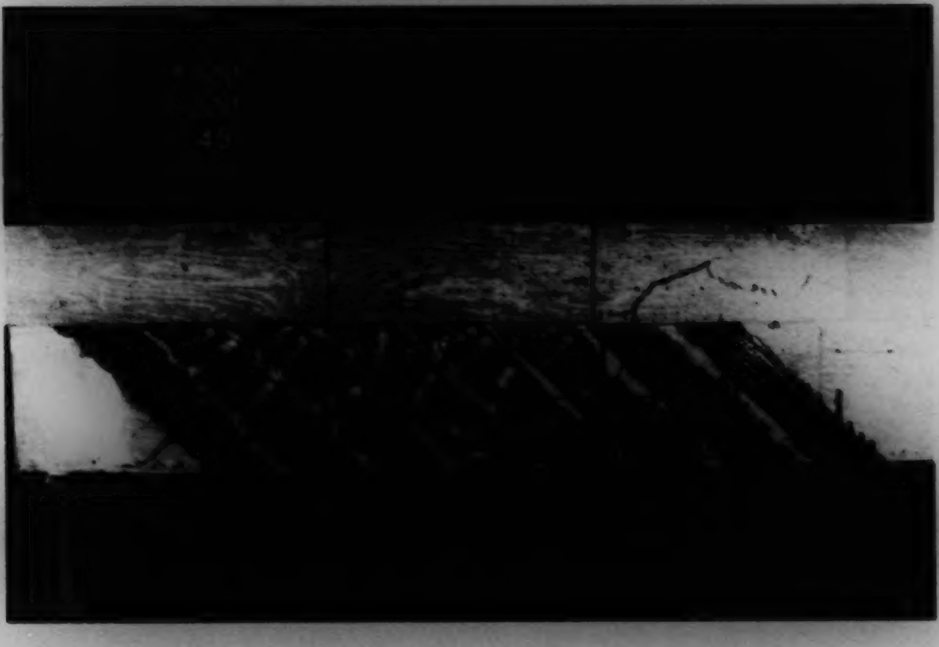

Figure B.14 T4S2C45 Specimen after Failure (Face B)

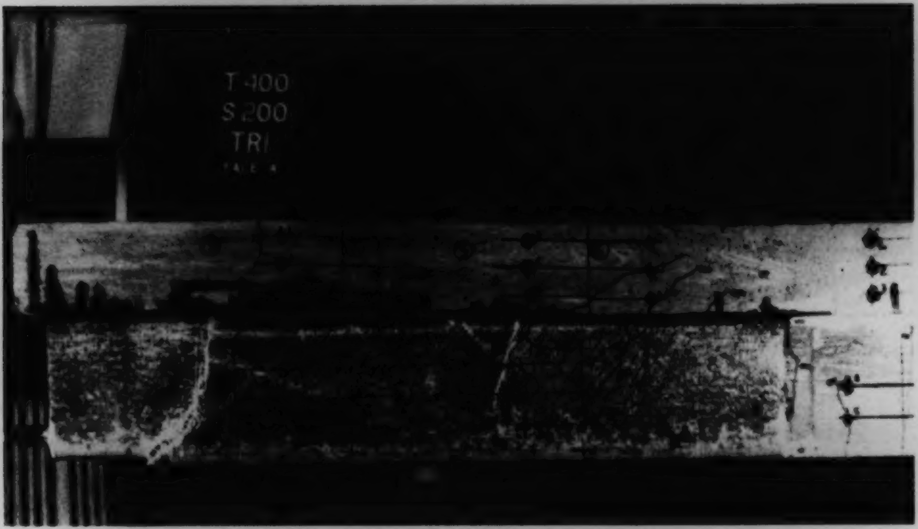
T 400
S 200
TRI

Figure B.15 T4S2Tri Specimen after Failure (Face A)

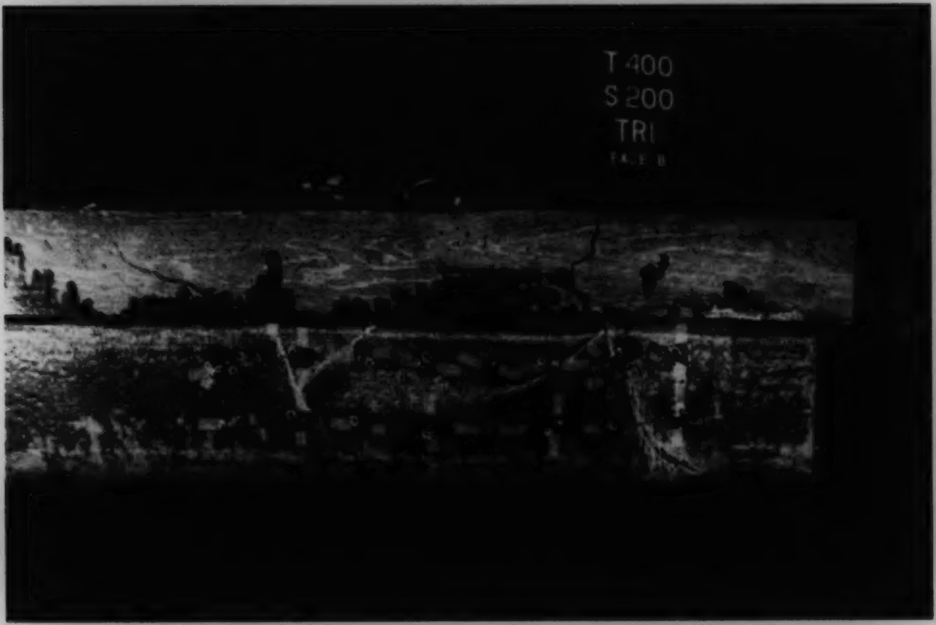
T 400
S 200
TRI

Figure B.16 T4S2Tri Specimen after Failure (Face B)

B.2 Schematic Shear Crack Patterns

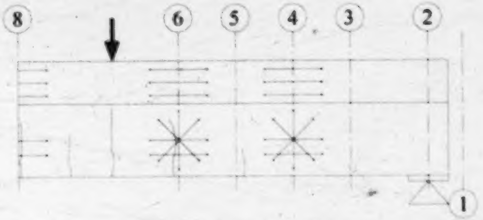

a) At 103 kN

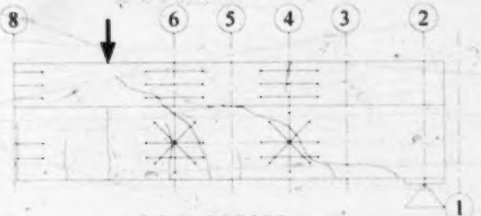

b) At 155 kN

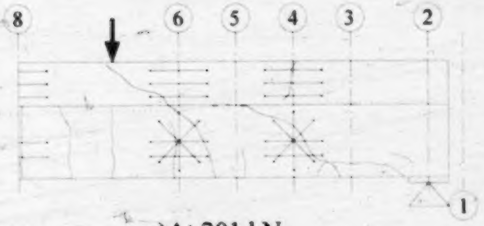

c)At 201 kN

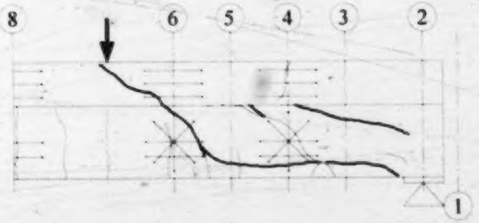

d) At 231 kN (Ultimate)

Figure B.17 Cracking growth of T4NS Specimen

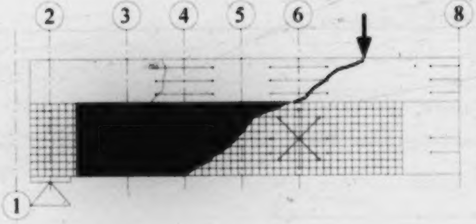

At 318 kN (Ultimate)

Figure B.18 Cracking of T4NSG90 Specimen at Ultimate

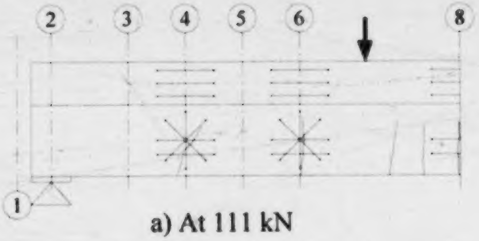

a) At 111 kN

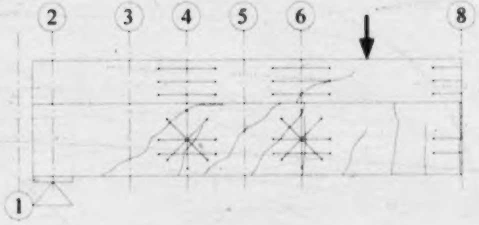

b) At 206 kN

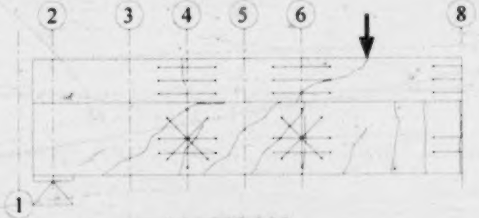

c)At 313 kN

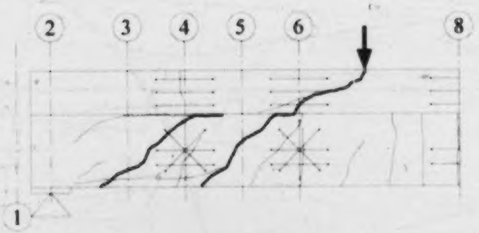

d) At 292 kN (Ultimate)

Figure B.19 Cracking Growth of T4S4 Specimen

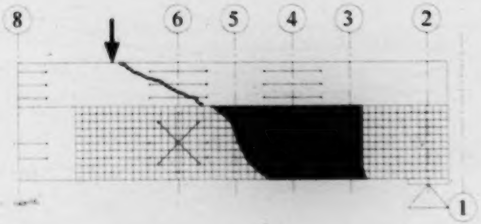

At 411 kN (Ultimate)

Figure B.20 Cracking of T4S4G90 Specimen at Ultimate

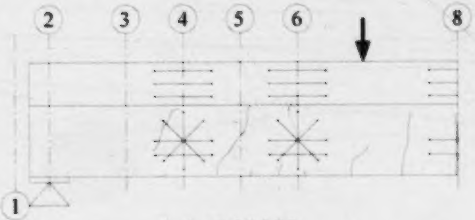

a) At 146 kN

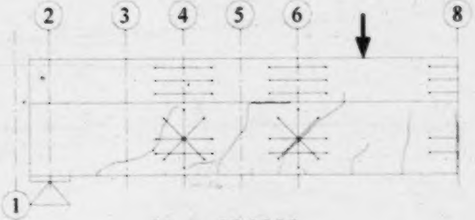

b) At 196 kN

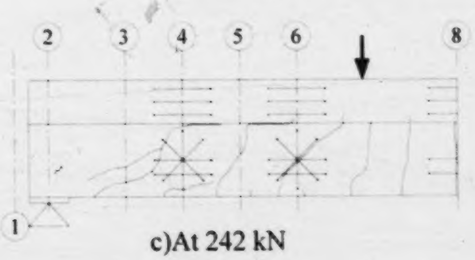

c)At 242 kN

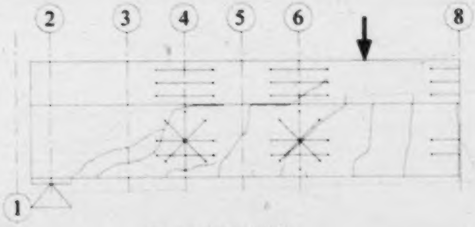

d) At 285 kN

Figure B.21 Cracking Growth of T4S2 Specimen (continued)

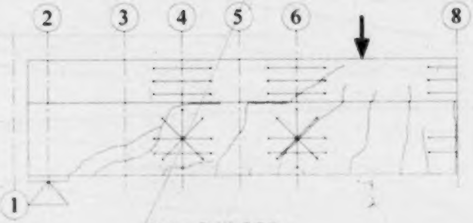

e)At 341 kN

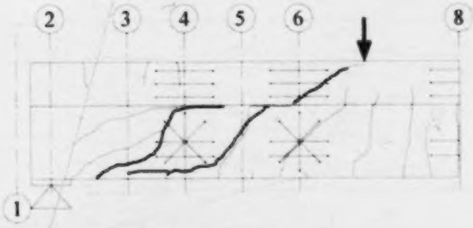

f) At 402 kN (Ultimate)

Figure B.21 Cracking Growth for T4S2 Specimen (concluded)

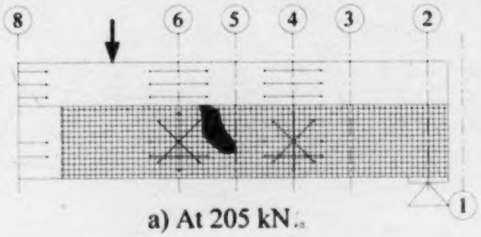

a) At 205 kN

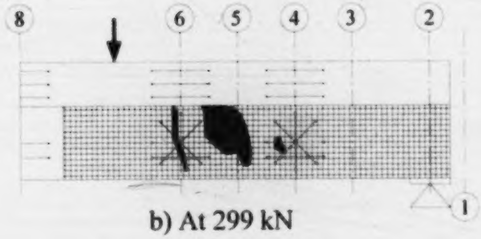

b) At 299 kN

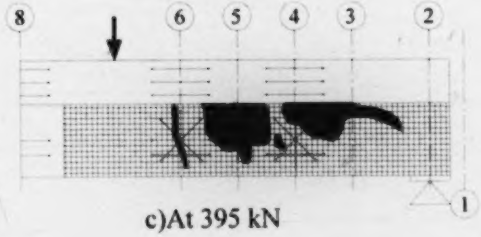

c)At 395 kN

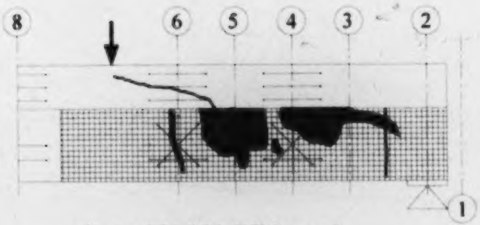

d) At 451 kN (Ultimate)

Figure B.22 Cracking Growth for T4S2G90 Specimen

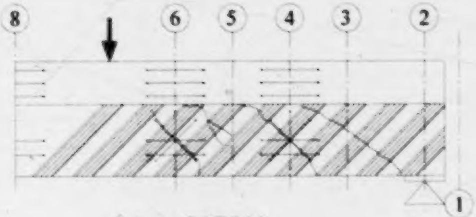

a) At 207 kN

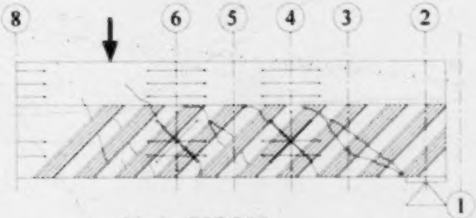

b) At 303 kN

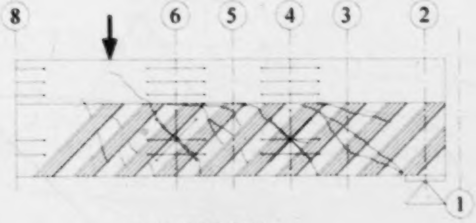

c)At 389 kN

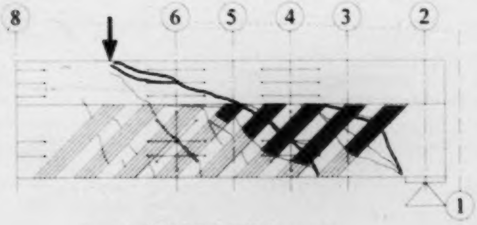

d) At 438 kN (Ultimate)

Figure B.23 Cracking Growth for T4S2C45 Specimen

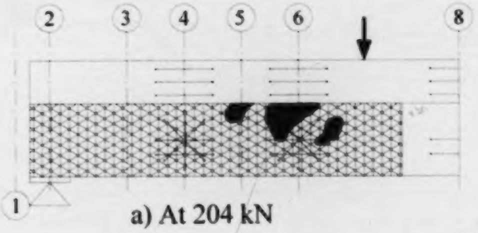

a) At 204 kN

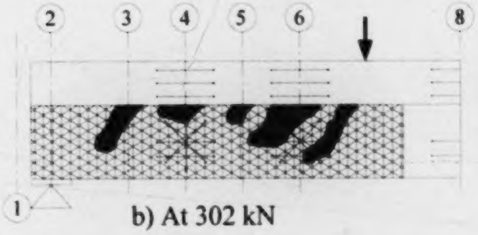

b) At 302 kN

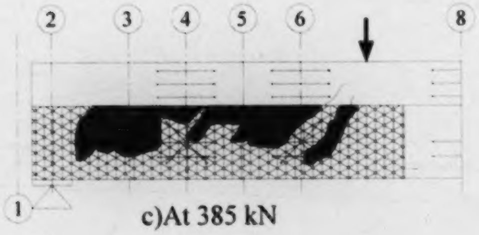

c)At 385 kN

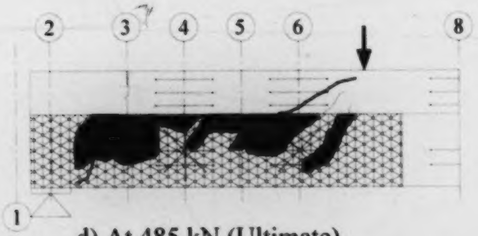

d) At 485 kN (Ultimate)

Figure B.24 Cracking Growth for T4S2Tri Specimen

B.3 Strain Distribution Through the Depth of the T-beam

T4NS T4NSG90

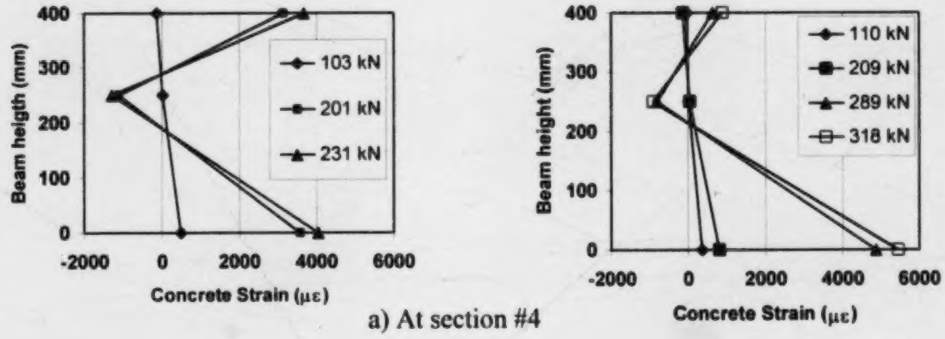

a) At section #4

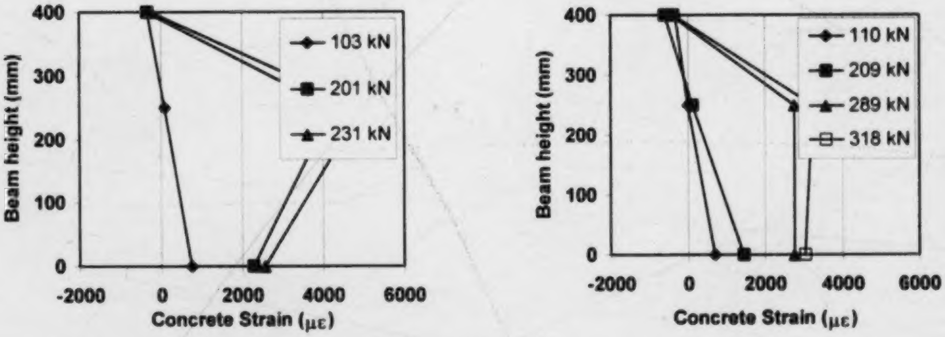

b) At section #6

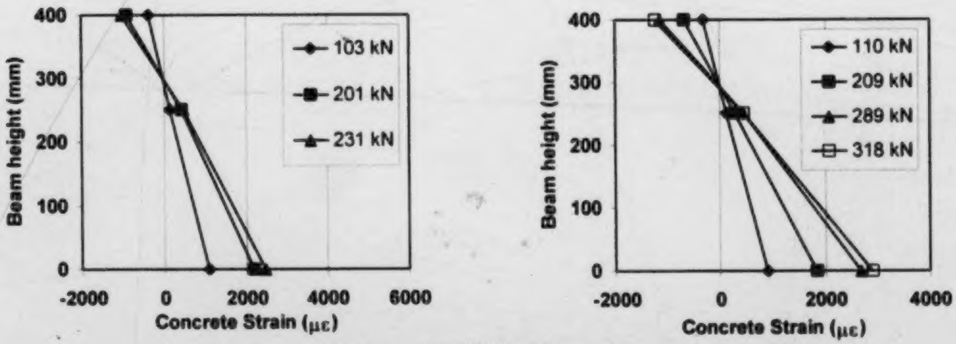

c) At section #8 (mid span)

Figure B.25 Horizontal LVDT Data for T4NS and T4NSG90 Specimens

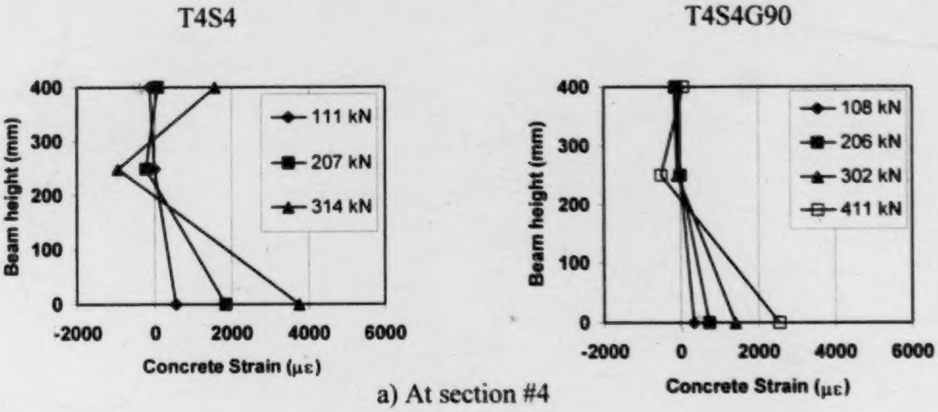

a) At section #4

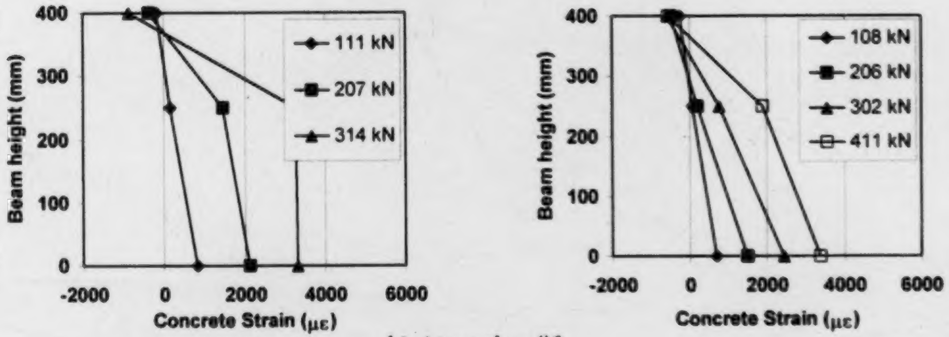

b) At section #6

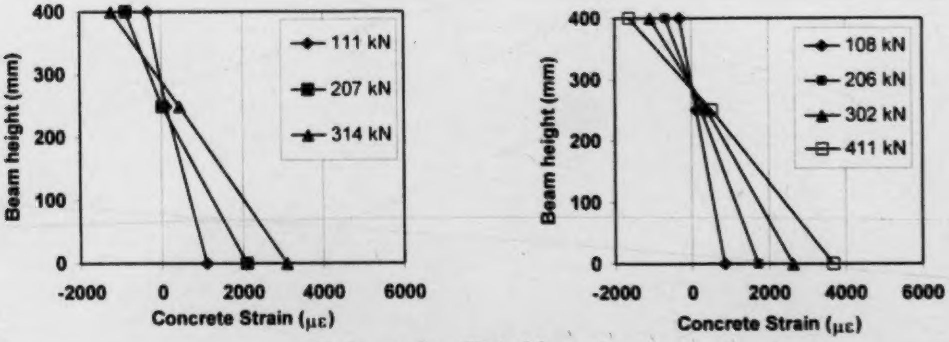

c) At section #8 (mid span)

Figure B.26 Horizontal LVDT Data for T4S4 and T4S4G90 Specimens

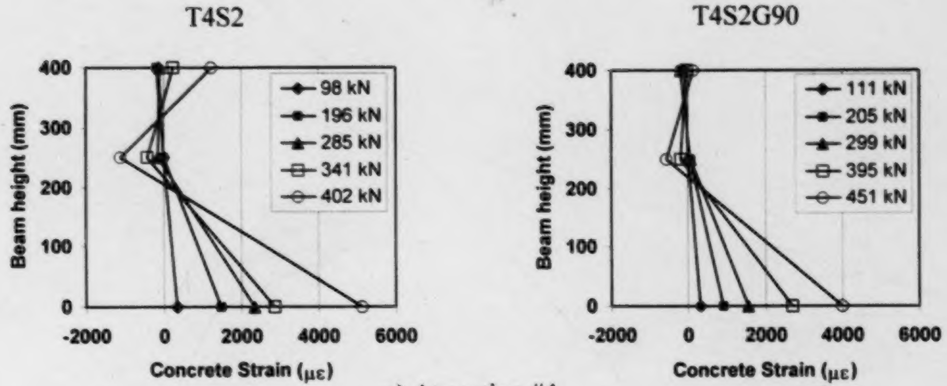

a) At section #4

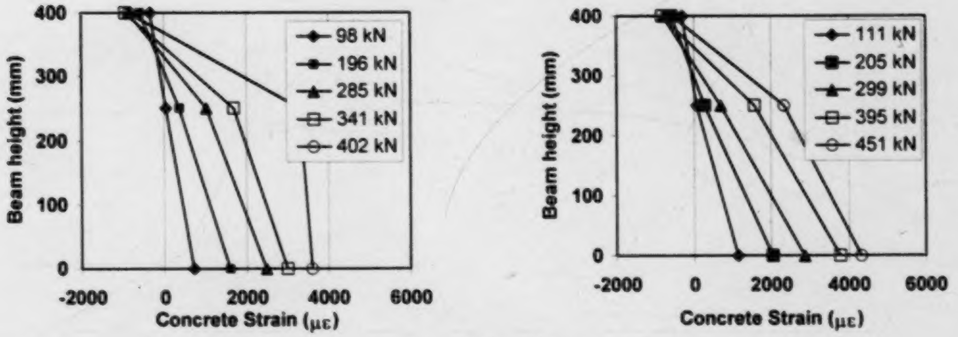

b) At section #6

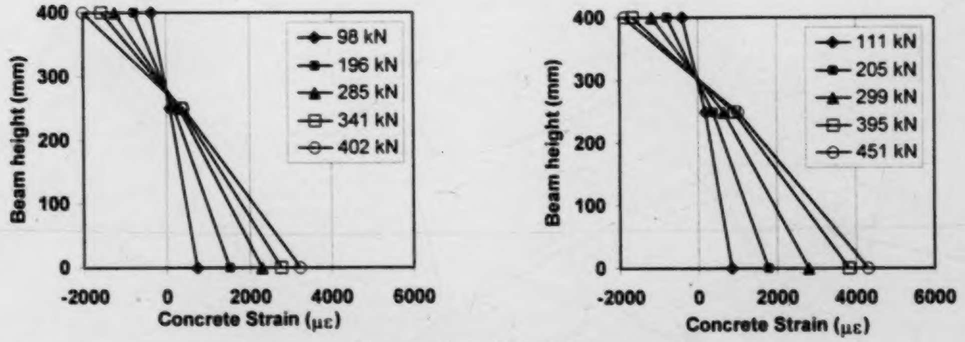

c) At section #8 (mid span)

Figure B.27 Horizontal LVDT Data for T4S2 and T4S2G90 Specimens

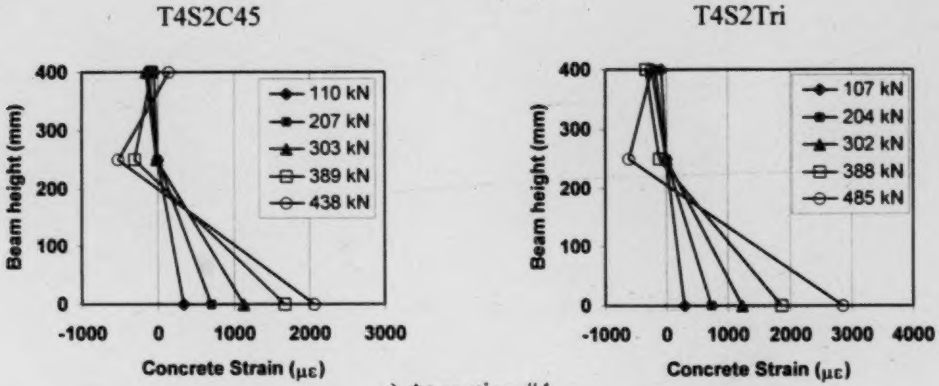

a) At section #4

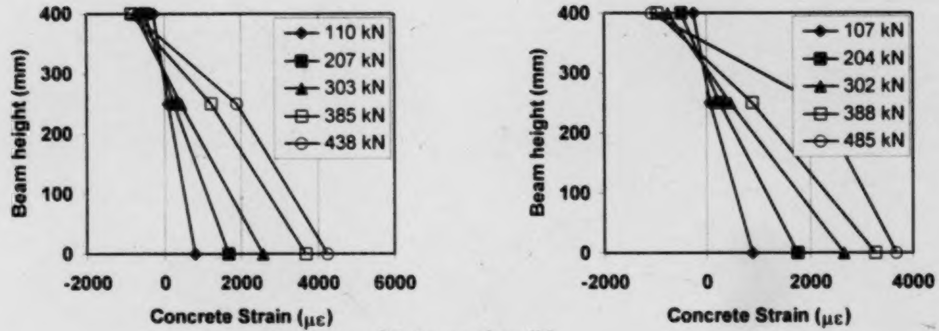

b) At section #6

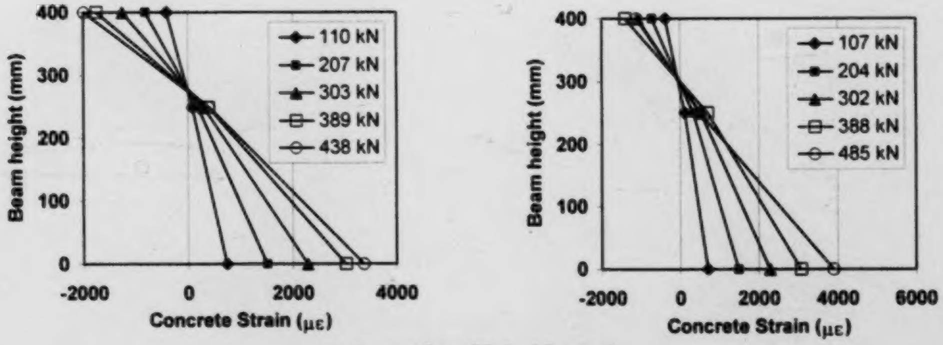

c) At section #8 (mid span)

Figure B.28 Horizontal LVDT Data for T4S2C45 and T4S2Tri Specimens

B.4 Crack Pattern Prediction

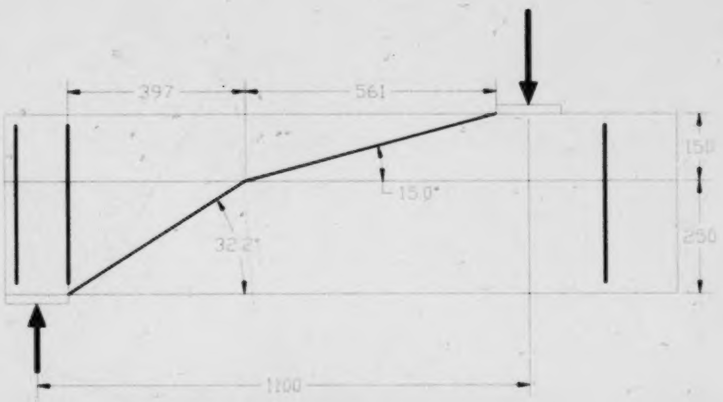

397
561
150
15.0°
32.2°
250
1100

Figure B.29 Crack Prediction for T4NS Specimen with a Linear FRP Strain Assumption

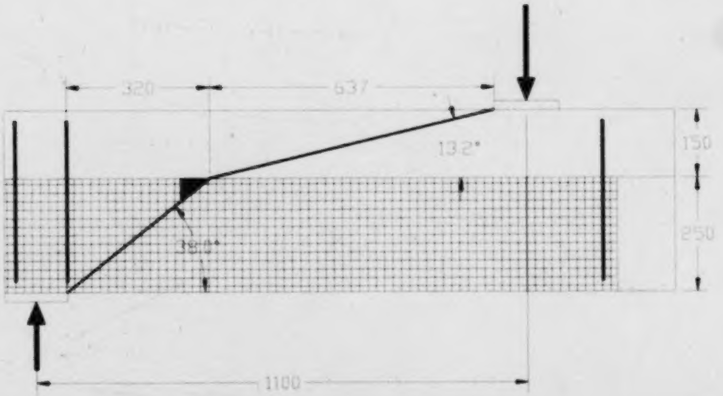

320
637
150
13.2°
38.0°
250
1100

Figure B.30 Crack Prediction for T4NSG90 Specimen with a Linear FRP Strain Assumption

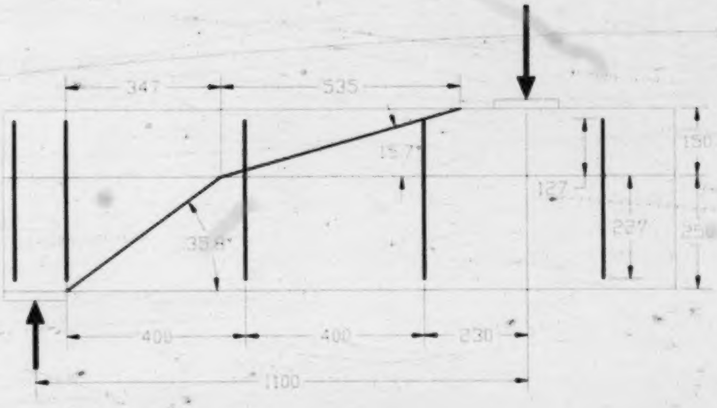
347
535
15.7°
35.8°
127
227
150
250
400
400
230
1100

Figure B.31 Crack Prediction for T4S4 Specimen with a Linear FRP Strain Assumption

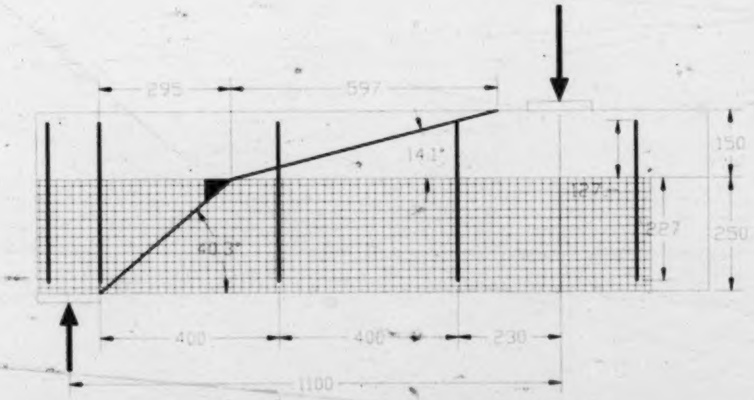
295
597
14.1°
60.3°
127
227
150
250
400
400
230
1100

Figure B.32 Crack Prediction for T4S4G90 Specimen with a Linear FRP Strain Assumption

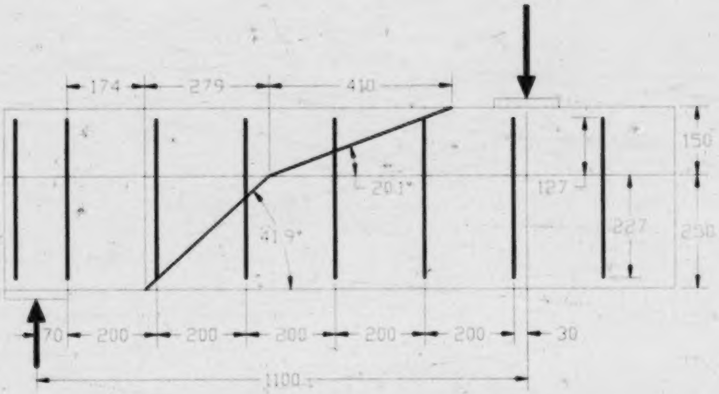
174
279
410
20.1°
41.9°
150
127
227
250
70
200
200
200
200
200
30
1100

Figure B.33 Crack Prediction for T4S2 Specimen with a Linear FRP Strain Assumption

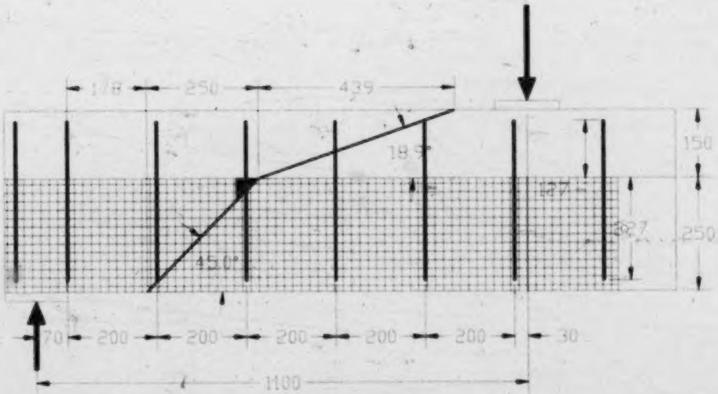
178
250
439
18.9°
45.0°
150
127
227
250
70
200
200
200
200
200
30
1100

Figure B.34 Crack Prediction for T4S2G90 Specimen with a Linear FRP Strain Assumption

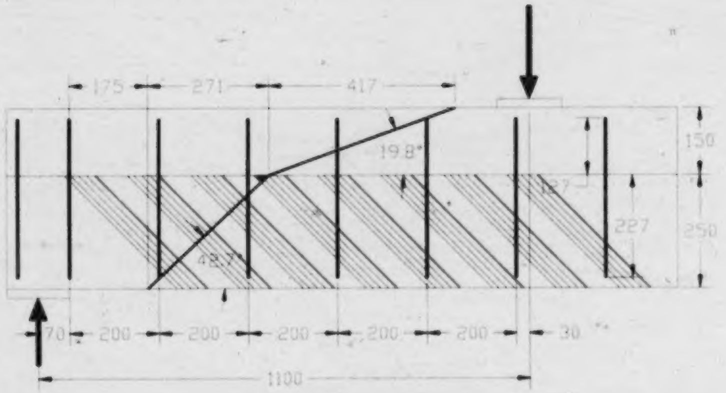

175
271
417
19.8°
127
227
150
250
48.7°
70
200
200
200
200
200
30
1100

Figure B.35 Crack Prediction for T4S2C45 Specimen with a Linear FRP Strain Assumption

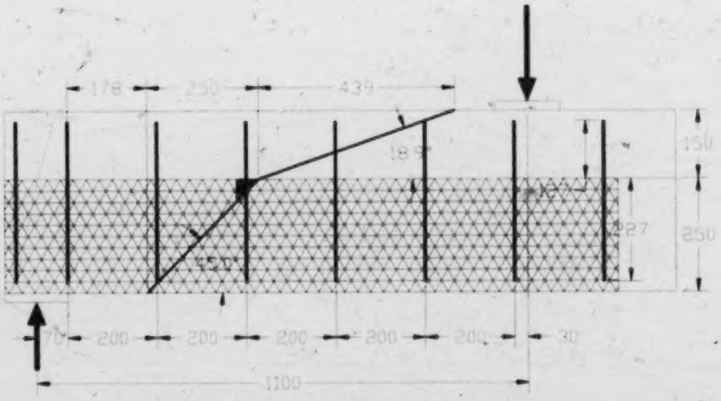

178
250
439
18.9°
227
150
250
70
200
200
200
200
200
30
1100

Figure B.36 Crack Prediction for T4S2Tri Specimen with a Linear FRP Strain Assumption

APPENDIX C ADDITIONAL T600 BEAM DATA

C.1 Photographs

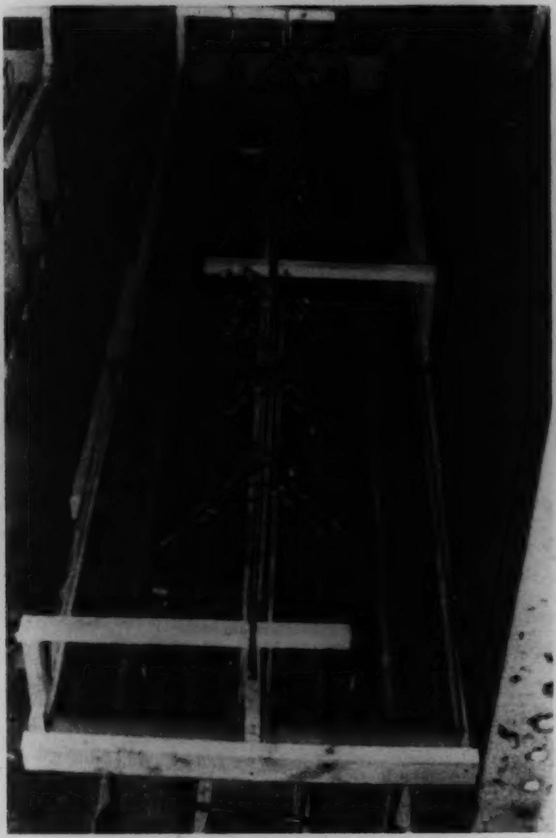

Figure C.1 Formworks and Bar Placement Prior to Casting the Concrete

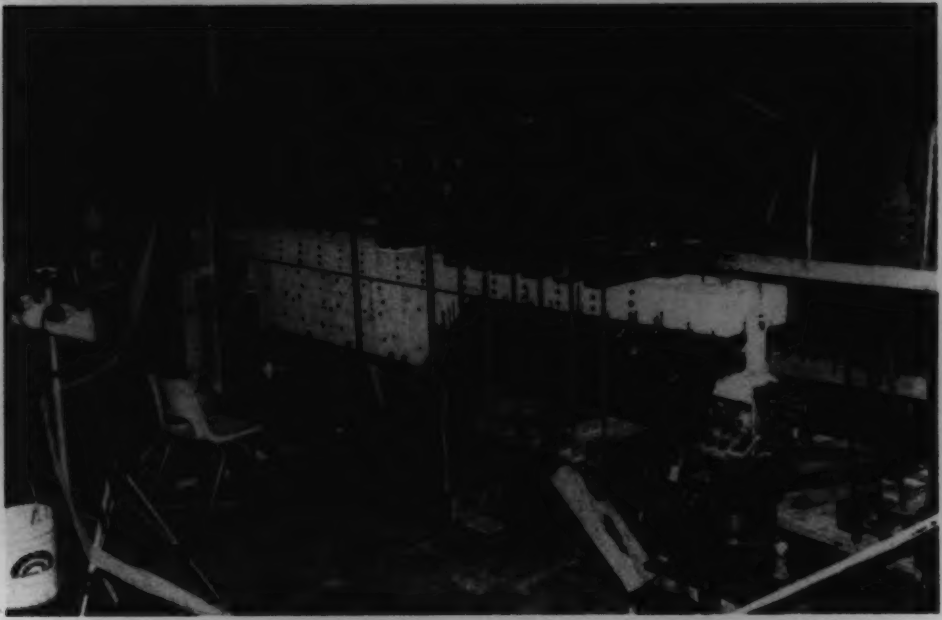

Figure C.2 Test Set-up

Figure C.3 Horizontal LVDTs on the Side of the Beam

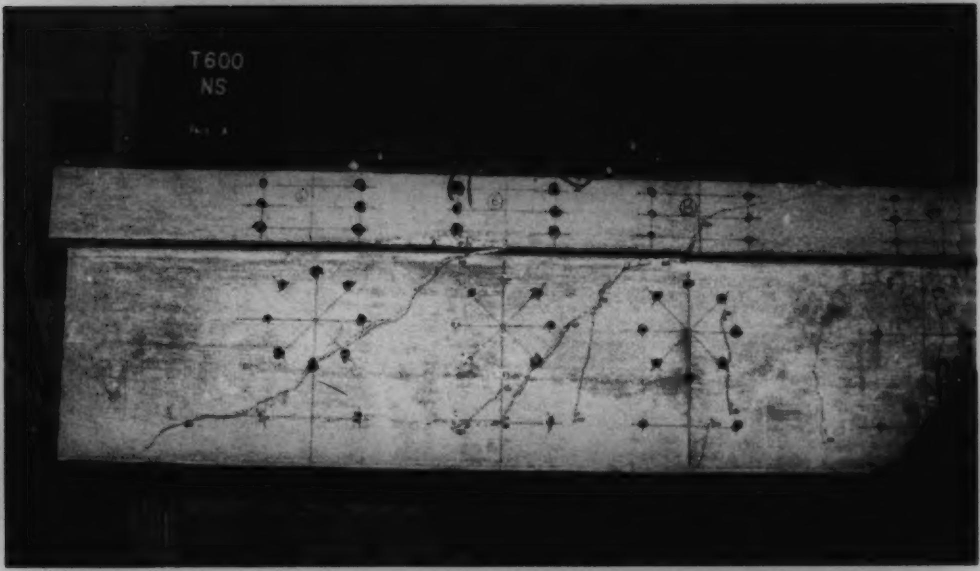

Figure C.4 T6NS Specimen after Failure (Face A)

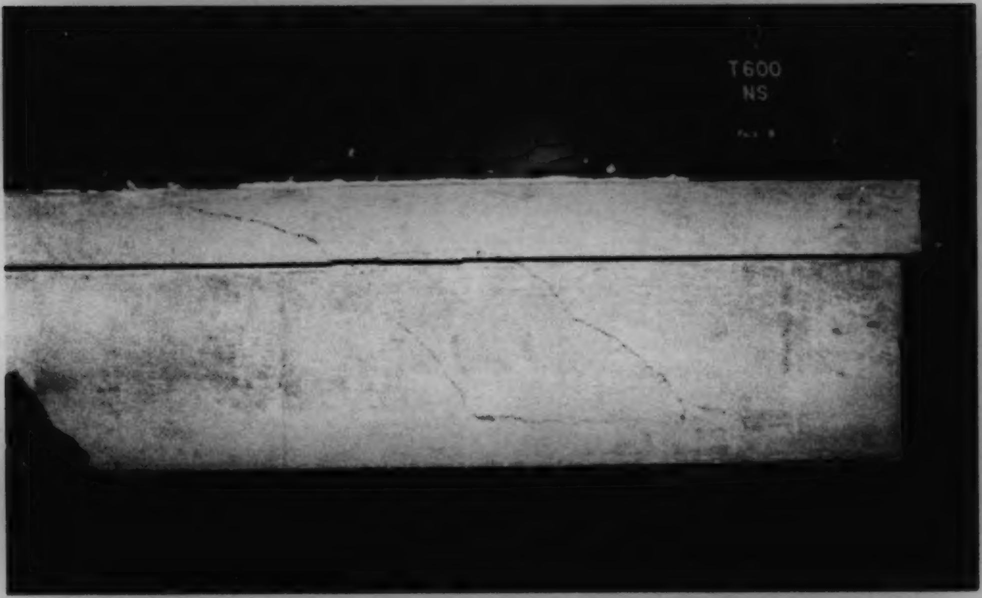

Figure C.5 T6NS Specimen after Failure (Face B)

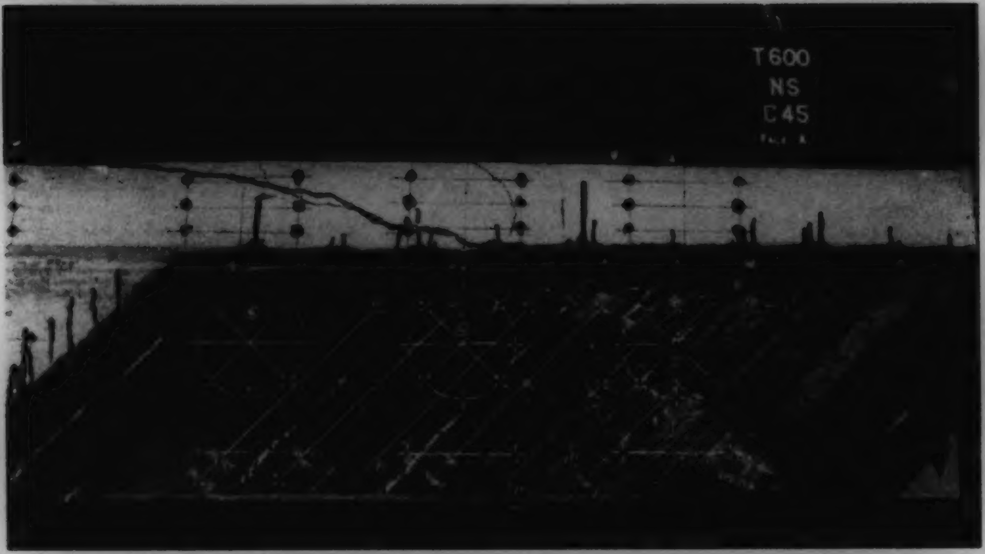

Figure C.6 T6NSC45 Specimen after Failure (Face A)

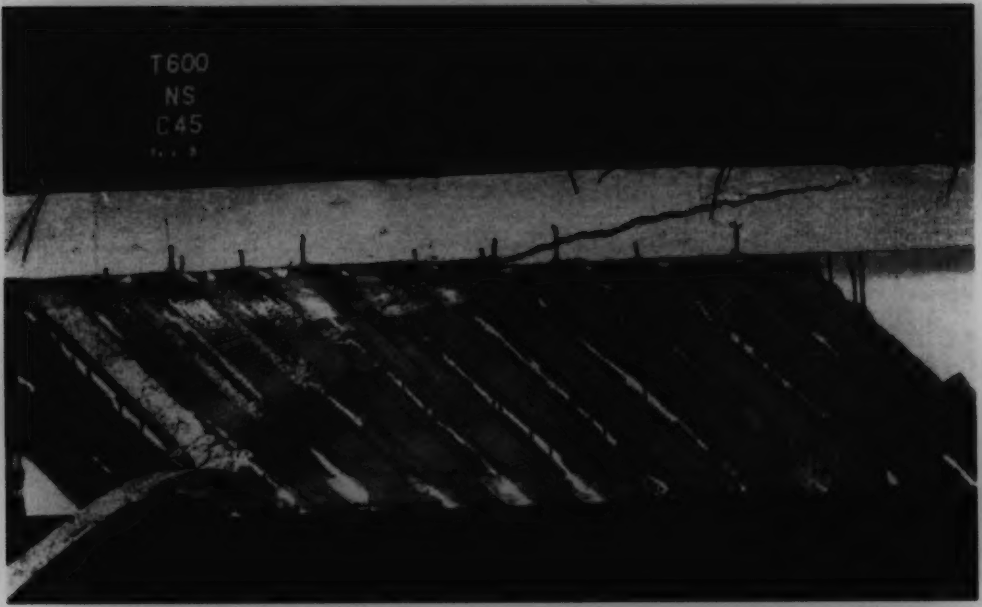

Figure C.7 T6NSC45 Specimen after Failure (Face B)

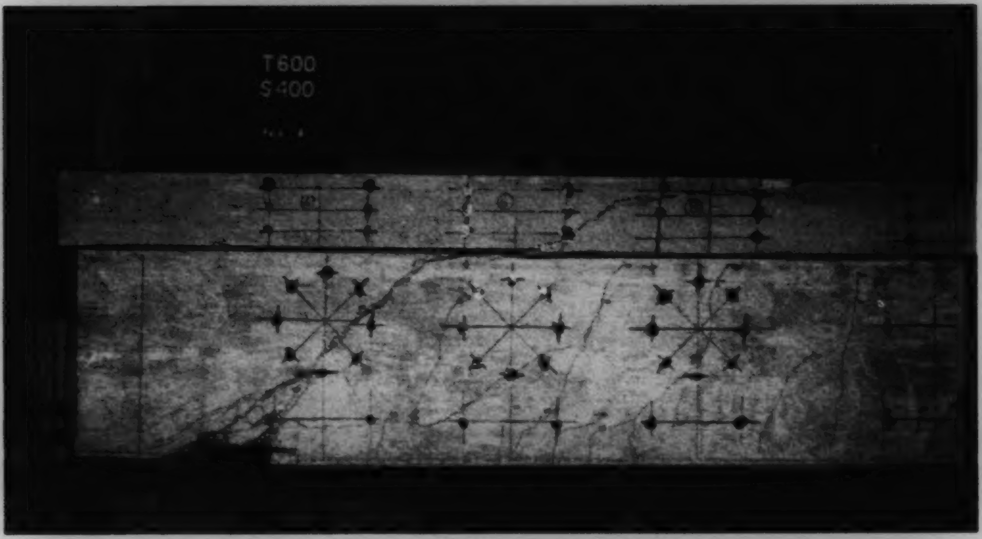

Figure C.8 T6S4 Specimen after Failure (Face A)

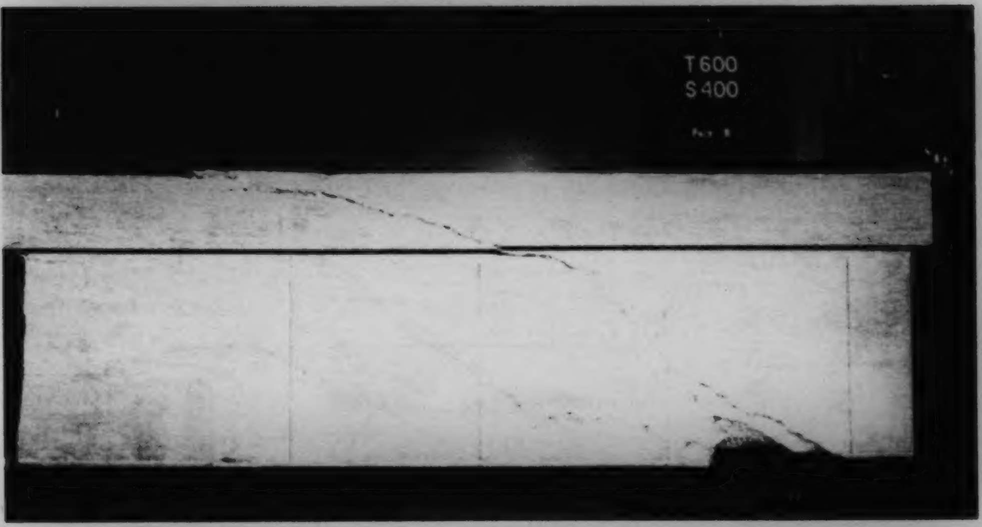

Figure C.9 T6S4 Specimen after Failure (Face B)

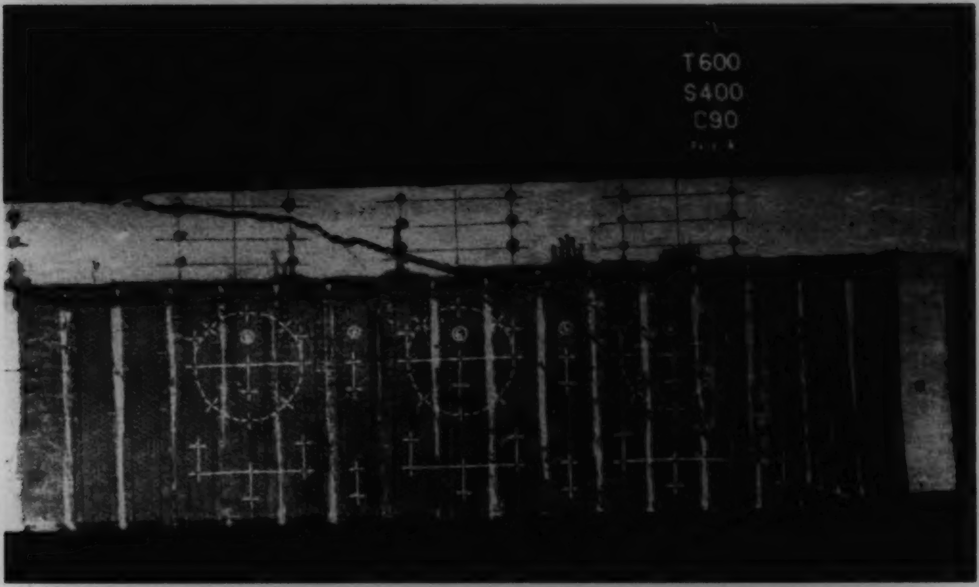
T600
S400
C90

Figure C.10 T6S4C90 Specimen after Failure (Face A)

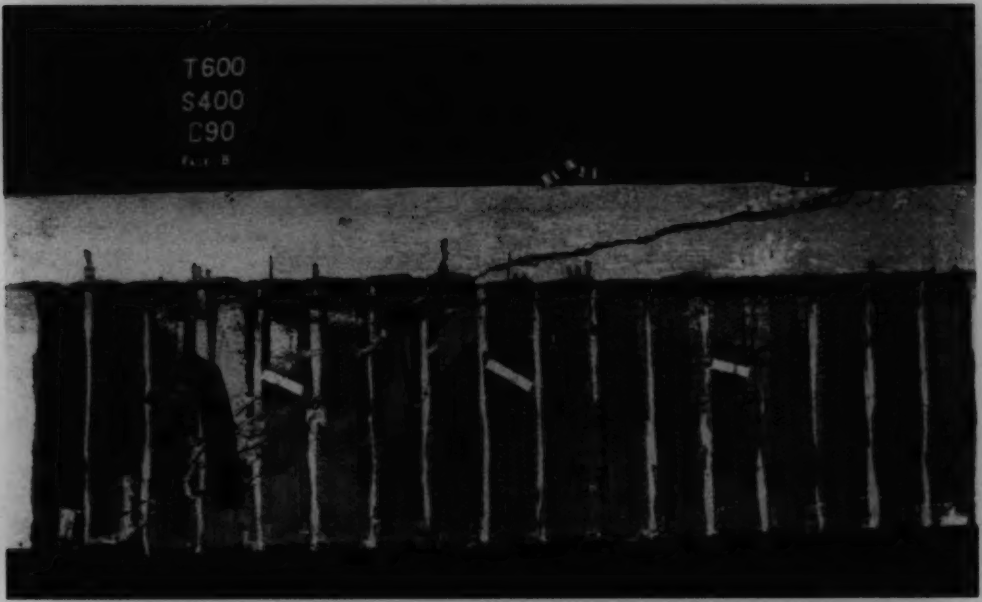
T600
S400
C90

Figure C.11 T6S4C90 Specimen after Failure (Face B)

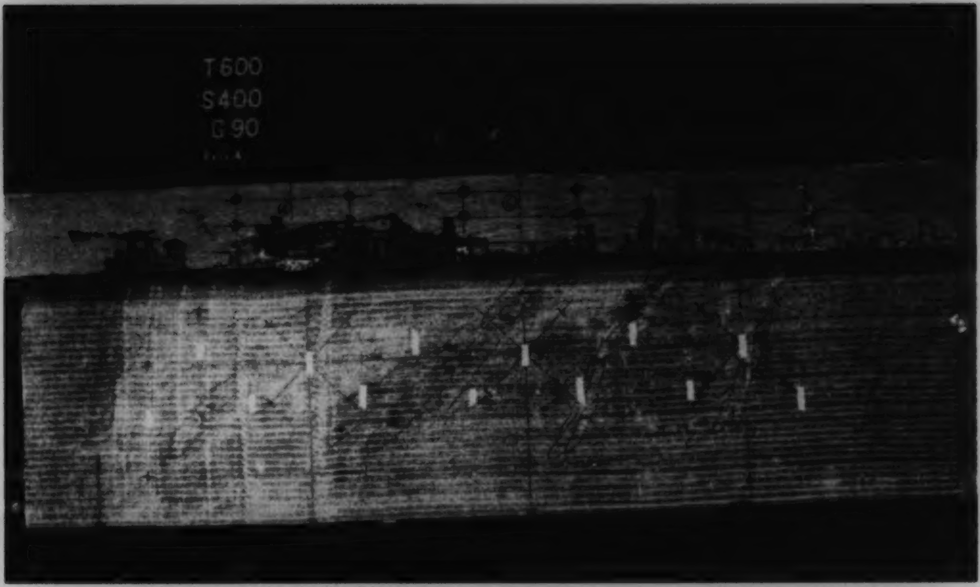
T600
S400
G90

Figure C.12 T6S4G90 Specimen after Failure (Face A)

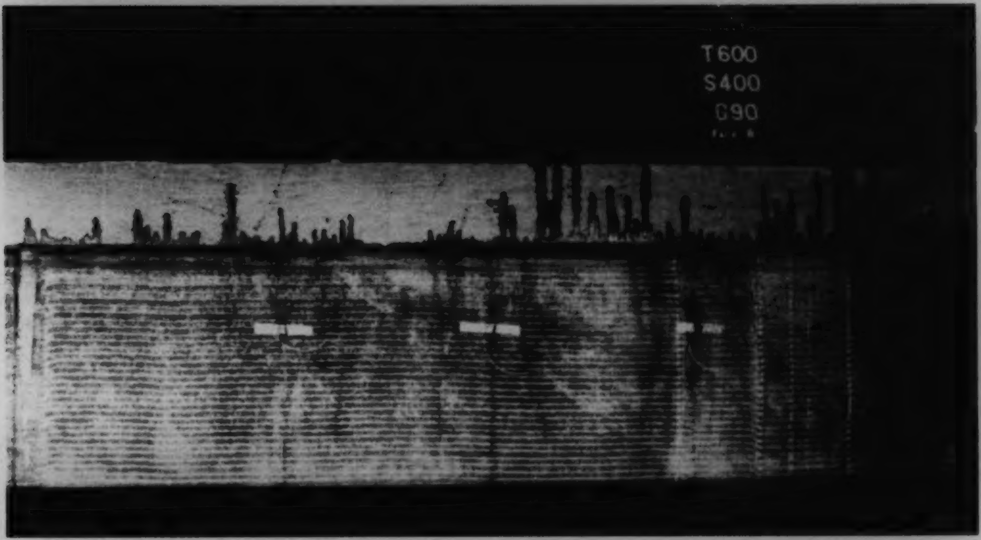
T600
S400
G90

Figure C.13 T6S4G90 Specimen after Failure (Face B)

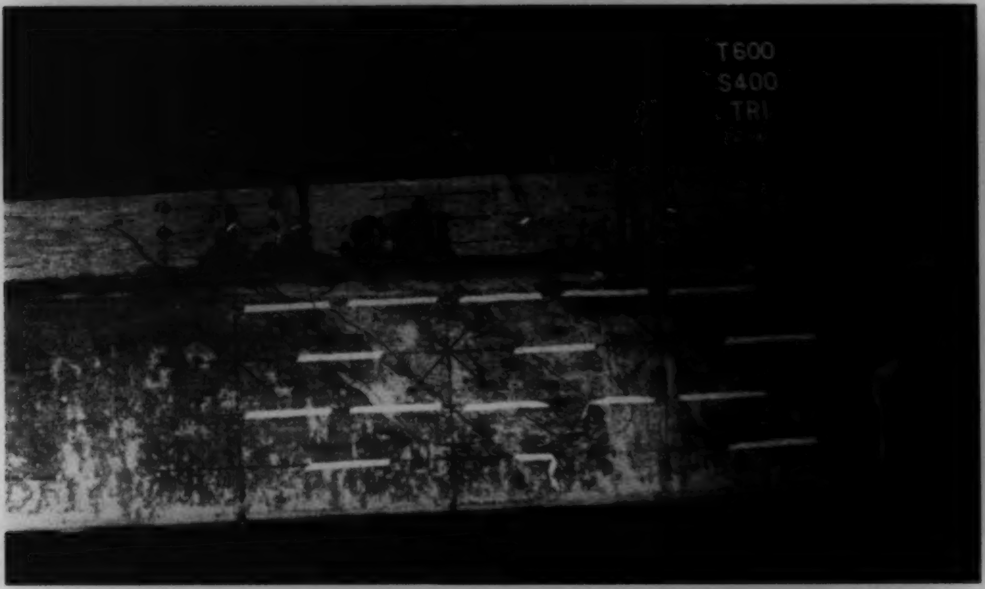
T600
S400
TRI

Figure C.14 T6S4Tri Specimen after Failure (Face A)

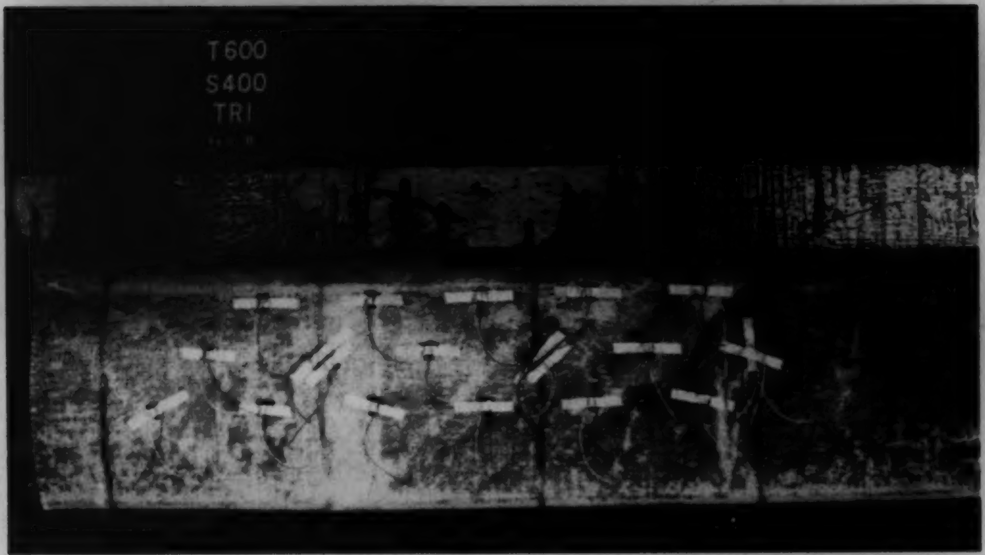
T600
S400
TRI

Figure C.15 T6S4Tri Specimen after Failure (Face B)

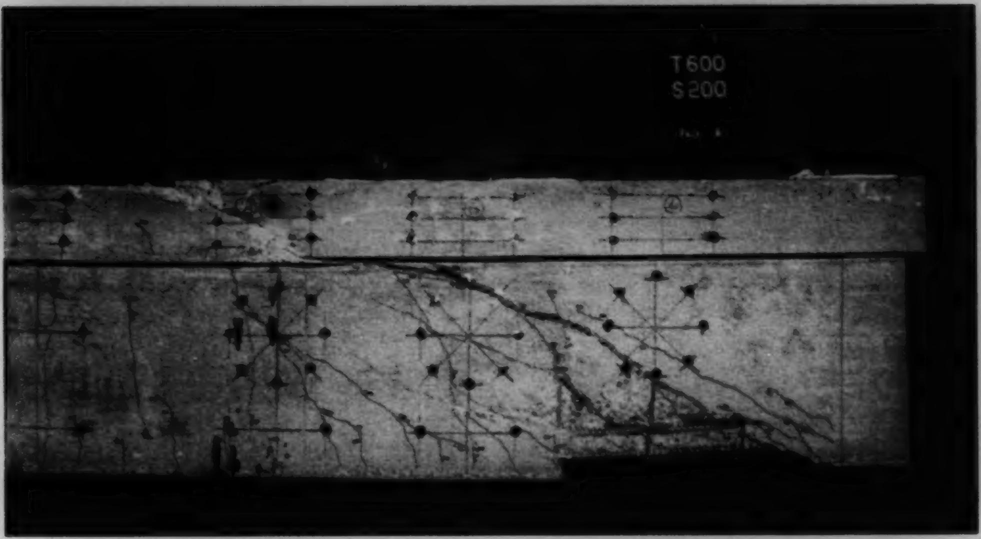

Figure C.16 T6S2 Specimen after Failure (Face A)

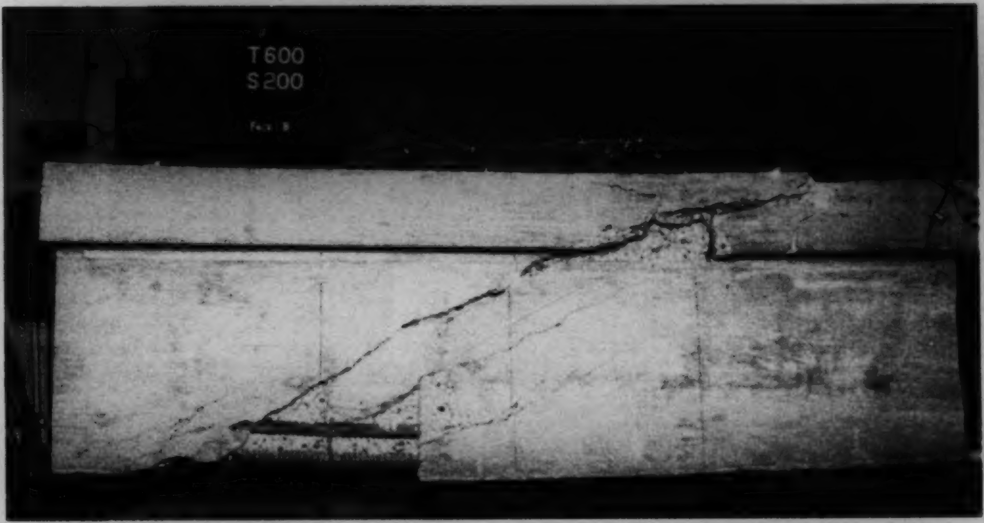

Figure C.17 T6S2 Specimen after Failure (Face B)

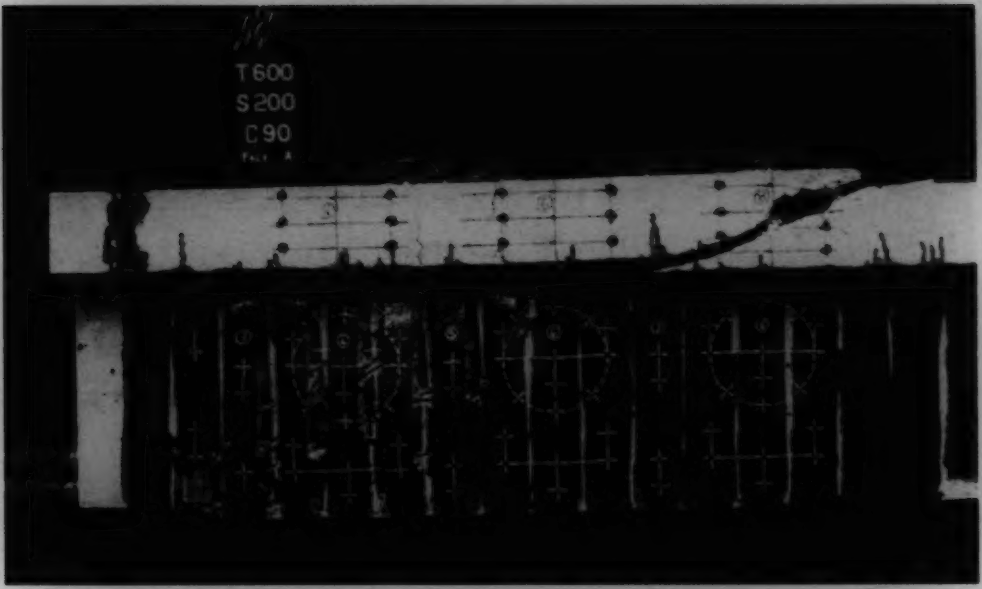
T600
S200
C90

Figure C.18 T6S2C90 Specimen after Failure (Face A)

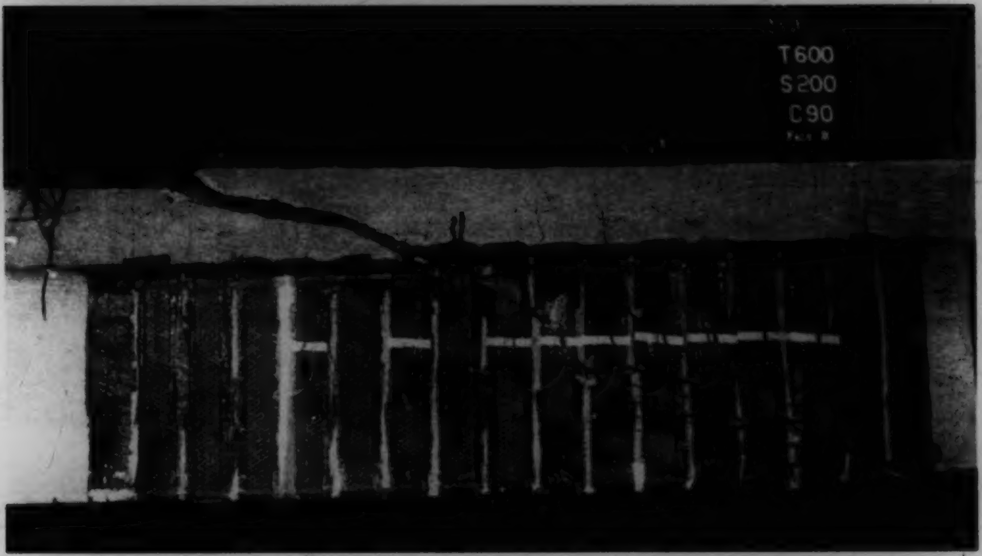
T600
S200
C90

Figure C.19 T6S2-C90 Specimen after Failure (Face B)

C.2 Schematic Shear Crack Patterns

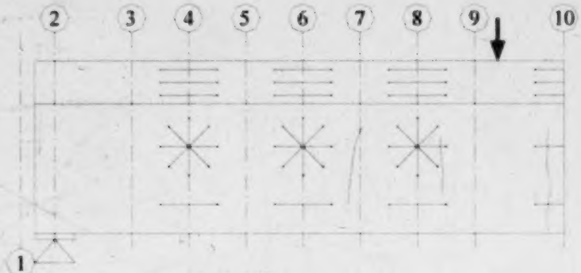
2
3
4
5
6
7
8
9
10
1

a) At 111 kN

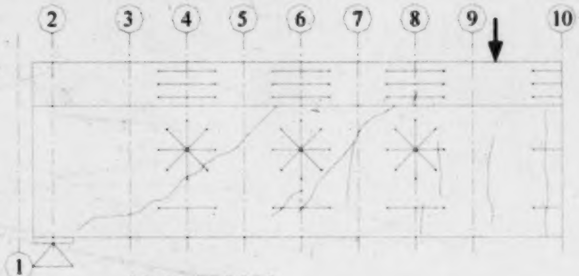
2
3
4
5
6
7
8
9
10
1

b) At 205 kN

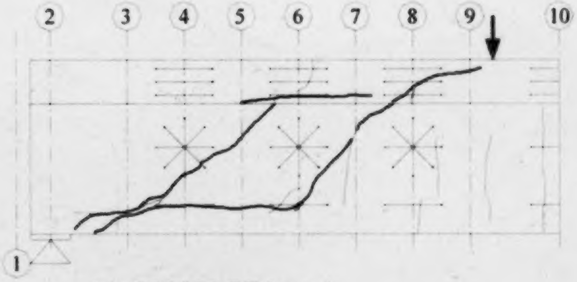
2
3
4
5
6
7
8
9
10
1

c)At 220 kN (Ultimate)

Figure C.20 Cracking Growth for T6NS Specimen

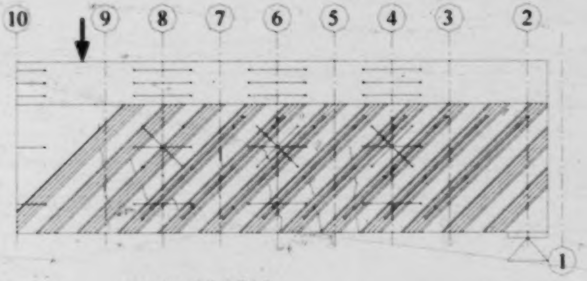
10
9
8
7
6
5
4
3
2
1

a) At 114 kN

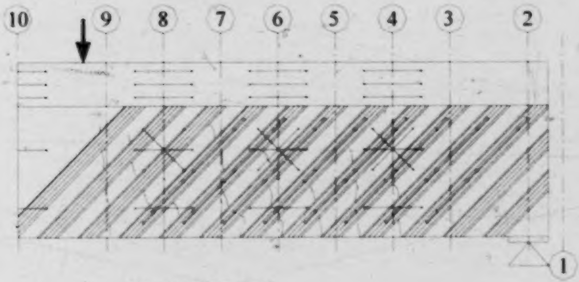
10
9
8
7
6
5
4
3
2
1

b) At 212 kN

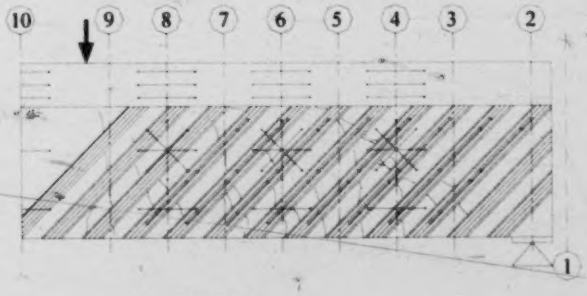
10
9
8
7
6
5
4
3
2
1

c)At 305 kN

Figure C.21 Cracking Growth of T6NSC45 Specimen (continued)

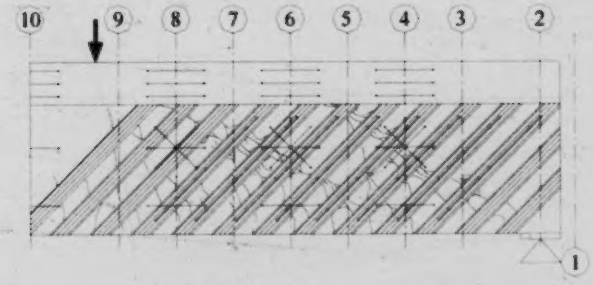
10
9
8
7
6
5
4
3
2
1

d)At 400 kN

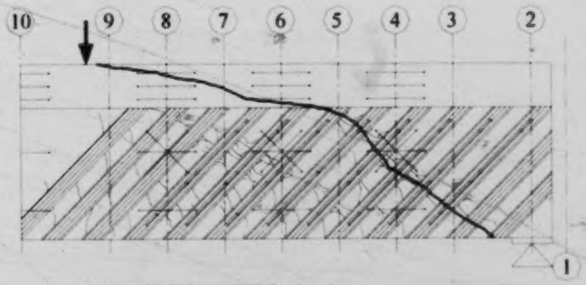
10
9
8
7
6
5
4
3
2
1

e)At 427 kN (Ultimate)

Figure C.21 Cracking Growth for T6NSC45 Specimen (concluded)

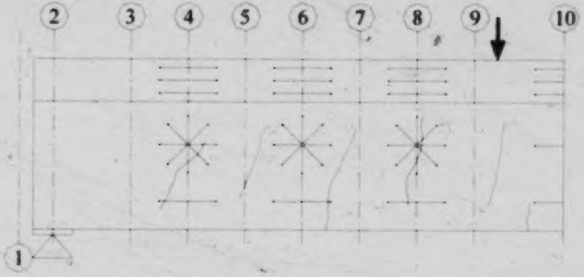
2
3
4
5
6
7
8
9
10
1

a) At 154 kN

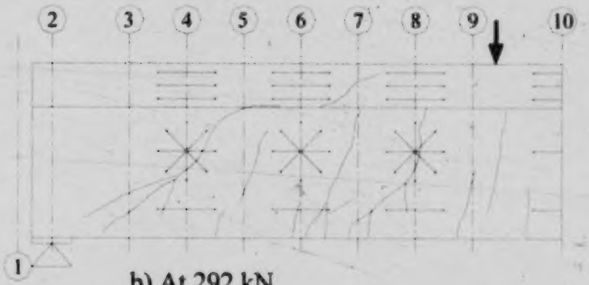
2
3
4
5
6
7
8
9
10
1

b) At 292 kN

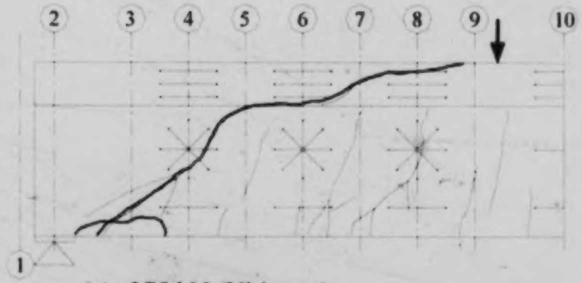
2
3
4
5
6
7
8
9
10
1

c)At 375 kN (Ultimate)

Figure C.22 Cracking Growth of T6S4 Specimen

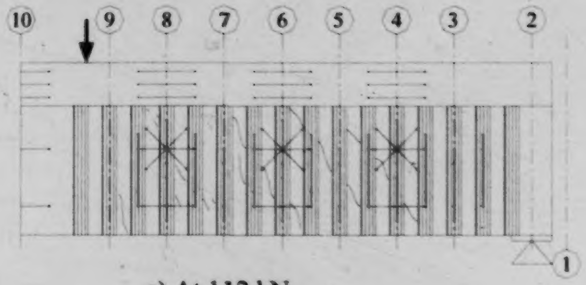
10
9
8
7
6
5
4
3
2
1

a) At 112 kN

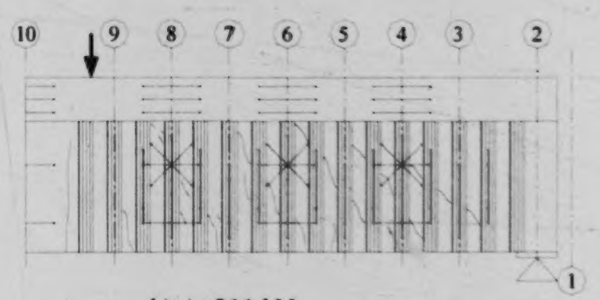
10
9
8
7
6
5
4
3
2
1

b) At 211 kN

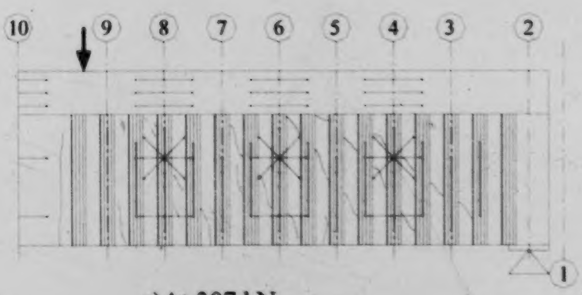
10
9
8
7
6
5
4
3
2
1

c)At 307 kN

Figure C.23 Cracking Growth for T6S4C90 Specimen (continued)

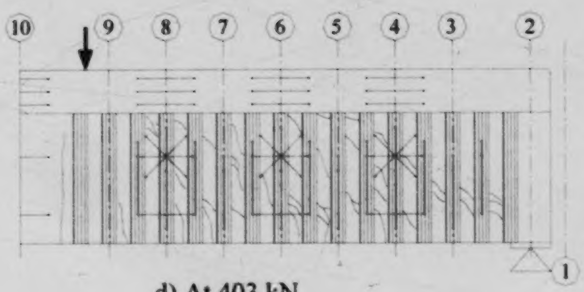
10
9
8
7
6
5
4
3
2
1

d) At 403 kN

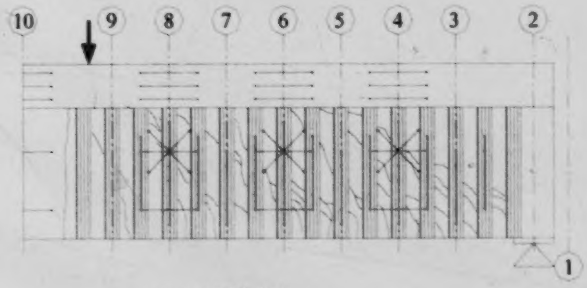
10
9
8
7
6
5
4
3
2
1

e) At 501 kN

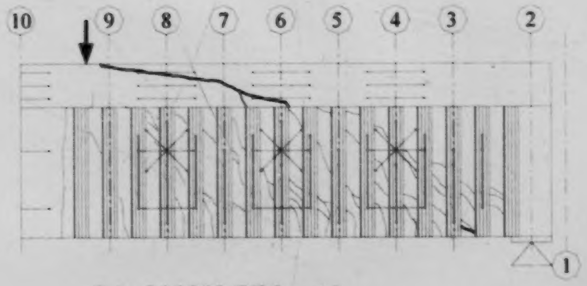
10
9
8
7
6
5
4
3
2
1

f)At 546 kN (Ultimate)

Figure C.23 Cracking Growth for T6S4C90 Specimen (concluded)

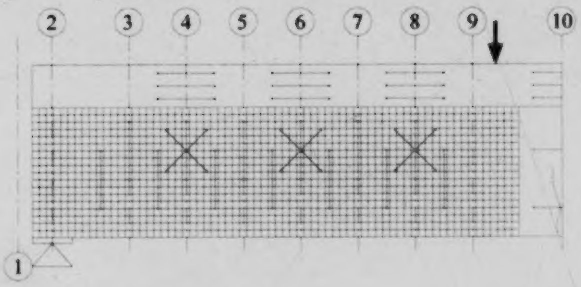
2
3
4
5
6
7
8
9
10
1

a) At 113 kN

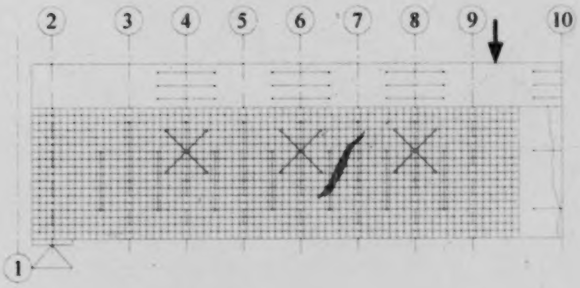
2
3
4
5
6
7
8
9
10
1

b) At 211 kN

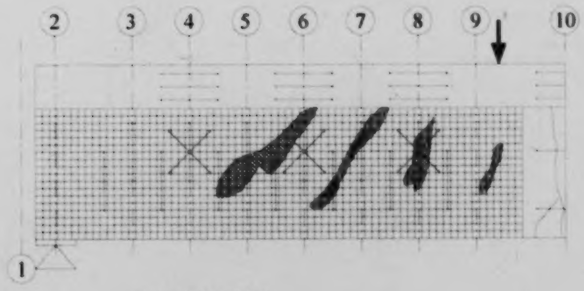
2
3
4
5
6
7
8
9
10
1

c)At 308 kN

Figure C.24 Cracking Growth for T6S4G90 Specimen (continued)

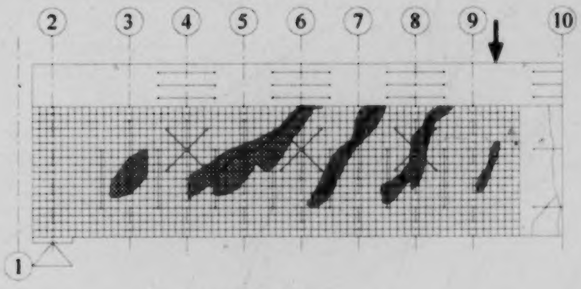
2
3
4
5
6
7
8
9
10
1

d) At 404 kN

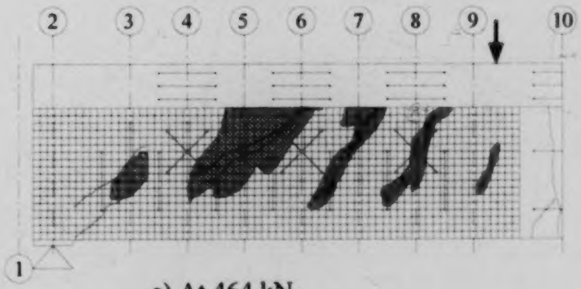
2
3
4
5
6
7
8
9
10
1

e) At 464 kN

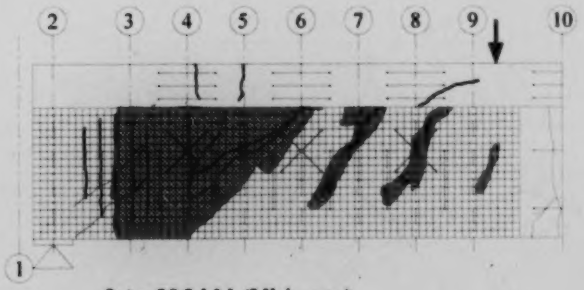
2
3
4
5
6
7
8
9
10
1

f)At 595 kN (Ultimate)

Figure C.24 Cracking Growth for T6S4G90 Specimen (concluded)

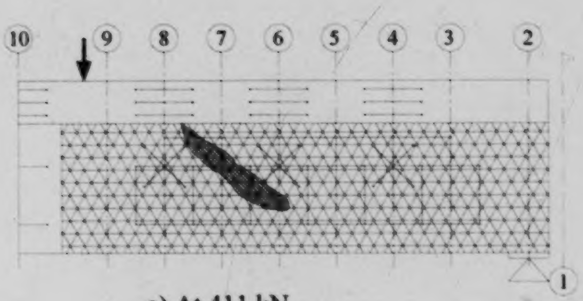
10
9
8
7
6
5
4
3
2
1

a) At 411 kN

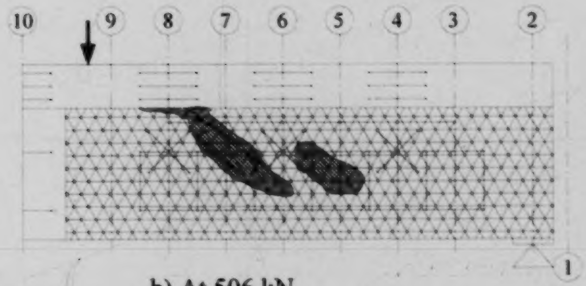
10
9
8
7
6
5
4
3
2
1

b) At 506 kN

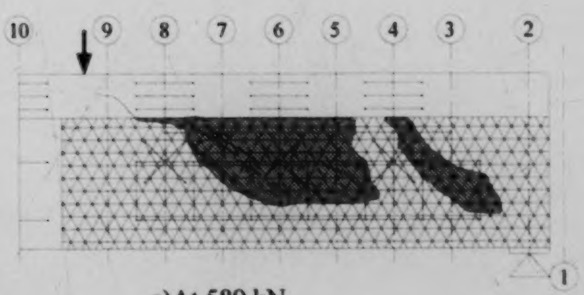
10
9
8
7
6
5
4
3
2
1

c)At 589 kN

Figure C.25 Cracking Growth for T6S4Tri Specimen (continued)

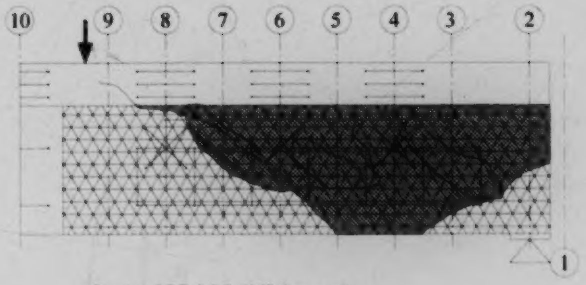
10
9
8
7
6
5
4
3
2
1

d) At 633 kN (Ultimate)

Figure C.25 Cracking growth for T6S4Tri Specimen (concluded)

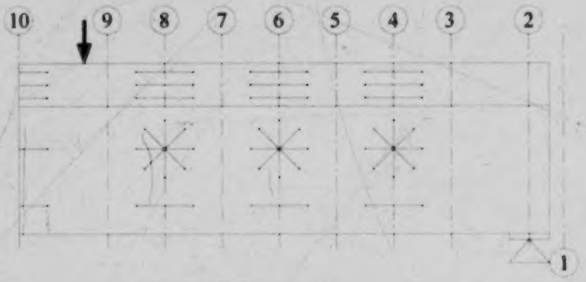
10
9
8
7
6
5
4
3
2
1

a) At 112 kN

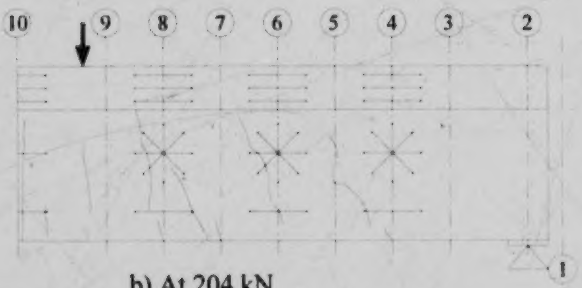
10
9
8
7
6
5
4
3
2
1

b) At 204 kN

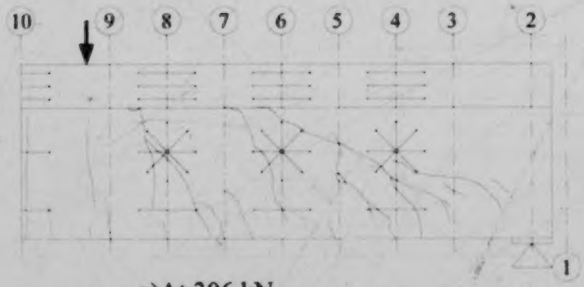
10
9
8
7
6
5
4
3
2
1

c)At 306 kN

Figure C.26 Cracking Growth for T6S2 Specimen (continued)

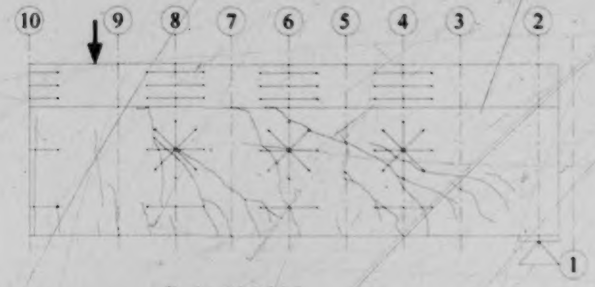
10
9
8
7
6
5
4
3
2
1

d) At 406 kN

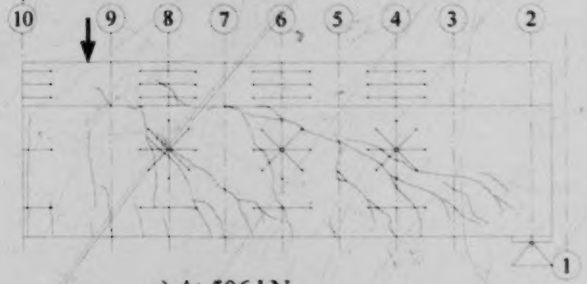
10
9
8
7
6
5
4
3
2
1

e) At 506 kN

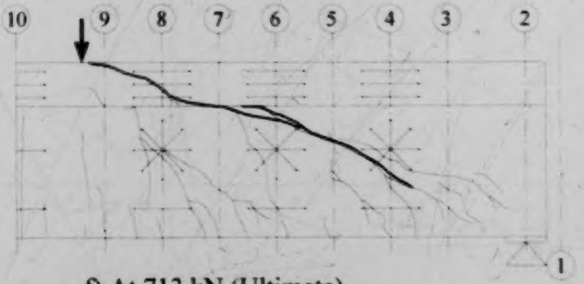
10
9
8
7
6
5
4
3
2
1

f) At 713 kN (Ultimate)

Figure C.26 Cracking Growth for T6S2 Specimen (concluded)

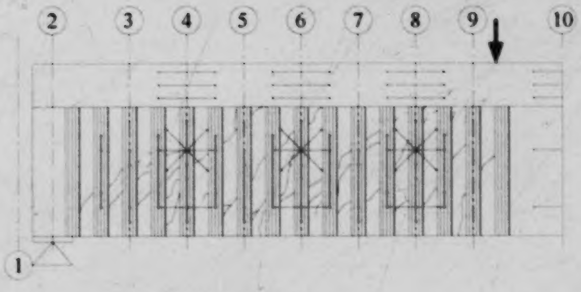
2
3
4
5
6
7
8
9
10
1

a) At 0 kN (Initial)

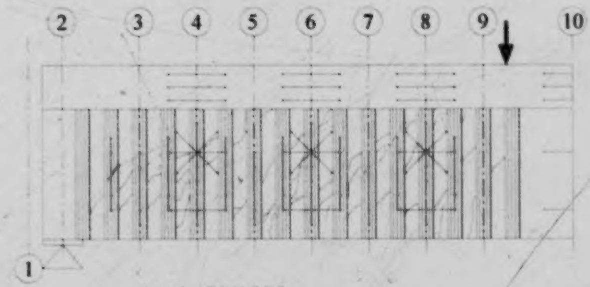
2
3
4
5
6
7
8
9
10
1

b) At 310 kN

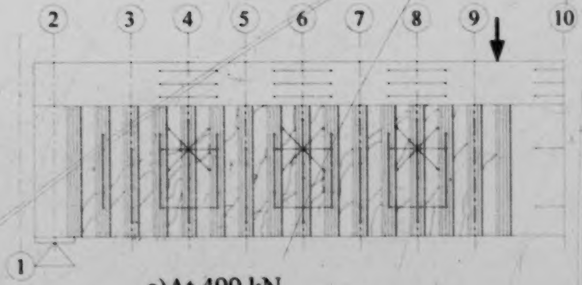
2
3
4
5
6
7
8
9
10
1

c)At 499 kN

Figure C.27 Cracking Growth for T6S2G90 Specimen (continued)

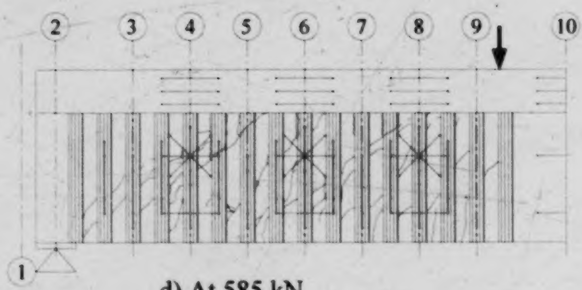
1
2
3
4
5
6
7
8
9
10

d) At 585 kN

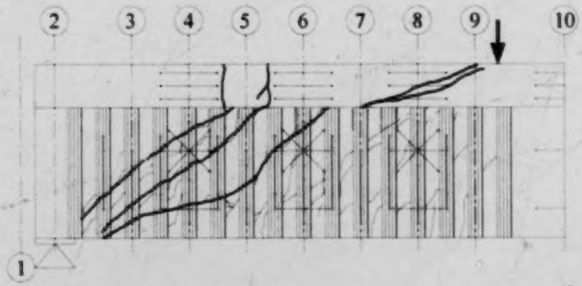
1
2
3
4
5
6
7
8
9
10

e) At 620 kN (Ultimate)

Figure C.27 Cracking Growth for T6S2C90 Specimen (concluded)

C.3 Beam and Arching Shear Actions

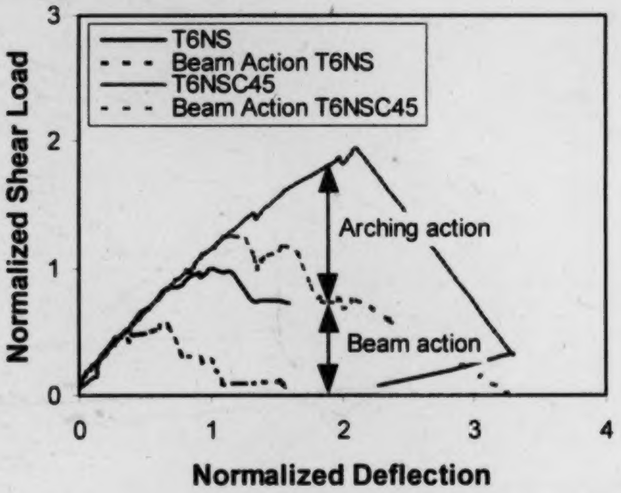

Figure C.28 Beam and Arching Actions for T6NS and T6NSC45 Specimens

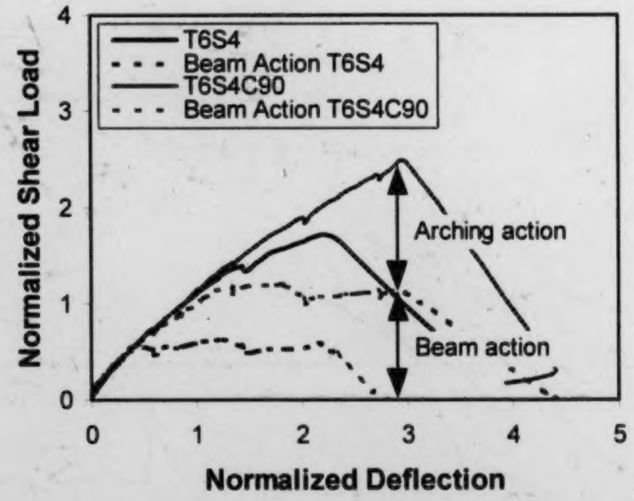

Figure C.29 Beam and Arching actions for T6S4 and T6S4C90 Specimens

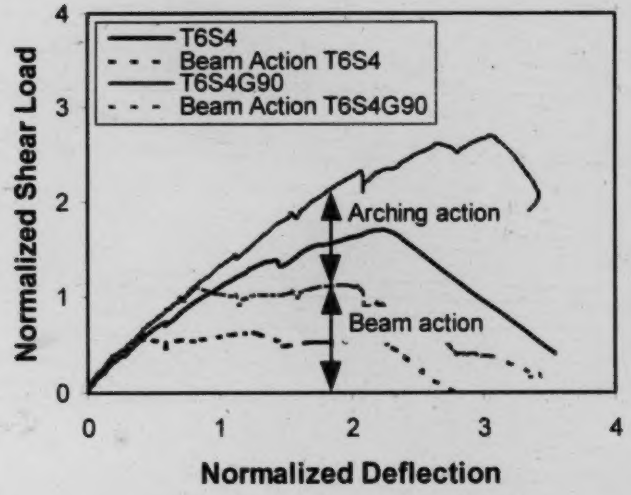

Figure C.30 Beam and Arching actions for T6S4 and T6S4G90 Specimens

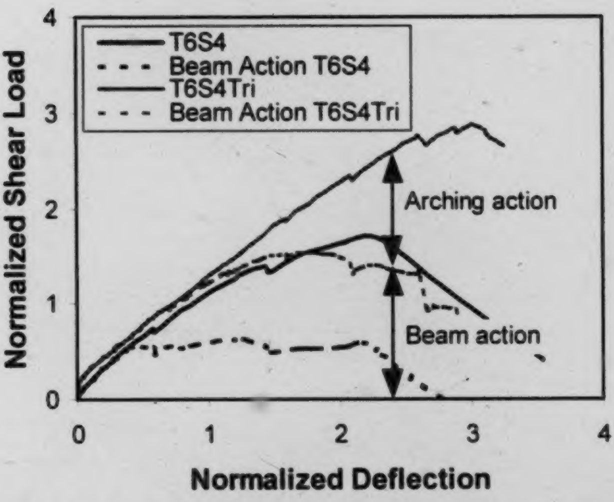

Figure C.31 Beam and Arching Actions for T6S4 and T6S4Tri Specimens

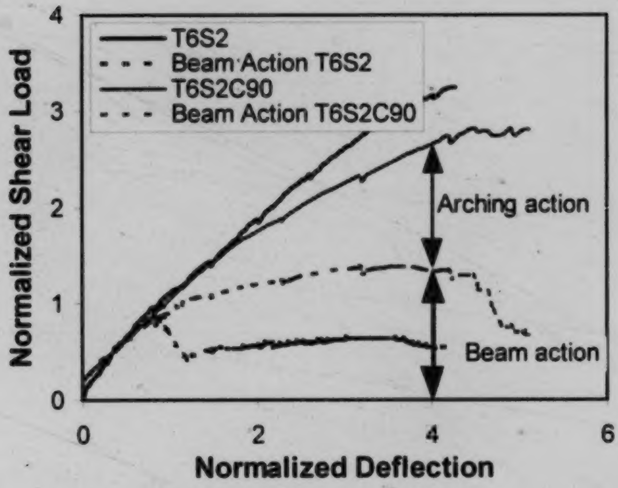

Figure C.32 Beam and Arching Actions for T6S2 and T6S2C90 Specimens

C.4 FRP Strain in the Principal Direction of the Fibre

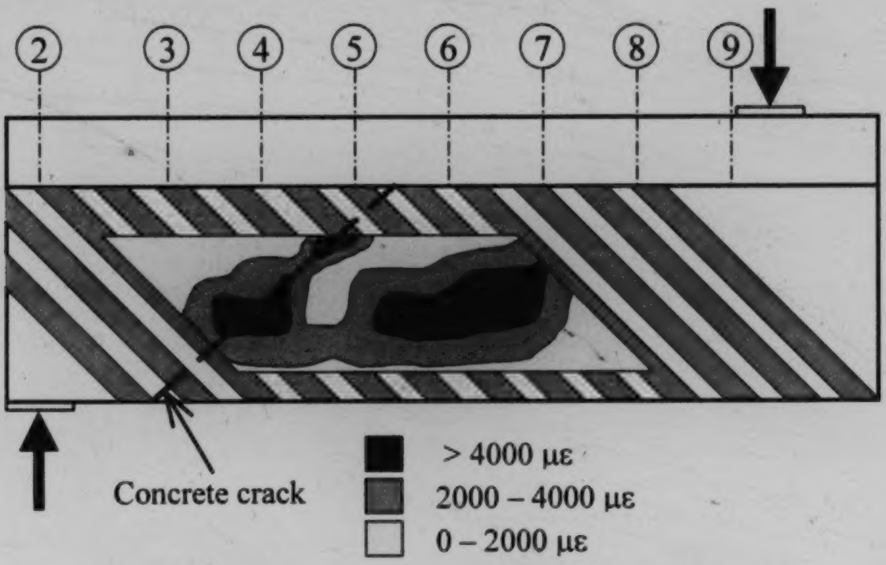
2
3
4
5
6
7
8
9
Concrete crack
■ > 4000 με
▨ 2000 – 4000 με
☐ 0 – 2000 με

Figure C.33 FRP Strains for T6NSC45 Specimen at 400 kN.

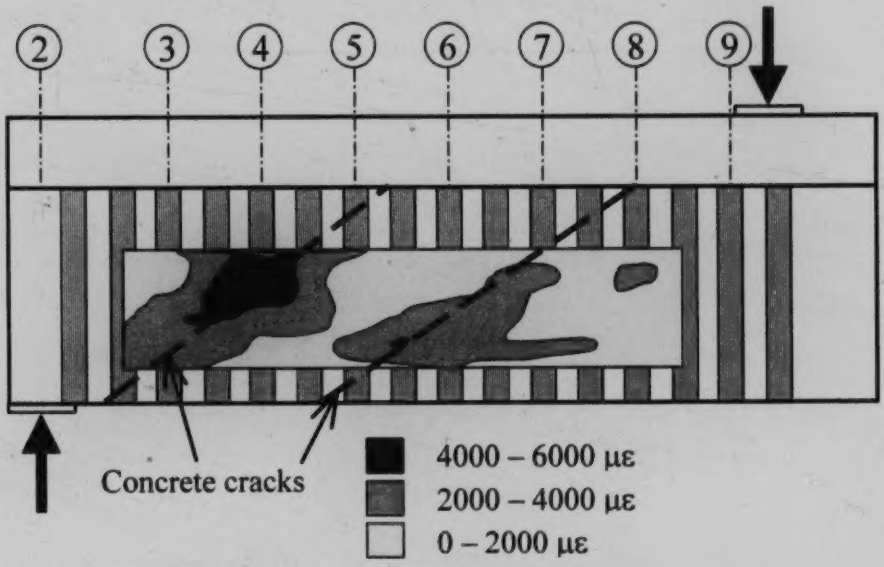
2
3
4
5
6
7
8
9
Concrete cracks
■ 4000 – 6000 με
▨ 2000 – 4000 με
☐ 0 – 2000 με

Figure C.34 FRP Strains for T6S4C90 Specimen at 501 kN

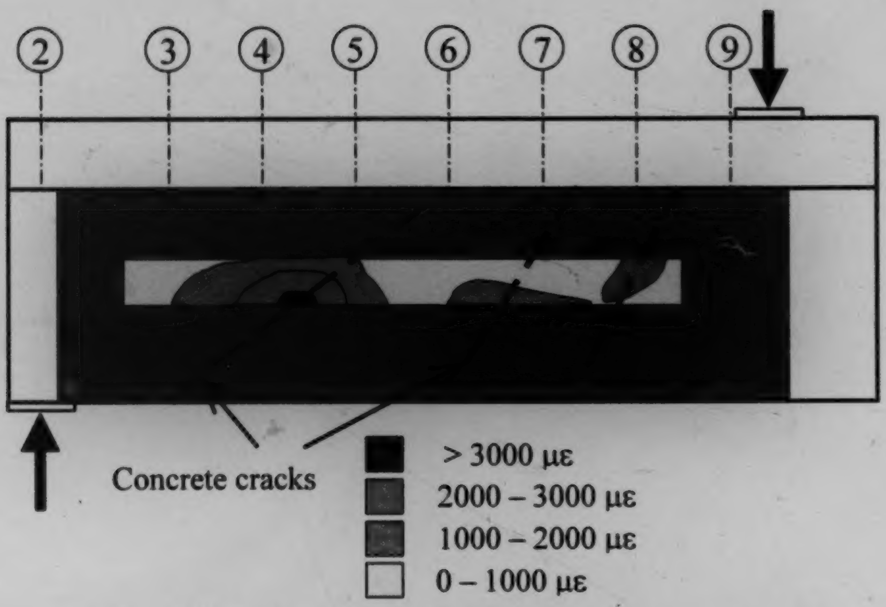
②
③
④
⑤
⑥
⑦
⑧
⑨
Concrete cracks
> 3000 με
2000 – 3000 με
1000 – 2000 με
0 – 1000 με

Figure C.35 FRP Strains for T6S4G90 Specimen at 464 kN

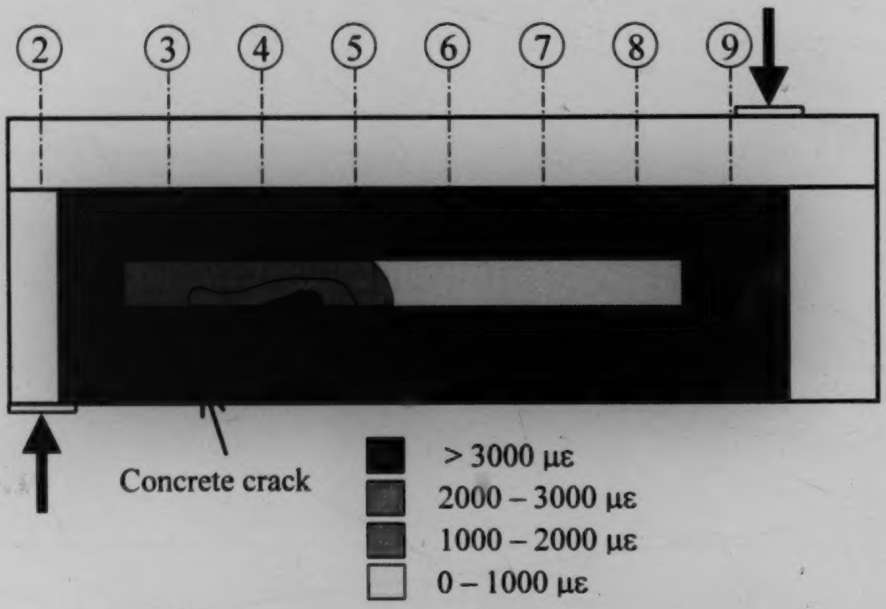
②
③
④
⑤
⑥
⑦
⑧
⑨
Concrete crack
> 3000 με
2000 – 3000 με
1000 – 2000 με
0 – 1000 με

Figure C.36 FRP Strains for T6S4Tri Specimen at 589 kN

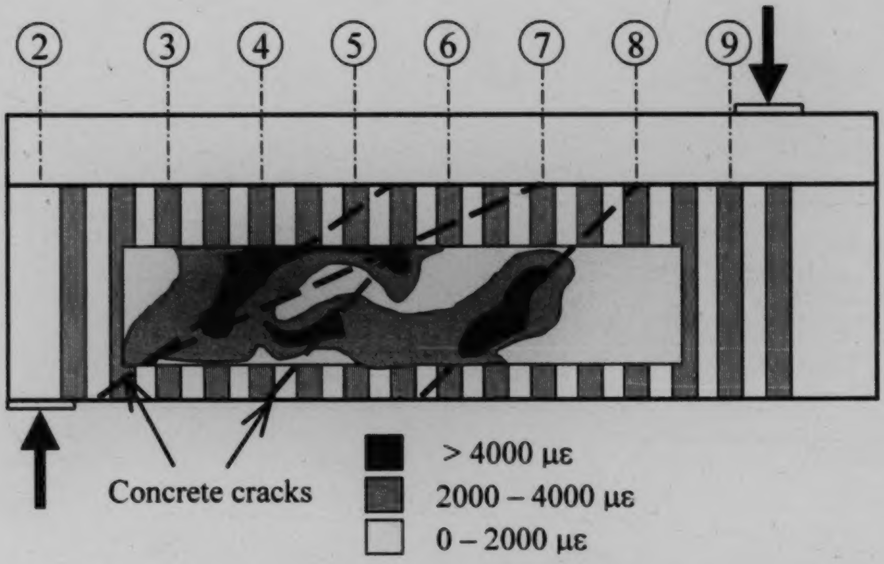
2
3
4
5
6
7
8
9
Concrete cracks
> 4000 με
2000 – 4000 με
0 – 2000 με

Figure C.37 FRP Strains for T6S2C90 Specimen at 585 kN

C.5 Crack pattern Predictions with a Uniform FRP Strain Distribution

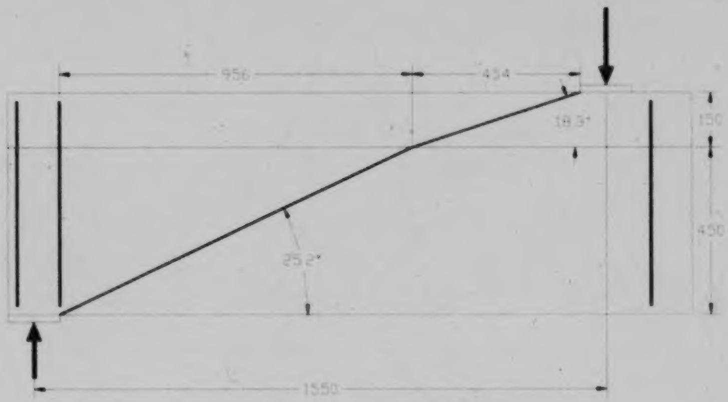
956
454
18.3°
150
450
25.2°
1550

Figure C.38 Crack Prediction for T6NS Specimen with a Uniform FRP Strain Assumption

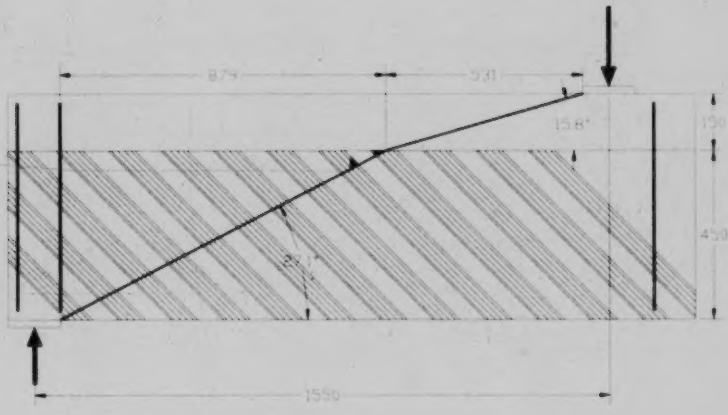
879
531
15.8°
150
450
27.1°
1550

Figure C.39 Crack Prediction for T6NSC45 Specimen with a Uniform FRP Strain Assumption

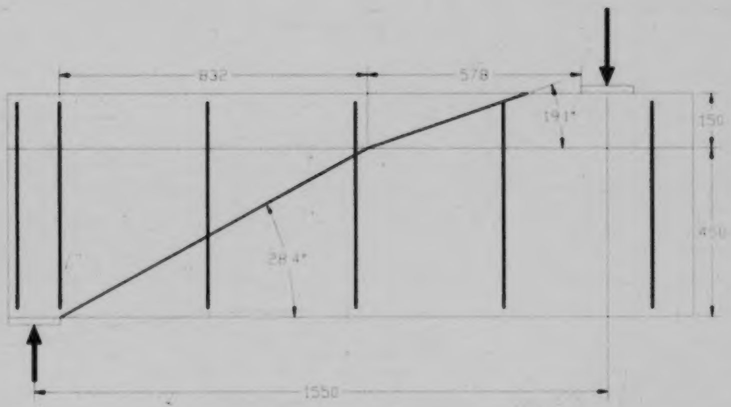
832
578
19.1°
150
450
28.4°
1550

Figure C.40 Crack Prediction for T6S4 Specimen with a Uniform FRP Strain Assumption

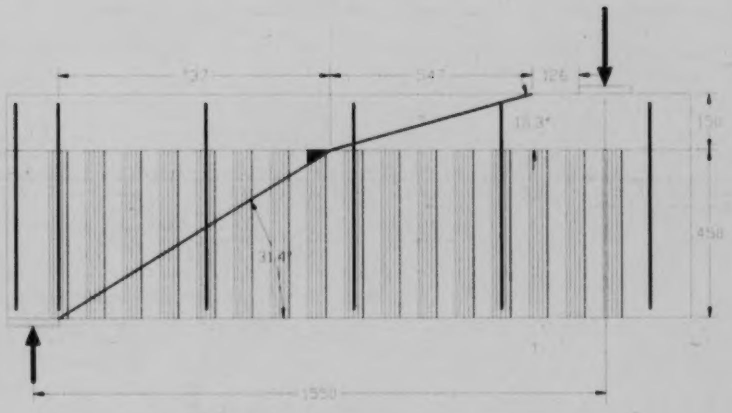
547
126
18.3°
150
450
31.4°
1550

Figure C.41 Crack Prediction for T6S4C90 Specimen with a Uniform FRP Strain Assumption

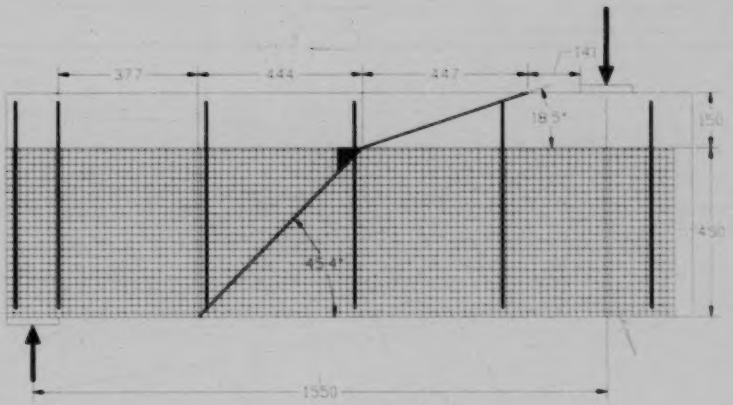
377
444
447
141
18.5°
150
450
43.4°
1550

Figure C.42 Crack prediction for T6S4G90 Specimen with a uniform FRP Strain Assumption

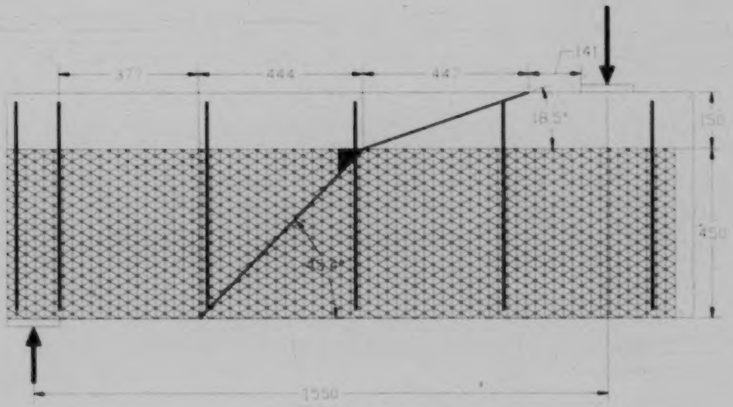
377
444
447
141
18.5°
150
450
43.4°
1550

Figure C.43 Crack Prediction for T6S4Tri with a Uniform FRP Strain Prediction

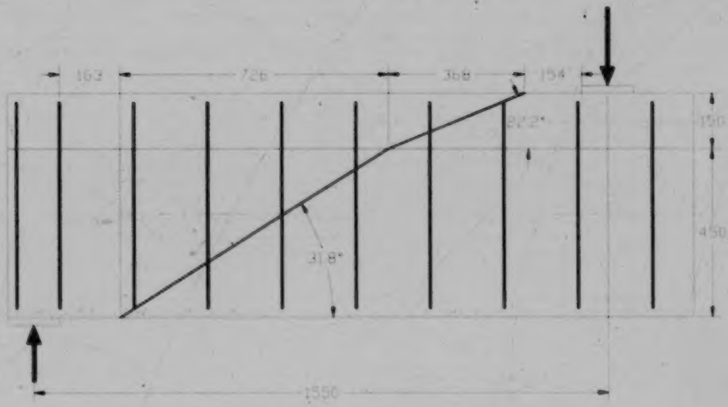
163
726
368
154
22.2°
150
450
31.8°
1550

Figure C.44 Crack Prediction for T6S2 Specimen with a Uniform FRP Strain Assumption

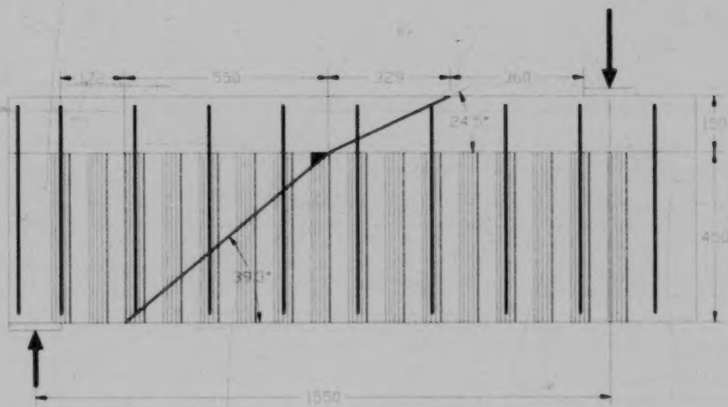
172
550
329
360
24.5°
150
450
39.3°
1550

Figure C.45 Crack Prediction for T6S2C90 with a Uniform FRP Strain Assumption

APPENDIX D ADDITIONAL SHEAR DESIGN METHOD DATA

D.1 T400 Crack Pattern Predictions with a Uniform FRP Strain Distribution

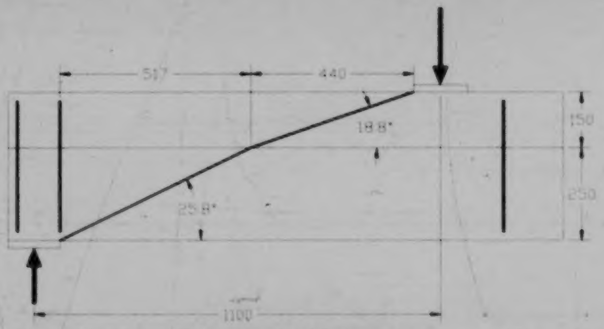
517
440
18.8°
25.8°
150
250
1100

Figure D.1 Crack Prediction for T4NS Specimen with a Uniform FRP Strain Assumption

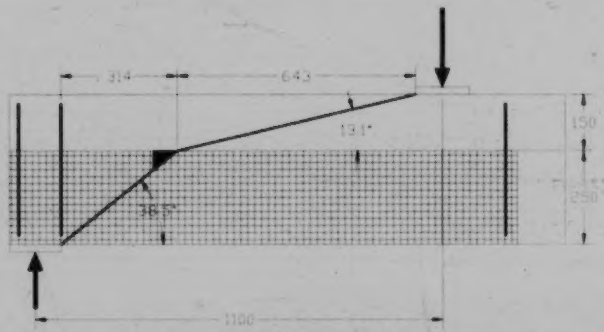
314
643
13.1°
36.5°
150
250
1100

Figure D.2 Crack Prediction for T4NSG90 Specimen with a Uniform FRP Strain Assumption

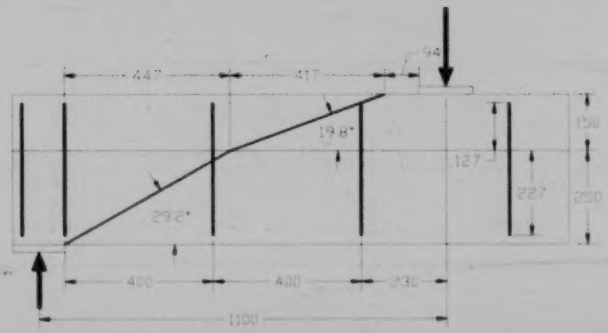
94
447
417
19.8°
29.2°
150
127
227
250
400
400
230
1100

Figure D.3 Crack Prediction for T6S4 Specimen with a Uniform FRP Strain Assumption

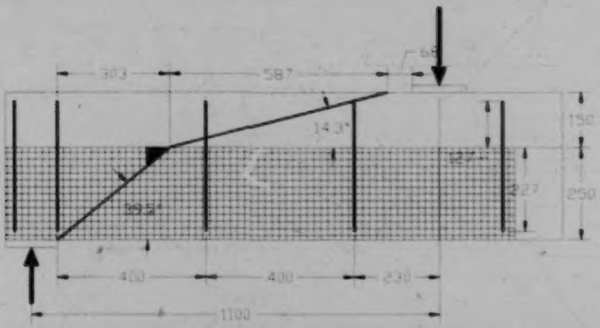
68
303
587
14.3°
150
127
227
250
400
400
230
1100

Figure D.4 Crack Prediction for T6S4G90 Specimen with a Uniform FRP Strain Assumption

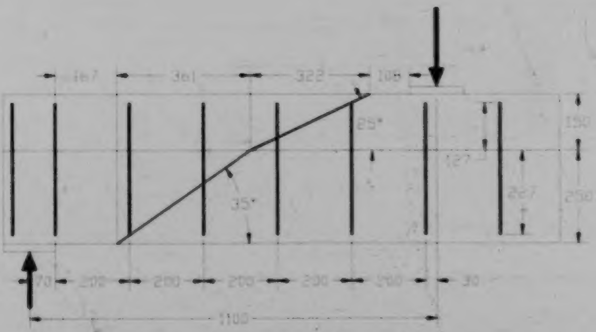
167
361
322
108
25°
150
127
227
250
35°
70
200
200
200
200
200
30
1100

Figure D.5 Crack Prediction for T4S2 Specimen with a Uniform FRP Strain Assumption

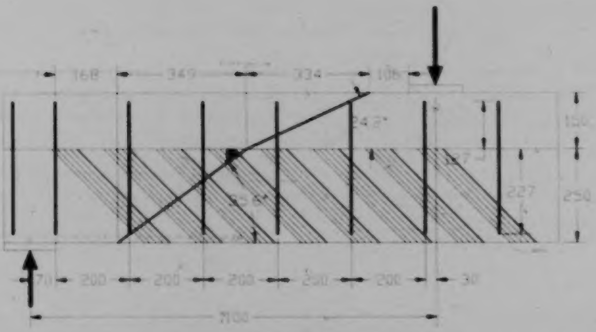
168
349
334
108
24.3°
150
127
227
250
70
200
200
200
200
200
30
1100

Figure D.6 Crack Prediction for T6S2C45 Specimen with a Uniform FRP Strain Assumption

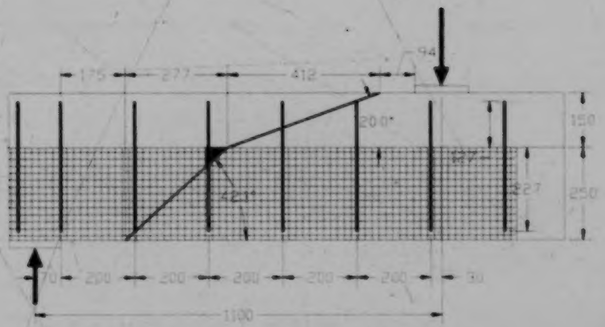
94
175
277
412
20.0°
150
127
227
250
42.1°
70
200
200
200
200
200
30
1100

Figure D.7 Crack Prediction for T6S2G90 Specimen with a Uniform FRP Strain Assumption

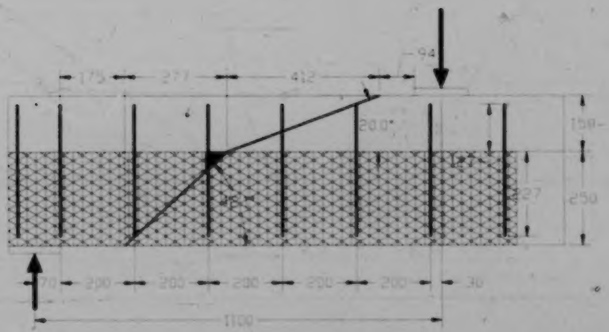
94
175
277
412
20.0°
150
127
227
250
70
200
200
200
200
200
30
1100

Figure D.8 Crack Prediction for T6S2Tri Specimen with a Uniform FRP Strain Assumption

D.2 Detailed Design Procedure Proposed by MALEK and SAADATMANESH (1998)

In 1998, MALEK and SAADATMANESH have worked out the section equilibrium of the forces acting along a concrete crack inclined at an angle θ_c. The method proceeds by steps that are reported below:

1. Assume the shear load V and the angle θ_c.
2. Calculate the axial force ΔN developed in the longitudinal reinforcement with:

[D.1] $$\Delta N = \frac{V}{\tan\theta_c}$$

3. Calculate the corresponding axial strain ε_x neglecting the effect of the FRP sheets with respect to the longitudinal reinforcement.

[D.2] $$\varepsilon_x = \frac{\Delta N}{A_s E_s} \le \frac{f_y}{E_s}$$

4. Compute the compressive stress in the concrete strut with:

[D.3] $$f_2 = \frac{V}{b_w d_v \sin\theta_c \cos\theta_c}$$

5. Assume ε_1 and compute the maximum compressive stress f_{2max} from:

[D.4] $$f_{2max} = \frac{f'_c}{0.8 - 0.34\dfrac{\varepsilon_1}{\varepsilon_{cu}}} \le f'_c$$

6. Calculate the compression strain in the concrete strut with the following equation (COLLINS and MITCHELL, 1989).

[D.5] $$\varepsilon_2 = \varepsilon_{cu}\left(1 - \sqrt{1 - \frac{f_2}{f_{2max}}}\right)$$

where ε_{cu} is the compressive uniaxial strain corresponding to f_c'.

7. Knowing ε_x and ε_2, ε_l and ε_y are obtained using the following transformation equations from the Mohr's circlD.

[D.6a] $$\varepsilon_1 = \frac{\varepsilon_x\left[1+\tan^2(\theta_c)\right]-\varepsilon_2}{\tan^2(\theta_c)}$$

[D.6b] $$\varepsilon_y = \varepsilon_1\left[1+\tan^2(\theta_c)\right]+\varepsilon_x\tan^2(\theta_c)$$

8. Check the assumption on ε_l.

9. The total shear force resisted by the beam is then expressed by

[D.7] $$V_i = F_{FRP} + F_s$$

with

[D.8a] $$F_s = E_s\,\varepsilon_y\,A_v\,\frac{d_v}{s\tan\theta_c} \le f_{yv}\,A_v\,\frac{d_v}{s\tan\theta_c}$$

[D.8b] $$F_{FRP} = 2d_{FRP}\,t_{FRP}\left(\sigma_{12}+\frac{\sigma_{11}}{\tan\theta_c}\right)$$

where σ_{12} and σ_{11} are the shear and normal stresses of the FRP sheet along the crack in the direction 1 and 2. The laminate theory is used to transform the FRP sheet stiffness from the axis l and t to the axis 1 and 2.

Step 1 through 9 are repeated until the assumed shear load V and V_i converge for a given angle θ_c. The inclination angle θ_c corresponding to the maximum shear load is the governing anglD.

Once the governing angle θ_c is found, the concrete contribution V_c can be found with the Equation (6.2) and the appropriate value of β. The total shear capacity of the beam becomes then:

[D.9] $$V_r = V_i + V_c$$

APPENDIX E CONFERENCE PAPERS

E.1 5th International Conference on Short and Medium Span Bridges – July 13-16, 1998, Calgary, Alberta

SHEAR REHABILITATION OF TYPE G GIRDERS USING ACM: EXPERIMENTAL STUDY

Christophe DENIAUD and J.J. Roger CHENG
Department of Civil and Environmental Engineering
University of Alberta
Edmonton, Alberta
Canada

Summary

Type G-girders have been used extensively in Alberta for highway bridges in 1950's and 60's, with approximately 1500 of these bridges still in service all over the province today. Structural deficiency, especially in shear, of the G-girders plus economic constraints of the government has demanded an economical and efficient method of rehabilitation for these bridges. A research program at the University of Alberta, in collaboration with Alberta Transportation and Utilities has been established to study the feasibility of using advanced composite materials (ACM) to rehabilitate those concrete bridge girders deficient in shear. This project is designed to find the most efficient repair scheme for type G-girders. This paper will address the structural deficiency of the G-Girders and present the results from the full scale tests.
A total of eight tests were carried out from four G -Girders removed from the existing bridges. Three of them have round end diaphragms and the remaining one has square end panels. Fibre reinforced plastic (FRP) sheets, both carbon and glass fibres, were used in the rehabilitation. Two shear repair schemes on the inside face of the girders were investigated: vertical sheets of 250 mm wide spaced at 300 mm (gap of 50 mm) and inclined sheets at 45° with the same width and gap perpendicular to the principal direction of the fibres. One girder (two ends) was strengthened with glass fibres. Three ends (one square and two round diaphragms) were strengthened with carbon fibres. At the end diaphragms, vertical straps of 50 mm wide sheets were provided on the inside face of the round diaphragms. Additional horizontal carbon fibres were also added for the square end diaphragm. All girders were subjected to eccentric loading in order to produce shear and torsion in the end panels. In order to avoid the flexural failure, full length longitudinal steel plates were glued at the bottom face of the girders.
Preliminary results show that the maximum load capacity of the girders is increased by 47% and 39 % when strengthened with inclined and vertical sheets, respectively. A large portion of the increased capacity comes from the glued steel plates. However, different failure modes were observed for the specimens with and without FRP strengthening. The type of fiber (carbon or glass) showed little influence on the capacity of the girders when sheets are applied at 45 degrees.

INTRODUCTION

Type G-girders as shown in Figure 1 have been used extensively in Alberta for highway bridges in 1950's and 1960's. Today, there are approximately 1500 of these bridges still in service across the province. Today, these girders are deficient in shear with regard to current code requirements and evaluation specifications. The deficiency is mainly due to the increase of allowable loads for the last 40 years as well as better understanding of shear behavior in reinforced concrete since the early 1970's. It is a major concern for the Alberta Transportation and Utilities (AT&U) to find a reliable technique to rehabilitate and strengthen these girders at the lowest cost. A research program is carried out at the University of Alberta in collaboration with AT&U using removed girders as full scale test specimens.

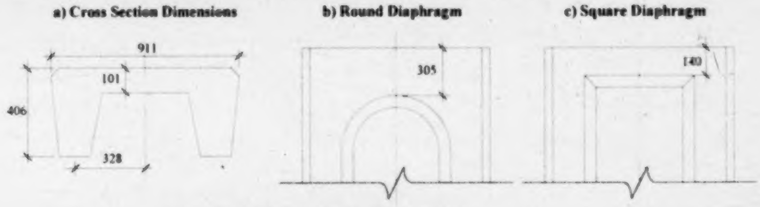
a) Cross Section Dimensions

b) Round Diaphragm

c) Square Diaphragm

Figure 1: Typical Type G-Girder

A preliminary investigation on type G girders was conducted at the University of Alberta in 1996 [1]. The results of that study showed that type G girders always failed in flexure if loaded through the centroid of the section, regardless of the longitudinal location of load application. This flexural failure still resulted despite the provision of four full length longitudinal layers of CFRP sheets along the extreme fibre. Therefore, the girders were loaded eccentrically about the centroid of the cross section in order to fail these girders in combination of shear and torsion. It was also shown that the end panel ended up being the weakest part of the girder under eccentric loading. Special considerations are therefore required to reinforce not only the inner faces of the legs but also the end diaphragm.

The objective of this series of tests was to establish a comparison between two different types of fibre reinforced plastic (FRP), namely glass and carbon fibres, with various configurations, as a shear repair technique. Reinforcement of the end diaphragm is also provided by the use of composite sheets. Because the flexural strength of the girders is not the principal investigation, a 9.5 mm thick steel plate is bonded along the bottom faces of the girders to avoid the flexural failure.

STRUCTURAL DEFICIENCY

Type G-girder bridges were designed using AASHO-49 specifications [2]. The design truck used was H20-S16 which corresponds to a total weight of 320.3 kN (36 t). The maximum wheel load was 71.2 kN. Today, bridges in Alberta are designed with CAN/CSA-S6-88 standard [3]. Three trucks, CS1 to CS3, are used in practice with a total weight increasing from 274.7 to 618 kN, respectively, The maximum wheel load is now 103 kN which represents a 44.7% increase.

In 1973, following a series of research programs, a better understanding of the shear resistance of the concrete members has resulted in a complete review of reinforced concrete design in shear [4]. Two major changes have been reported: concrete shear strength resistance and stirrups spacing. The AASHO-49 and CAN/CSA-S6-88 codes give different values using concrete design strength of 27.6 MPa and effective depth (d) of 376 mm for type G girder.

Concrete shear strength

AASHO-49: $v_c = 0.03\ f'_c$ $v_c = 0.828$ MPa

CAN/CSA-S6-88: $v_c = 0.19\ (f'_c)^{1/2}$ $v_c = 0.998$ MPa

Stirrups Spacing

AASHO-49:	$s = \frac{1}{2} h$	when required to carry shear	$s = 203$ mm
or			
	$s = \frac{3}{4} h$	when not required	$s = 304$ mm
CAN/CSA-S6-88:	$s = d/2 < 600$ mm		$s = 188$ mm

It shows that the shear strength might be increased by 20.5%. But the spacing of stirrups would need to be reduced from 304 to 188 mm which represents a 38.2% difference. Furthermore, it was found, with help of steel detector, that the spacing of G-girders tested did not even meet the requirements of AASHO-49. The actual spacings were more than twice the maximum spacing allowed by current CAN/CSA-S6-88 standard.

CAN/CSA-S6-88 also stipules that minimum area of shear reinforcement must be provided where the design shear is greater than one half the permissible shear resistance (v_c) carried by the concrete [3]. In other words, when minimum stirrups requirements are not satisfied, the concrete shear strength should be reduced by half to give, in this example, $v_c = 0.499$ MPa. The later result is then compared to 0.828 MPa.

Overall, the design shear capacity has decreased by 40% while the applied loads have increased by about 45% over the last 40 years. These two effects added together plus the aging of the bridges result in the shear deficiency of type G-girders.

EXPERIMENTAL PROGRAM

Test Specimen

Two types of specimens were used in this series. Three of the girders investigated had round end diaphragms and the last girder had square end panels. The girders were 6.1 m long. The girder dimensions are presented in Figure 1.

When the specimens were strengthened, the concrete surface was prepared using a grinder to remove any bumps where the steel plates and composite sheets were to be applied. The steel plates were also sand blasted before gluing it underneath each leg. The epoxy used to bond the steel plate to concrete was *Sikadur 31 Hi Mod* provided by Sika Inc. This paste comes in two parts with a mixing ratio of 3 parts A to 1 part B by volume.

In order to avoid sharp corners for the ACM, putty was used to round the corners when necessary. This procedure was particularly difficult in the end panel, as can be seen in Figure 2. Figure 3 shows a typical layout of the end diaphragm where vertical carbon fibre sheets were used. One end of the sheet extended underneath the flange and the other end extended on the top of the steel plate or underneath the end panel as shown in Figure 4. In any case, at least 100 mm development length was provided for the FRP sheets. The bands were 250 mm wide on the side of the legs. However, bands of 50 mm wide were used in the end diaphragm to be able to bond them properly to the round surface.

Two main repair schemes were used in this series. CFRP sheets were glued vertically to the inside legs for the first scheme and at an angle of 45° degrees for the second scheme. Round end panels were strengthened using 50 mm wide bands applied vertically in both cases. One square end panel (*G4 West*) was strengthened with horizontal carbon sheets. A Full description of the various configurations and materials used at each end is described in Table 1. The maximum load in the Table 1 is the applied load on the top of the girder at ultimate.

Both repair schemes are presented with dimensions and layout in Figure 4.

Test Set Up

In order to provide an eccentric loading frame, a stiff steel beam was used to distribute the load from the MTS 6000 testing machine to the top of one leg of the girder. The test set-up is presented schematically in Figure 5. The applied load on the top of the girder in each test was then computed using two methods: summation of all four load cells located at each supports, and subtraction of the distributing steel beam support and the MTS 6000.

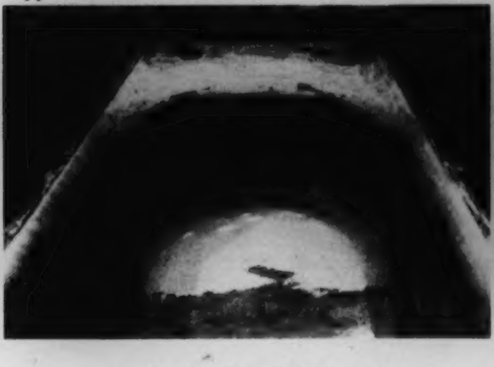

Figure 2: Putty Applied in the End Panel

Figure 3: Typical End Diaphragm Layout

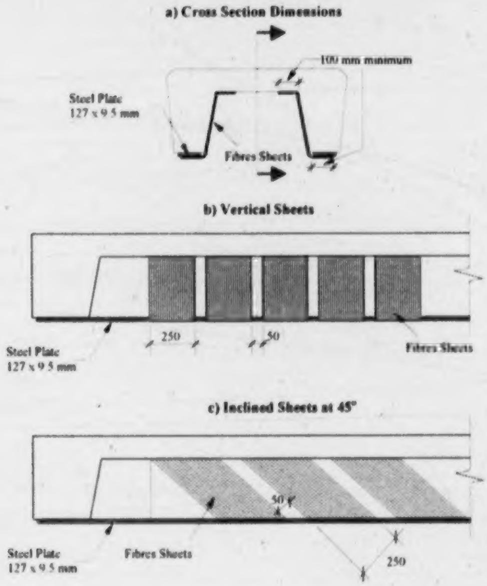

a) Cross Section Dimensions

b) Vertical Sheets

c) Inclined Sheets at 45°

100 mm minimum
Steel Plate
127 x 9.5 mm
Fibres Sheets
250
50
Fibres Sheets
Steel Plate
127 x 9.5 mm
50
Steel Plate
127 x 9.5 mm
Fibres Sheets
250

Figure 4: Repair Schemes Used

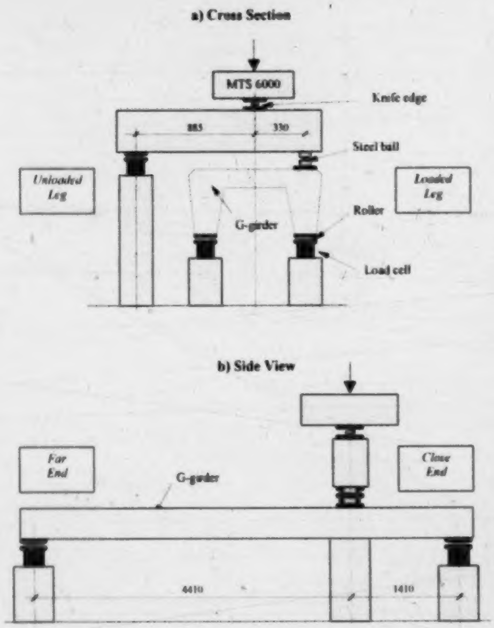

a) Cross Section

b) Side View

MTS 6000
Knife edge
885
330
Steel ball
Unloaded Leg
Loaded Leg
G-girder
Roller
Load cell
Far End
Close End
G-girder
4410
1410

Figure 5: Test Set-Up

Table 1: Test matrix and Results

Girder	Steel Plate	*In Situ* f_c' MPa	ACM Repair Scheme	Max. Load on girder kN	% Increase	Failure Mode
G1 East	Yes	45.9	None	382	35.5	Torsion in the end panel and plate debonding
G1 West	No	45.9	None	282	0.0	Torsion in end panel
G2 East	Yes	46.2	Vertical carbon	350	24.1	Shear in loaded leg
G2 West	Yes	46.2	Inclined carbon	412	46.1	Torsion in end panel/ partial concrete crushing
G3 East	Yes	42.8	Vertical glass	394	39.4	Torsion in end panel
G3 West	Yes	42.8	Inclined glass	415	47.2	Shear in loaded leg
G4 East*	No	32.5	None	259	0.0	Torsion in *Close Unloaded* (CU) corner
G4 West*	Yes	32.5	Inclined carbon	395	52.5	Torsion in *Close Unloaded* (CU) corner

* Square end Diaphragm

Special terminology used in testing program is specified in Figure 5. This system used the following keywords: *Close*, *Far*, *Unloaded* and *Loaded*. These terms serve as a general cardinal orientation because the loaded leg could be either one for each end tested.

Instrumentation

The side of each leg of the girders was instrumented with numerous sets of Demec gauges. A Demec gauge of 250 mm was used on the outside of each girder leg and an 200 mm Demec gauge was used on the inside to speed up the recording process by two crews. Electrical strain gauges were provided on the steel plate.

In order to record flexural deflection, eight cable transducers were used along each leg. Four LVDTs were also installed at two stirrup locations of interest, between the point load and the *close* supports. An extra LVDT was set up later during the test program to record the *Far Unloaded* support which was lifting up during each test

Test Procedure

Each test was performed under stroke control by the MTS6000. The following steps were followed:

1. Initial reading of all Demec points were taken.
2. Initial electronic data were recorded using a data acquisition system.
3. The specimen was loaded at a rate of 10 to 20 μm/s to give approximately 15 kN per minute in the elastic range.
4. Any sound or noise was recorded during the test.
5. For every load step of 25 kN applied on the top of the girder, a complete set of data was collected by the data acquisition system.
6. At every 100 kN load step, called *stage* in the remaining part of this paper, up to 300 kN when applicable, the loading process was paused in order to record manually all Demec gauge readings. During each stage, visual inspection of the girder was made to record any cracks and/or damage that may have occurred.
7. The girder was continuously loaded until failure with all visual cracks and noises being recorded.

Only the load applied to the top of the girder was recorded. Therefore, the dead load of the specimen is not taking into account for any results presented here.

After the first end of each girder was completed, external stirrups were provided to the failed end prior to testing the second end. These stirrups consisted of two HSS steel tubes with tie rods on both ends.

EXPERIMENTAL RESULTS

Material Properties

Concrete strength was obtained by drilling 100 mm diameter cores in accordance with the ASTM Standard C-42 [5]. Three cores were taken in each girder at three different locations to average the data. Core specimens were then soaked for at least 48 hours prior to testing. Correction factors developed by Bartlett and Mac Gregor [6] were used to find the equivalent *in situ* strength presented in Table 1.

Coupon tests were carried out in accordance with ASTM Standard A-370 [7], to determine the stress strain curve for each steel component. Two coupons were cut from the plate used as external reinforcement. Three coupon test specimens were taken from the #9 longitudinal reinforcement bars and one coupon test specimen from the #3 stirrup bars for each girder. Coupons from girder 1 could not be taken because of further scheduled testing. Table 2 gives relevant information on steel coupon test results.

Table 2: Steel Coupon Tests

		Yield Stress f_y *MPa*	Elastic Modulus E *MPa*	Ultimate Strength F_u *MPa*
Steel Plate		327	202000	502
Girder 2	#9	306	203000	494
	#3	311	186000	455
Girder 3	#9	263	191000	414
	#3	302	252000	423
Girder 4	#9	267	194000	448
	#3	336	203000	511

Two composite materials were used in this series. Unidirectional carbon fibres *Replark Type 20* from Mitsubishi Canada Limited and woven glass fibres *SEH41* from Excel Fyfe Canada Ltd were used to strengthen the sides of the girder legs and the end panel of the girders. The first one is in the form of a prepregnated tape that is mixed with two parts epoxy resin. The later is not prepreg but is also mixed with two components epoxy resin. The epoxy resin used with glass fibres was less viscous because the sheets need to be soaked in it before positioning on the concrete. Training was received on campus from Excel Fyfe on the proper use of their product. Only one layer was applied on the concrete surface. The same repair schemes were used with both composites.

ACM coupon specimens were made at the same time as the bands were being bonded. Material properties for the two composites are given in Table 3. It should be noted that a premature failure was observed from the glass fibre coupons.

Table 3: Advanced Composites Material Properties

ACM Name	Type of fibres	Test source	Ultimate Strength *MPa*	Modulus of Elasticity *MPa*	Thickness *mm*
Replark Type 20	Carbon	Fibre strength	3400	230000	0.11
		Coupon specimens	422	44800	0.70
SEH41	Glass	Fibre strength	-	-	-
		Coupon specimens	106*	17700	1.80

* Premature failure

Girder Tests

This test program includes the test results of four girders. Because both ends of each girder are tested, eight test results are reported. Table 1 summarizes the maximum loads reached and the failure modes observed for each test. Figure 6 shows the load vs point load deflection for all tests with round end diaphragm. The two tests with square end diaphragm are presented in Figure 7.

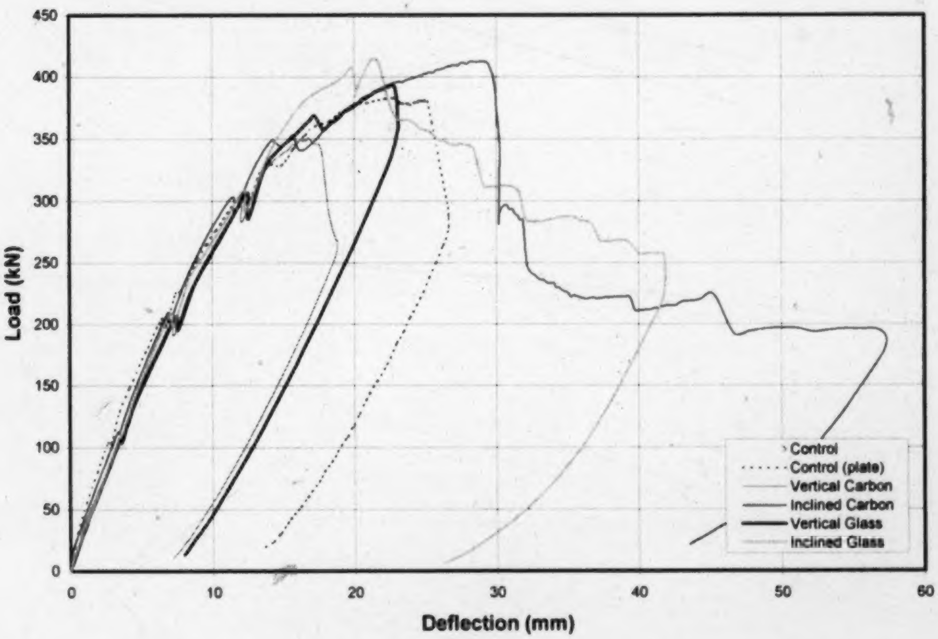

Figure 6: Load vs Point Load Deflection Curves for Specimens with Round End Diaphragm

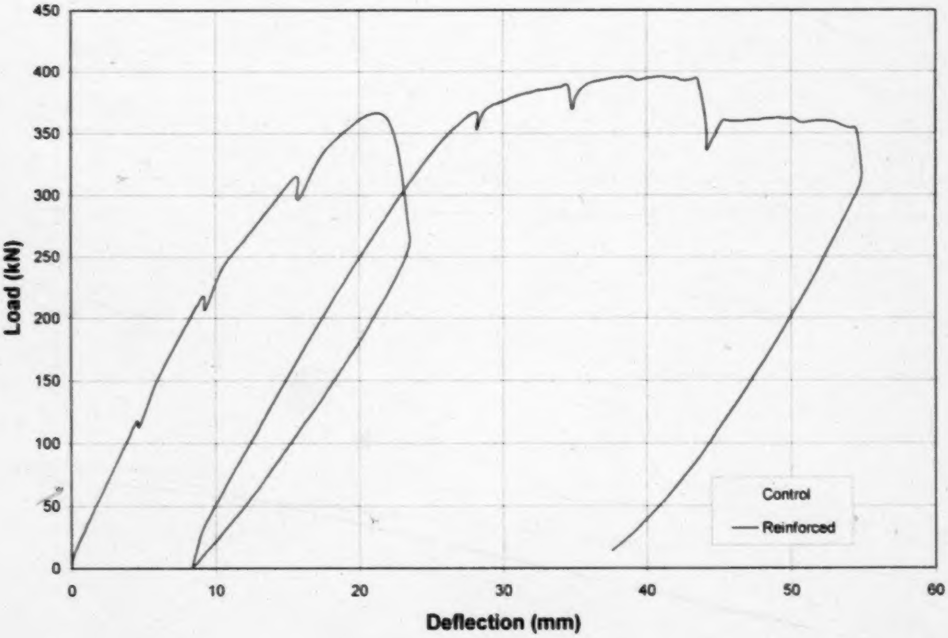

Figure 7: Load vs Point Load Deflection Curves for Specimens with Square End Diaphragm

DISCUSSION

General Behavior

When the girders are eccentrically loaded over one leg as described above, the load is distributed among the four supports in similar manner for all tests. About 70 to 75% of the total load was carried by the *Close Loaded* support reaction and 20 to 25% went to the *Far Loaded* support. The remainder of the load, no more than 7%, was carried by the *Close Unloaded* support. The *Far Unloaded* support was lifting up in all cases. It appears from these observations that the load-sharing path is not significantly affected by the external plate or ACM strengthening. Furthermore, only the loaded leg carries majority of the shear load.

From the deflection data recorded along each leg, the ratio of *Loaded* over *Unloaded* leg at the load point location is about 1.5 during the first stages. This value increases significantly at ultimate, but it should be noted that by then the section is fully damaged. The girder no longer behaves as a whole inverted U section. However, because the deflections of the leg are proportional to the applying moment, load sharing occurs between the two legs in bending. During the first stages, flexure loads are distributed as follows: *Loaded* and *Unloaded* legs carry 60% and 40% of the bending moment, respectively.

Failure Mode

All of the test results in this series showed that FRP sheets helped to hold flexural reinforcement in place. No debonding of the steel plate occurred when composite materials were used because FRP sheets were extended to cover the steel plate. This technique was proved to be very efficient to avoid premature failure by steel plate debonding. Except for *Girder 2 East*, where the test was stopped prematurely, and *Girder 3*

West, the failure mode observed was torsion in the end panel that induced shear cracks in the end diaphragm. *Girder 3 West* failed in shear in the *Loaded* leg with no crack in the end panel. This result is the most promising in shear evaluation of this type of girder and tentative explanations are provided in the next sections.

End Panel Cracks

For all the round diaphragms, a major crack occurred in the end panel (*Girder 2 East* is discarded as mentioned before because of premature test stop) except *Girder 3 West*, which will be discussed later.

It should be recalled that bands of 50 mm wide were applied vertically in the end panel. From the control test with the steel plate (*Girder 1 East*), the crack in the end panel was inclined at about 60 to 70 degrees from the soffit of the diaphragm. The vertical fibres provided prevented any vertical displacement or appearance of cracks perpendicular to the principal orientation of fibres (i.e. horizontal in this case). The crack path in the diaphragm then became vertical which was now the weakest orientation. This behavior is clearly observed with *Girder 2 West*. *Girder 3 East* is similar but the crack in the end panel was initiated by the peeling-off of a band underneath the diaphragm.

With *Girder 3 West*, such peeling off did not occur. The woven glass fabric used also presented fibres in both directions (0° and 90° with a ratio of 20 and 80%, respectively). This material was stronger than the unidirectional carbon fibres in the principal axis perpendicular to the main fibre orientation. Even if bands of only 50 mm wide were used, horizontal tension in this product can be mobilized and partially explains why the end panel did not fail in this case. Unfortunately, no strain in the horizontal direction was measured to confirm this hypothesis.

For the square end panel specimen, the carbon sheets were applied horizontally in the end panel (*Girder 4 West*). Therefore, the crack, which was running along the *Close Unloaded* corner, was covered by ACM. A vertical crack can still be developed because of the sharp corner but then the fibres become extremely effective. Twisting of the fibres can be seen in Figure 8. In this case, the horizontal sheets were long enough to provide good anchorage and to avoid peeling off.

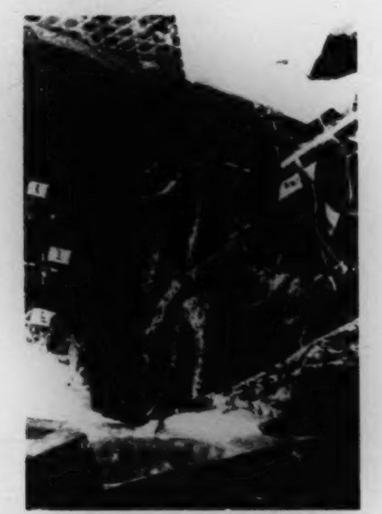

Figure 8: Twisting of Carbon Fibres in CU Corner (Girder 4 West)

Shear Span Cracks

Two major inclined cracks were usually observed in each shear span. The first one was initiated at the support location and the second one started to open up about 500 mm away from the support slopping toward the load point. These cracks were initially oriented at about 45 degree. However the ultimate crack orientation decreased to roughly 30 degree.

The steel plate alone did not affect the inclination and start up of these cracks. However, the failure crack without any ACM was closer to the support as opposed to the failure crack of the girder strengthened by composites. For this later case, the failure crack initiated at the leg-end panel joint, where the legs become wider and it grows toward the point load. In other words, the failure crack is shifted away from the support face when the ACM was used. For example, Figure 9 shows a comparison of two typical cases with and without ACM (*Girders 2 West* and *1 East, respectively*).

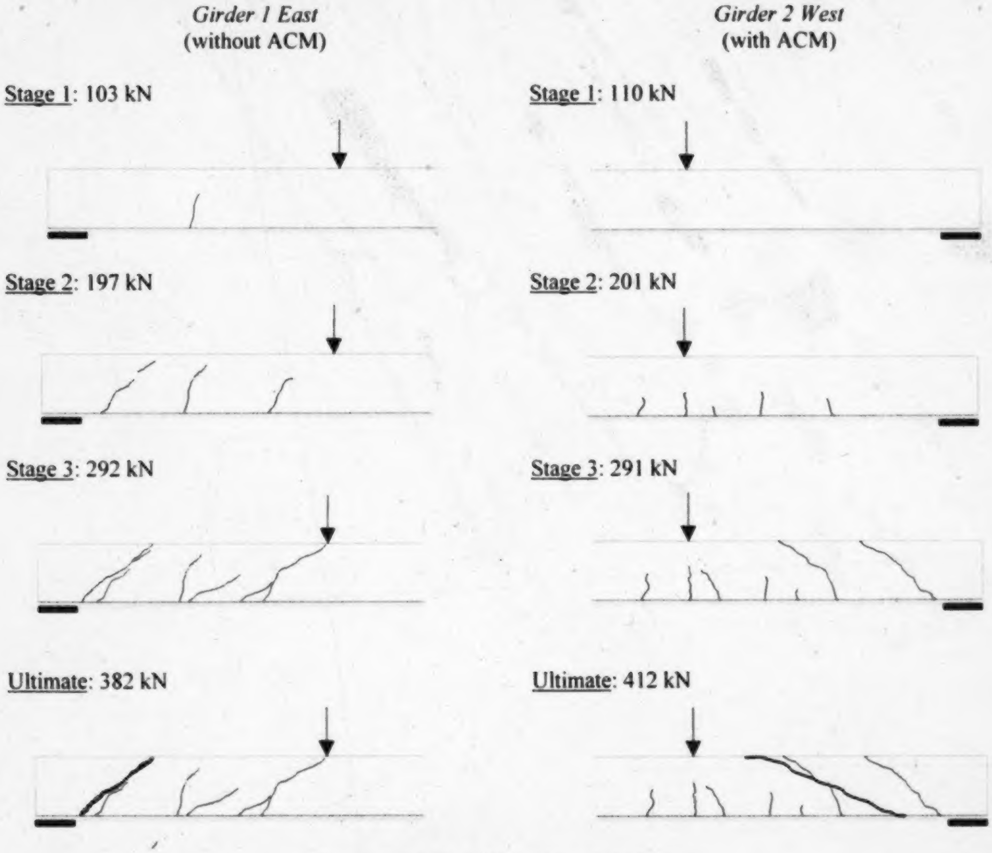
Girder 1 East
(without ACM)
Girder 2 West
(with ACM)
Stage 1: 103 kN
Stage 1: 110 kN
Stage 2: 197 kN
Stage 2: 201 kN
Stage 3: 292 kN
Stage 3: 291 kN
Ultimate: 382 kN
Ultimate: 412 kN

Figure 9: Typical Shear Crack Patterns

Maximum Load

The overall comparison of the total load applied on the girder (Table 1) shows that the external steel plate by itself increases the capacity of the girder by 35%. This large amount comes from the large stiffness the plate adds at the bottom of the legs. Therefore, deflections of the legs are reduced and the plate acts to hold the above concrete in place thereby allowing greater shear transfer to occur.

The effect of ACM can be found by superposition and is equal to 5 and 12% for the vertical and inclined sheets, respectively. It should be noted that *Girder 2 East* increased only by 24% but the test was stopped prematurely. With the square end panel, and assuming the same percentage attributed by the external steel plate, the presence of carbon sheets increased the applied load by another 15%. Even tough the difference between inclined and vertical sheets is not so large, the repair scheme using inclined sheets gave better performance. This phenomena can be explain by the fact that cracking cannot occurs in the gap between the sheets when the fibres are inclined. In fact vertical cracks were observed between vertical sheets during the test, compared to cracks oriented at 90° from principal axis of the inclined sheets.

ACM and Steel Strains

From the experimental data, the maximum steel strain was never greater than the yield strain measured during coupon tests. Therefore, the flexural capacity was therefore not an issue when steel plate was used.

The values of strain recorded in the FRP sheets at each stage were relatively small compared to the maximum deformation that these materials can sustain. The maximum strain recorded was 0.18% while ACM usually deform up to and more than 1%.

However, an interesting observation can be seen between inclined and vertical repair schemes. For the inclined sheets, the measured strains were similar in magnitude in both legs. For the vertical sheets, the loaded leg sheet sustained twice more strain than the unloaded leg. Therefore, the inclined repair scheme seems to evenly distribute the strains and stresses in the fibres to both legs. Torsion in the end panel is then reduced because inclined sheets stiffen both legs to rotate one from the other. This result cannot be observed, of course, with *Girder 3 West* because the failure occurs in the shear span. It shows much more deformation in the loaded leg than for torsion and shear failure occurring in the end panel.

CONCLUSIONS

This series of tests has investigated the benefit of ACM in shear rehabilitation of type G girders. Several conclusions can be drawn from the test results.

1. The steel plate used as flexural reinforcement provides significant increase in shear capacity.
2. From two repair schemes investigated, the inclined sheets were more effective than the vertical sheets.
3. Woven fabric materials also perform better than unidirectional fibres, when principal stresses are not obvious *a priori* or are not constant during loading process.
4. The end panel remains the weakest part of the girder under eccentric loading because it does not contain steel reinforcement. Strengthening can only be applied from the inner face and therefore presents a challenge, due to the convex surface.
5. Vertical bands of composites applied in the round diaphragm were not efficient, except for one case to avoid failure in the end panel. Better results were obtained with horizontal sheets in the square end diaphragm.
6. The FRP sheets do not fully develop their maximum capacity throughout the test. Therefore, the maximum strength of the fibres is not a criterion to consider in this type of application.
7. Proper anchorage of the composite sheets must be provided to avoid fibre peeling off.
8. The combination of the steel plate and the composite sheet along the inner faces of the girder legs tends to shift the failure crack from the support face to the leg end panel joint, inducing less torsion in the diaphragm.

RECOMMENDATIONS

In order to complete this investigation of repair technique for girders, further tests should be carried out to evaluate and to study particular elements to improve the efficiency of the repair technique by ACM. The recommendations for these further tests are as follows:

1. Other types of flexural reinforcement, such as composite straps should be used because they are likely to be used in combination with ACM sheets.
2. Reinforcement of the end panel of type G girder should be investigated with horizontal sheets.
3. Bi-directional or multi directional composite materials should be used as shear reinforcement rather than unidirectional sheets.
4. A detailed investigation of the development length for various composites should be carried out to develop design criteria.
5. External reinforcement cannot be placed between the support abutment and the girder without removing the girder. Flexural reinforcement with cut off close to the support should be studied.

ACKNOWLEDGEMENTS

This work was supported by ISIS (Intelligent Sensing for Innovative Structures) Network of Centre of Excellence. ACM materials were supplied by Mitsubishi Canada Limited, Hexcel Fyfe Canada Ltd and Sika Canada Inc. The authors would also like to thank technical crew from Hexcel Fyfe Canada Ltd for their work contribution, the U of A I.F. Morrison Structures Lab technicians and helpful graduate students for their time.

REFERENCES

[1] ALEXANDER J and CHENG J.J.R., "Shear Rehabilitation of G-Girder Bridges using CFRP Sheets", *Structural Engineering Report No 218,* Department of Civil and Environmental Engineering, University of Alberta, Canada, 1997, 181 p.

[2] AASHO-49, "Standard Specifications for Highway Bridges", *American Association of State Highway Officials*, 5th edition, 1949, 284 p.

[3] CAN/CSA-S6-88, "Design of Highway Bridges", *Canadian Standard Association*, 1988.

[4] ACI-ASCE Committee 426, "The Shear Strength of Reinforced Concrete Members", *American Society of Civil Engineers*, 1974, 96 p.

[5] ASTM C-42, "Standard Test Method for Obtaining and Testing Drilled Cores and Sawed Beams of Concrete", *Annual Book of ASTM Standards*, American Concrete Institute, 1994, p 24-27.

[6] BARTLETT F.M. and MAC GREGOR J.G., "Assessment of Concrete Strength in Existing Structures", *Structural Engineering Report No 198*, Department of Civil and Environmental Engineering, University of Alberta, Canada, 1994, 287 p.

[7] ASTM A-370, "Standard Test Methods and Definitions for Mechanical testing of Steel Products", *Annual Book of ASTM Standards*, American Concrete Institute, 1996, p 164-200.

E.2 27th Annual Conference of the Canadian Society for Civil Engineering – June 2-5, 1999, Regina, Saskatchewan (Paper #1)

Shear Rehabilitation of Type G-Girders Using FRP Sheets – An Analytical Study

Christophe Deniaud and J.J. Roger Cheng
Department of Civil and Environmental Engineering
University of Alberta
Edmonton, Alberta, T6G 2G7

ABSTRACT

Type G-girders have been used extensively in Alberta for highway bridges in 1950's and 60's. There are approximately 1500 bridges still in service in the province today. Structural deficiency, especially in shear, of the G-girders plus economic constraints has demanded a more economical and efficient method of rehabilitation for these bridges. This research program is established to study the feasibility of using Fibre Reinforced Polymers (FRP) to rehabilitate the G-girders in shear and evaluate the applicability of existing design and analytical models for this new technology. Three analysis methods for shear evaluation, the strut and tie model, the grid analysis, and the Modified Compression Field Theory (MCFT) were investigated in the paper. The methods were used to predict and compare the full-scale G-girder test results.

All three methods gave reasonable and conservative prediction of the test results and were consistent with each other. The methods can be used conservatively as design tools for the shear strength of the concrete girders strengthened by FRP sheets. The strut and tie model and the MCFT provide only the ultimate shear capacity of the girder whereas the grid analysis provides also the load deflection curves but the accuracy is limited to the elastic range. The shear contribution of FRP sheets at any angle can be accurately accounted for in the analysis.

INTRODUCTION

Precast concrete type G-Girder was used extensively in highway bridges (with a span length around 6 to 9 meters long) in Alberta around 1960's. Today in Alberta, there are approximately 1500 of these bridges still in service. These girders were found structurally deficient in shear based on current code requirements. It is a need to seek a reliable technique to rehabilitate and strengthen these girders as well as analytical methods to evaluate the repaired girder strength. A research program is carried out at the University of Alberta in collaboration with Alberta Transportation and Utilities (AT&U) to assess these needs.

An experimental research program testing full-scale type G-girders was conducted at the University of Alberta (Alexander and Cheng, 1997; Deniaud and Cheng, 1998). These studies investigated the potential of using Fibre Reinforced Polymer (FRP) sheets as shear reinforcement materials. Two different types of FRPs, namely carbon and glass fibres, with various repair configurations were studied in the program.

In this paper, three analysis methods for shear evaluation, the strut and tie model, the grid analysis, and the Modified Compression Field Theory (MCFT), were investigated. The methods were used to predict and compare the G-girder test results obtained by Deniaud and Cheng (1998).

EXPERIMENTAL PROGRAM DESCRIPTION

The test set-up consisted of four supports at each corner of the girder. The load was applied on the top of one leg of the girder through a distributing beam, as shown in Figure 1. Before the FRP sheets were applied, a 9.5 mm thick steel plate was provided underneath each leg to increase the flexural capacity of the girder. Bands of 250 mm FRP sheets were then glued to the inside face of the webs with a gap of 50 mm in either vertical or inclined layouts. The end diaphragm of the girder was also reinforced by FRP bands of 50 mm applied vertically in all cases.

The flexural reinforcement of each girder consisted of three 28.5 mm diameter steel bars per leg. One of three bars in each leg was bent up 45° at 1085 mm from the support. The stirrups were made of 9.5 mm steel reinforcements and were spaced at 254 mm and 381 mm close to the support and at mid span, respectively.

A total of eight tests were conducted on four G-girders. Each end of girders was tested separately to provide eight test results. *Girder 1* was used as a control beam without FRP reinforcement with the *West End* tested "as is" condition and the *East End* reinforced with a steel plate. *Girder 2* was reinforced with carbon fibre sheets in shear. Vertical bands and inclined bands were applied on the *East* and *West End*, respectively. *Girder 3* was identical to the *girder 2* but glass fibre sheets were used instead. Finally, *Girder 4* had a square end diaphragm rather than round in other three girders. Therefore, only the *West End* was reinforced with inclined carbon sheets while the *East End* was used as a control specimen.

The in-situ concrete strength ranged from 32 to 46 MPa, as shown in Table 1. The steel reinforcements showed a yield stress around 300 MPa with usual characteristic of the steel properties for both the stirrups and the longitudinal bars. FRP coupons were made at the same time the fibres were applied. The carbon coupons were 0.7 mm thick with a modulus of elasticity of 44800 MPa and an ultimate strength of 422 MPa. The glass coupons were 1.8 mm thick and the modulus of elasticity equaled 17700 MPa. Unfortunately, the ultimate strength of the glass fibres was not available because a premature failure within the grips occurred.

The experimental tests were presented previously in detail (Deniaud and Cheng, 1998). The test results will be summarized later in this paper. However, the *Girder 2 East* and *Girder 3 East* were discarded here because the test was stopped prematurely and a FRP band peeled off in the end diaphragm, respectively. The failure mode for all other tests was by cracking in the end panel due to the applied torque except the *Girder 3 West*. In this case, the end diaphragm did not fail but a shear failure occurred in the loaded leg.

ANALYTICAL MODELS FOR TEST SPECIMENS

In all cases, the shear load is assumed to be carried by the loaded leg only as observed during the tests. The bending loads were shared between the two legs. However, the contribution of the unloaded leg varied from test to test as well as it increased with the load level. Therefore, the L/U (*Loaded/Unloaded*) ratio from experimental results at the ultimate was used. No FRP strain measurements were recorded at the ultimate. A linear extrapolation was used from the last two Demec records to evaluate the maximum FRP strains at the ultimate load. Table 1 summarizes the parameters used for the analysis. As mentioned before, three shear design models, the strut and tie model, the grid analysis, and the Modified Compression Field Theory (MCFT) were used to evaluate the shear strength of the girders.

Struts and Ties

The loaded leg of the specimen was modeled as shown in Figure 2. Vertical ties were located at the stirrup locations. The longitudinal bar that bent up at 1080 mm from the support was also introduced into the scheme (Figure 2). The 300-mm level arm between the bottom tie and the top chord was used in all cases regardless whether external flexural reinforcement was provided or not.

The effect of the load shearing in flexure by unloaded leg will be considered in the grid analysis. The area of the bottom steel tie was increased accordingly to the L/U ratio given in Table 1. It was also assumed that the concrete stresses in struts were not critical.

The truss model shown in Figure 2 was loaded until a first tie reached its elastic limit with respect to the material properties of the steel. The yielded tie then removed from the model and a new scheme was created. This process was repeated until the truss collapses by yielding all ties. The ultimate load was the summation of all incremental loads from each mechanism. The effect of the composite sheets was integrated in the method by increasing the load level required to yield the vertical ties.

Grid Analysis

In this approach, the girder was modeled by the use of beam elements. Two longitudinal beams spaced 660 mm apart representing the two legs. Two and seven transverse beams were used for the end panel and flange elements, respectively. The spacing between two consecutive transverse beams was 750 mm except for the first transverse element where 660 mm to the end panel element was used.

Material and Section Properties – The material properties of the girder were computed from the experimental data. The in situ concrete strength f'_c obtained from core tests was used to calculate the modulus of elasticity using the equation in CSA-A23.3-94 (1994). The shear modulus of the concrete was computed assuming an elastic material with Poisson's ratio $\nu = 0.2$.

Section properties of each element were also evaluated. The moment of inertia of the leg elements was calculated using the transformed section method (CSA-A23.3-94, 1994) to account for cracking from service loads after 30 years.

The St. Venant torsion constant J was estimated using membrane analogy. The cross section of the elements was discretized by a two-dimensional mesh. The equation of compatibility for torsion of a prismatic section is:

$$\frac{\partial^2\Phi}{\partial y^2}+\frac{\partial^2\Phi}{\partial x^2}=-2G\theta \qquad [1]$$

where Φ is the stress function at any point (x, y). G is the shear modulus and θ is the angle of twist per unit length. The stress function Φ was then determined by finite difference method. Iteration processes were employed until equilibrium was reached for each discrete point of the grid (Oden and Ripperger, 1981).

The constant J can then be easily found by the membrane analogy. The material and section properties used in the analysis are summarized in Table 2.

The cracking moment in the end panel was evaluated by using the calculated stress function. The shearing stresses can be computed as well as the principal stresses at any discrete point. The maximum principal tensile stress was then compared to the direct cracking strength of the concrete $f_{cr} = 0.33\sqrt{f'_c}$, presented by Collins and Mitchell (1987). The cracking torque in the end panel can then be evaluated by linear interpolation. The maximum shearing stress was found along the inner face of the end diaphragm. When composite sheets are applied on this surface, the maximum shearing stress that leads to cracking of the end panel was shifted to the exterior face of the girder.

Flexural Strength of the Leg – The flexural strength of each individual leg was computed by a combination of two strength calculations. The first method uses a triangular compression zone as shown in Figure 3 to compute the flexural strength M^T_r. The second method uses a rectangular compression block to obtain M_r^R. The former method accounts for unsymmetrical beam section (i.e. inverted L-shape when considering only half the hat-shaped G girder) and the later describes symmetrical beam section behavior. The flexural strength of the leg was then estimated using an exponential decay relationship that is a function of the ratio L/U from Table 1. The flexural strength M^R_r occurs at L/U equals one whereas the flexural strength M^T_r is assumed to occur when L/U reaches infinity. Table 3 gives the flexural strength of the girder elements for each test.

Shear Strength of the Leg –

Concrete: The statistically derived equation (Eq. 2) by Zsutty (1968) for the shear strength of concrete member was used to evaluate the concrete shear strength of the loaded leg.

$$v_c = 2.137\left(f'_c\,\rho_w\,\frac{d}{a}\right)^{1/3} \quad \text{(in MPa)} \qquad [2]$$

where ρ_w is the longitudinal reinforcement ratio, d and a are the effective depth and shear span, respectively. It is important to note that the contribution of the flexural reinforcement and the type of the beam are included in the above formulation through the use of ρ_w and a. The strengthening effect from the flange is ignored for design purposes.

Stirrups: The stirrup contribution was computed by the simplified equation given in CSA-A23.3-94 (1994):

$$V_s = \frac{A_v f_y d}{s} \qquad [3]$$

where A_v, f_y and s are the area, yield strength, and spacing of the stirrups, respectively.

FRP Sheets: Shear friction formulations in CSA-A23.3-94 (1994) were used to evaluate the shear contribution of FRP sheets with some modifications to the specifics of the sheets. Equations used are described below:

$$v_r = k\sqrt{\sigma f'_c} + \rho_v E_f \varepsilon_f \cos\alpha_f \qquad [4]$$

where $\sigma = \rho_v E_f \varepsilon_f \sin\alpha_f$; $\rho_v = \frac{A_{vf}}{A_{cv}}$; k = 0.6 for concrete placed monolithically; E_f and ε_f are the elastic tensile modulus and maximum measured strain of the sheets, respectively. α_f is the angle between the shear friction reinforcement and the shear plane. A_{vf} and A_{cv} are the area of shear friction reinforcement and concrete section resisting shear transfer, respectively.

For consistency with stirrups and concrete shear contribution previously defined, a shear plane at 45° was assumed. Only half of the concrete web was assumed to transfer shear stresses due to the FRP sheets glued only on one face, as shown in Figure 4. Finally, the contribution of the FRP sheets becomes:

$$V_{FRP} = (v_r - v_c)A_{cv} \sin\alpha_f \qquad [5]$$

The shear strength of the leg is then the summation of all its components as follows:

$$V_r = V_c + V_s + V_{FRP} \qquad [6]$$

The calculated shear strengths for each test are summarized in Table 3.

The elastic grid analysis was conducted using the finite element program SAP90. The boundary conditions of the grid model were such that the FU support was able to lift up. The maximum load applied on the top of the girder was calculated when one of elements reaches its assumed capacity (see Table 3). If the end diaphragm failed first, a second elastic analysis was performed with the end diaphragm element removed. The maximum applied load was determined by the failure of one of the loaded leg elements.

Modified Compression Field Theory (MCFT)

This method was developed by Collins and Mitchell (1987). It is the basis of the general method used in CSA-A23.3-94 (1994) with a variable angle truss model. A computerized program was created to include the contribution of the FRP sheets. The procedure requires iterations to converge to the appropriate solution. The solution technique and relevant information of the method can be found in Collins and Mitchell (1987). The predicted strength using MCFT is summarized in Table 4.

DISCUSSION

The analytical results of each test obtained by using the three methods along with the test results are shown in Figure 5 to Figure 12. The test girders behave nonlinearly as the load increases (Deniaud and Cheng, 1998). This behavior can not be fully assessed with the methods of analysis presented. A more sophisticated analysis such as finite element method could be used.

The FRP stiffness per unit width (modulus of elasticity E_f times the thickness h_f of the coupons) provided by the glass and carbon fibres are found to be 31.9 and 31.4 kN/mm, respectively. The fibres oriented at 45° performed better than vertical sheets. In the former case, the concrete cracks were almost at right angle to the principal orientation of the fibres. The composite sheets became then very effective to restrain the opening of cracks to stiffen the leg in shear. This effect is also well described by analysis when computing the strength of the girder element using the grid method (see Table 3).

Comments on Each Model

The strut and tie model is known to be a lower bound solution. The experimental result is therefore expected to be higher than predicted. Predicted results are in fact conservative except for *Girder 2 East* but as mentioned before this test was stopped prematurely.

The grid analysis can accommodate easily various loading conditions or combinations. Load deflection curves in the initial stage can then be performed with reasonable accuracy. However, the flexural strength of the element along the longitudinal axis needs to be evaluated with care. The load sharing between the two legs varies with the position of the applied load. Further investigations should be carried to evaluate this aspect.

The grid analysis gives a very good agreement with the test results in the elastic range. This method is obviously limited to the elastic analysis and cannot include any plastic behavior of the elements. The difficulty comes to assess the cracking moment in the end panel of the girder. *Girder 3 West* for instance did not fail in the diaphragm but the prediction gives end panel cracking. However, if one ignores the cracking at the end diaphragm in the grid analysis, the failure occurs by exceeding the shear capacity of the leg element at almost the same load level.

The shear friction approach used to evaluate the contribution of the composite sheets gives simple but reasonable results. The Canadian standard CSA-A23.3-94 (1994) however presents two methods that give a range of shear strength. More research works should be undertaken to refine or specify a preferred method between these two formulations when applied to composites.

The MCFT method considers only a rectangular concrete block for the T-beam section when computing a plane section analysis to find the corresponding flexural moment. This assumption can only lead to an approximation of the capacity of the leg under eccentric loading. As shown in Figure 3, a triangular compression block represents a better solution for loads applied on the top of one leg.

Comparison of the Models

A good correlation between the MCFT and the strut and tie models was found for almost all tests except *Girder 1 East*. In this test, the girder was strengthened only by a steel plate that gave a heavy longitudinal reinforcement. The stirrups spacing of 380 mm is then too large to assume uniform concrete struts as describe in the MCFT method.

The overall predictions for each method are presented in Table 4. A ratio P_{Test} over P_{Pred} is included to facilitate the comparison. The ratios range from 0.857 to 1.514. Because of the complex loading with combination of bending, shear and torsion, it is difficult to expect better accuracy with the assumptions and simplifications made in the analysis. However, these three methods are consistent with each other and give for most cases conservative and similar ultimate loads.

CONCLUSION

Based on the three models analyzed, several conclusions can be drawn as below:

1. The three methods presented in this study are consistent with each other. They can be used conservatively as tools to design the rehabilitation of existing structures.
2. The strut and tie model and the MCFT give only the ultimate load capacity of the girder whereas the grid analysis provides also the load deflection curves but the accuracy is limited to the elastic range.
3. The shear contribution of FRP sheets at any angle can be accurately accounted for in the analysis. The shear friction method using 45° crack angle provided simple and reasonable results. The method can be be extended for variable crack angle.

REFERENCES

ALEXANDER J. and CHENG J.J.R. (1997) Shear Rehabilitation of G-Girder Bridges using CFRP Sheets, *Structural Engineering Report No 218*, Department of Civil and Environmental Engineering, University of Alberta, Canada, 181 p.

ASCE-ACI COMMITTEE 426 (1973) The Shear Strength of Reinforced Concrete Members, *American Society of Civil Engineers*, 96 p.

COLLINS M.P. and MITCHELL D. (1987) Prestressed Concrete Basics, *Canadian Prestressed Concrete Institute*, 1st Edition, Ottawa, 614 p.

CSA-A23.3-94 (1994) Design of Concrete Structures, *Canadian Standard Association*, Rexdale, Ontario.

DENIAUD C. and CHENG J.J.R. (1998) Shear rehabilitation of type G-girder using ACM: experimental study, *Developments in Short and Medium Span Bridge Engineering*, Canadian Society for Civil Engineering, Calgary, Alberta.

ODEN J.T. and RIPPERGER E.A. (1981) Mechanics of Elastic Structures, *MacGraw Hill*, 2nd Edition, 460 p.

ZSUTTY T.C. (1968) Beam Shear Strength Prediction by Analysis of Existing Data, *American Concrete Institute Structural Journal*, **65**, 943--951.

Table 1 Parameters Used for Analysis of test Specimens

Girder	f'_c *MPa*	L/U Ratio At Ultimate	V/M Ratio	ε_f $\mu\varepsilon$
G1W	45.9	1.62	1.147	-
G1E	45.9	3.95	0.889	-
G2E	46.2	2.11	1.045	1502
G2W	46.2	8.29	0.795	1783
G3E	42.8	4.07	0.883	2267
G3W	42.8	2.34	1.012	3907
G4E	32.5	3.99	0.887	-
G4W	32.5	4.50	0.867	1409

Table 2 Material and Section Properties of Girder Elements

Girder	Density γ *kg/m³*	E *MPa*	G *MPa*	Leg with 2#9 I_{cr} 10^6 mm^4	Leg with 2#9 J 10^6 mm^4	Leg with 3#9 I_{cr} 10^6 mm^4	Leg with 3#9 J 10^6 mm^4	Diaphragm J 10^6 mm^4
G1W	2084	25239	10516	932.2	137.9	1108.8	181.3	7742.1
G1E	2084	25239	10516	1663.8	231.6	1765.3	288.0	7742.1
G2	2111	25792	10747	1639.1	231.6	1740.4	288.0	7742.1
G3	1942	22109	9212	1820.6	231.6	1922.1	288.0	7742.1
G4E	2197	24002	10001	967.9	137.9	1148.8	181.3	1373.2
G4W	2197	24002	10001	1722.1	231.6	1823.8	288.0	1373.2

Table 3 Strength of Girder Elements

Girder	Leg with 2#9 M_r *kN m*	Leg with 2#9 V_r *kN*	Leg with 3#9 M_r *kN m*	Leg with 3#9 V_r *kN*	Diaphragm T_{cr} *kN m*
G1W	130.4	168.7	181.2	153.4	49.1
G1E	267.6	200.1	308.6	178.0	49.1
G2E	284.4	213.0	332.3	194.2	55.7
G2W	272.0	235.3	312.9	216.4	55.7
G3E	258.8	222.1	296.7	203.8	53.6
G3W	264.2	266.3	305.0	248.0	53.6
G4E	120.3	161.8	163.6	144.0	14.3
G4W	249.5	210.2	282.3	188.8	14.3

Table 4 Ultimate Point Load Predictions

Girder	Test Results	Methods					
		MCFT		Strut and Tie		Grid Analysis	
	kN	*kN*	P_{Test}/P_{Pred}	*kN*	P_{Test}/P_{Pred}	*kN*	P_{Test}/P_{Pred}
G1W	281.9	210.6	1.339	230.2	1.225	195.9	1.439
G2E	351.0	393.3	0.892	409.5	0.857	281.1	1.248
G2W	412.6	320.1	1.289	313.4	1.316	310.5	1.329
G3E	393.0	330.4	1.190	319.1	1.232	293.1	1.341
G3W	414.8	373.8	1.110	364.6	1.138	340.6	1.218
G4E	259.0	171.1	1.514	172.6	1.501	179.5	1.443
G4W	395.7	313.7	1.261	315.7	1.254	277.4	1.427
G1E	383.1	226.3	1.693	331.7	1.155	264.1	1.451

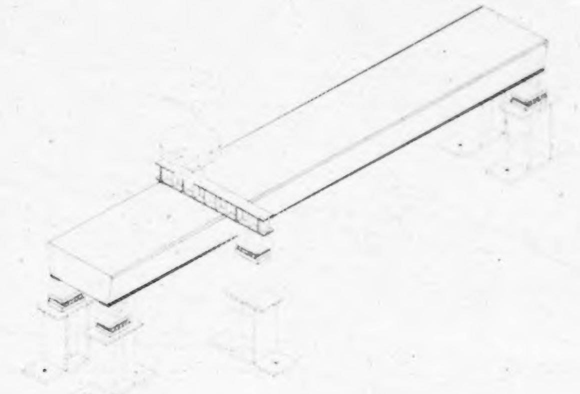

Figure 1 Isometric View of the Test Set-up

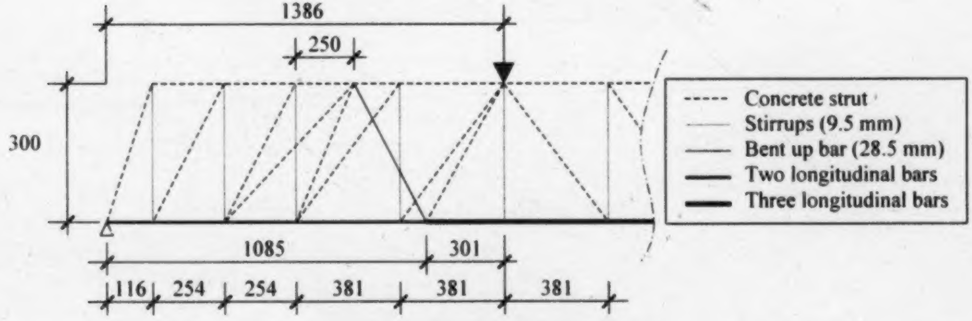
1386
250
300
1085
301
116
254
254
381
381
381
Concrete strut
Stirrups (9.5 mm)
Bent up bar (28.5 mm)
Two longitudinal bars
Three longitudinal bars

Figure 2 Strut and Tie Scheme

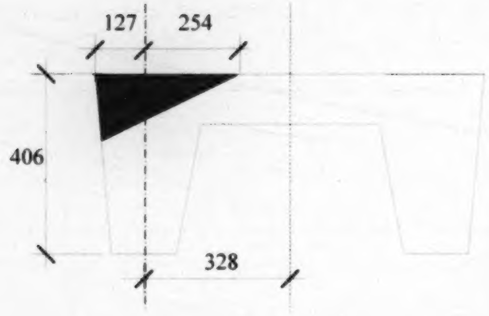
127
254
406
328

Figure 3 Geometry for the Triangular Stress Block

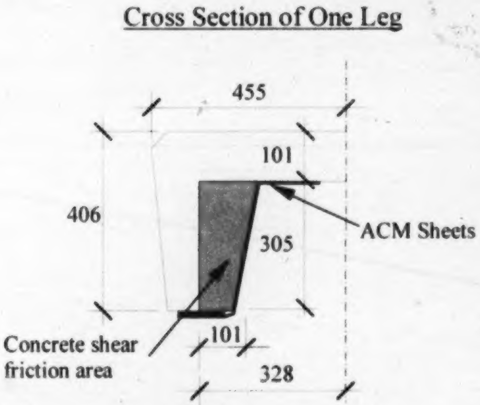
Cross Section of One Leg
455
101
406
305
ACM Sheets
Concrete shear friction area
101
328

Figure 4 Shear Friction Assumptions with FRP Sheet

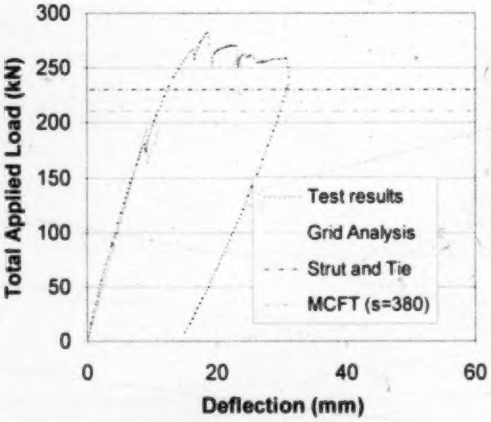

Figure 5 Point Load deflection comparisons with Girder 1 West

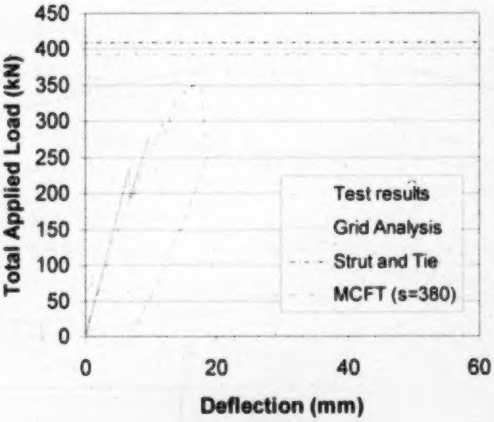

Figure 6 Point Load Deflection Comparisons with Girder 2 East

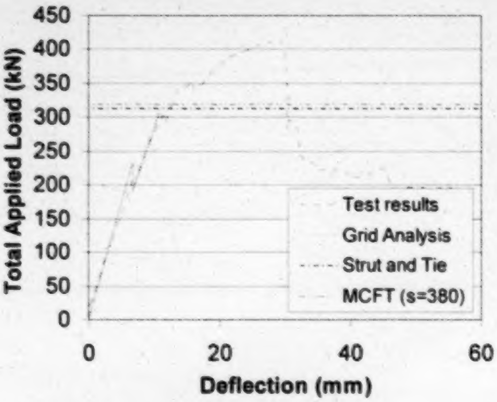

Figure 7 Point Load Deflection Comparisons with Girder 2 West

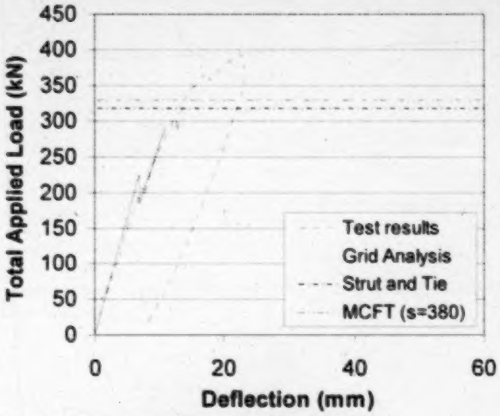

Figure 8 Point Load Deflection Comparisons with Girder 3 East

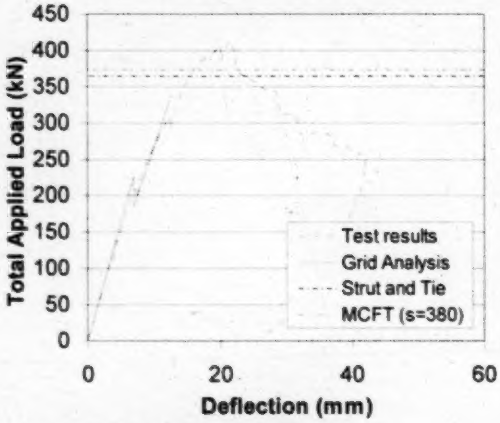

Figure 9 Point Load Deflection Comparisons with Girder 3 West

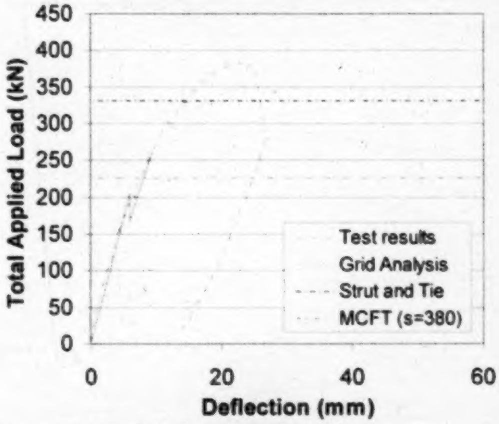

Figure 10 Point Load Deflection Comparisons with Girder 4 East

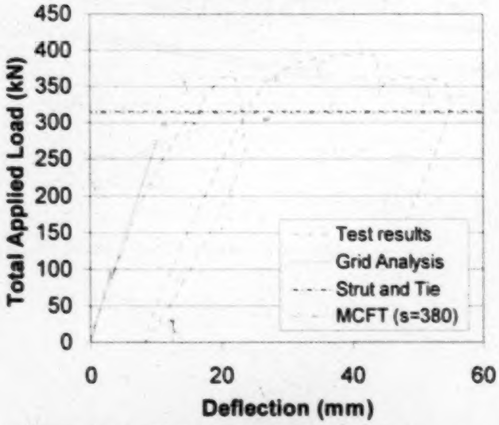

Figure 11 Point Load Deflection Comparisons with Girder 4 West

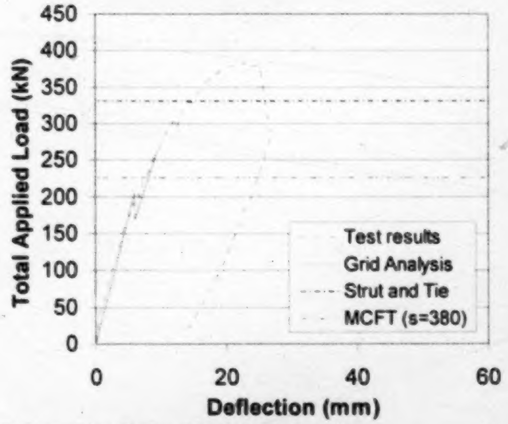

Figure 12 Point Load Deflection Comparisons with Girder 1 East

E.3 27th Annual Conference of the Canadian Society for Civil Engineering – June 2-5, 1999, Regina, Saskatchewan (Paper #2)

Tests of Reinforced Concrete T-beams Strengthened in Shear by FRP Sheets

Christophe Deniaud and **J.J. Roger Cheng**
Department of Civil & Environmental Engineering
University of Alberta
Edmonton, Alberta, T6G 2G7

ABSTRACT

This research is designed to study the interaction of the concrete, the steel stirrups, and the external fibre reinforced polymers (FRP) reinforcement in carrying shear loads in reinforced concrete beams. A total of eight tests were conducted on four concrete T-beams. The flange of the T-beams was 400 mm wide and 150 mm thick. The height of 250 mm and thickness of 140 mm was used in the web. All the beams had a length of 3 m. The nominal concrete strength of 25 MPa was used. The flexural reinforcement was provided by two Dywidag bars with a nominal diameter of 26 mm. The Dywidag bars were extended 150 mm from the end of the beams and were anchored with 50 mm thick steel plate to avoid longitudinal de-bonding shear failure. Closed stirrups of plain steel (6 mm diameter) were used with three different spacing: 200 mm, 400 mm and no stirrups. The beams were subjected to a four point loading. Each end of the beam was tested separately. Three types of FRP were used to strengthen externally the web of the T-beams: uniaxial glass fibre, uniaxial carbon fibre, and tri-axial glass fibre. The glass fibres were applied at the right angle along the full length of the shear span. The carbon fibres were placed inclinedly at 45° with a width of 50 mm and a gap of 50 mm perpendicular to the direction of the fibres. The test results showed that the FRP reinforcement increased the maximum shear strengths from 15.4% to 42.2% compared to the ones with no FRP. The magnitude of the increased shear capacity is not only dependent of the type of FRP but also the amount of internal shear reinforcement. The failure mode of the beams reinforced by FRP was by vertical zipping of the fibres close to the support. The tri-axial glass fibre reinforced beam exhibited a more ductile failure than other beams reinforced by two other types of fibre.

INTRODUCTION

After World War II, many concrete bridges were built in North America and elsewhere in the world due to the reconstruction. Since then, the volumes of traffic and the allowable loads of trucks have increased steadily. As a result, most of the old bridges are now underdesigned according to the current bridge design codes, such as Canadian bridge design standard CAN/CSA-S6-88 (1988). At the same time, bridges have shown signs of aging, such as corrosion of steel and spalling of concrete due to the use of de-icing salt.

In order to accommodate these deficiencies, a few options are available for designers: limit the traffic loads, upgrade the structures to carry additional loads, or construct new bridges. The first choice is not likely desirable because it creates inconvenience in the redirection of the traffic, and the last option is extremely expensive and can cause serious traffic flow problems. Therefore, the strengthening of existing structures becomes a new challenge and cost effective rehabilitation methods are in demand.

The rehabilitation of infrastructures is not new and various projects were realized in the world in the last two decades. In general, steel was the primary material used to strengthen concrete bridges or buildings. External bonded steel plates or external stirrups have been successfully used to repair concrete girders that were deficient in bending or in shear (SWAMY *et al.*, 1987; JONES *et al.*, 1988). However, strengthening by steel elements adds additional dead loads on the structures and corrosion protection to the steel is normally required.

The construction market started only a few years ago to include Fibre Reinforced Polymers (FRP) as structural materials, generally used in combination with other construction materials, such as wood, steel, and concrete. The main attractive properties of FRP are low weight to strength ratios, non-corrosive and electromagnetically neutral behavior.

The use of FRP sheets or plates bonded to concrete beam was investigated by several researchers (RITCHIE *et al.*, 1991). They have shown that bonded FRP plates are a feasible method of upgrading the flexural strength of reinforced concrete beams. AL-SULAIMANI *et al.* (1994) investigated the feasibility of using glass fibre sheets to repair shear deficient concrete beams. A series of small-scale concrete beam specimens deficient in shear were cast. The specimens were loaded until the first visible cracks appeared, then repaired with glass fibre sheets. But, even the beams were designed to yield a flexural capacity 1.5 times higher than the shear capacity, some beams still failed in bending and the full potential of the FRP shear strengthening could not be reached. Similar concrete beam specimens without stirrups were also tested by CHAJES *et al.* (1995) but they concluded that full-scale tests should be conducted and more tests were required with internal shear reinforcement.

The University of Alberta and the Alberta Transportation and Utilities (AT&U) have worked together to demonstrate in the field the potential of FRP for bridge rehabilitation (ALEXANDER and CHENG, 1996). Meanwhile, old concrete girders removed from existing bridges were strengthened by carbon fibre reinforced plastic (CFRP) sheets and tested in laboratory (Drimoussis and Cheng, 1994; Alexander and Cheng, 1997). Although the tests showed increased shear strength by using CFRP sheets, however, no information was obtained on the interaction between the internal stirrups and CFRP sheets.

This project is to provide a series of laboratory controlled concrete beam specimens strengthened in shear with FRP sheets. The objectives are to study the effects of the concrete strength, the stirrups spacing, the height of the beam web, and the type of FRP on the FRP strengthened concrete beams. The experimental results of the first series of tests with a beam height of 400 mm are reported in this paper.

EXPERIMENTAL PROGRAM

Test Specimen

The size of the specimens is designed to provide a reasonably true behavior of such structure element and to minimize scale effect. T-beam shape is selected to increase the flexural capacity relatively to the shear resistance. In addition to the T shape, two high strength Dywidag bars with a nominal diameter of 26 mm were used. The length of these beams was 3 m. Closed stirrups of plain steel (6 mm diameter) were used with three different spacing: 200 mm, 400 mm, and no stirrups. Figure 1 shows a typical cross section of a selected T-beam. The beam was designed to give a flexural capacity between 2.0 to 3.5 times the shear capacity without FRP contribution. The specimens were cast with ready-mix concrete from a local supplier. The nominal concrete strength for this series was 25 MPa.

This test series includes the test of four beams. Because both ends of each beam were tested, a total of eight tests were conducted. The test matrix for these four beams is presented in Table 1.

Table 1: Test matrix of the T400 series

Specimen	Stirrups Spacing *mm*	End	External FRP Reinforcement
T4S2	200	1	None
T4S2–C45		2	Mitsubishi carbon sheets at 45° (50 mm wide, 50 mm gap)
T4S4	400	1	None
T4S4–G90		2	Fyfe glass fibres SEH51 at 90° (No gap)
T4NS	None	1	None
T4NS–G90		2	Fyfe glass fibres SEH51 at 90° (No gap)
T4S2–G90	200	1	Fyfe glass fibres SEH51 at 90° (No gap)
T4S2–Tri		2	Triaxial glass fibres (No gap)

Three types of FRP were used to strengthen externally the web of the T-beams: a) uniaxial carbon fibre; b) uniaxial glass fibre SEH51; and c) triaxial [0/60/-60] glass fibre. The glass fibres were applied at right angle along the full length of the shear span. The carbon fibre sheets were placed inclinedly at 45° with a width of 50 mm and a gap of 50 mm perpendicular to the direction of the fibres. In all cases the fibres were extended underneath the flange to provide a minimum anchor length of 100 mm. The FRP sheets were also bonded to the specimens prior to the test.

Test Set-up

The test setup shown in Figure 2 consisted of four points loading system that created a constant moment region at mid span. Because of the symmetric loading, the non-tested shear span of the beam was always strengthened by external stirrups to avoid the premature failure. These stirrups consisted of two HSS steel tubes with tie rods on both ends.

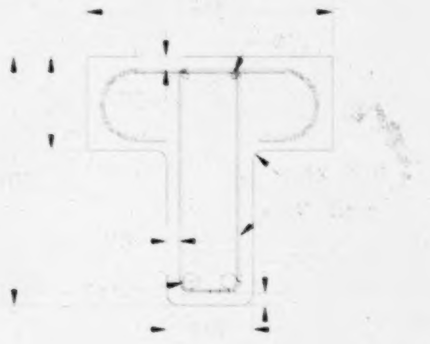

Figure 1 T-Beam cross section

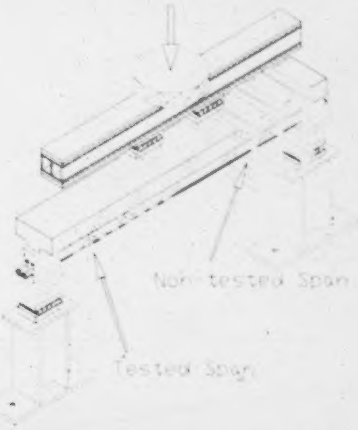

Figure 2 Isometric view of the test set-up

The two longitudinal Dywidag bars, as shown in Figure 1, were extended 150 mm from the end of the beams and were anchored with a 50 mm thick steel plate. L-shaped steel angles were also provided on each side of the web to be used as a passive confinement for the anchor zone of the flexural reinforcement. These details (plate and angles) are also shown in Figure 2 and were designed to avoid longitudinal de-bonding failure.

Instrumentation

Up to 20 electrical strain gauges were provided on the FRP sheets on one side of the T-beam. These gauges were either vertically or horizontally orientated. While the other side was instrumented with numerous sets of Demec gauges. A Demec gauge of 200 mm was used for most of the measurements. However, a Demec gauge of 50 mm was used to record vertical and inclined at 45° strains on the side of the web when glass fibre sheets and carbon fibre bands were glued, respectively.

The Dywidag bars were instrumented along the full length with nine electrical strain gauges. Both legs of the stirrups located in the shear span were also instrumented at mid height. These gauges were protected with waterproof coating and silicon prior to casting the concrete.

The flexural deflection was recorded by three cable transducers that were located at each load point and at mid span. A total of nine horizontal LVDTs were also installed at two locations (section #4 and section #6) within the shear span (470 mm and 870 mm from the support, respectively) and at mid span of the T-beam to measure the strain distribution through the depth of the beam. At each section, a steel apparatus was fixed on the side of the beam to hold three LVDTs at various elevations.

The total load applied by the MTS6000 on the top of the T-beam was recorded from a load cell and checked with the two load cells provided at each support. The dead load of the specimen is not considered in the results presented here.

EXPERIMENTAL RESULTS

The ultimate loads obtained from each test are summarized in Table 2. From the LVDT data, the strain distribution through the height of the beam was computed by the least square method. The coefficient of variation (COV) of the compressive strain at the concrete extreme fibre was then calculated with the best fit line from all the three LVDTs and with the only first two LVDTs. At the mid span the COV was never greater than 5%, it validated the assumption of plane section remains plane. However, at the sections #4 and #6 (470 mm and 870 mm from the support, respectively) this value increased drastically after certain loads, it implies that the plane section no longer remains plane. The corresponding loads when the plane section no longer remains plane at these two locations are shown in Table 2 for each test.

Table 2: Maximum loads and loads corresponding to the change of behavior when plane section no longer remains plane

Test	Maximum load *kN*	At Section #4 *kN*	At Section #6 *kN*
T4NS	230.8	34.6	155.4
T4NS–G90	318.0	9.1	269.1
T4S4	313.9	0.0	140.6
T4S4–G90	411.2	0.0	313.3
T4S2	402.5	83.2	232.1
T4S2–C45	438.1	0.0	406.9
T4S2–G90	451.2	0.0	361.8
T4S2–Tri	485.3	59.4	415.6

For ease of comparison, the loads and deflections obtained from each test were normalized to the test results of the one with no FRP and no stirrup (T4NS). Figure 3 to Figure 5 show normalized load vs. normalized deflection curves for three different stirrup arrangements. Figure 6 illustrates the increase of shear strength with use of glass fibre and decrease of stirrup spacing. Table 3 summarized the normalized ultimate loads and the net increase in shear strength over the respective control specimen.

Table 3: Normalized loads

	Normalized Load			Net increase (%)		
	Stirrups Spacing (mm)			*Stirrups Spacing (mm)*		
FRP reinforcement	*None*	*400*	*200*	*None*	*400*	*200*
control	1.00	1.36	1.74	-	-	-
glass fiber SEH51	1.38	1.78	1.96	37.8%	42.2%	21.1%
carbon sheets at 45°	n.a.	n.a.	1.90	n.a.	n.a.	15.4%
tri-axial Glass	n.a.	n.a.	2.10	n.a.	n.a.	35.9%

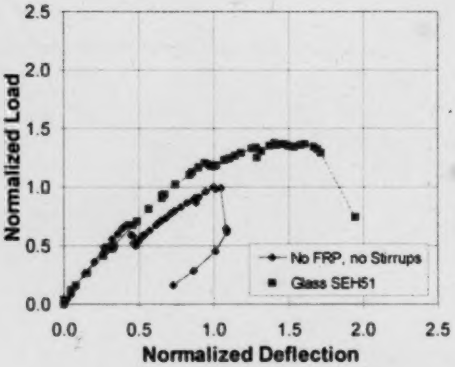

Figure 3 Normalized load deflection curves with no stirrups

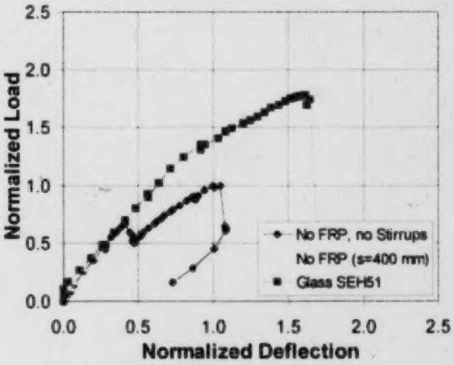

Figure 4 Normalized laod deflection curves with 400 mm stirrup spacing

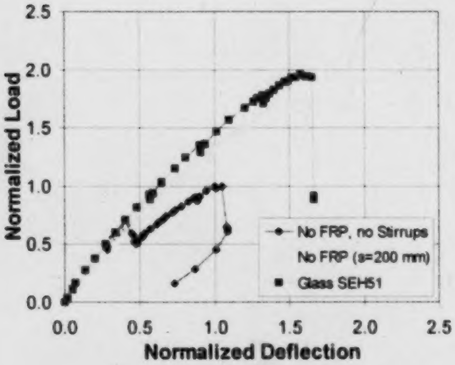

Figure 3 Normalized load deflection curves with no stirrups

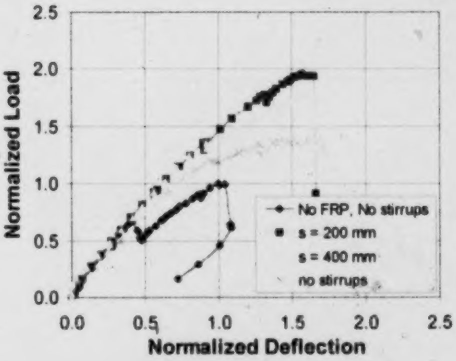

Figure 4 Normalized load deflection curves with 400 mm stirrup spacing

The shear force V can be expressed by two components: namely arching action and beam action. At any location in a beam when a moment gradient $\frac{dM}{dx}$ is present, these two effects are combined to give the total shear resistance. For a cracked concrete member, these components can be written as follows:

[Eq. 1] $$V = \frac{dM}{dx} \quad \text{and} \quad M = T \cdot jd$$

Where T and jd are the tensile force in the bottom chord and lever arm, respectively. Thus,

[Eq. 2] $$V = T\frac{djd}{dx} + jd\frac{dT}{dx}$$

The first term of the above equation is referred to the arching action while the second term describes the beam behavior. These two effects can be evaluated between two known sections along the length of the beam with the recorded strain gauge data and the applied moment at each location. Beam and arching actions were calculated using Eq. 2 between the sections #4 and #6. The calculated results corresponding to the change of beam action to arching action, equal share between beam and arching actions, and remaining beam action at the maximum load are summarized in Table 4.

Table 4: Beam and arching shear actions

Test	Beam action until *kN*	Equal share *kN*	Remaining beam action at the P_{max} %
T4NS	83.0	136.8	0.0%
T4NSG90	214.0	276.0	12.2%
T4S4	65.5	162.2	16.1%
T4S4G90	85.7	313.3	19.6%
T4S2	62.8	162.8	24.8%
T4S2C45	59.8	303.1	20.3%
T4S2G90	111.5	313.2	21.8%
T4S2Tri	91.1	360.6	34.5%

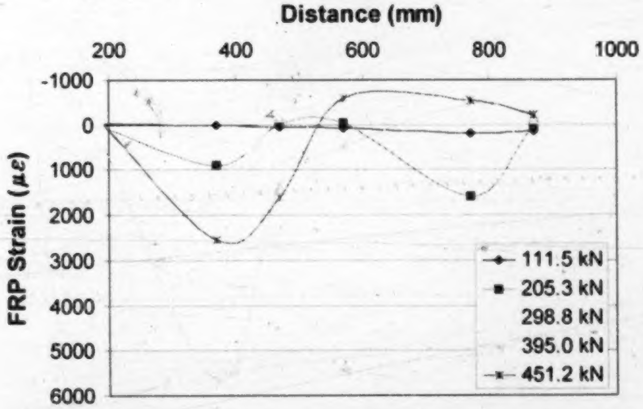

Figure 7 Horizontal FRP strain distribution for T4S2–G90

From the strain gauges on the FRP sheets, horizontal strain distribution can be drawn along the length of the T-beam. A typical distribution is shown in Figure 7.

DISCUSSION OF TEST RESULTS

Initial flexural stiffness: As expected, the external and internal shear reinforcements did not increase the initial flexural stiffness of the beams. Figure 3 to Figure 6 show that the initial slope of the curves is identical for all tests. Only the maximum load and the final deflection (ductility) are increased by the reinforcement.

Amount of stirrups: When the same type and amount of fibre (glass fibre SEH51) is used with various stirrup spacing, different degrees of increase in the shear capacity were observed. With 200 mm stirrup spacing (heavy internal shear reinforcement) the net increase by using SEH51 was 21% while with no stirrups or with s = 400 mm, the glass fibre sheets provided about 40% increase in shear strength (see Table 3). These results indicated that the benefit from the use of FRP reinforcement was reduced when beams were heavily reinforced by internal shear stirrups.

Strain distribution through the depth: From the data recorded by the horizontal LVDTs, section #4, located at 470 mm from the support, did not behave as a plane section for most of the tests from early stages of the loading. However, at section #6, 870 mm from the support, the external FRP reinforcement delayed the non-plane section behavior. In all cases but one (T4S2–G90 test), the section strengthened with FRP did not remain plane when the maximum load level of the corresponding control test with the same internal reinforcement was reached.

Beam and arching actions: The shear components calculated by Eq. (2), between sections #4 and #6, confirmed the results found with the LVDTs. At the beginning of the test, the shear is carried by beam action until the concrete cracks and the struts start to form (second column of Table 4). Equal share of the shear between beam action and arching action is reported in the third column of Table 4. The last column shows the remaining beam action in percentage that carries the shear. It should be noted that with no reinforcement in test T4NS the load is transferred from the point load to the support only by arching action. Therefore, 0% remaining beam action is shown in Table 4. No significant increase of the remaining beam action in percentage at the maximum load was observed for the beams with FRP. However, the arching action behavior was delayed when FRP sheets were applied to the web of the specimens. The equal share between beam and arching actions occurred at a load level close to the lost of the plane section behavior observed with the LVDTs (see Table 2).

Failure modes: In general, for the tests of no FRP, two major shear cracks were observed within the shear span, as shown in Figure 8. The ultimate load was reached when the concrete cracked through the flange near the load point. However, the failure of the glass fibre sheets occurred in all cases by vertical zipping through the fibres close to the support as shown in Figure 9. This effect can be explained by strain compatibility between the flange and the web. When the concrete strut was formed in the web, it created a secondary effect in the top flange. At about 400 mm from the support, horizontal tensile strains were observed in the flange. Eventually, these strains reached the tensile strength of the concrete. A vertical crack therefore formed from the top of the flange and extended downward through the flange thickness reaching the web and the FRP sheets, leading to a vertical zipping of the fibres. The horizontal strain gauges on the FRP sheets captured this behavior, as shown in Figure 7 where strains up to 0.6% were observed at ultimate in the weakest direction of the FRP sheets.

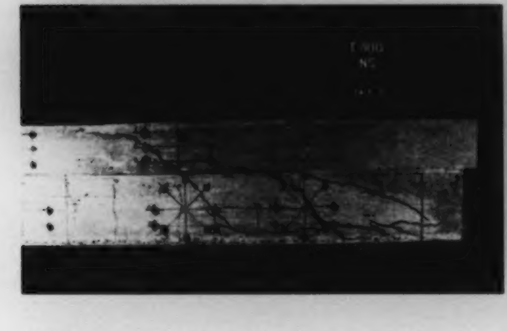

Figure 8 Photo of the crack pattern for T4NS

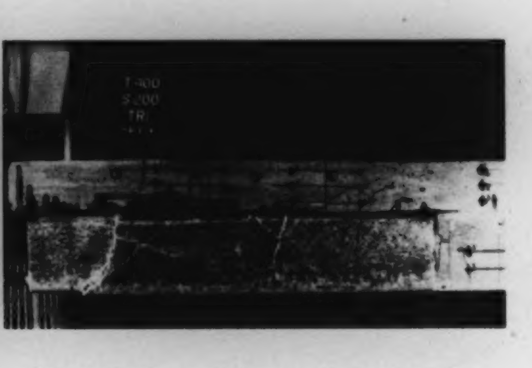

Figure 9 Photo of the crack pattern for T4S2-Tri

Type of FRP: The type of FRP has a significant effect on the final failure mode. With tri-axial glass fibres, the strength of the sheet is more uniform and homogeneous. Therefore, the failure is progressive and the zipping of the fibre can be observed throughout the test. When the SEH51 product is applied, the zip occurred suddenly since little resistance existed in the transverse direction of the sheet. The unidirectional carbon bands at 45° were crossing the concrete cracks almost at right angle and were therefore very effective. However, these bands with a gap of 50 mm generated large shear forces to be transferred to the surrounding concrete and thus peeled off suddenly from the concrete by shear failure.

CONCLUSION

This series of test investigated the behavior of reinforced concrete beams with external FRP shear strengthening. Several conclusions can then be drawn as follows:

1. The effectiveness of shear contribution of the FRP strengthening is dependent of the amount of internal shear reinforcement. It appears that the composites are less effective when beams are heavily reinforced by internal shear reinforcement.
2. The plan section does not remain plane in the shear span after the certain load levels, but the external FRP sheets delay the lost of plane section behavior.
3. The shear forces carried by arching action are also delayed when FRP are used. The remaining beam action at ultimate with significant shear reinforcement either by internal steel stirrups or external FRP sheets accounts for about 20% of the total shear force.

4. The failure mode of the beams reinforced by FRP was by vertical zipping of the fibres close to the support. The geometry of the T-beam is obviously a significant factor of such failure.
5. Tri-axial glass fiber reinforcement provided the beam a more ductile failure than the ones strengthened by unidirectional glass fibre and unidirectional carbon fibre with 50 mm gap.

ACKNOWLEDGEMENTS

This work was funded by ISIS Canada, a Network of Center of Excellence in Canada. The authors would like to thank Mitsubishi Canada Limited and Fyfe LLC Limited for providing FRP materials to the test program.

REFERENCES

ALEXANDER J. and CHENG J.J.R. Field Application and Studies of using CFRP Sheets to Strengthen Concrete Bridge Girders. 2nd International Conference in Advanced Composite Materials in Bridges and Structures, CSCE, Montreal, Quebec, 1996, pp. 465--472.

ALEXANDER J. and CHENG J.J.R. Shear Rehabilitation of G-Girder Bridges using CFRP Sheets. Structural Engineering Report No 218, Department of Civil and Environmental Engineering, University of Alberta, Canada, 1997, 181 p.

AL-SULAIMANI G.J., ISTEM A. BASUNBUL A.S., BALUCH M.H. and GHALEB B.N. Shear Repair for Reinforced Concrete by Fiberglass Plate Bonding. American Concrete Institute Structural Journal, Vol. 91, 1994, pp. 458--464.

CAN/CSA-S6-88 Design of Highway Bridges. Canadian Standard Association, 1988.

CHAJES M.J., JANUSZKA T.F., MERTZ D.R., THOMSON T.A. and FINCH W.W. Shear Strengthening of Reinforced Concrete Beams using Externally Applied Composite Fabrics. American Concrete Institute Structural Journal, Vol. 92, 1995, pp. 295--303.

DRIMOUSSIS E.H. and CHENG J.J.R. Shear Strengthening of Concrete Girders using Carbon Fibre Reinforced Plastic Sheets. Structural Engineering Report No 205, Department of Civil Engineering, University of Alberta, 1994, 177 p.

JONES R., SWAMY R.N. and CHARIF A. Plate Separation and Anchorage of Reinforced Concrete Beams Strengthened by Epoxy-Bonded Steel Plates. The Structural Engineer, Vol. 66, 1988, pp. 85--94.

RITCHIE P.A., THOMAS D.A., LU L.W. and CONNELLY G.M. External Reinforcement of Concrete Beams using Fiber Reinforced Plastics. American Concrete Institute Structural Journal, Vol. 88, 1991, pp. 490--500.

SWAMY R.N., JONES R. and BLOXHAM J.W. Structural Behaviour of Reinforced Concrete Beams Strengthened by Epoxy-Bonded Steel. The Structural Engineer, Vol. 65A, 1987, pp. 59--68.

E.4 3rd International Conference on Advance Composite Materials in bridges and Structures – August 15-18, 2000, Ottawa, Ontario

EVALUATION OF SHEAR DESIGN METHODS OF REINFORCED CONCRETE BEAMS STRENGTHENED WITH FRP SHEETS

Christophe DENIAUD and J.J. Roger CHENG
Department of Civil and Environmental Engineering
University of Alberta
Edmonton, Alberta, Canada T6G 2G7
Rcheng@civil.ualberta.ca

ABSTRACT

The rehabilitation of concrete structures using Fiber Reinforced Polymer (FRP) materials has become a growing market in the construction industry over the last few years. Many research projects in Canada and elsewhere in the world were carried out to promote this efficient repair technique to extend the service life of these structures. However, most of the research was focussed on the flexural reinforcement. As the results, the flexural design methods are well developed and accepted in the design offices. In contrary, few researchers have proposed design methods to evaluate the shear capacity of beams strengthened in shear by FRP. This paper will review the different FRP shear design methods found in the literature and compare the adequacy of each method by using the test results from the University of Alberta. The FRP shear design methods presented include: the effective FRP strain and the bond mechanism criteria, the Strut and Tie model, the Modified Compression Field Theory (MCFT), and a mechanical model based on the shear friction approach. Sixteen full scale T-beam test results were used in the comparison. Two web heights of 250 and 450 mm and two ready mix concrete batches of 29 and 44 MPa were used in the test specimens. Closed stirrups were used with three spacings: 200 mm, 400 mm and no stirrups. Three types of FRP were used to strengthen externally the web of the T-beams: a) uniaxial glass fibre; b) triaxial [0/60/-60] glass fibre; and c) uniaxial carbon fibre. The results showed that the shear friction approach evaluates better the FRP shear contribution. The predicted capacities from this mechanical model are also found conservative and in excellent agreement with the test results.

INTRODUCTION

Fibre Reinforced Polymers (FRPs) are used with a great success in the construction market for over ten years. These materials have been used primarily for the repair and the rehabilitation of existing structures in many structural aspects (Neale, 1999). The FRP shear reinforcement of reinforced concrete beams was investigated successfully with laboratory controlled specimens (Al-Sulamani *et al.*, 1994; Chajes *et al.* 1995). Girders removed from existing bridges were also strengthened in shear with FRP and tested in laboratory (Drimoussis and Cheng, 1994; Alexander and Cheng, 1997).

In 1998, several researchers developed design equations and analytical models to evaluate specifically the FRP shear strengthening of R/C beams (Triantafillou; Malek and Saadatmanesh; Khalifa *et al.*, Chaallal *et al.*). These approaches were found successfully in predicting the beam shear strength. However, the experimental specimens considered were small in scale with the depth less than 300 mm. Chajes *et al.* (1995) concluded that full-scale specimens should be studied and more tests were required with internal reinforcement, different geometry, and various shear span to depth ratio. Collins and Mitchell (1980), and MacGregor (1997) state that the size of the beam is one of the factors affecting the shear strength of reinforced concrete beams. Conceptually, beams strengthened in shear with FRP sheets should also be affected by scale-effect. Furthermore, Deniaud and Cheng (1999a, 1999b) have shown that the amount of internal reinforcement affected the net shear contribution of the FRP sheets.

This paper aims to review, discuss, and compare six recently published FRP shear models with existing full-scale R/C beams tested by Deniaud and Cheng (1999b, 1999c).

EXPERIMENTAL PROGRAM

A brief description of the test specimens is presented below as well as a summary of the testing program results. The testing program details have been published elsewhere and will not be discussed here (DENIAUD and CHENG, 1999b; 1999c).

Test Specimens

A total of eight T-beams (four T-beams of each height) were cast in the program, as shown in Figs. 1 and 2, with a length of 3 m and 3.7 m, respectively. The specimens were subjected to four point loading. The shear spans were 1100 and 1550 mm for the short and long beam, respectively.

Each end of the T-beam was tested separately while the other end was strengthened using external stirrups. The flexural reinforcement was provided by two and four Dywidag bars for the 3 m and 3.7 m beams, respectively. The design provided a flexural capacity between 2.0 and 3.5 times the shear capacity without FRP. The concrete strength was 29 and 44 MPa for the short and the long beams, respectively. Closed stirrups of plain steel (6 mm diameter, 550 MPa yield strength) were used with three spacings: 200 mm, 400 mm, and no stirrups.

The material properties of the three types of FRP sheets used to strengthen externally the web of the T-beams are summarized in Table 1. Coupon specimens were prepared in accordance with ASTM Standard D-3039M (1995). Table 2 presents the test matrix with the total load applied to each specimen at ultimate.

The contribution of the FRP strengthening to the shear capacity of the beam was dependent on the amount of internal reinforcement. The FRP sheets were less effective when beams were heavily reinforced with internal shear reinforcement. The external FRP reinforcement could eventually reduced the shear capacity of the beam by changing the critical path that led to an even more sudden shear failure (DENIAUD and CHENG, 1999b).

The failure mode of the beams strengthen with FRP was significantly affected by the web height of the T-beam as well as the layout and the type of the FRP sheets. With the 400 mm beam height, tensile strain was observed at the top of the flange. This strain caused crack in the concrete. The crack then extended downward and eventually reached the web and unzipped the FRP sheets vertically. The failure mode of the 600 mm beams was mostly affected by the layout of the FRP. The CFRP bands with a 50 mm gap peeled off above the shear crack in the web. The GFRP sheets fully wrapped without any gap showed a debonded area surrounding the path of the concrete shear crack. Once a large area of GFRP sheets debonded, the sheets behaved like a thin shell. The compressive concrete strut ended up buckling the FRP sheets.

SHEAR EVALUATION METHODS

Most of the current design codes (CSA A23.3, 1994; ACI, 1998) in North America evaluate individually the shear contribution of each material used in the structural member. The general formulation of the shear capacity of a reinforced concrete beam including the FRP sheets can be written as follows:

[1] $$V_r = V_c + V_s + V_{FRP}$$

where the subscripts c, s and FRP stand for concrete, steel and FRP sheets, respectively. The shear contributions of the concrete and transverse steel reinforcement are well established and can be found in the current design standards.

In determining the FRP shear contribution, the effective FRP stress, f_{FRP}, in the principal direction of the fibre is the most difficult and sensitive parameter to evaluate. Many researchers have published different expressions for f_{FRP}. Due to the page limitation of the paper, no formulas are given below.

Effective FRP Strain and Bond Mechanism Criteria

In the following models, the shear crack angle θ_c is assumed equal to 45°.

CHAALLAL *et al.* (1998) – The effective FRP stress f_{FRP} in this model is determined based on the FRP sheets' capability to stay bonded to the web surface of the web. They proposed an empirical equation to determine the ultimate bond stress between concrete and fibre.

KHALIFA *et al.* (1998) – This model expresses the effective FRP stress as a fraction of the ultimate FRP strength, f_{ultFRP}, with the use of a reduction factor R. Thus, f_{FRP} is expressed as $R \cdot f_{ultFRP}$. Three requirements for the value of the reduction factor R are considered to include different failure modes of the bond.

CSA-S806 (draft 1999) – The Canadian Standard Association is currently preparing a new design standard for the construction of buildings with FRP. The effective FRP stress shear is simply given by $E_{FRP}\,\varepsilon_{eff}$. The effective FRP strain ε_{eff} is taken as 0.004 (or 4000 $\mu\varepsilon$).

Modified Compression Field Theory (MCFT)

In 1998, Malek and Saadatmanesh have worked out the section equilibrium of the forces acting along a concrete crack inclined at an angle θ_c and followed the procedures similar to MCFT proposed by Collins and Mitchell (1989).

Shear Friction Method

This method was presented with a great success by Loov (1998) to review the simplified method of shear design in the Canadian Standard CSA-A23.3 (1994). Deniaud and Cheng (1999c) extended the shear friction method to include the effect of the FRP sheets. The effective FRP stress is expressed by :

$$f_{FRP} = E_{FRP}\,\varepsilon_{max}\,R_L \qquad [2]$$

where ε_{max} and R_L are evaluated with the strip method summarized below.

The FRP sheets crossing the concrete shear crack are described as a series of strips. Each strip is evaluated individually to find its allowable strain ε_{all} (i.e. the smallest strain) from the geometry of the FRP sheets. The geometry includes the bonded length of the strip above and below the concrete crack as well as the anchorage detail at each end of the strip. The load is assumed linearly distributed among the fibres. When the FRP sheets are in a form of U-jacket, the allowable strain ε_{all} of the strip close to the web-flange corner is very small and will first fail. The load is then redistributed to the remaining strips with a larger critical ε_{all} Eventually, as the critical ε_{all} increases, the number of remaining strip decreases until the load carried by the remaining FRP strips reaches a maximum. At this point the maximum FRP strain ε_{max} as well as the ratio R_L (bonded over total length) are recorded. The lowest shear strength among all potential failure planes is the governing shear.

Strut-and-Tie Model

With this method, a truss describes the shear span of the test specimen. For the beam without stirrups, the approach proposed successfully by Al-Nahlawi and Wight (1992) with tension concrete ties within the truss model was used. The concrete compressive struts were assumed adequate and were not checked. The predicted failure load was obtained when the vertical steel reinforcement yielded and when the tension concrete ties exceeded the cracking strength of the concrete. The effect of the composite sheets was integrated in the method by increasing the load level required to yield the vertical ties and to crack the concrete tension ties.

DISCUSSION

The above six models were used to predict the 16 experimental test results. The predicted shear loads are plotted against experimental shear loads for each method, as shown in Figs 3 to 8 respectively, to evaluate each model's efficiency and for comparison between the models.

CHAALAL *et al.* (1998) – The FRP stresses were limited in this model by the ultimate strength of the sheets. In other words, the model assumes that the bond shear stresses at the end of the sheets do not govern the failure. This model thus assumed that the full strength of the sheets could be mobilized. Fortunately, the assumed 45° concrete crack angle limited the overall shear capacity of the FRP U-jacket. However, all the specimens strengthened with the glass fibre sheet were overly over-estimated. Furthermore, allowing the full strength of the FRP sheets implies also that the ultimate FRP strain could be reached. In most cases, the ultimate FRP strain of 1% would have a significant impact on the concrete integrity.

KHALIFA *et al* (1998) – In this model, a wide range of possible failure modes are identified. The T400 beams strengthen with the uniaxial glass fibre is found to be governed by the bond limit. But for all the other cases and in particular when the beam height increases to 600 mm, the FRP sheet rupture becomes the governing failure mode. The shear load carried by the FRP sheet then is limited to one third of the FRP strength. Combined with the assumed 45° concrete crack angle, the predicted values were generally found conservative.

CSA-S806 – The limitation of the FRP strain to 4000 $\mu\varepsilon$ gives lower bound and conservative results, as shown in Fig. 5. This method is very efficient and can be used for a preliminary design. However, the mode of failure of the FRP cannot be determined.

MALEK and SAADATMANESH (1998) (MCFT) – This model uses the compatibility of the stirrups and FRP strains without crushing the concrete strut. The vertical shear components are then evaluated consistently with each other. The model tends to overestimate the FRP shear contribution when fewer steel stirrups are present. In fact, the method converges to a smaller concrete crack angle, which leads to a substantial increase of the fully wrapped FRP sheets.

Shear Friction – Good correlation between predicted and experimental results is shown in Fig. 7 using shear friction method. The model can also predict with a very good accuracy the critical shear crack path. The shear contribution of the FRP sheets and the number of stirrups crossing the concrete crack are also accurately evaluated. The model does not address at this point the buckling failure of the wrapped FRP sheets. Two test results (T6S4-G90 and T6S4-Tri) are thus over-estimated by this model but the predicted capacity remains within 10%.

Strut-and-Tie – The Strut-and-tie model is well known as a lower bound solution. Therefore, conservative values were expected and indeed this approach under estimated largely the capacity of all the specimens. The FRP shear contribution is also limited in this method by the yield strain of the stirrup or the tensile strength of the concrete. The full tensile potential of the FRP sheets is thus significantly reduced.

Comparison of the Models

For ease of comparison, the mean, the standard deviation and the coefficient of variation were computed with the 16 ratio V_{exp}/V_r found for each model. Table 3 summarizes these calculations. The shear friction method seems the most accurate and reliable with a mean value of 1.233 and a coefficient of variation of 16.7%. The models proposed by CSA-S806 and Khalifa *et al* (1998) follow quite closely with a mean value of roughly 1.5 and a coefficient of variation of about 20% for both of them. However, the CSA-S806 equation is fast and very simple to use but is lacking in providing the FRP failure modes. The other three models presented in this study have very scattered results with a coefficient of variation over 30%. Three approaches gave conservative results for all the 16 tests used in this study: CSA-S806, Khalifa *et al* (1998) and Strut-and-Tie. The shear friction method was also conservative except for the two specimens which failed by FRP buckling. But none of the models investigated here has addressed this mode of failure.

CONCLUSION

Six FRP shear design models proposed recently in the literature were reviewed and compared with sixteen full-scale concrete T-beam tests. The shear friction approach seems very promising to evaluate adequately the shear contribution of the FRP sheets. It is also the most reliable and consistent method among the models investigated for this T-beam test series. The interaction of each individual component resisting shear loads is probably the key element for a successful model. The shear friction model accommodates very well the influence of the concrete, the stirrups and the FRP sheets in combination with each other. The size of the beam affects the shear behavior of the specimen. This factor must thus be accounted for in any shear evaluation method. The buckling of the FRP sheet needs to be addressed as a potential failure mode and needs to be included in any FRP shear evaluation model. None of the presented shear models included this failure mode.

ACKNOWLEDGEMENTS

This work was funded by ISIS Canada, a Network of Centers of Excellence in Canada.

REFERENCES

ACI. 1998. ACI Committee 318 – Building Code Requirements for Structural Concrete, American Concrete Institute, Detroit, MI, 369 p.

Alexander, J. and Cheng, J.J.R. 1997. Shear Rehabilitation of G-Girder Bridges using CFRP Sheets, Struc. Engrg. Rep. No 218, University of Alberta, 181 p.

Al-Nahlawi, K.A., and Wight, J.K. 1992. Beam Analysis using Concrete Tensile Strength in Truss Models, American Concrete Institute Structural Journal, **89:** 284--289.

Al-Sulaimani, G.J., Istem, A., Basunbul, A.S., Baluch, M.H., and Ghaleb, B.N. 1994. Shear Repair for Reinforced Concrete by Fiberglass Plate Bonding, ACI Struc. J., 458--464.

ASTM. 1995. ASTM D-3039M - Standard Test Methods for Tensile Properties of Polymer Matrix Composite Materials, Annual Book of ASTM Standards, 98--144.

Chaallal, O., Nollet, M.-J., and Perraton, D. 1998. Strengthening of Reinforced Concrete Beams with Externally Bonded Fiber-Reinforced-Plastic Plates: Design Guidelines for Shear and Flexure, Can. J. of Civil Engineering, **25:** 692--704.

Chajes, M.J., Januszka, T.F., Mertz, D.R., Thomson, T.A., and Finch, W.W. 1995. Shear Strengthening of Reinforced Concrete Beams using Externally Applied Composite Fabrics, ACI Structural Journal, **92:** 295--303.

Collins, M.P., and Mitchell, D. 1987. Prestressed Concrete Basics, 1st Edition, Canadian Prestressed Concrete Institute, Ottawa, ON, 614 p.

Collins, M.P., and Mitchell, D. 1980. Shear and Torsion Design of Prestressed and Non-Prestressed Concrete Beams, Prestressed Concrete Institue Journal, **5:** 1--70.

CSA. 1994. CSA-A23.3 - Design of Concrete Structures, Canadian Standard Association.

CSA. 2000. CSA-S806 - Design and Construction of Building Components with Fiber Reinforced Polymers, Canadian Standard Association.

Deniaud, C., and Cheng, J.J.R., 1999a. Shear Rehabilitation of Type G-girders in Alberta using FRP Sheets, Canadian Journal of Civil Engineering, (accepted).

Deniaud, C., and Cheng, J.J.R., 1999b. Full Size Reinforced Concrete T-beams Strengthened in Shear by FRP Sheets, J. of Comp. for Const., ASCE (accepted).

Deniaud, C., and Cheng, J.J.R., 1999c. Further Full Size Reinforced Concrete T-beams Strengthened in Shear by FRP Sheets, ACI Structural Journal (submitted).

Drimoussis, E.H., and Cheng, J.J.R. 1994. Shear Strengthening of Concrete Girders using CFRP Sheets, Struc. Engrg. Rep. No 205, Dept. of Civil Engrg., Univ. of Alberta.

Khalifa, A., Gold, W.J., Nanni, A., and Aziz, M.I. 1998. Contribution of Externally Bonded FRP to Shear Capacity of RC Flexural Members, J. of Comp. for Const., ASCE, Vol.2.

Loov, R. 1998. Review of A23.3-94 Simplified Method of Shear Design and Comparison with Results using Shear Friction, Can. J. of Civil Engineering, **25**: 437--450.

Malek, A.M., and Saadatmanesh, H. 1998. Analytical Study of Reinforced Concrete Beams Strengthened with Web-Bonded FRPPlates or Fabrics, ACI Structural Journal, **95:** 343--352.

MacGregor, J.G. 1997. Reinforced Concrete – Mechanics and Design, 3rd edition, Prentice Hall, Upper Saddle River, NJ, 939 p.

Neale, K. 1999. FRPs for Structural Rehabilitation: A Survey of Recent Progress, Progress in Structural Engineering and Materials (in press).

Triantafillou, T.C. 1998. Shear Strengthening of Reinforced Concrete Beams using Epoxy-Bonded FRP Composites, ACI Structural Journal, **95:** 107--115.

Table 1. Fibre Reinforced Polymer Material Properties

FRP Name	Type of fibers	Test source	Ultimate Strength *MPa*	Modulus of Elasticity *MPa*	Thickness *mm*
Replark Type 20	Carbon	Fiber strength	3400	230000	0.11
(Mitsubishi)		Coupon specimens	422	44800	0.70
Triaxial	Glass	Fiber strength	-	-	-
(Owens Corning)		Coupon specimens	124	8100	2.10
SEH51	Glass	Fiber strength	-	-	-
(Fyfe LLC)		Coupon specimens	250*	17700	1.80

* Assumed with roughly ε_{ultFRP}=1.5%

Table 2. Test Matrix and Ultimate Loads

Specimen	Stirrup Spacing, *mm*	End	External FRP Reinforcement	Ultimate load *kN*
T4NS		1	None	230.8
T4NS–G90	None	2	Glass fibers SEH51 at 90° (No gap)	318.0
T4S4		1	None	313.9
T4S4–G90	400	2	Glass fibers SEH51 at 90° (No gap)	411.2
T4S2		1	None	402.5
T4S2–C45	200	2	Carbon sheets *Replark Type 20* at 45° (50 mm wide, 50 mm gap)	438.1
T4S2-G90		1	Glass fibers SEH51 at 90° (No gap)	451.2
T4S2–Tri	200	2	Tri-axial glass fibers (No gap)	485.3
T6NS		1	None	220.2
T6NS–C45	None	2	Carbon sheets *Replark Type 20* at 45° (50 mm wide, 50 mm gap)	427.2
T6S4		1	None	375.0
T6S4–C90	400	2	Carbon sheets *Replark Type 20* at 90° (50 mm wide, 50 mm gap)	545.6
T6S4–G90		1	Glass fibers SEH51 at 90° (No gap)	594.9
T6S4–Tri	400	2	Tri-axial glass fibers (No gap)	633.4
T6S2		1	None	713.7
T6S2–Tri	200	2	Carbon sheets *Replark Type 20* at 90° (50 mm wide, 50 mm gap)	619.6

Table 3. Model Comparison

Model Name	Average	Sdt dev.	c.o.v. %
CHAALLAL *et al* (1998)	1.348	0.456	33.8
KHALIFA *et al* (1998)	1.561	0.305	19.6
CSA-S806	1.512	0.304	20.1
MALEK and SAADATMANESH (1998)	1.346	0.590	43.8
Shear Friction	1.233	0.206	16.7
Struts-and-Ties	2.074	0.632	30.5

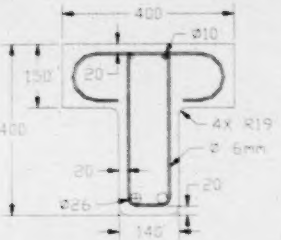
400
Ø10
150
20
400
4X R19
Ø 6mm
20
20
Ø26
140

Figure 1: T400 beam cross section

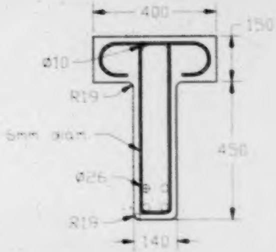
400
150
Ø10
R19
6mm diam
450
Ø26
R19
140

Figure 2: T600 beam cross section

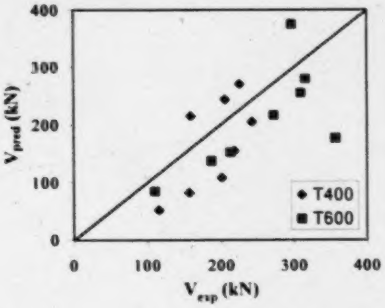

Figure 3 : Chaallal *et al.* model predictions

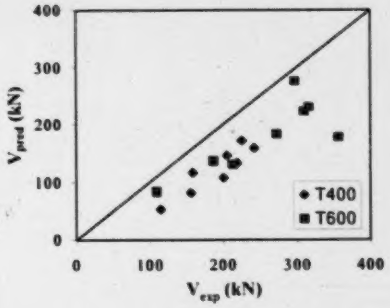

Figure 4: Khalifa *et al.* model predictions

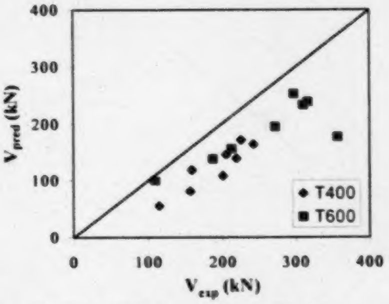

Figure 5: CSA-S806 model predictions

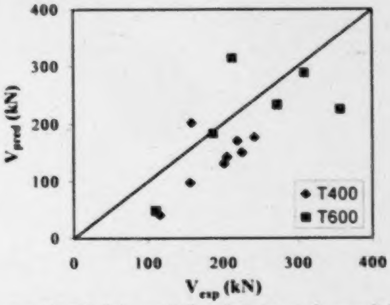

Figure 6: Malek and Saadatmanesh model

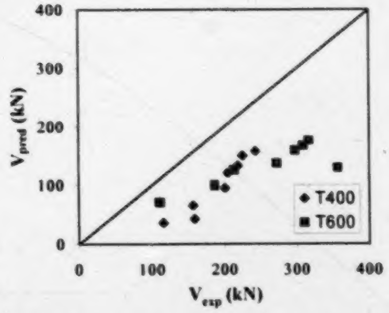

Figure 7: Strut-and-Tie model predictions

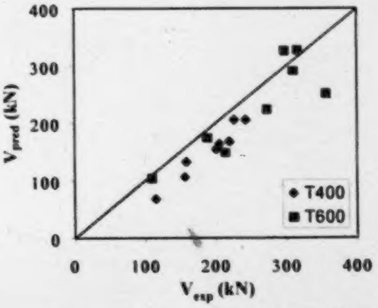

Figure 8: Shear Friction model predictions